MCCRINDLE, ROBERT IAN

ETHANOL LOADING IN AN INDUCTIVELY COUPLED PLASMA

DPhil UP 1995

Ethanol Loading in an Inductively Coupled Plasma

by

Robert Ian McCrindle

Submitted as partial fulfilment of the requirements for the degree

Doctor Philosophiae in Chemistry

in the Faculty of Science

University of Pretoria

Pretoria

18 August 1995

Declaration

I hereby declare that this dissertation which is submitted for the degree of Doctor Philosophiae at the University of Pretoria, has not been submitted for a degree at any other University and that it is my own work.

_____

R I McCrindle

"Show me your ways, O Lord,
teach me your paths,
guide me in your truth and teach,
me,....." Ps 25.

To my wife and family.

ACKNOWLEDGEMENTS

I wish to thank Prof C. J. Rademeyer for his patience, support and friendship over a long period of time.

My thanks to my wife who not only supplied the inspiration, but also did much of the work to make it understandable.

To Prof Kobus Visser for the programme that made the calculations possible

The technical staff of the University of Pretoria were constantly on hand to enable work to continue. Thanks to Reg, Robin, Corrie and Leon.

The students of both the University of Pretoria and Technikon Pretoria for assisting with many of the experiments.

Thanks to the personnel of the Department of Chemistry and Physics for support over a long period of time.

Thanks to Driekus van der Westhuizen for programming and assisting with interfacing the computer.

To Mark Saunders and SMM instruments for assistance and loan of the Liberty ICP-OES.

SAMEVATTING

"Ethanol-loading in an Inductively Coupled Plasma" deur Robert Ian McCrindle, voorberei onder leiding van prof. C. J. Rademeyer in die Departement van Chemie, voorgelê vir die gedeeltelike vervulling van die vereistes vir die graad Doctor Philosophiae in Chemie.

Die kwanitatiewe bepaling van elemente in oplossings bevattende 30 % en meer etanol of metanol deur gebruik te maak van plaaslike beskikbare induktiefgekoppeldeplasma-optiese-emissiespektrometers (IGP-OESs), was tot onlangs nie in Suid-Afrika moontlik nie. Onvermoë om die plasma vol te hou terwyl etanoliese oplosings verstuif word, plaas 'n ernstige beperking op die analise van sekere elemente, aangesien etanol 'n uitstekende oplosmiddel is. Voorheen was dit nodig om etanol uit die monster te verwyder voordat 'n analise met IGP-OES gedoen kon word. Hierdie studie was geloods om die oorsake vir die uitdoof van die plasma, wanneer hoë etanoliese konsentrasies verstuif word, te ondersoek.

Fundamentele eienskappe van die plasma soos temperatuur, elektrondigtheid, verspreiding van druppelgrootte, massavloeitempo en waterstofemissie is ondersoek. Die invloed van bogenoemde op analitiese parameters soos sensitiwiteit, opsporingsgrense en agtergrond-ekwivalente-konsentrasie (AEK) is daarna bepaal.

Opwekkingstemperatuur is met behulp van die "twee lyn"-metode bepaal. Die intensiteit van twee waterstoflyne (H_α en H_β), is by verskillende posisies in die plasma tydens verstuiwing van verskillende konsentrasies etanol, gemeet. Om akkurate antwoorde met die metode te verkry, is dit nodig dat die plasma in 'n toestand van lokale termodinamiese ewewig (LTE) moet wees. Daar is voldoende getuienis beskikbaar dat IGPs nie 'n toestand van LTE bereik wanneer waterige oplossings verstuif word nie, maar vir die doel van hierdie ondersoek was dit nie as 'n probleem beskou nie. Die doel van die ondersoek was om die veranderinge in temperatuur te meet wanneer die konsentrasie van etanol verhoog word, eerder as om die opwekkingstemperatuur akkuraat te probeer bepaal. Resultate het getoon dat die opwekkingstemperatuur saam met die etanolkonsentrasie verhoog en dat 'n maksimum temperatuur van 10400 K bereik word wanneer 15 % etanol verstuif word.

Elektrondigtheid is bepaal deur die Stark-verbreding van die H_{β}-lyn te meet. Daar is gevind dat die elektrondigtheid verhoog wanneer die etanolkonsentrasie verhoog word. Die grootste verhoging het in die omgewing van die sentrale kanaal plaasgevind (gemeet na Abel-inversie). Die hoogste elektrondigtheid was 8 x 10^{15} cm^{-3} wat naby die vereiste waarde vir LTE is.

Druppelgrootte-verspreiding is met behulp van 'n laser deeltjieteller gemeet. Die aërosol is met argon verdun en deur die meetsel gestuur. Slegs die neiging van die druppelgrootte-verspreiding tydens veranderinge in die etanolkonsentrasie, is gemeet. Die druppeldeursnit het toegeneem namate die etanolkonsentrasie verhoog is. Hierdie toename in druppelgrootte het tesame met 'n toename in die massa materiaal wat na die plasma deurgedring het, plaasgevind. Laasgenoemde is gravimetries bepaal.

Daar is gevind dat die waterstofinhoud van die plasma verhoog namate die etanolkonsentrasie van die verstuifde vloeistof verhoog word. Die waterstofemissiesein (H_{α}-lyn by 656.3 nm) het viervoudig toegeneem wanneer die etanolkonsentrasie na 25 % verhoog is.

Die invloed van veranderinge in die fundamentele eienskappe van die plasma op die analitiese vermoë van die IGP-OES is hierna ondersoek. Kalibrasiekrommes vir Pb, Cd, Al, Cr, Fe, Na, Mn, Mo en V in 'n reeks oplossings met toenemende etanolkonsentrasies, is bepaal. Vir elk van die elemente is die maksimum sensitiwiteit by 'n etanolkonsentrasie van 15 % verkry. Analitiese parameters het van element tot element gevarieer.

Daar is vasgestel dat die vloeitempo van die aërosoldraaergas 'n groter invloed het in die geval van etanolbevattende oplossings as in die geval van waterige oplossings. Optimering van die aërosoldraergastempo met waterige oplossings het 'n verdubbeling in emissie veroorsaak, terwyl 'n 15 % etanoloplossing 'n viervoudverhoging in seinsterkte tot gevolg gehad het.

Met die beskikbaarstelling in Suid-Afrika van 'n nuwe IGP-OES wat die vermoë besit om 100 % etanoloplossings te hanteer, is die ondersoek uitgebrei om die invloed van hoër konsentrasies etanol vas te stel. Dieselfde elemente is weer ondersoek, maar die hoogste etanolkonsentrasie wat gebruik kon word, was 95 %. Deur 1.5 kW drywing en optimum

verstuiwergasdruk te gebruik, is gevind dat die sensitiwiteit oor die volle etanol gebied verhoog.

Opsporingsgrense het nie in elke geval verbeter nie omrede die AEK verhoog het soos wat die etanolkonsentrasie verhoog is. Nogtans is dit voordelig dat oplossings met etanol as oplosmiddel nou geanaliseer kan word.

Elektrondigtheid, soos deur die verhouding tussen twee Mg-lyne bepaal, was 'n maksimum by 25 % etanol. By dié konsentrasie was die lynverhouding 14, wat toon dat die plasma naby aan 'n toestand van LTE is, wat weer die bepaling van die opwekkingstemperatuur met sekere oplossings meer akkuraat maak.

Ter uitbreiding van die studie is die invloed van etanolbyvoegings tot 'n organiese oplosmiddel ook ondersoek. Vir hierdie ondersoek is 30 en 45 % oplossings van etanol in xileen voorberei. Al, Pb, Fe, Cr en Cu is in 'n standaardverwysingsoliemonster opgelos in die etanol/xileen mengsels en ook suiwer xileen as oplosmiddel, bepaal. Simpleksoptimering is toegepas om die hoogste sein-tot-geraas-verhouding te kry. Resultate wat vir die verwysingolies verkry is, was naby die gesertifiseerde waardes. Byvoeging van etanol het tot groot verlaging in sensitiwiteit gelei en het ook negatief op die ander analitiese parameters ingewerk. Die elektrondigtheid het ook drasties met etanolbyvoeging afgeneem. Die massa materiaal wat deur die spuitstuk gegaan het, het met die etanoloplossings meer as verdubbel. Dit word gepostuleer dat dit tot 'n verlaging in die energie, wat vir dissosiasie van die monster beskikbaar was, gelei het.

Hierdie ondersoek het bygedra tot uitbreiding van kennis oor die plasma en prossese wat plaasvind wanneer 'n monster en matrys in 'n omgewing van hoë temperatuur ingespuit word. Die belangrikheid van die veranderinge in die fundamentele eienskappe vir analitiese werk word beskryf. 'n Metodiek wat die nuutste tegnologie gebruik, is ontwikkel om die analise van monsters wat in etanol opgelos is, moontlik te maak.

SYNOPSIS

"Ethanol-loading in an Inductively Couple Plasma", by Robert Ian McCrindle, prepared under the leadership of Prof. C. J. Rademeyer in the Department of Chemistry, as partial fulfilment of the requirement for the degree Doctor Philosophiae in Chemistry.

Inductively coupled optical emission spectrometers (ICP-OES's) that have been commercially available in South Africa have, until recently, been unable to determine elements in solutions containing more than 30 % ethanol or methanol. Inability of the plasma to be sustained while aspirating ethanolic solutions is a severe limitation to the analysis of certain elements as ethanol is an excellent solvent. Previously, ethanol had to be removed from samples prior to analysis using ICP-OES. This investigation was launched to determine the cause of the plasma being extinguished when higher ethanolic concentrations were nebulized.

Fundamental characteristics of the plasma were investigated. These were temperature, electron density, drop size distribution, mass flow rate and hydrogen emission. Effects on the analytical parameters of sensitivity, detection limits and background equivalent concentration were then determined.

Excitation temperature was determined by the "two line" method. The intensity of two lines of hydrogen (H_α and H_β), at different positions in the plasma and while different concentrations of ethanol were being aspirated, was measured. For accurate answers to be obtained with this method the plasma must be in a state of local thermodynamic equilibrium (LTE). Sufficient evidence is available to indicate that ICP's do not reach LTE when aqueous solutions are aspirated, but for the purpose of this work this was not considered a problem. The aim of the investigation was to measure the changes that occurred to the temperature as the ethanol concentration being aspirated increased rather than to measure accurately the excitation temperature. Results showed that excitation temperature increased as ethanol concentration increased and reached a maximum of 10400 K when 15 % ethanol was nebulized.

Electron density was determined using Stark broadening of the H_β line. It was found that electron density increased as the ethanol concentration increased. Furthermore, the major increase occurred on the region of the central channel, as measured after Abel inversion had been applied. The highest electron density determined was 8 x 10^{15} cm^{-3}, close to the requirements for LTE.

Drop size distribution was measured by means of a laser particle counter. The aerosol was diluted with argon and then passed through the measuring cell. Again, only the tendency of the drop size distribution was measured, as changes in the ethanol concentration occurred. Droplets increased in diameter as the ethanol concentration increased. This increase in drop size diameter was found to be accompanied by an increase in the mass of material entering the plasma as determined by gravimetry.

It was discovered that the hydrogen content in the plasma increased as the ethanol concentration of the aspirated solution was increased. There was a fourfold increase in hydrogen emission signal (H_α line at 656.3 nm) as the ethanol was increased to 25 %.

The effects that changes to the fundamental properties of the plasma would have on the analytical performance of the ICP-OES was then investigated. Calibration curves for Pb, Cd, Al, Cr, Fe, Na, Mn, Mo and V in a series of solutions containing increasing ethanol concentration were determined. For each element, the most sensitive results were obtained with 15 % ethanol solutions. Analytical parameters were found to vary according to the element analysed.

Aerosol carrier gas flow rates were found to be more important for the ethanol containing solutions than for aqueous solutions. Optimization of aerosol carrier gas flow rates with aqueous solutions led to a doubling in emission intensity, while with 15 % ethanol solutions there was a fourfold increase in signal intensity.

The introduction into South Africa of an ICP-OES capable of measuring 100 % ethanol, resulted in the investigation being extended to study higher concentrations of ethanol. The same elements were again investigated, but the highest concentration of ethanol which could

now be used as solvent was 95 %. Using 1.5 kW power and optimum nebulizer gas pressure, the sensitivity of the determinations was found to increase throughout the ethanol range. Detection limits did not necessarily improve, as the BEC increased with increase in ethanol concentration. However, the advantage was that solutions where ethanol had been used as solvent could now be analysed.

Electron density, as determined by the ratio of two Mg lines, was a maximum for 25 % ethanol. For that concentration of ethanol the ratio was 14, indicating that the plasma was close to being in a state of LTE, which made the determination of the excitation temperature with certain solutions more accurate.

In addition to aqueous solutions, the effects of ethanol additions to an organic solvent were investigated. For this investigation, 30 and 45 % solutions of ethanol in xylene were prepared and Al, Pb, Fe, Cr and Cu were measured in a standard reference material using the ethanol/xylene mixtures as well as pure xylene. Simplex optimization was applied to achieve the greatest signal-to-background-ratio. Results obtained for the reference oil were close to those certified. Additions of ethanol resulted in severe degradation of the sensitivity and other analytical parameters. The electron density measured from the ratio of Mg lines also decreased drastically when the ethanol was added. The mass of material exiting the nozzle more than doubled for the ethanol solutions, and it is proposed that this led to a decrease in energy available to dissociate the sample.

This investigation has led to a further understanding of the plasma and the processes that occur as the sample and matrix are injected into a region of high temperature. The significance of changes in fundamental properties for analytical work was described. A methodology was developed which utilized new technology so as to allow analysis of samples dissolved in ethanol.

CONTENTS

LIST OF FIGURES

LIST OF TABLES

LIST OF PLATES

LIST OF SYMBOLS AND ABBREVIATIONS

a	a-parameter indicated contribution from Gaussian and Lorenzian components to Voigt function.
A	Absorbance.
A_{pq}	Transitional probability for spontaneous emission between states p and q.
AAS	Atomic absorption spectrometer/spectrometry.
ASDF	Atomic state distribution function.
B	Rotational constant for upper vibrational level.
$B(\lambda,T)$	Spectral radiance.
BEC	Background equivalent concentration.
c	Velocity of light.
C_{DL}	Detection limit.
d_c	Cutoff diameter of drops.
d_s	Sauter mean diameter of the droplets of the aerosol.
ds	Exchange area.
D	Drop diameter.
D_{50}	Droplet distribution diameter below 50 % of the cumulative aerosol volume.
D_v	Diffusion constant.
E	Evaporation factor.
E_d	Energy of dissociation.
E_i	Ionization energy.
E_p	Energy difference between excited and ground states.
E_t	Translational energy.
E_x	Energy difference between excited state x and ground state.
FAAS	Flame atomic absorption spectrometry.
g_o	Statistical factor (statistical weight) of the ground state.
g_p	Statistical factor (statistical weight) of the excited state.
GVMS	Gas viewing module sensor.
h	Planck's constant.
h_t	Height above injector nozzle.

H_α	Hydrogen line at 656.28 nm.
$H_ß$	Hydrogen line at 486.13 nm.
H_δ	Hydrogen line at 483.05 nm.
ICP	Inductively couple plasma.
ICP-MS	Inductively coupled plasma mass spectrometer/spectrometry.
ICP-OES	Inductively coupled plasma optical emission spectrometer/spectroscopy.
i(r)	Local radiance intensity, a function of the radius.
I(x)	Intensity of radiation distributed along horizontal direction.
I_b	Intensity of background.
I_{cont}	Intensity of continuum.
I_{pq}	Observed intensity for transition between states p and q.
J	Quantum number.
k	Boltzmann's constant.
K	Rotational quantum number.
K_n	Equilibrium dissociation constant.
l	Path length.
LPS	Laser particle spectrometer.
LTE	Local thermodynamic equilibrium.
m_x	Mass of species x.
M	Atomic mass.
n_a	Total concentration of atoms.
n(D)	Number of drops with diameter D.
$n(E_x)$	Population density of atoms excited by energy x.
n_e	Electron number density.
n_i	Concentration of ions.
n_o	Number of atoms in the ground state.
n_p	Number of atoms in an excited state.
OB	Obscuration factor.
P_s	Saturated pressure.
Q_{CPL}	Plasma carbon load.
Q_g	Volume flow rate of gas.
Q_l	Volume flow rate of liquid.

Q_{SPL}	Solvent plasma load.
R	Gas constant.
R_o	Radius of the source.
Rf	Radio frequency.
RSD	Relative standard deviation.
S	Sensitivity.
S_n	Saha-Eggert constant for mass action.
S_{tot}	Solvent transport.
SSA	Specific surface area.
T_D	Doppler temperature.
T_e	Electron temperature.
T_{exc}	Excitation temperature.
T_{rot}	Rotational temperature.
TE	Thermodynamic equilibrium.
V	Difference in velocities of gas and liquid entering nebulizer.
V(a,0)	Voigt function.
W_{tot}	Mass transport.
Z_a	Partition function of atom a.
Z_i	Ionic partition function.
Z_x	Partition function of x.

δ	Dummy integral (for Voigt function).
$\Delta\lambda_C$	Collisional halfwidth.
$\Delta\lambda_D$	Doppler halfwidth.
$\Delta\lambda_H$	Halfwidth of hydrogen line.
$\Delta\lambda_N$	Wavelength spread.
ϵ	Transport efficiency.
η	Viscosity.
η_i	State density per statistical weight.
θ	Thermal conductivity.
λ	Wavelength.

λ_o	Wavelength at centre of line.
ξ	Radiant power.
ρ	Density.
$\rho(\lambda,T)$	Spectral volume density of radiant energy.
σ	Surface tension.
σ_l	Standard deviation of limiting noise.
τ	Mean life-time of a level.
υ	Frequency.
ϕ	Function of normalized distribution.

CHAPTER 1

INTRODUCTION

1.1 Introduction to Inductively Coupled Plasma-Optical Emission Spectrometry

Inductively Coupled Plasma-Optical Emission Spectrometer (ICP-OES) has become the work horse of the analytical laboratory in many instances. Though the technique is primarily limited to liquid samples, its analytical parameters are such that it is the chosen technique for most applications. The sensitivity achieved and low detection limit for most elements make it a trace element technique. The calibration curves exhibit long linear working ranges (between four and six decades) and therefore make continual dilutions or multiple standards unnecessary.

Simultaneous measurement or fast sequential measurement makes rapid determination of many elements in a single sample possible. In the case of a simultaneous ICP-OES only the number of channels limit the number of elements that may be determined in a reading period which is normally of about ten seconds. Auto-samplers make routine analysis even without the presence of an operator, a possibility. Further developments, like the addition of a mass spectrometer as detector, or the use of laser ablation as a means of generating atomic vapour from solids, give the technique a wide range of possibilities.

There are unfortunately some disadvantages to the technique, most being economic in nature. Even simple instrumentation is not cheap, costing in excess of R 200 000.00 (1995 prices) and is computer driven. Although this has the advantage that the instrument may be operated from the keyboard, it does mean that the operator must be sufficiently skilled to be able to use the computer. The system uses Argon to support and maintain the plasma. The consumption of Argon can be considerable

(a cylinder every two days) and the price of Argon must therefore also be taken into consideration.

1.2 Brief description of an ICP-OES

The instrument itself consists of several units, and is represented schematically in Fig. 1.1.

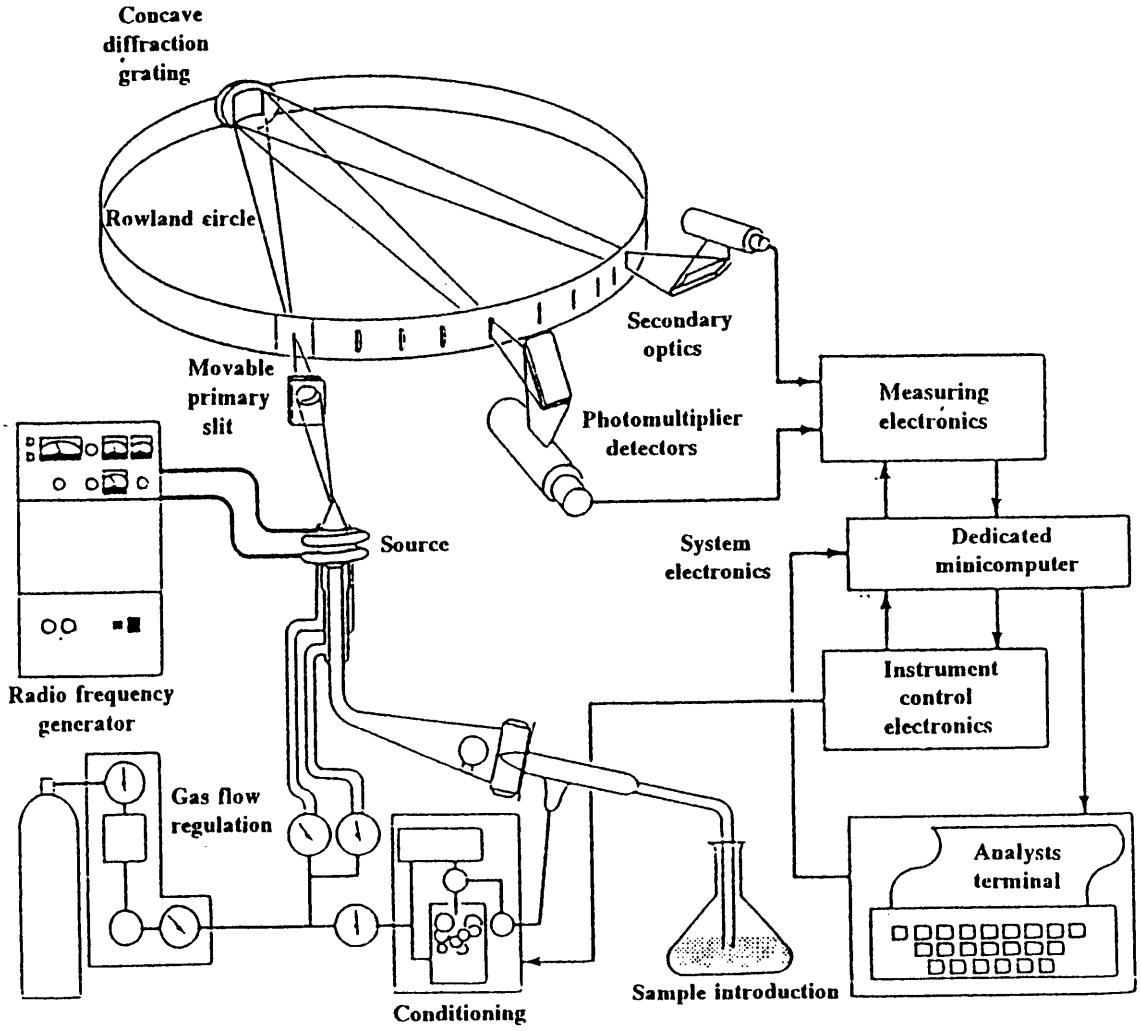

Figure 1.1 Schematic diagram of a non-scanning (simultaneous) ICP-OES using a holographic concave grating in the Rowland circle configuration (Willard *et al*: 1988).

1.2.1 The Plasma

A plasma consists of ionized gas a mixture of fast moving anions and cations and is schematically shown in Fig. 1.2. The plasma itself is electrically neutral, but does

conduct electricity. It is initiated by seeding a few electrons from a Tesla discharge coil. These seeded electrons interact with the magnetic field of the coil and gain sufficient energy to ionize argon atoms by collisional excitation. Electrons and cations, generated by the seeding, are accelerated by the magnetic field in a circular flow perpendicular to the argon emerging from the torch (Fig. 1.3a and b). The direction of the current in the induction coil is reversed and this reverses the direction of the magnetic field applied to the mixture of electrons, ions and atoms. Eddy currents are induced in the gas by the rapidly changing magnetic field, and resistance to these currents results in intense Joule heating. The process becomes self sustaining once ionization temperatures have been reached. The sample is blown into the plasma through the nozzle of the torch, "punching" a hole in the plasma as it enters a region of high temperature. This causes some cooling in the central channel formed by the entry of the sample.

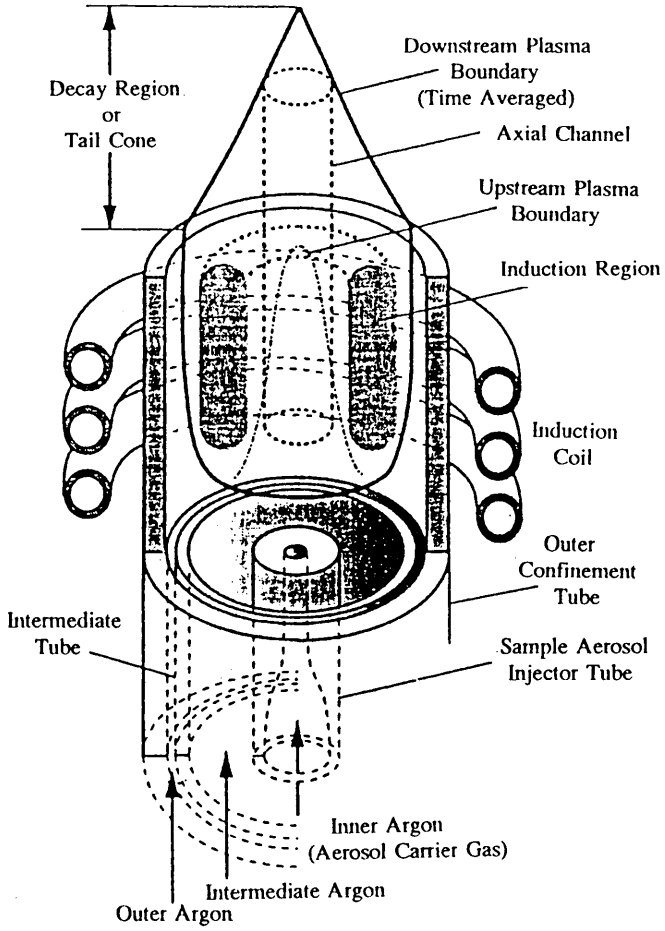

Figure 1.2 Schematic representation of an ICP (Weir and Blades: 1994).

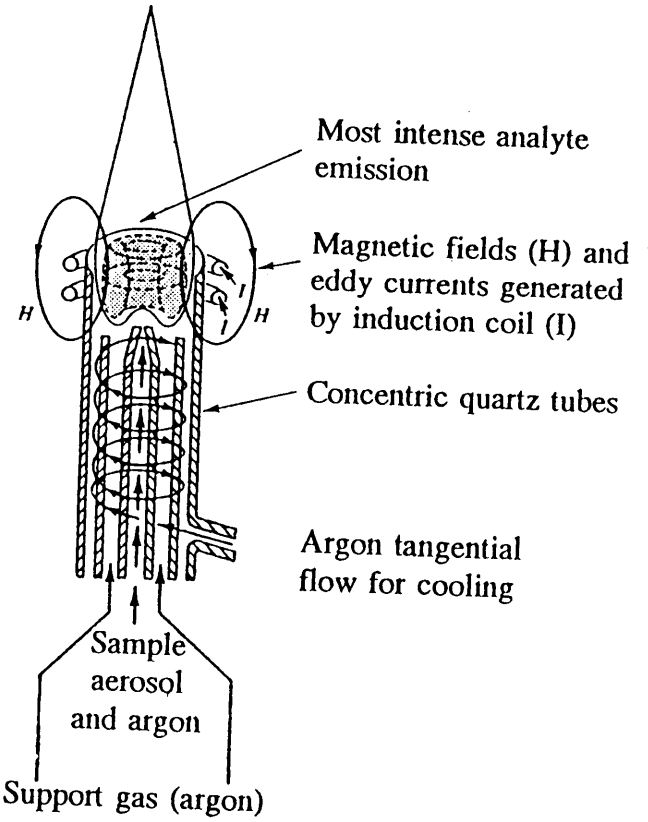

Figure 1.3a Configuration of an ICP-OES torch and gas flows (Willard *et al*: 1988 p266).

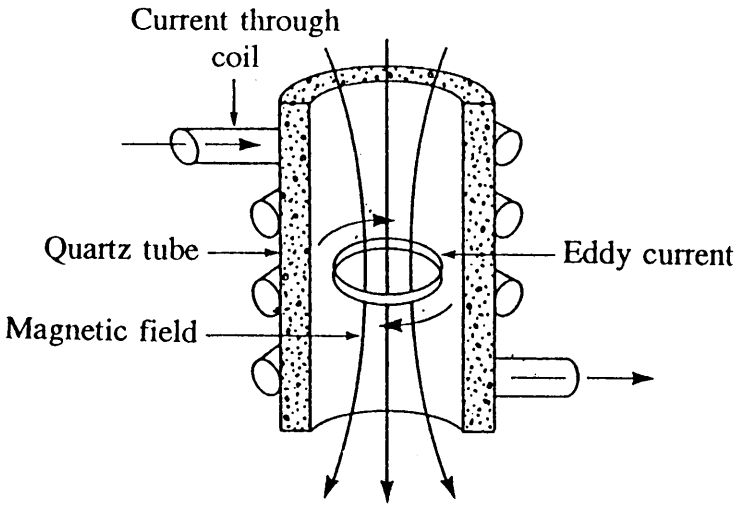

Figure 1.3b Schematic representation of the operation of an ICP source (Willard *et al*: 1988 p266).

1.2.2 Power Generator

The generators used to supply the radio frequency, rf, are oscillators generating alternating current at the required frequency. The circuit supplying the current, a "tank circuit", is a capacitor in parallel with an inductor. As the capacitor is discharged through the inductor, the magnetic field collapses causes build up of charge in the capacitor. Without losses due to resistance the oscillatory process would continue indefinitely, but this does not occur. Instead the tank circuit is connected to the grid of a vacuum tube which amplifies the voltage. A portion of the amplified voltage is then feed back into the tank circuit to overcome the resistance losses.

Two types of oscillators are used, namely "crystal controlled" or "free running". Crystal controlled oscillators have a piezoelectric crystal to control the feedback to the tank circuit in order to maintain the established frequency. The alternative free running oscillator is such that the basic frequency is fixed by values in the tank circuit which can be modified by changes in the plasma impedance and load coil. The majority of instruments available use a frequency of 27.12 MHz and have a nominal power output of 2 kW.

1.2.3 Sample Introduction

In most ICP-OES instruments sample is fed into a spray chamber by a peristaltic pump. The pump rate may be fixed or can be changed to supply a required flow rate. Also the dimensions (and type) of tubing may be adjusted depending on the circumstances. The sample enters the spray chamber though a nebulizer.

There are two types of pneumatic nebulizers used in ICP-OES. In cross-flow nebulizers the capillary transporting the sample is at right angles to the gas stream as may be seen in Fig. 1.4a. With concentric nebulizers the sample capillary is surrounded by a high velocity argon stream parallel to the capillary (Fig. 1.4b). A commercial glass version of the concentric nebulizer is the Meinhard type having a small Venturi at the one end. A Babington nebulizer is a modified cross flow nebulizer less prone to blocking as the sample emerges through a larger orifice. For this reason they have been used extensively (sometimes with adaptions) for the

analysis of slurries or sample containing a large amount of undissolved solids. There are more sophisticated and complex nebulizers available such as MAK and ultrasonic nebulizers. In the latter type a transducer vibrating at frequencies higher than 20 kHz is used to break the liquid mass into smaller particles. It is often accompanied by the dissolution of the sample. This investigation was, however, limited to the more standard types and consequently no detailed discussion of these nebulizers will be given.

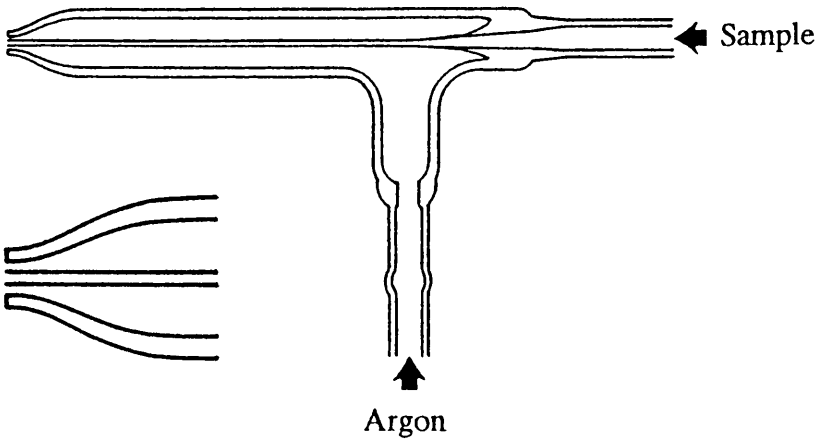

Figure 1.4a Concentric nebulizer (Boss and Fredeen: 1989).

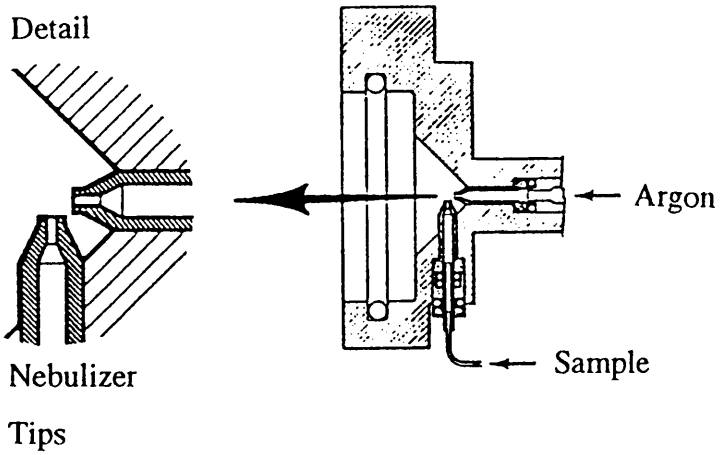

Figure 1.4b Cross-flow nebulizer (Boss and Fredeen: 1989).

Only droplets with diameters less than 10 μm should enter the plasma, and the spray chamber is a means to remove unwanted larger drops. The Scott spray chamber consists of two barrel type chambers, one inside the other as may be seen in Fig. 1.5.

The nebulizer is placed at the entrance of one chamber (the inner chamber) and the spray must proceed into the outer chamber before moving into the torch. The drain is at the opposite end of the spray chamber to the entrance of the droplet cloud to the plasma.

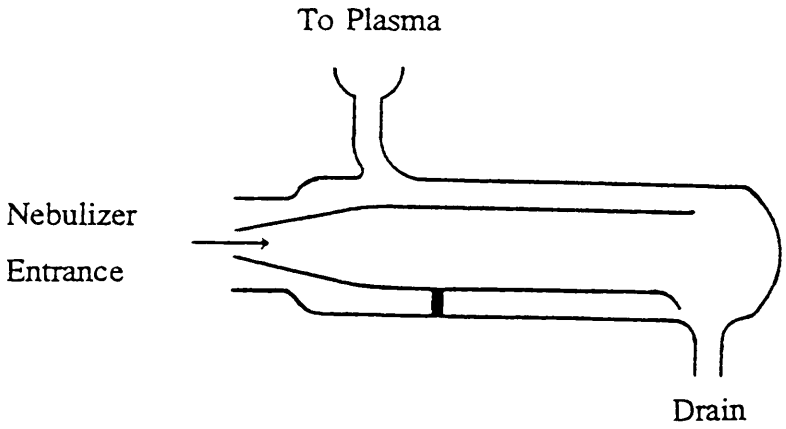

Figure 1.5 The Scott spray chamber (Scott *et al*: 1974)

1.2.4 Torches

A torch consists of three concentric quartz tubes. The innermost tube is used to transport the aerosol carrier gas, and argon passes through at a rate between 0.4 and 1 l min^{-1}. The major portion of argon is transported through the other tubes and is used to sustain the plasma and to cool the quartz, the coolant flow being tangential to the aerosol carrier gas and support gas.

Torches are divided into either Greenfield or Fassel types. Variations of each type are available. The size of Greenfield torches is such that a frequency of about 100 MHz is required to maintain the plasma. Fassel torches are much smaller and therefore less power is needed to maintain the reduced frequency required by the plasma. The three tubes of the Fassel torch are shown in Fig. 1.6.

The aerosol enters from the spray chamber into the injector tube which is normally narrowed at the exit to increase flow rate. Around the inner tube is the second tube through which flows the inner gas or the coolant gas. The outer tube finally transports the support gas.

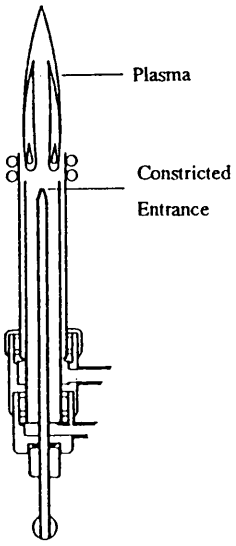

Figure 1.6 The Fassel torch (Dickerson and Fassel: 1969)

1.2.5 Spectrometers

Concave and plane diffraction gratings are used as dispersive elements. A concave grating may act as its own focusing devise whereas with a plane grating, mirrors or lenses may be required. Dispersion within the monochromator is usually affected by the grating being in a Czerny-Turner or Ebert mounting, whereas the Paschen-Runge mount is used for direct reading spectrometers. In the Paschen-Runge mount the grating and entrance slits are in fixed positions while the exit slits are mounted on a portion of the Rowland circle. The essential difference between the Czerny-Turner and Ebert mountings is that two smaller mirrors are used to focus the light in the Czerny-Turner configuration, while only one large spherical mirror is used in the Ebert mount as is demonstrated in Fig. 1.7.

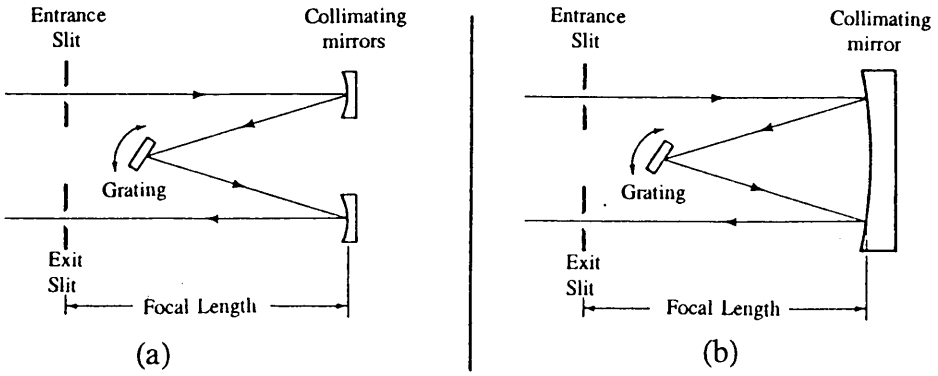

Figure 1.7 Czerny-Turner (a) and Ebert (b) monochromator mounts (Boss and Fredeen: 1989).

1.2.6 Radiation Processes

Radiation emitted from an excitation source will include all the contributions from the different processes occurring in the region of emission. These include the contributions from the gaseous atmosphere, free atoms, ions and molecules of the sample, and any species which may have been formed between the constituents of the gaseous atmosphere itself, or between the atmosphere and sample components. The emission spectrum of the source will then consist of the line and band spectra superimposed upon the continuum. The source of the continuum could be the result of various types of interactions between free electrons and ions including recombination, recombination of atoms, and thermal emission from incandescent solid particles.

1.3 Introduction to the Problem

Ethanol and methanol are most convenient solvents in chemistry. Because of their polarity they may be used as solvents for organic matrices and at the same time they easily form aqueous mixtures. They are relatively cheap and easy to use without giving rise to dangerous wastes which have to be disposed of at great expense. Unfortunately they cannot be used in any analysis in which the final stage is to measured by means of an ICP-OES since most plasmas are unable to be sustained if concentrations of alcohols above 25 % are introduced. This restriction on the use of the alcohols as solvents in ICP-OES analyses has resulted in them being avoided in favour of other organic solvents often at much greater expense. Additions of ethanol or methanol to the analyte at concentrations above the 25 % resulted in the plasma being extinguished and, in most cases experience showed that the torch and spray chamber had to be dismounted and cleaned before the plasma could be restored.

Boorn and Browner (1987) describes the reasons for the plasma being extinguished as follows:

"The influence of alcohols on the plasma is difficult to explain, but the instability results from a gradual quenching of the luminous plasma core from beneath the load coil, which finally reaches the core region at which point the plasma extinguishes". Unfortunately this description was insufficient to explain the problem, as it was a dissertation as to how the plasma died rather than how and why it was extinguished.

After consideration of the problem the following explanation seemed likely. The addition of ethanol to a solution will clearly alter the surface tension and the aerosol size distribution would be influenced. This lowering of surface tension could possibly result in more smaller droplets entering the plasma. The mass of material being nebulized would reach a stage at which the temperature and electron density could no longer manage to cope with the increased aerosol and the plasma would be extinguished. The smaller droplets would result in an increase in sensitivity just prior to the plasma being quenched.

Additional power requirements to dissociate organic matrices have been reported by Boumans and Lux-Steiner (1982). This additional power referred to organic solvents usually used in the analysis of oil and it was not expected that ethanol would present the same problem as these solvents.

If too much material reaches the plasma then it should be possible to construct a spray chamber with a variable exit to overcome the problem. The amount of aerosol reaching the plasma could be kept constant. Sensitivity should still be greater with ethanol present than with pure water because the reduced flow reaching the plasma would consist of smaller droplets and the mass flow rate should still be maintained.

The solution would be the development of a new spray chamber but before the investigation led to the construction of expensive glass adaptions for the existing spray chamber it was decided to consider the influence that additions of ethanol would have to the system. To understand these influences more fully the various aspects of such an addition should be considered.

1.4 **Aspects to be considered**

1.4.1 Generators

In South Africa almost all ICP-OES's sold are equipped with crystal controlled oscillators. Benli (1983) reported that using free running rf generator ethanol concentrations up to 100 % had been investigated. The problem would appear initially

that while crystal controlled generators are unable to cope with additions of ethanol to the sample, free running generators can accommodate high concentrations of ethanol.

1.4.2 Temperature and electron density

The two properties of temperature and electron density are of fundamental importance to any emission process and particularly one generated by a plasma. If the addition of ethanol results in an increase in mass flow rate (as speculated above) then this should lead to a cooling of the plasma and the temperature and electron density would finally reach some values below which the plasma could no longer be maintained. Changes in the temperature would result in the electron density within the plasma being altered.

1.4.3 Solvent introduction

The addition of ethanol (or any solvent) will clearly change the physical characteristics of the solution. These characteristics include those of density, surface tension, viscosity, vapour pressure, etc. Changes in the physical characteristics will influence the sample introduction. The peristaltic pump ensures that the rate at which the sample enters the spray chamber is kept constant, irrespective of changes to the physical characteristics of the solution. It is once the sample has entered the spray chamber that these changes will become of great importance. As mentioned in the speculations above it could be expected that the decrease in surface tension would result in smaller drops being formed by the nebulizer. This in turn should lead to an increase in the mass flow rate of sample reaching the torch.

1.4.3 Analytical parameters

According to Benli (1983) addition of ethanol to the analyte leads to signal enhancement and consequently to an increase in the sensitivity of the analysis. Any increase in sensitivity is to be considered important since the continual demands for improved trace element analysis makes such increases of major significance. The degree to which sensitivity was increased and under which conditions that increase was obtained thus required further investigation.

1.4.4 Processes within the Plasma

Aerosol is transported into the region of high temperature by means of a stream of argon. This flow is stabilized by the vortex flow of argon used to cool the torch. A phenomenon called the skin effect causes the toroidal shape of the plasma. This lengthens the time in which the analyte spends in the plasma. Aerosol enters the region near the coils at ambient temperature. Within the space of a few millimetres and in milliseconds, the temperature reaches thousands of Kelvin. During that time the sample is vaporized, desolvated, dissociated, atomized, ionized and excited. It is the first few steps which are the most time-consuming (milliseconds), while the atomization, ionization and excitation only take nanoseconds. Only those chemical processes are considered due to the time constraints that would be imposed on any other type of reaction.

1.4.5 Classification of Emission Lines

There are several methods used to classify emission lines. Spectral lines originating from neutral atoms are designated with a "I" immediately after the symbol of the element. Emission signals from singly charged ions are denoted by a "II" after the symbol, and a "III" indicates a doubly charged ion, and so on.

Intensity of the spectral line is thought of as a function of temperature, then the intensity will pass through a optimum at a certain temperature, referred to as the "norm temperature". The value of the spectral line on a "norm temperature" scale is used to divide the lines into "soft" and "hard". Assuming the "norm temperature" to be 9000 K, then atomic lines of elements with low to medium ionization potential (<8 eV) and ionic lines with low second ionization potential are designated as "soft", since they will have "norm temperature" less than 9 000 K. All the other atomic and ionic lines are called "hard". Generally, the alkali and alkali earth metals all fall into the category of elements having "soft" lines, while examples of elements having "hard" spectral lines include Cd II (226.5 nm), Mn II (257.6 nm), Zn I (213.9 nm) and Cd I (228.8 nm).

1.5 Visual Changes

Additions of ethanol visibly change the shape and colour of the plasma. These changes may seen in plates 1.1 to 1.5, taken when using the Liberty ICP-OES of Varian. The frequency used was 40 MHz and 1.5 kW power, while a nebulizer pressure of 150 kPa was applied. The pump speed was 15 rpm.

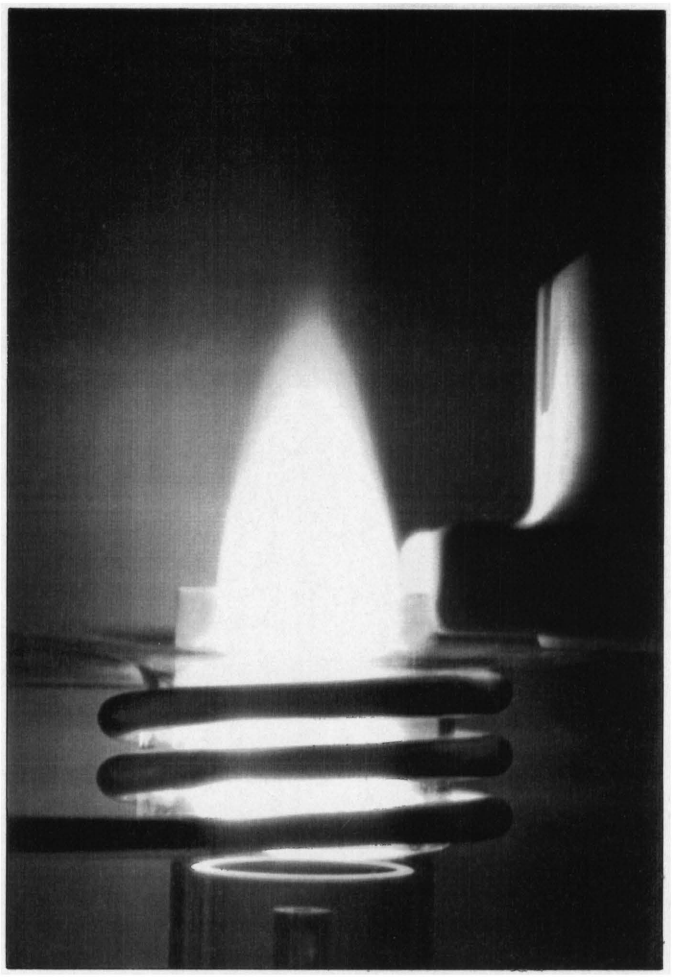

Plate 1.1 Plasma when water was aspirated.

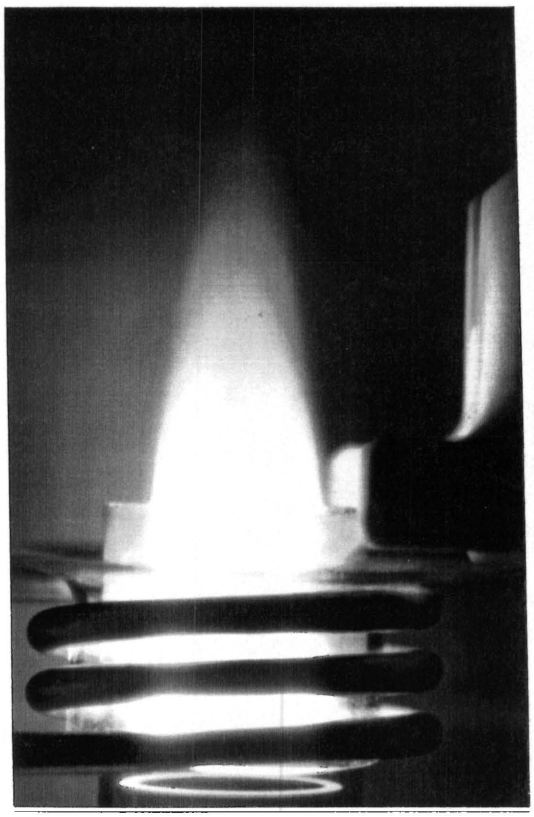

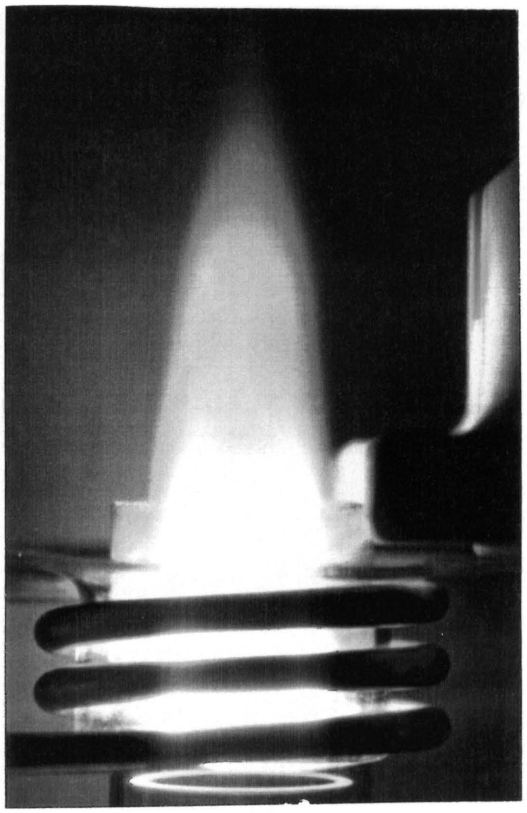

Plate 1.2 and 1.3 Plasma when 25 and 50 % ethanol was aspirated, respectively.

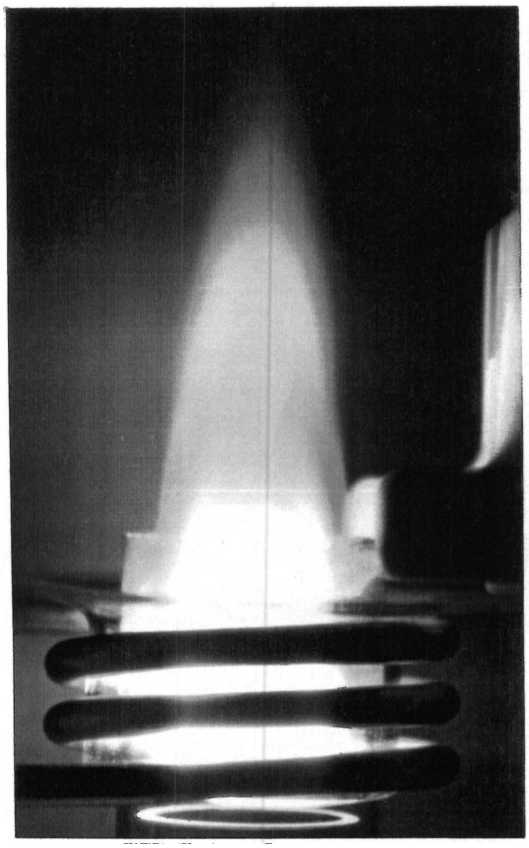

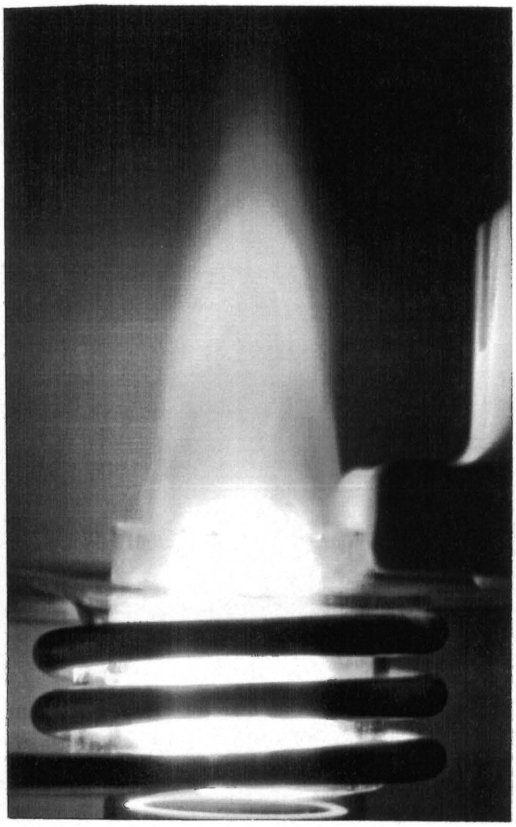

Plate 1.4 and 1.5 Plasma when 75 and 95 % ethanol was aspirated, respectively.

CHAPTER 2

TEMPERATURE AND ELECTRON DENSITY

2.1 Introduction

Temperature is a major consideration when an emission process is taking place since the greater the number of excited atoms or ions, the larger the emission signal will be. In its simplest form the Boltzmann distribution equation which relates the population of excited species to temperature may be given as follows:

$$n_p/n_o = g_p/g_o \exp(E_p/kT) \qquad 2.1$$

where n_p and n_o are the number of atoms in an excited state and the ground state respectively, k is the Boltzmann constant (1.38×10^{-23} J/K), T is the temperature in Kelvin, and E_p is the energy difference in joules between the excited state and the ground state. The quantities g_p and g_o are statistical factors (statistical weights) that are determined by the number of states having equal energy at each quantum level.

Clearly, in terms of the above equation, an increase in the temperature will result in an increase in the number of atoms in the excited state and once these atoms return to their ground state the emission intensity or signal intensity will be increased.

Electron density plays an important role in the maintenance of a plasma. By definition, a plasma is an ionized gas and many of the reactions occurring within it are as a result of the plasma itself. Changes of electron density will thus influence these reactions.

Associated with the whole topic of temperature and electron density is the problem of thermodynamic equilibrium and since this is usually unobtainable, local

thermodynamic equilibrium (LTE) and any factors which would result in line broadening must be considered considered before an ICP-OES may be characterized.

2.2 Thermodynamic Equilibrium

When a system is in contact with a heat bath at uniform temperature and is subjected to no changes, then a steady thermodynamic state will eventually be reached. In the case of a gaseous vapour, all the particles in that cloud may possess various forms of energy. The distribution of this energy over the various degrees of freedom and the distribution of any dissociated or ionized particles, as well as the spread of spectral energy, are subject to one universal parameter, temperature, T, in some form for the system (Alkemade *et al*: 1982).

According to Boumans (1966), a plasma in complete thermodynamic equilibrium can be characterized by the conditions discussed further below:

2.2.1 The distribution function for the velocity or translational energy of all the free particles is given by the Maxwell-Boltzmann equation,

$$dn(E_t)/n_a = 2\pi(E_t)^{1/2}[\exp(-E_t/kT)]/([\pi/kT]^{3/2})dE_t \qquad 2.2$$

where E_t is translational energy, n_a is the total concentration of atom a and $n(E_t)$ is the population density.

2.2.2 For each separate type of particle, the relative electron population of the various discrete levels of internal energy is determined by particle collision processes and follows the Boltzmann distribution law, equation 2.1, which for the total concentration of neutral atoms, becomes,

$$n(E_p)/n_a = (g_p/Z_a)\exp(-E_p/kT) \qquad 2.3$$

where E_p is the energy of the p^{th} level with respect to that of the ground level (E_o=0) and g_p the statistical weight of that level. Z_a is the partition function of atom a.

When E_p is expressed in eV and T in K, then

$$\exp(-E_p/kT) = 10^{-5040Ep/T} \qquad 2.4$$

2.2.2.1 The ionization of atoms, molecules and radicals is described by the Saha-Eggert equation which is the law of mass action,

$$S_n = (n_e n_i/n_a) \qquad 2.5$$

n_e is the electron number density and n_i is the concentration of ions.
Because of the spin of an electron it has a statistical weight of 2 and its mass m_e compared to the mass of the atom, molecule or radical is very small, the equation becomes

$$S_n = (2Z_i/Z_a)(2\pi m_e kT/h^2)^{3/2}\exp(-E_i/kT) \qquad 2.6$$
$$= (n_i n_e/n_a)$$

where E_i is the (positive) ionization energy and Z_i the ionic partition function. Expressing E_i in eV, T in K and S_n in cm^{-3} the equation becomes

$$S_n = 4.83 \times 10^{15} T^{3/2}(Z_i/Z_a)10^{-5040Ei/T} \qquad 2.7$$

2.2.2.2 The general equation for equilibria can be used to describe the dissociation of molecules and radicals,

$$K_n = (n_x n_y/n_{xy}) \qquad 2.8$$
$$= (2\, m_x m_y kT/m_{xy}h^2)^{3/2}(Z_x Z_y/Z_{xy})\exp(-E_d/kT) \qquad 2.9$$

where E_d is the energy of dissociation, m is the mass and Z the partition function of the various species.

2.2.2.3 The spectral volume density of radiant energy (black body radiation) is given

by the Planck law, which in a vacuum reads,

$$\rho(\lambda,T) = (8\pi h\upsilon^3/c^3)/(\exp[h\upsilon/kT] - 1) \qquad 2.10$$

or, in terms of the Planck function, i.e. the spectral radiance,

$$B(\lambda,T) = (2h\upsilon^3/c^2)/(\exp[h\upsilon/kT] - 1) \qquad 2.11$$

Radiance is defined as the radiant flux per unit solid angle and per unit area perpendicular to the direction of radiation. Alternatively,

$$B(\lambda,T) = 2hc^2\,\lambda^{-5}/(\exp[hc/\,kT] - 1) \qquad 2.12$$

2.2.2.4 The radiance of an arbitrary thermal radiator is expressed by Kirchoff's law (Lochte-Holtgreven: 1968),

$$\xi(\lambda) = K(\lambda)B(\lambda,T) \qquad 2.13$$

where $\xi(\lambda)$ is the radiant power and $K(\lambda)$ the absorption coefficient.

A necessary and sufficient condition for complete thermodynamic equilibrium is when the total number of ions leaving a certain state in a fixed time is equal to the number arriving in that state in the same length of time. True thermodynamic equilibrium (including radiation), cannot be attained if the observation of radiation implies that some radiation has been lost by the plasma. Discharges as used in spectroscopy can therefore never be in thermodynamic equilibrium.

The plasma is not truly an adiabatic system. Heat is radiated to the environment, and heat losses occur due to conduction and convection. Concentration gradients of all the constituent substances will be present. The transportation of heat, radiation and mass will occur throughout the plasma. Under these conditions thermodynamic equilibrium cannot be maintained and a single temperature which would characterize

the plasma will not exist. If, however, the rate of transportation of these processes is slow with respect to the rate at which energy is partitioned over the various degrees of freedom, then the plasma can be regarded as reaching a state of "incomplete equilibrium" or "local thermodynamic equilibrium" (LTE). In this state the distribution functions will still be given by Boltzmann's Law, but black body radiation will be partially or entirely missing. Since the system can no longer be characterized by one temperature, different "temperatures" can be defined which will become numerically equal should the state of thermodynamic equilibrium be obtained. The various temperatures and the techniques used to obtain are discussed below.

2.3 Excitation Temperature, T_{exc}

The temperature which will govern the population of an excited level will be determined by the Boltzmann distribution [equation 2.1]. Should the radiation source be optically thin, then the observed intensity, I_{pq} (ergs/sr cm^2 s) of a transition from a higher level p to a lower level q is given by (Hasegawa and Haraguchi: 1987),

$$I_{pq} = [(l/4\pi)n(E_p)A_{pq}hc]/\lambda_{pq} \qquad 2.14$$

$$= (l/4\pi)n_a(g_p/Z_a)A_{pq}(hc/\lambda_{pq})\exp(-E_p/kT) \qquad 2.15$$

where l is the path length of the source and A_{pq} is the transition probability for the spontaneous emission; c, h, and g_p having their standard meanings. If n_a and the absolute transition probability are known, then T_{exc} can be determined from the intensity of an emission line using 2.15. In the case of an argon ICP, n_a can be estimated from the ideal gas law and hence this method is applicable to Ar. The logarithmic form of 2.15 is

$$\ln(I_{pq}\lambda_{pq}/g_pA_{pq}) = -E_p/kT + \ln(n_alhc/4\pi Z_a) \qquad 2.16$$

and hence using the relative intensities of two lines, T_{exc} can be determined from the slope of the straight line (-1/kT) fitted to a plot of the left hand side of 2.16 against E_p, where only the relative transition probability is now required.

When the "two-line" method is used, n_a cancels out and need not be known:

$$I_{pq}/I_{kl} = (g_pA_{pq}\lambda_{kl}\exp[\{-E_p+E_k\}/kT])/(g_kA_{kl}\lambda_{pq}) \quad 2.17$$

In the above methods the determination of T_{exc} is dependent on the accuracy of the transition probability data and errors using this method often arise from the inadequacies of A.

An absorption method is also available for the determination of T_{exc}. The absorbance of radiation emitted from a narrow-line source is given by (Kirkbright and Sargent: 1974):

$$A = [(\lambda^4 g_p/4\pi^2 c g_q)n(E_p)lA_{pq}V(a,0)(\pi \ln 2)^{1/2}/\Delta\lambda_D \quad 2.18$$

where V is the Voigt function, and a is the a parameter of an absorption line and $\Delta\lambda_D$ its Doppler width. The ratio of emission intensity to absorbance gives T_{exc} (Kornblum and de Galan: 1977)

$$I/A = [\Delta\lambda_D(\pi/\ln 2)^{1/2}hc^2]/[\lambda^5 V(a,0)\exp(-E_p/kT)] \quad 2.19$$

2.4 Rotational Temperature, T_{rot}

The emission intensities of rotational lines emitted from a diatomic molecule are related by (Alder and Mermet: 1973)

$$\ln[\{I\lambda^4(K+1)\}/\{(K+1)^2 - 1\}] = D - [BhcK(K+1)]/kT \quad 2.20$$

where I is the intensity of the line, K is the rotational quantum number, D is a constant and B is the rotational constant for the upper vibrational level. The rotational temperature can be determined from a plot using equation 2.20 in which case two parallel straight lines are obtained. The rotational temperature is regarded as being the same as the kinetic temperature of the gas due to the rapid exchange between rotational and kinetic energy of the molecule (Kornblum and de Galan: 1977).

2.5 Ionization Temperature, T_{ion}

The concentration of neutral atoms and ions which are collisionally equilibrated is given by the Saha equation 2.5. Combining equations 2.5 and 2.15

$$n_e(I_{kl}{}^{+}A_{pq}\lambda_{kl}{}^{+})/I_{pq}A_{kl}{}^{+}\lambda_{pq}=(2g_k/g_p)(2\ m_ekT/h)^{3/2}\exp(-[E_i+E_k-E_p]/kT) \qquad 2.21$$

where the + superscript denotes the positive ion. The implication of equation 2.21 is that the ionization temperature is calculated from the ratio of spectral line intensities of the atom and ion and from the electron number density.

2.6 Electron Temperature, T_e

The transition of an electron from the free to bound state is accompanied by the emission of continuum radiation and is called radiative recombination. The intensity of this continuum is dependent on the density and kinetic temperature of the electrons. If the plasma is electrically neutral, then the emission intensity within a narrow wavelength is:

$$I_{cont} = (1/4\pi)g(\lambda,T_e)n_e n_{Ar}{}^{+} \qquad 2.22$$

$$= (1/4\pi)g(\lambda,T_e)n_e{}^{2} \qquad 2.23$$

where $g(\lambda,T_e)$ is a function of λ and T_e (Hasegawa and Haraguchi: 1985b), and $n_{Ar}{}^{+}$ is the number density of argon ions. If the absolute emission intensity and the electron number density are known then the electron temperature can be calculated from equation 2.23.

An estimation of T_e can be obtained by plotting $\ln(I_{cont})$ against λ without knowing n_e (Kleinmann and Cajko: 1970),

$$d\ \ln(I_{cont})/d\lambda = \delta \ln[g(\lambda,T_e)]/\delta\lambda \qquad 2.24$$

Another expression for T_e can be obtained by combining 2.23, 2.5 and 2.16 (Bastiaans and Mangold: 1985). This may be seen in equation 2.25

$$I_{cont}/I_{line} = \{[g(\lambda,T)\lambda\Delta\lambda/A_{pq}hc](2\pi m_e kT)^{3/2}\exp(-[E_i-E_p]kT)\}/h^3(2g_i/g_p) \qquad 2.25$$

where g_i is the statistical weight of the ground state of the argon ion. The electron temperature can thus be obtained from the ratio of the emission intensity of an argon atomic line and the adjacent continuum.

2.7 Doppler Temperature, T_D

The temperature which governs the velocity distribution, is the electron temperature, in the case of an electron, and the Doppler temperature, for heavy particles. Doppler broadening caused by the relative motions of atoms in a plasma results in a line width $\Delta\lambda_D$, which is related to T_D by

$$\Delta\lambda_D = 2(2R\ln 2)^{1/2}(\lambda_0/c)(T_D/M)^{1/2} \qquad 2.26$$

where R is the gas constant, λ_0 the wavelength at the centre of the line and M is the atomic mass.

2.8 Line Broadening in an ICP

The shape and width of the spectral line carries information pertaining to the physical conditions at the source of the line and therefore serves as a non-interacting probe (Lochte-Holtgreven: 1968). The line profiles are of finite width as a result of several sources of line broadening. These are natural, Doppler, Lorentz, Holtzmark and Stark broadening. These will be discussed in more detail below.

2.8.1 Natural Broadening

The Heisenberg uncertainty principle implies that the energy of an atomic level cannot strictly be determined, i.e.

$$\tau.\Delta E \sim h/2\pi \qquad 2.27$$

For a resonance line,

$$\Delta \upsilon_N = \Delta E/h = 1/2\pi\tau \qquad 2.28$$

where τ is the mean lifetime of the level. The spectral line corresponding to any resonance transition will thus have a wavelength spread, $\Delta\lambda_N$. The broadening profile is found to be a Lorentzian function (Griem: 1974):

$$P(\lambda) = \text{const}/[1 + \{2(\lambda - \lambda_o)/\Delta\lambda_N\}^2] \qquad 2.29$$

where λ is the wavelength and λ_o the wavelength at the intensity maximum. The halfwidth, $\Delta\lambda_N$, is independent of wavelength and of the order of 0.01 pm (Alkemade *et al*: 1982). This figure is negligibly small when compared to the halfwidths due to other line broadening mechanisms in spectroscopic light sources.

2.8.2 Doppler Broadening

The movement of a radiating particle towards or away from an observer leads to a wavelength shift of the emitted line, called the Doppler shift. The random motion of the radiating particles in a plasma results in Doppler broadening of the lines. The species in the plasma are hot and so follow the Maxwell-Boltzmann velocity distribution because atoms having different velocities emit radiations which result in a wavelength spread. The line profile follows a Gaussian distribution:

$$I(\lambda) = \text{const} \times \exp\{-\ln 2[2(\lambda - \lambda_o)/\Delta\lambda_D]^2\} \qquad 2.30$$

where $\Delta\lambda_D$ is given by equation 2.26.

2.8.3 Lorentz Broadening

Collisions between species result in line broadening, called Lorentz or pressure broadening. This is interpreted as perturbation of atomic structure in the quantum theory (Foley: 1946). According to the impact theory, the perturbations shift each energy level E_i by an amount ΔE_i. This amount depends on the distance between the atoms, x. The frequency of emission from level 2 to level 1 will then be given by:

$$\upsilon(x) = [E_2(x) - E_1(x)]/h \qquad 2.31$$

Rapid changes in x result in the spread of the frequency. In an argon ICP, the main perturber is the argon ground-state atom because of its high number density.

2.8.4 Holtzmark Broadening

When an excited atom, usually in a resonance state, X^*, collides with an identical atom in the ground state, X, Holtzmark or resonance broadening occurs:

$$X^* + X \rightarrow X + X^* \qquad 2.32$$

At high concentrations of emitting and ground-state atoms this type of broadening becomes important (Hasegawa and Haraguchi: 1987).

2.8.5 Stark Broadening

When subjected to a strong electric field, the degenerate levels split into several components. The charged particles in a plasma cause the Stark effect, resulting in broadening of the spectral lines (Griem: 1974). The line shape once again approximates the Lorentzian form.

2.8.6 Effects of Line Broadening

A spectral line emitted by a plasma will be subject to all the broadening processes discussed and so the profile will not be that of a simple Gaussian or Lorentzian function, but rather a combination of both components. This is called the Voigt function and defined by:

$$V(a,\omega) = (a/\pi) \int_{-\infty}^{\infty} \exp(-t^2)/[a^2 + (\omega - t)^2]\, dt \qquad 2.33$$

if, $$a = (\ln 2)^{1/2} \Delta\lambda_C / \Delta\lambda_D \qquad 2.34$$

$$t = 2(\ln 2)^{1/2}\ \delta/\Delta\lambda_D \qquad 2.35$$

and

$$\omega = 2(\lambda - \lambda_o)(\ln 2)^{1/2}/\Delta\lambda_D \qquad 2.36$$

where, δ is a dummy integration variable, λ_o the wavelength at the maximum of the profile, λ_C and λ_D the collisional and Doppler halfwidths, respectively. The a-parameter (a value) indicates the contributions of the Gaussian and Lorentzian components.

The spectral line of an element that has several isotopes or a non-zero nuclear spin will show splitting, or fine structure, known as hyperfine structure (hfs) (Herzberg: 1944). The resulting line profile will be given by the sum of all the hyperfine components.

Self-absorption is the selective absorption by identical atoms of the emission line from an optically thick light source (Human and Scott: 1976). Because this effect occurs at the intensity maximum it causes apparent broadening of the line profile. This will be more likely to occur if the light source has fringes that are cooler than the inner core. The high number density of absorbing atoms in the fringes may result in severe intensity depression at the line centre. This phenomenon is called self reversal.

2.9 Electron Number Density

The argon ICP is a partially ionized plasma consisting mainly of argon atoms, argon ions and electrons. Among the most important properties which can be used to characterize the plasma are "temperature" and electron number density, n_e, the number of free electrons per unit volume (Blades: 1982). The problems relating to temperature have already been discussed. The definition of n_e makes it a simple concept, unfortunately, the experimental determination of n_e is not as simple for various reasons. The methodology used for calculating the electron density will be discussed in more detail below.

2.9.1 Stark Width Method

The broadening of the spectral lines as a result of the Stark effect has already been discussed. Although the primary cause of line broadening for analytes introduced into an ICP is due to the Doppler effect (Human and Scott: 1976, Hasegawa and Haraguchi: 1985a), atomic hydrogen is subject to a large linear Stark effect. For hydrogen lines, therefore, Stark broadening is dominant. The hydrogen profile can hence be used for the determination of n_e in the plasma.

According to the quasi-static theory of Kepple and Griem (1968) the halfwidth of the hydrogen line, $\Delta\lambda_H$, is proportional to $n_e^{2/3}$. n_e can be determined from the following relationship:

$$n_e = C_H(n_e,T)\ \Delta\lambda_H^{3/2} \qquad 2.37$$

where C_H is a constant depending only slightly on n_e and the temperature.

The formula expanded to four terms is as follows:

$$n_e = [C_0 + C_1(\ln\Delta\lambda) + C_2(\ln\Delta\lambda)^2 + C_3(\ln\Delta\lambda)^3]\Delta\lambda^{3/2}10^{13} \qquad 2.38$$

where the coefficients are $C_0 = 36.84$, $C_1 = -1.430$, $C_2 = -0.133$ and $C_3 = 0.0089$. The H_β line (486,1 nm), which is the second line of the Balmer series, is the one that is most commonly used for the measurement of Stark halfwidths. The reason for this is as follows:

(i) reliable data for C_H are available (Griem: 1964, Griem: 1974),
(ii) the H_β line is relatively free from interferences caused by the emission lines of other plasma components (Inglis and Teller: 1979), and
(iii) the profile is sufficiently intense and broadened (Kepple and Griem: 1968).

The precision of n_e calculated using this method is better than 5 % (Walters, Gunter and Zeeman: 1986). Furthermore the method does not require the assumption of

thermal equilibrium for the plasma. For these reasons the use of Stark broadening of the Hβ line is more reliable than other spectroscopic methods.

For elements other than hydrogen the perturbation is quadratic and due to electron impact. The halfwidth, $\Delta\lambda_S$, is proportional to n_e;

$$n_e = C_S(n_e,T)\Delta\lambda_S \qquad 2.39$$

Argon lines which originate from higher energy levels are most commonly used for measurement, since their Stark widths are relatively large compared to that of their Doppler widths. The accuracy of these measurements (between 20 and 30 %) have resulted in them being used less frequently (Griem: 1964).

2.9.2 The Saha Method

The Saha equation, 2.5, can be applied to the determination of n_e. The temperature (normally T_{exc}) is calculated and substituted into equation 2.5, then n_e can be obtained from the intensity ratio of the atomic and ionic lines by

$$n_e = \frac{I_{pq}A^{+}_{kl}\lambda_{pq}\,2g_k}{I^{+}_{kl}A_{pq}\lambda^{+}_{kl}\,g_p} \times (2\,m_e kT/h)^{3/2}\exp\left(-\frac{E_i+E_k-E_p}{kT}\right) \qquad 2.40$$

The use of the Saha equation implies that thermal equilibrium exists between atom and ion.

2.9.3 The Continuum Method

If the electron temperature can be determined by the slope or line-continuum method, then n_e can be calculated from equation 2.22 using the absolute intensity of a continuum.

$$n_e = [\{(4\pi/l)I_{cont}\}/\{\Delta\lambda g(\lambda,T_e)\}]^{1/2} \qquad 2.41$$

For the continuum around 430 nm, $g(\lambda,T_e)$ is given by (Kornblum and de Galan: 1977, Kornblum and de Galan: 1974):

$$g(\lambda,T_e) = 1.1013 \times 10^{-27} T_e^{-1/2} \text{ (erg s}^{-1} \text{ cm}^{-3} \text{ } \mu\text{m)} \qquad 2.42$$

n_e can be obtained from a suitably chosen T_e because of its slight dependence on that parameter ($n_e \propto T_e^{1/4}$).

Problems that are associated with the determination of the electron number density using this technique result mainly from the theoretical error that arises in the calculation of the proportionality constant, or to experimental error in the measurement of the intensity of the continuum.

2.9.4 Series Limit, Line Merging Method

The probability that a spectral line will be split as a result of the Stark effect increases as the principal quantum number, increases. At the same time the energy difference between the adjacent states rapidly decreases and the broadening lines start to merge, reaching a continuum before the series limit. The principal quantum number of the last discernible line in the series is related to n_e by the Inglis-Teller equation (Montaser and Fassel: 1982):

$$\log(n_s) = 23.23 - 7.5\log(n_m) \qquad 2.43$$

where n_m is the principal quantum number of the last discernible line and n_s is the sum of n_e and the number density of the ion, n_i cm^{-3}:

$$n_s = n_e + n_i \qquad 2.44$$

This equation is only valid for hydrogen and hydrogen-like atoms, while equation 2.40 is approximately true for other species. Using the Series limit line merging method, the Abel inversion is hardly applicable. There are, however, other causes of line broadening (Griem: 1974), which will result in the lowering of the apparent series

limit and therefore this method is suitable for the estimation of n_e in the central channel of an ICP-OES (Hasegawa and Haraguchi: 1987).

2.10 Abel Inversion

Any spectroscopic information, either emission or absorption, read from an ICP, is obtained from a side-on projection. The information thus given is the integrated intensity over the entire length of the light source. The Abel inversion is a mathematic means of transforming this side-on data, i.e. the lateral profile, into a radial profile.

If the plasma is cylindrically symmetric and no self-absorption takes place, then the relationship between the local radiation intensity i(r) as a function of radial distance r and the distribution of the radiation I(x) measured by scanning the plasma in the horizontal x direction perpendicular to the optical axis is given by the Abel integral equation (Prost: 1982)

$$I(x) = 2\int_{x}^{R_o} i(r)r(x^2 - r^2)^{-1/2}dr \qquad 2.45$$

where R_o is the radius of the source. The radial intensity is then given as

$$i(r) = -1/\pi\int_{r}^{R_o} \{[dI(x)/dx]/[(x^2 - r^2)^{-1/2}]\}dx \qquad 2.46$$

Physically, these equations represent the convolution between the physical i(r) and I(x) and the space coordinate as can be seen in Figure 2.1.

The following sequence is usually carried out in order to obtain a numeric value for the radial intensity from the lateral intensity that is measured. The observed lateral intensities along the x-axis are usually asymmetric, so the symmetric intensity data must first be calculated by averaging the intensity information from both sides of the central vertical axis (Blades: 1983). Once this has been achieved this information is

fitted into an n^{th} order polynomial expression by the least-squares regression method (Goode and Deavor: 1984). The integration of polynomial expression using equation 2.26 yields the radial profile.

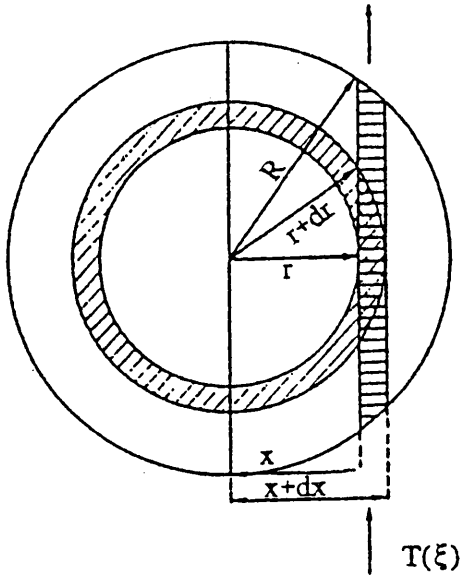

Figure 2.1 Relation between I(x) and i(r) for a symmetrical ICP-OES torch, where T(ξ) is the region observed (Prost: 1982).

2.11 Departure from LTE

In order to investigate the departure of the plasma from LTE, van der Mullen in three tutorial reviews (1989, 1990a and 1990b) studied four types of balances, denoted by Maxwell, Boltzmann, Saha and Planck. These led to comments which related to the relationship between atomic state distribution function (ASDF) and plasma parameters. ICP's will deviate from TE since they are created by external forces in a limited space. Van der Mullen considered three features:

(i) external forces are needed to create, maintain and limit the plasma,
(ii) radiation will escape from the plasma, and
(iii) temperature and density gradients will be present.

By considering these three features he was able to find three causes for the distortion of the Boltzmann and Saha balances and therefore the ASDF.

(i) A difference between translational temperatures of the various particles will be induced because the different particles respond differently to applied forces.

(ii) The escape of photons from the plasma will affect Planck's balances and, in turn, the Boltzmann and Saha balances.

(iii) The transport of particles due to gradients may result in imbalances in the various processes.

Summarizing the affect of different forces to different particles van der Mullen noted that the electron was the most important particle in the maintenance of Boltzmann and Saha balances. Furthermore, if the plasma is non-isothermal and the electron ruled balances of Boltzmann and Saha are sufficiently effective, then the electron temperature as determined by the Saha-Boltzmann equation may be used to describe the ASDF. The transport of radiation which violates Planck's equilibrium will not disturb the Boltzmann balance to any great extent provided the number of electron induced transitions per radiative lifetime is much larger than unity. This places demands on the electron density, which depends on the atomic system and level. The Griem criterion is not, he concluded, sufficient condition for LTE.

When considering the influence of transport, van der Mullen found that the presence of density gradients caused inward or outward movement of charged particles. In the ionizing part of the ICP an overpopulation of the ground state was found, while an underpopulation occurred when recombining took place. The levels between the ground and ion state are interconnected by Boltzmann balances in a stepwise manner and this implied that the Saha deviations from ground state will propagate the system to higher excited states. For LTE to exist two conditions had to satisfied

(i) the absolute concentration must be so large that all collision transitions dominate radiative decay, and

(ii) the gradient length of the electron density must be so large that transport processes will not affect the local Saha equation.

Weir and Blades (1994) when determining electron density from the intensity of a single argon line considered the error of the method owing to departures from local Saha equilibrium, LSE. To understand the error more fully they used the non-equilibrium parameter b to describe the departure of ASDF's from LSE. This parameter is defined as the ratio of the experimental population of the i^{th} energy level b_i(expt) to the Saha, or theoretical LTE value b_i(LSE):

$$b_i = \eta_i(\text{expt})/\eta_i(\text{LSE}) \qquad 2.47$$

where η is the state density per statistical weight.

Each energy level has a unique value for b. When they considered the dependence of b on the energy levels for argon they found that due to losses caused by the transport processes, the thermal balances shift such that ionization is favoured so as to sustain the population of charged particles in the plasma. The result is that lower atom levels are overpopulated with respect of Saha distribution, while the ion levels are underpopulated. i.e. $b_1>b_2>b_3>...>b_n$.

When considering the departure of the plasma from LTE, they found that for the Ar I line at 687.129 nm, b_1 was such that $0.1<b_1<10$. This, in turn yielded a possible error in determination of a maximum of 15 %.

2.12 Literature Values for the Temperature and Electron Number Density

Following the introduction, in 1963, of the inductively coupled plasma as an excitation source for emission spectroscopy (Greenfield, Jones and Berry: 1964, Weldt and Fassel: 1965) it became important to determine the optimal analytical conditions of the plasma. The temperature and its distribution within the plasma torch remains one of the most important parameters since the emission lines are so dependent on that value. The results initially reported (Goldfarb and Dresvin: 1965, Johnston: 1966, and Hughes and Wooding: 1967) characterized the temperature environment in the support gas. They generally were not made on plasmas that were used for analytical purposes (Kalnicky, Kniseley and Fassel: 1975). Some of the earliest work using a

plasma designed for analytical work was reported by Kornblum and de Galan in 1974. The temperature distributions reported in that work exhibited large scatter and peculiarly steep off-axis peak behaviour. The authors cautioned that "only the overall shapes of the distributions and the order of magnitude of the quantities" were of real significance.

Kornblum and de Galan (1974) only measured the excitation temperature and they used iron in the investigation for the following reasons:

(i) It is known that the complex spectrum of iron provides many spectral lines which are close together. This means that calibration of the detector system may be avoided.

(ii) Reliable transition data was available. Oscillator strengths of iron are considered more reliable than for most other elements (Faires *et al*: 1984).

(iii) The iron lines are easily identified since the iron spectrum is a traditional wavelength standard.

(iv) The excitation energies of the upper levels are greatly different which enhances the precision of the temperature measurements.

It is a distinct advantage that most of the work has been done using iron as it is easy to compare results obtained by different research-workers.

Radial temperatures were calculated with the aid of the slope and two line method according to Reif and co-workers (Reif *et al*: 1973). Abel inversion was then applied. The assumption was made that the central portions of the argon supported inductively coupled plasma used were in a LTE state. The results yielded a bell-type graph for a plot of relative intensity, versus horizontal displacement from the plasma edge (or radial position from the plasma centre). Above an observation height of 25 mm the bell-shape prevailed, while below that height a toroidal temperature distribution was found (Fig. 2.2).

In a later paper, the same authors, Kalnicky, Fassel and Kniseley (1977) once again investigated excitation temperature, but this time in the presence of an easily ionizable element (EIE). The results obtained for the Fe I line were in agreement with their previous findings. However when the Ar I line the results were indeterminable. No noteworthy difference in the radial excitation temperature was found after the addition of 6900 μg/ml sodium (an EIE). Electron density profiles were also reported after both the H_α line for Stark broadening and Saha-Eggert profiles were investigated. The Stark broadening values of n_e obtained were about five-fold smaller than those reported by Mermet (1975). They were two-fold smaller than those found by Kornblum and de Galan (1974), who used a continuum and the Saha method. The electron densities obtained by Kalnicky *et al*, using magnesium, were at least a factor 10 times smaller than the results obtained using Stark broadening. Again the addition of an EIE had little effect except at an observation height of 25 mm, when the value of n_e at the wings of the plasma was suppressed.

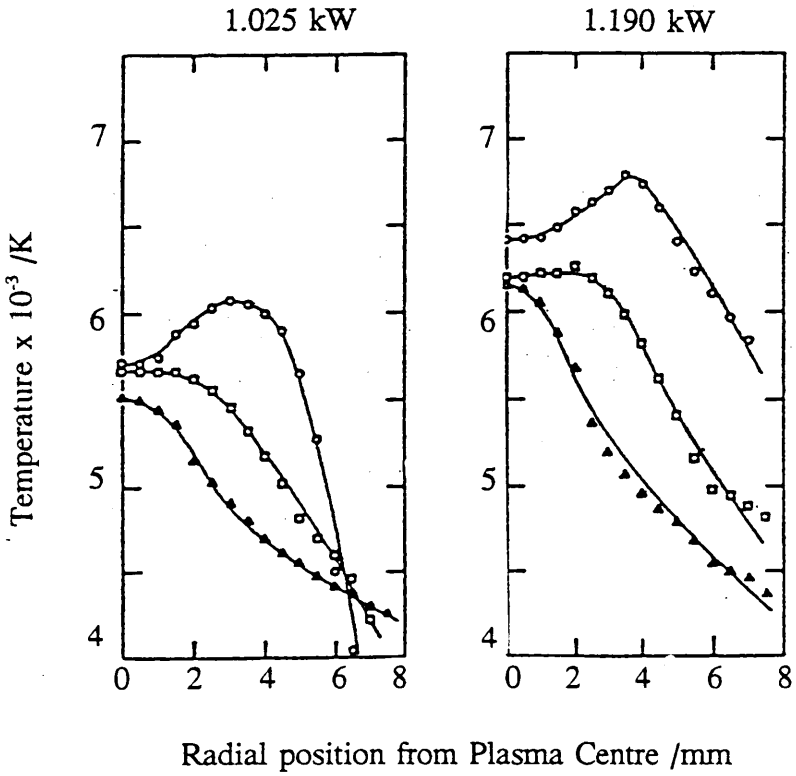

Figure 2.2 Radial excitation temperatures for two power levels and three observation heights using Fe I: (o), 15 mm; (□), 20 mm; (Δ), 25 mm (Kalnicky *et al*: 1975).

The spatial characteristics of the temperature were explained by Hasegawa and Haraguchi (1985b) by considering the gas flow and heat conduction within a plasma. In the off-axis region, the temperature decreases with distance from the hottest region inside the load coil due to the heat being conducted to the surrounding atmosphere Hasegawa and Haraguchi: 1985b). They went on to comment that in the central core of the plasma, the temperature is slightly lower because of the large flow of cool injector gas (>50 m/s). At the observation height usually used the temperature increases due to the mixing of the gas between the inner core and the hot surrounding zone. The temperature decreases once more in the plume, where the mixing is nearly complete.

This explanation by Hasegawa and Haraguchi clarified the temperature and velocity distribution model of Barnes and Schleicher (1981). They (Barnes and Schleicher) investigated the temperature and velocity distributions under conditions which allowed a direct comparison with computer calculations. Pure argon was used for the central gas flow and no solution aerosol was applied. After modifying an empirical model, they obtained better than 15 % agreement between experimental and calculated temperature profiles inside the core and up to 15 mm above the coil. Blades and Caughlin (1985) studied the complicated spatial characteristics using photodiode array detectors and confirmed the behaviour of T_{exc}.

Fourier transform spectroscopy was used by Faires and co-workers (Faires *et al*: 1984) to determine the excitation temperature of Fe I, Co I, Ni I, V I and II. The criteria for LTE set by Griem (1964) stated that the collision rate of depopulation from excited states should be at least ten times greater than the radiative state of depopulation. This was calculated by Alder *et al* (1980) to require an electron density of at least 10^{16} cm^{-3} for an argon plasma at 7000 K. Values that have been reported lie between 10^{13} and 10^{17} cm^{-3} (Kornblum and de Galan: 1977, Kalnicky *et al*: 1977), implying that it is dubious to consider that the ICP-OES is in a state of LTE. Fourier transform spectroscopy was used to collect spectroscopic data and Boltzmann plots were drawn. It was impossible to conclude anything about the absolute value of the excitation temperature due to the variations obtained using different oscillator strength (g_p) data.

Vertically resolved profiles of T_{exc} were derived by Houk, Schoer and Crain (1987) using emission profiles from Fe I, Mn I, Cr I, Ba II and Ca II lines. They described a method whereby the spatial behaviour of T_{exc} and the adherence of the excited state populations to a Boltzmann distribution could be studied without knowledge of transition probabilities for the lines monitored. The various species all yielded a hump-shaped T_{exc} profile with a maximum value for T_{exc} at or near the peak of the intensity profile for "hard" lines. Because the values of T_{exc} varied between species and also energetically different excited states of the same species, they concluded that the excited state deviated from a Boltzmann distribution.

The experimental conditions greatly affect the excitation temperature (Kornblum and de Galan: 1977, Kalnicky *et al*: 1977). Capelle *et al* (1982) found that the temperature and electron density decreased with increasing generator frequency. Even considering the variations that conditions and inaccuracies in the oscillator values employed, the range in T_{exc} found, 3000 - 7000 K cannot be explained in this way.

Alder and co-workers (Alder *et al*: 1980) measured the different intensities of Fe I for 20 different transitions and after dividing the data up into three groups with increasing energy found that three different values for T_{exc} were obtained. Kornblum and Smeyers-Verbeke (1982) found that T_{exc} increased continuously as the excitation energy increased, which indicated as did the results of Alder *et al* (1980), that there was a departure from the Boltzmann distribution.

Only species that have sufficiently intense atomic and ionic lines can be used for the determination of the ionic temperature. When investigating the influence of water vapour on plasma conditions, Alder and co-workers also measured T_{ion} for seven different elements as well as investigating T_{exc} using iron. Their findings showed that T_{ion} was in good agreement with the values of T_{exc} resulting from high energy levels.

Using an ICP-mass spectrometer (MS), Houk and co-workers (Houk, Svec and Fassel: 1983, Houk, Montaser and Fassel: 1983) were able to measure the concentration of

singly and doubly charged ions directly and could then calculate T_{ion} from the Saha equation, 2.5. The measurements they found for T_{ion} for barium and strontium were in good agreement with those reported by Alder and co-workers.

The value obtained for the rotational temperature was dependent on the species investigated. The T_{rot} found using N_2^+ and C_2 (Batal, Jarosz and Mermet: 1982, Abdullah and Mermet: 1982, and Zeeman *et al*: 1978) was relatively high (4500 - 8000 K), while other species such as OH resulted in T_{rot} values in the region of 3000 K (Crosley and Smith: 1982). In the work done by Zeeman *et al* a 9.2 MHz ICP-OES was used and T_{rot} found for the N_2^+ band was between 6400 and 8000 K. The temperature was determined from the equation

$$\ln(I_{em}/[J'+J''+1] = A - B'J'(J'+1)hc/kT \qquad 2.47$$

where A is a constant, B′ the rotational constant of the upper state and J′ and J″ are the quantum numbers of the upper and lower rotational levels, respectively. The graph of the left hand side versus J′(J′+1) gives a straight line with slope -Bhc/kT. The N_2^+ bands arise from a $^2\Sigma \rightarrow {}^2\Sigma$ transition. The strongest (0,0) band is at 391.4 nm, while the (0,1) band is at 427.8 nm.

Air is entrained in an ICP and molecular emission bands from N_2, N_2^+ and NO will result. The emission spectra of OH, NO and NH molecules was observed by Reeves *et al* (1980) as a function of observation height, rf power and the environment surrounding the plasma. They found that the emission intensities of the NH and NO bands were enhanced by increasing the observation height and input power as well as by adding nitrogen to the gas mixture. The power dependency indicated that the nitrogen and oxygen molecules were decomposed into atoms with an increase in temperature. Niebergall, Brauer and Dittrich (1984) measured the spatial distribution of N_2^+ bands by photographing the plasma after the signal had passed through a slitless spectrograph. From their results they proposed an air entrainment model where the atmospheric gases were directed inward and upward through the forced aerosol flow.

Atomic fluorescence spectrometry (AFS), using the ICP as an atomization source has several advantages (Omenetto *et al*: 1980, Kosinski *et al*: 1983, and Krupa *et al*: 1985). There are less quenching reactions and greater freedom from chemical and ionization interferences than when a chemical flame is used. The excited atom lifetimes in the ICP measured by time resolved laser fluorescence indicate quantum efficiencies in the range of 0.2 - 1.0 (Uchida *et al*: 1983, Uchida *et al*: 1984). The quantum efficiency of the sodium atomic resonance line was equal to 1.0 up to a height of 60 mm above the load coil when using an extended long sleeve torch. This must be compared with a figure of 0.044 when using an air-acetylene flame (Russo and Hieftje: 1982).

Hasegawa and Winefordner (1987) published the results of their investigation into the temperature of the neutral nitrogen molecule in an ICP. They found that T_{rot} using the second positive bands of N_2 and a medium resolution monochromator was approximately 4000 K at an observation height of 70 mm. The rotational temperature was calculated from the correlation plot of half-width of over-all band profile against T_{rot}. The value for T_{rot} for the OH species was only 2000 K. The T_{vib} was in the range 2500 - 5500 K and the spatial profile was an annular structure which changed to a bell-shape at increasing observation heights. They proposed that the energy gained by the N_2 through energy collisions was lost by the radial heat conduction and that collisions between N_2 and Ar were thermally equilibrated.

The thermometric species N_2^+ and OH were also investigated by Raeymaekers, Broekaert and Leis (1988). They used an ICP-OES operating at 2 kW and with argon and oxygen as outer gases when determining T_{rot} for OH and N_2 or air when determining N_2^+. Their findings that the OH radical did not comply with Boltzmann behaviour were in agreement with those of Hasegawa and Winefordner (1987). The low rotational temperatures described for O_2 were probably due to the fact that its dissociation is also 10^5 higher than the neutral N_2 molecule. A cooler channel in the plasma centre was visibly discernible and this agreed with the theoretical model of Barnes and Schleicher (1981).

Very few determinations of T_D have been made because of the difficulty of measuring spectral line widths and the associated convolution procedures. Human and Scott (1976) used a Fabry-Perot interferometer, while Faires *et al* (1985) applied Fourier transform spectroscopy to the problem. Their findings were consistently in the range 4000 to 6000 K for T_D.

If the plasma cannot be assumed to be in a LTE state then the value of all the temperatures except that of T_D and T_e, when the latter is calculated using Stark broadening, is in doubt. The electron temperature can thus be regarded as the most important for characterizing an ICP. The determination of T_e from the background emission of argon still presents problems and complicated theoretical calculations relating to the continuum radiations must be carried out (Bastiaans and Mangold: 1985, Batal *et al*: 1982). Batal and co-workers (Batal *et al*: 1982, Batal *et al*: 1981) determined T_e from the ratio of an Ar I line to the continuum in the visible region of the ICP spectrum, 400 - 700 nm. The value for T_e they obtained, i.e. 8000 - 10 000 K was considerably higher than they had found previously for T_{exc} or T_{rot} (5000 K) using the same source.

Hasegawa and Haraguchi (1985b) determined the spatial distribution of T_e by fitting the theoretical curve to the observed continuum profile. The T_e value of 8400 K that they obtained at a distance of 15 mm above the load coil was comparable with the results of Batal and co-workers using similar equipment.

In an article, van der Mullen and co-workers reported their findings for electron density and T_e (Van der Mullen *et al*: 1988). They used both the Stark broadening of the H_β line and Saha-Boltzmann plots for the determination of n_e, and obtained results for the two methods which agreed within 20 %. This supported the close-to-LTE concept. They further proposed a b_1 parameter which could characterize the LTE-departure in an ICP. The electron temperature calculated by these authors for different values of b_1 ranged between 7000 and 9000 K.

One further method for the determination of T_e was used by Huang and Hieftje (1985 and 1989) and Hanselman *et al* (1994), namely Thomson scattering. This method had the advantage that LTE was not in any way assumed and the temperature could be measured exactly. The experimental Stark broadened line profile must normally be deconvoluted for instrumental and Doppler broadening before applying Abel inversion, and each step can generate errors. The advantages of applying the theory of Thomson scattering to determine the electron density and temperature are as follows:

(i) direct and simultaneous measurement of spatially resolved electron temperatures and density without the need for assuming LTE or performing Abel inversion,
(ii) temporal resolution,
(iii) no interferences with or perturbations to the plasma if the laser power is limited.

The method is, however, experimentally complex. Anti-Stokes Thompson scattering (CATS) has the scattered light concentrated in a very small solid angle, and produces a signal which has quadratic dependence on electron concentration and cubic dependence on laser power. The enhancement of the absolute scattering by CATS occurs only when both laser beam diameter and observation path lengths are small and when the electron density is high. The laser beam can unfortunately not be focused tightly into an ICP because of heating and ionization problems. The temperatures obtained using CATS were in the region of 9200 to 11 600 K (Huang, Marshall and Hieftje: 1986).

A further method for determining electron temperature was reported by Pei-qi, Pei-zhong and Tie-zheng (1988). A Langmuir probe was constructed of tungsten in a magnesium oxide sleeve and this was immersed in the plasma. The electron temperature was calculated from the variations of measured current with applied potential. The results obtained at 1.0 kW were about 7500 K, only slightly lower than the spectroscopic values, but considerably lower than the results obtained using Thomson scattering.

By far the most commonly reported method for the determination of electron number density uses the Stark broadening of the Hβ line. This laborious process has been speeded up by using photodiode array detectors (Caughlin and Blades: 1984) or two stepping motors (Walters, Gunter and Zeeman: 1986). Considering that this method is regarded as being the most reliable, wide variations in the value of n_e have been reported, i.e. from 5 x 10^{14} to 5 x 10^{15} cm^{-3}. This inconsistency may be attributable to factors such as:

(i) error introduced by the Abel inversion,
(ii) uncertainty with respect to the instrumental or Doppler broadening,
(iii) misalignment of the optical system,
(iv) asymmetry of the plasma, and
(v) different operating conditions.

Goode and Deavor (1984) used the least squares fit to improve precision and by comparing data obtained by the halfwidth method to that of the curve-fitting approach, they showed that the halfwidth method had a tendency to overestimate, by a factor of 2 or 3, the value of n_e. The electron density was obtained using Stark broadening of the Hβ line and then subjected to a curve-fitting algorithm in which the single parameter, n_e, was adjusted to achieve a least-squares fit to a theoretical profile.

A comparison of the radial electron number density distribution obtained from Stark broadening of the Hβ line and Saha calculations may be seen in Fig. 2.3.

Further plots were published by Blades and Caughlin (1985) and Furuta *et al* (1985). The values for n_e show small variation. These might be attributable to the uncertainty in the transition probabilities. There is, however, a considerable difference (factors of between 30 and 50) between the values for n_e found using the Saha method and equivalent values obtained from Stark broadening of the Hβ line. The only conclusion is that the differences must be due to the plasma not being in LTE.

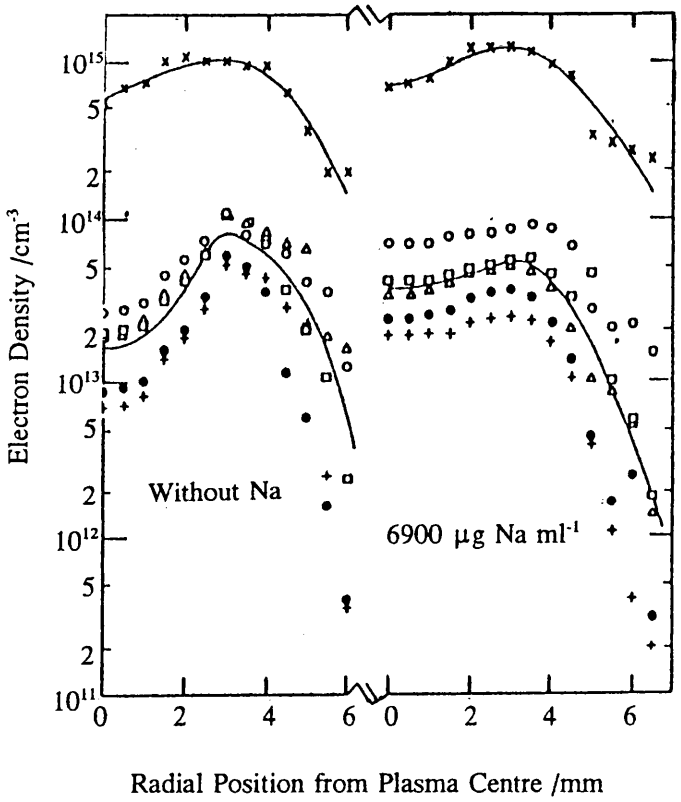

Figure 2.3 Radial electron number density distributions obtained from Hβ Stark broadening (x) and Saha calculations: 10 µg/ml of Ca (o), 150 µg/ml of Fe (□),10 µg/ml of Mg (Δ), 10 ug/ml of Cd (+), 10 µg/ml of Zn (●) (Kalnicky *et al*: 1977).

Thomsen and Helbig (1991) compared the experimental and theoretical values obtained for the electron density from the Stark broadening of the Hβ line. They were investigating the electron density range of 6.4 x 10^{14} and 1.3 x 10^{15} cm^{-3} by using the Hβ and Dβ half widths and line profiles. For larger electron densities (3 x 10^{16} and 2 x 10^{17} cm^{-3} an error of possibly 4 % had been reported (Helbig and Nick: 1981). They concluded that for the lower electron density the half width of the Hβ line could be used as a sensitive and accurate electron density probe for laboratory diagnostics of analytical plasmas.

The temperature and electron density was determined for a helium/hydrogen capacitively coupled microwave plasma by Masamba, Ali and Winefordner (1992). The excitation temperature was determined using Boltzmann plots of six iron emission lines in the 370 - 377 nm region. The rotational temperature was calculated from the

relative intensities of the rotational lines of the Q_1 branch of the (0,0) transition of the OH radical in the 307 - 310 nm region. The electron density was determined from Stark broadening of the H_β line.

Kornblum and de Galan (1977) used the continuum method for the determination of electron density. They calculated n_e from the absolute continuum at 450 nm in low- and high-gas ICP's. The value for n_e at the centre of the plasma with a low gas flow was about 1 x 10^{15} cm^{-3} which is comparable to the value found using the Saha method.

The method of Series limit-line merge was applied by Montaser and co-workers to the determination of n_e (Montaser and Fassel: 1982, Montaser, Fassel and Larson: 1981). Values of n_e obtained from the line merging of six elements were comparable to, or lower than, those found with the Stark method, even though the application of the Inglis-Teller formula tended to give higher values.

In an attempt to establish a new basis for the discussion of electron density without non-thermodynamic "temperatures", Meeks (1993), derived an equation in terms of the thermodynamic temperature and the electronic potential of the parent species in the ionization of a slightly ionized gas. The new expression for the electron number density was found without use of the Boltzmann partition function. Electrons were allowed to follow the Boltzmann distribution when in the gaseous phase, but were required to follow the Fermi-Dirac distribution when bound. The effect that this had was that the ratio of the Boltzmann partition functions in the Saha relationship with the quantity $e^{\mu/kT}$. Several advantages were claimed for this approach, including that the temperatures required to correlate the electron densities with experimental values were close to the gas and rotational temperatures.

2.13 Factors influencing temperature and electron density

The temperature and electron density are parameters fundamental to the plasma and any changes to the plasma will obviously effect these variable. The variations of these parameters within the plasma have been well documented. Even aerosol carrier gas

will effect the absolute number density of argon (metastable argon) as may be seen in Fig 2.4. These determinations were made by Nojiri *et al* (1983) when considering absorbance values 15 mm above the load coil. The addition of a solvent aerosol to this gas flow in turn changed the conditions within the plasma (Nowak *et al*: 1988, Alder *et al*: 1980 and Caughlin and Blades: 1987).

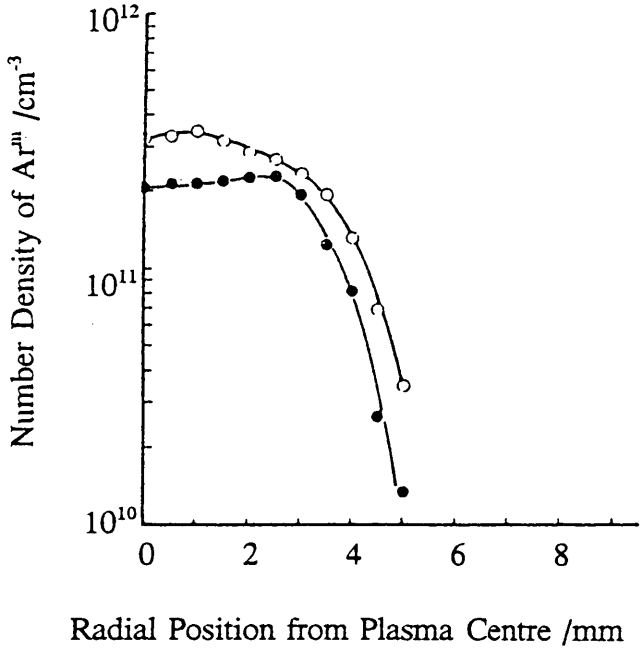

Figure 2.4 Radial distribution of number density of metastable argon with (●) and without (o) aerosol carrier gas (Nojiri *et al*:1983).

The findings of Long and Browner (1988) were that water changed the plasma low down, but the effect resulting from the water could be seen in the plasma at a height of 15 mm above the load coil. The authors differentiate between water vapour and water aerosol. They found that water vapour made very little difference to the electron density within the plasma, while water aerosol resulted in a dramatic difference. Their findings that the addition of water aerosol to the plasma resulted in an increase in electron density agreed with that of Alder *et al* (1980).

The article concerning this effect of water on the ICP by Long and Browner (1988) resulted in a letter to the editor by de Galan and a subsequent response by Long and Browner (1989). One of the criticisms levelled by de Galan was that in the calculations of Long and Browner they had not accounted for the increase in electron

density which would result from the presence of hydrogen and oxygen, which according to de Galan would cause an increase of 20 % on their own.

In their reply Browner and Long were prepared to accept that the validity of their measurements of temperature and electron density were subject to experimental and interpretational bias depending on the original article, but were based on careful consideration of the data. They had clearly distinguished between water vapour and water aerosol, the former making no difference to the plasma, the latter significantly altering the physical parameters.

The findings of Nowak *et al* (1988) were that the addition of water to the aerosol carrier gas resulted in the plasma shrinking in all dimensions and this caused the change in the electron density. They further found that the density along the axis decreased more rapidly as a function of height due the presence of water. What is also interesting is that the change in electron density resulting from the water could be most clearly seen in the electron density determined at the centre of the plasma (Fig. 2.5).

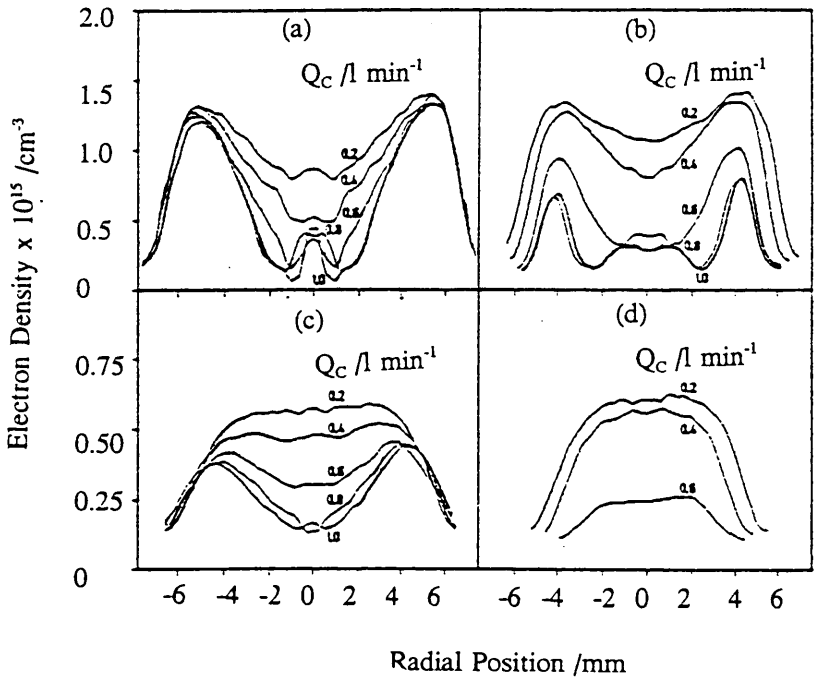

Figure 2.5 The radial profile of the electron density for different values of aerosol carrier gas flow rate at 0.8 kW; (a) z = 5 mm, no water, (b) z = 5 mm, water added, (c) z = 15 mm, no water, and (d) z= 15 mm, water added (Nowak *et al*: 1988).

A recombination channel could have been responsible for the observed decay in the number of electrons per unit length along the axis, but the authors felt that this was not of atomic nature.

The effect of ethanol on a free running ICP-OES was reported by Benli (1983) when he gave a survey of plasma spectroscopy in the People's Republic of China. As the concentration of ethanol was increased from zero to 90 % (v/v), the excitation temperature when measured 15 mm above the load coil increased, initially reaching a maximum at about 30 % ethanol, then decreased as shown in Fig 2.6.

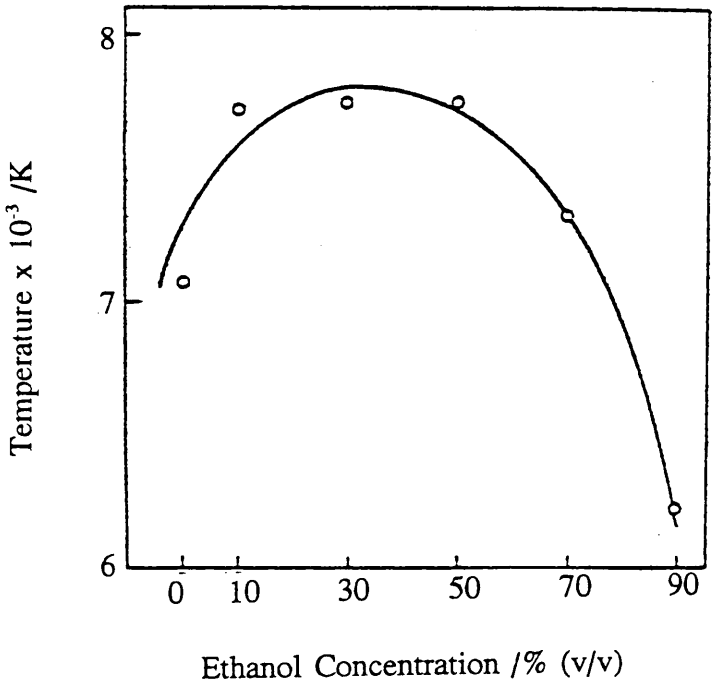

Figure 2.6 Effect of ethanol on the excitation temperature of a free running generator at anode grid voltage of 4.6 kV, aerosol carrier gas flow rate of 0.48 l min^{-1} and observation height 15 mm (Benli: 1983).

Excitation temperature was determined using a set of vanadium ion lines and Abel inversion was applied. At the same time, anode and grid currents of the free running generator were determined. It was found that both increased rapidly up to 30 % ethanol (anode from 0.71 to 0.78 A and grid from 140 to 185 mA) then continued to increase but less rapidly and almost linearly until 90 % ethanol. The frequency

decreased throughout the ethanol range and the change becoming greater as the input power was decreased. These effect were utilized to estimate the alcoholic content of drinks when compared to ethanol matched standards.

Excitation conditions of the plasma with other organic solvents has been widely investigated. Interest in the analysis using organic solvents results mainly from three applications:

(i) petroleum products (Brown: 1983 and Botto: 1987),
(ii) organic extract (Ward *et al*: 1977 and Seeverens *et al*: 1983), and
(iii) used as a detector for liquid chromatography (Hausler and Taylor: 1981 and Jinno *et al*: 1985).

In particular, the analysis of wear metals in oils has become an established procedure as they are an indication of the state of the engine and consequently most useful as a diagnostic tool (Granchi *et al*: 1987).

Boorn and Browner (1982) investigated the excitation conditions when chloroform and carbon tetrachloride were aspirated and compared the results to those found for water. In each case a decrease in excitation temperature was reported. They concluded that this decrease was a result of the absorption of rf power in the central channel produced by the volatile organics. Boumans and Lux-Steiner (1982) found that an additional 0.5 kW of power was required to achieve similar results with organic solvent when compared to water. The organic solvent they investigated was 4-methyl pentan-2-one (MIBK). These authors suggested that the difference between the "organic" and "aqueous" plasma could be explained by assuming that molecular constituents such as CO, C_2 and CN enhance the thermal conductivity of the gas.

These findings were in agreement with those of Blades and Caughlin (1985) when investigating xylene as solvent. They demonstrated that the energy absorbed by the plasma in vaporizing and dissociating the xylene in their plasma was equivalent to reducing the external power loading to the plasma by 500 W. Blades and Caughlin

attributed the decrease in excitation temperature to the dissociation of C_2 molecules in the central channel of the plasma.

Kreuning and Maessen (1989) investigated six organic solutions and compared the results with those found for water when considering the following measurements:

(i) axially resolved excitation temperature,
(ii) radially resolved emission intensities of C_2, CN and C,
(iii) axially resolved emission intensities of C_2, CN and C, and
(iv) axially resolved net line intensities of the spectral lines investigated by them.

The change in excitation temperature for ethanol relative to the height above the load coil is given in Fig. 2.7.

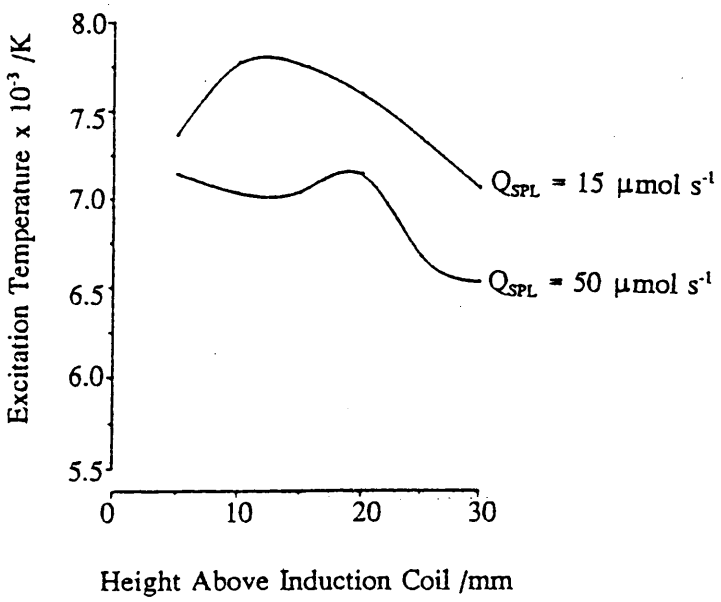

Figure 2.7 Excitation temperature as a function of observation height at two plasma loads (Kreuning and Maessen: 1989)

In Fig. 2.7, Q_{SPL} is the solvent plasma load as determined by a continuous weighing method, and Q_{CPL} the plasma carbon load. For ethanol they found that Q_{CPL} was twice Q_{SPL}. The excitation temperature was determined by considering Boltzmann plots of iron emission spectra. Kreuning and Maessen (1989) found that when the solvent plasma load was increased from 15 to 25 µmol s^{-1} the excitation decreased for the

entire axial zone considered. They found further that the excitation profiles for ethanol and methanol were virtually identical although their carbon loads differed by a factor of two. Also, between 10 and 20 mm above the induction coil the excitation temperatures of both methanol and ethanol was higher than that of water, contradicting the findings of Blades and Caughlin (1985).

Kreuning and Maessen concluded that not only the nature of the solvent played a role in determining excitation temperature profiles and spatial distribution of pyrolysis products, but also the solvent plasma load. They found the following features applied to the organic plasmas that they investigated:

(i) the distance between the axial position of the C_2 emission maximum and the axial position of the intensity maxima of the ionic lines remained constant,
(ii) there is a relationship between the shape of the axial C_2 emission profile and the excitation temperature profile, and
(iii) the position of the intensity maxima of "hard" atomic lines was always the same.

In two articles, Pan, Zhu and Browner (1990 and 1992) investigated the role of auxiliary gas flow in organic sample introduction with ICP-OES. They calculated the excitation temperature using Boltzmann distribution of iron lines. In the original article in 1990 they used carbon tetrachloride and noted that its mass transport rate was ten times that of water. In the second paper they looked at xylenes and amyl alcohol as well as carbon tetrachloride. They came to the conclusion that the distribution of solvent loading in the plasma central channel played a very important role in determining the plasma conditions. An increase of C_2 in the plasma channel resulted in more energy being consumed to dissociate the species. This in turn led to a decrease in the excitation temperature with increasing auxiliary gas flow rate.

Thomson and Rayleigh scattering was used by Hanselman *et al* (1994) to study the effect of sample matrix on electron density, electron temperature and gas temperature in an ICP. The effect that matrices and especially easily ionized elements (EIE) had

on the ICP was reported by Horlick and Blades (1980) and Blades and Horlick (1981) who found that the magnitude of the effect was spatially dependent and was inversely proportional to the elements ionization potential. Hanselman *et al* also found this inverse relationship, but also found that regardless of the ionization potential, additions of an interferent resulted in significant changes in analyte emission profiles. This was accompanied by large shifts in the electron density, electron and gas temperature. Depending on the operating conditions of the plasma, the magnitude and even the sign of these changes differed.

Ionization of the matrix was not solely responsible for the large increases in electron density (Hanselman *et al*: 1994), but rather that electrons may be redistributed from high-density to low-density regions, through altered energy coupling or transport. Further, at high central gas flow rates, a smaller analyte-atom diffusion cloud together with large increases in electron density and temperature, would result in enhanced atom and ion, emissions due to increased collisions.

In a most recent article, Weir and Blades (1994) had a look at the background spectra and visual features obtained with different solvents. According to the authors (Weir and Blades) solvents may be divided into three categories. Water, methanol and chloroform may be taken as a representative of each. They examined the plasma with both a minimum and maximum loading of each of these three solvents. A MAK cross-flow nebulizer was used together with a desolvator.

They found that when methanol was used as solvent, the atomic plasma translated downstream and both the diffuse and sharp diatomic carbon plumes extended along the central channel, as the methanol loading increased. In addition to this downstream translation of the atomic plasma, it also contracted, the amount of contraction increasing with methanol loading. This contraction may have resulted from the thermal pinch effect. The secondary plasma also appeared to bloom open in response to the increasing methanol loading. The bright secondary plasma retained its toroidal capped cone, but as the methanol load increased, the cone of the bright secondary plasma was almost completely penetrated leaving only a thin arch near its apex. This

blooming, Weir and Bloom decided, would alter the amount of energy available in the central channel to desolvate, vaporize, atomize, ionize and excite the analyte.

Directly linked to the blooming of the plasma they found that the diatomic carbon extended downstream. The cup and the plume grew downstream with increasing solvent load and the intense sharply defined green emission overtook and predominated the diffuse one. The authors intend to follow the publication with other giving the effect that these observed changes will have on electron density and temperature.

One final property of the plasma which would have an effect on electron density and temperature must be considered. Recent experimental evidence using laser light scattering measurements found that there were a number of incompletely desolvation droplets in the normal analytical zone of the plasma (Olesik and Fister: 1991). The presence of these droplets was found to be a function of the aerosol carrier gas flow rate and the applied power.

Hobbs and Olesik (1993) investigated the effect these droplets would have on the ionization and excitation in the plasma. Using time-gated laser-excited fluorescence they were able to show that Sr atom number density increased by more than a factor of 40 near incompletely desolvated droplets and by more than 60 near vaporizing particles. A 2.6 fold increase in Sr ion number density was found near incompletely desolvated droplets and a seven fold increase near vaporizing particles. They noted that there was a decrease in analyte ionization near the droplets.

Hobbs and Olesik calculated the temperature and electron density from ion to atom fluorescence ratios. They used an adaption of the Burton-Blades modification (Burton and Blades: 1990) of the LTE model. In the absence of droplets in the analytical zone they measured a temperature of 8040 K and an electron density of 1.8×10^{15} cm^{-3}. Near incompletely desolvated droplets the calculated temperature was only 6120 K and the electron density 4.3×10^{13} cm^{-3}. The presence then of these droplets meant a reduction in temperature of 1900 K and more than one and a half decades in

electron density. They also found a drop in the degree of ionization. In the absence of droplets, the Sr was 99.0 % ionized, while in the presence of droplets this was reduced to 85.9 %.

Temperatures and electron densities calculated from emission to fluorescence intensity ratios led to similar differences between the plasma condition with and without the presence of droplets. Similar measurements were made near vaporizing droplets and the same tendency was found, namely that near vaporizing droplets the temperature and electron density was reduced, though not to the same extent.

Hobbs and Olesik found that the incompletely desolvated drops had a large effect on atom and ion number densities. The Sr ion fluorescence signal more than doubled when droplets were introduced into the analytical zone. Since the droplets would not introduce analyte into the plasma, the change, they deduced, must have resulted from one of the following:

(i) increased gas density due to cooling,
(ii) changes in ionization equilibrium, and/or
(iii) variations in the fraction of ions in the ground state.

Allowing for a change from 65 to 100 % in the fraction of ions in the ground state, the fluorescence intensity would according to the authors calculations only increase from 22 to 34 and not the 57 found experimentally. Additional ions were not produced in the vicinity of the droplets as determined above, which meant that the increase in the gas density was the most likely contributor to the observed increase in fluorescence intensity.

A rapid and simple method for the determination of electron density within the plasma must also be mentioned. Several authors have reported on the usefulness of ionic to atomic lines assessing the deviations of a given plasma from LTE (Blades *et al*: 1987, Mermet: 1989 Mermet: 1991). The most common ionic and atomic lines used are those of magnesium. The ratio Mg II/Mg I should be in the region of 10 to 13 for

the plasma to be in a state of LTE. Should the ratio be smaller than 10 then deviations from LTE have been encountered, and the further the deviation from 10 is, the less the plasma will conform to LTE conditions (Mermet: 1991).

CHAPTER 3

DETERMINATION OF TEMPERATURE

AND ELECTRON DENSITY

3.1 Introduction

An investigation was carried out to determine the changes in temperature and other fundamental properties that occurred with changes in ethanol concentration in the sample solution. For this purpose it was decided that the excitation temperature, T_{exc}, would be determined. T_{exc} is the temperature that governs the energy population as defined by the Boltzmann distribution.

Changes in the excitation temperature, when organic solvents were used, according to the literature may be summarized as follows.

A decrease in the excitation temperature with the introduction of organic solutions was reported by Boorn and Browner (1982), Goldfarb and Goldfarb (1985), and Blades and Caughlin (1985). When studying the excitation temperature while increasing the ethanol concentration from 0 to 90 % (v/v), Benli (1983) reported that the temperature initially increased and then dropped to a value lower than that obtained with pure aqueous solutions. Kreuning and Maessen (1989) found that the nature of the solvent and the solvent plasma load were decisive in determining the excitation parameters. Pan *et al* (1990 and 1992) found that the plasma excitation temperature decreased with increasing vapour pressure.

Considerable criticism has come from the method for determining the temperature by means of a Boltzmann distribution because of the reliance of that method on LTE

conditions within the plasma. Deviations from LTE would result in the values found for the excitation temperature when using the Boltzmann distribution to be possibly inaccurate (Kornblum and Smeyers-Verbeke: 1982, and Alder *et al*: 1980). Raaijmakers *et al* (1983) suggested that the deviations from LTE in an ICP are limited.

Since this investigation was not used to determine the excitation temperature with great accuracy, but rather to determine **changes in excitation temperature** as conditions altered, it was decided to use the Boltzmann distribution as described by equation 2.17, even though the system would contain an inherent error due to deviation from LTE. For simplification, the "two line" method was used, since as indicated in section 2.3 n_a, the total number of atoms, cancelled out.

The Stark broadening of the hydrogen lines was the method used to determine the electron density as there is an abundance of literature references available for comparison of results. Also, the method is regarded as fairly simple and without serious errors (section 2. 11). This method depends on the Stark broadening of the H_β line (486.1 nm) and may be calculated from equation 2.38. The profile of the H_α line at 656.3 nm was measured, although the electron density was calculated using the H_β line itself since the precision of the results associated with such determinations are about 5 % (Thorne: 1974), better than any of the other hydrogen lines available.

As the two hydrogen lines were being determined for the purpose of calculating the electron density it seemed reasonable to use them for the determination of the excitation temperature. The conditions as given in section 2.9.1 for the "two line" method, namely that the transition probability data and statistical weight be accurately known are satisfied for the two hydrogen lines.

3.2 Experimental

3.2.1 Reagents

Analytical-grade purity ethanol was used. The water was distilled and de-ionized.

3.2.2 Apparatus

3.2.2.1 Spectrometer.

A Hilger Analytical microprocessor-controlled 1.5 m spectrometer was used. It was equipped with a Czerny-Turner grating (1800 lines mm^{-1}). The monochrometer was placed on an xz-table and incoming emission from the torch was focused onto the exit slit by means of a Helium laser. Details of the experimental setup may be seen in Fig. 3.1.

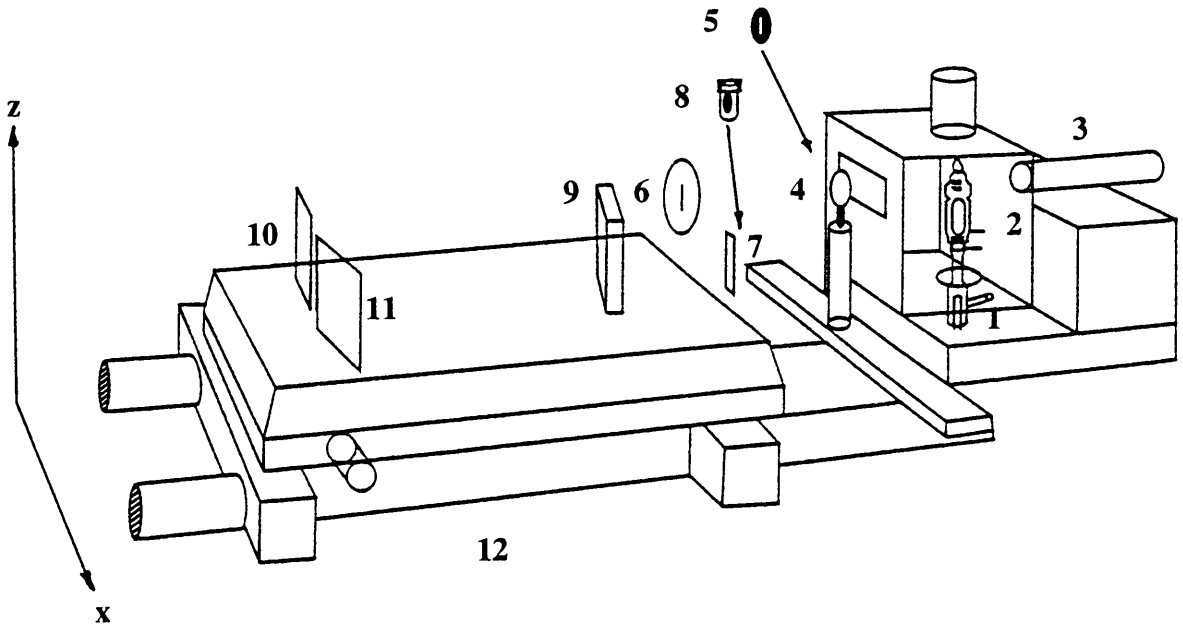

Figure 3.1 Schematic diagram of experimental setup: 1, sample inlet; 2, torch; 3, alignment laser; 4, lens, 5, removable or adjustable aperture; 6 and 7, entrance and exit slits; 8, photomultiplier tube; 9, 10 and 11, grating spectrometer; 12, xz table.

3.2.2.2 ICP spectrometer

The ICP-OES used was a Spectro Analytical Instruments Spectroflame operating under the conditions given in Table 3.1. It was fitted with a standard crossflow nebulizer and glass Scott spray chamber.

3.2.2.3 Read-out system

A Hamamatsu photomultiplier tube, R955, was used as detector. It was powered by a Brandenburg Power Supply, Model 4728, and the analogue signal was sent through a Philips PM 3350 oscilloscope to an analogue/digital converter (PCL-711S) in an IBM-compatible PC computer.

The voltage applied to the photomultiplier tube, PMT, was 850 V in the case of H_β readings and 600 V when H_α was measured.

3.2.3 **Procedure**

3.2.3.1 Electron density (n_e) determination

The electron density was calculated using equation 2.38. The temperature was assumed to be at 5500 K while both the entrance and exit slits were 15 μm. Correction was then calculated according to the method used by Xiao *et al* (1992).

3.2.3.2 Calculation of temperature

Temperature was calculated from equation 2.17.

Both the temperatures and the electron densities were calculated from a programme written for this purpose by Prof K Visser of Stellenbosch University. Due to the length of the programme only menus and manual are given in Appendix B, but the programme used for the calculations may be found on a computer disk. The programme "Abel", as written by Prof. Visser, applied the inversion, while the programme "Temp" calculated temperature and electron density.

3.2.3.3 Measurement of the emission intensities

The spectrometer was positioned so that the emission from just above the load coil (z = 0 mm) and at the extreme edge of the torch (x = -8 mm) could be measured. Both the H_β and H_α (486.133 and 656.272 nm, respectively) lines

were scanned while water was being nebulized and their intensities recorded. This recording was made for both the forward and reverse direction of scan. The lateral position of the spectrometer was changed (moved through 1 mm) and the scans repeated. This process was continued until the emission from the other outer edge of the torch was measured (x = 8 mm). The height of the spectrometer was changed so that the recording could be made from a position 5 mm above the load coil (z = 5 mm). The lateral measurements were then repeated. This procedure was carried out for z = 10 and z = 15 mm. The entire procedure was repeated for solutions containing 5, 10, 15, 20 and 25 % (v/v) ethanol.

3.2.3.4 Data processing methodology

In the initial stage of this investigation the emission intensities were recorded on an Apple 2e computer equipped with an analogue-to-digital converter. The digital data were transferred to an IBM compatible computer for further analysis. For this procedure two software programmes were used, the one for converting the analogue signal, the other for transferring the data. The method proved to be cumbersome and when the Apple computer began giving problems, the entire procedure was altered so that it could be carried out using an IBM compatible computer.

The analogue signal from the photomultiplier tube passed though an oscilloscope to an analogue-to-digital converter in an IBM compatible computer. The oscilloscope was used only to evaluate rapidly the signal from the PMT. The digital signal, after conversion, was recorded in ASCII on floppy disks by the computer using a programme written for this purpose (Manual and instructions given in Appendix A, while the programme is on the computer disc). The digital data in ASCII was transferred to a software package, Asystant (Asyst Software Technologies, Inc.). This data was then transformed, and the array thus obtained, smoothed by applying a Blackman window low pass filter to each row. The cutoff frequency of the filter was set so as to reduce most of the noise (0.15 relative units) and entered in units of cycles per point.

The wave generated by the program was either processed further in that the FWHM was calculated in order to determine the electron density, or the wave data was applied to the program for calculating the Abel inversion. In the case of the H_α lines, only the magnitude of the intensity was determined.

The flow diagram of the procedure may be seen in Fig. 3.2.

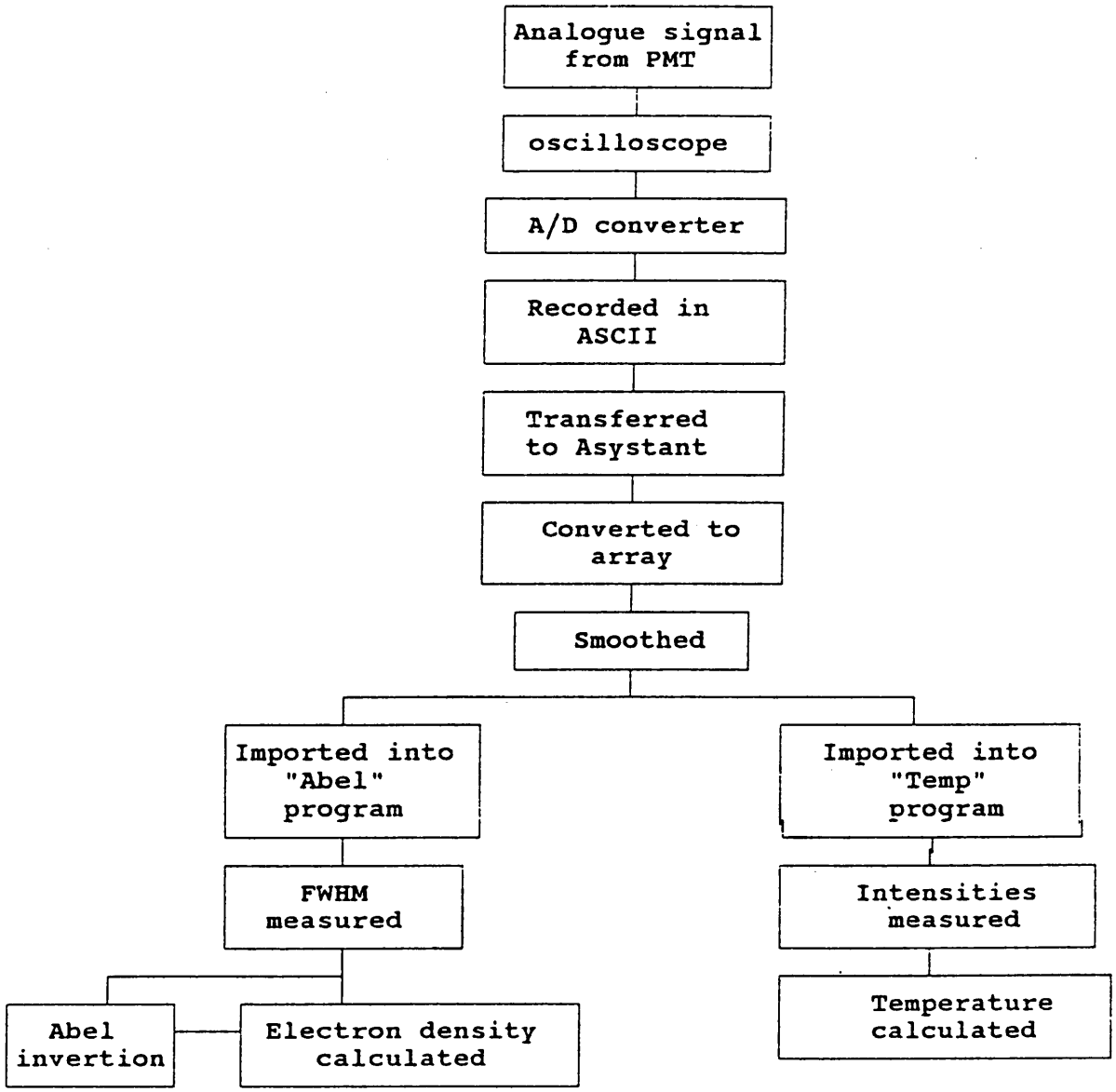

Figure 3.2 Procedure followed in calculating temperature or electron density.

3.2.4 Abel inversion

The Abel integral inversion was calculated, by the programme of Prof Visser, according to the technique of Freeman and Katz (1962). The intensity data, $I(x_i)$, was obtained for equidistant lateral x_i-coordinates from the cylindrical symmetric source. The wavelength index for the peak of the spectral line was determined for each lateral position and the wavelength distributions synchronized. Maximum and minimum wavelength indices that were used in the integral inversion calculation were determined from this skewness.

Radial origin of the plasma was extrapolated from symmetry considerations of the lateral intensities at the spectral line's peak wavelength. The Abel integral inversion was then calculated for each wavelength by fitting a sixth order polynomial over the lateral intensities at that particular wavelength, as well as a summation process, to calculate the radial intensities at the different radial indices, for that wavelength channel.

3.2.5 Instrumental parameters

The instrumental parameters as used are given in Table 3.1.

Table 3.1. ICP-OES operating parameters

Forward power	1.3 kW
Plasma gas flow rate	1 l min^{-1}
Coolant gas flow rate	14 l min^{-1}
Nebulizer	Crossflow
Nebulizer gas flow rate	1 l min^{-1}
Nebulizer gas pressure	1.0 bar
Sample uptake rate	2.5 ml min^{-1}
Spray chamber	Scott, glass
Torch	Internal diameter 16 mm

3.3 Results and Discussion

3.3.1 Electron density

The method used to determine the FWHM involved recording a number of data points as the line was scanned. The program, Asystant, allows 256 data points to be evaluated in one determination. The limited number of data points, together with the problems associated with smoothing, may have led to an inherent error in the system. In the smoothing process the peak may be reduced in size and this could influence the FWHM. The magnitude of this error is dependent upon the amount of smoothing required (i.e. the signal-to-noise ratio), and consequently was larger for peaks with small signal-to-noise ratio's. In the extreme case an error of 15 % was possible, which decreased to 7.5 % when a large signal-to-noise ratio was obtained. The uncertainties due to the application of the Abel inversion were discussed by Cremer and Birkebak (1966). Even taking these possible errors into consideration, the values calculated for n_e and given in Figs. 3.3a, b, c, and d are in agreement with those found in the literature (Grieg *et al*: 1968 and Hill: 1968).

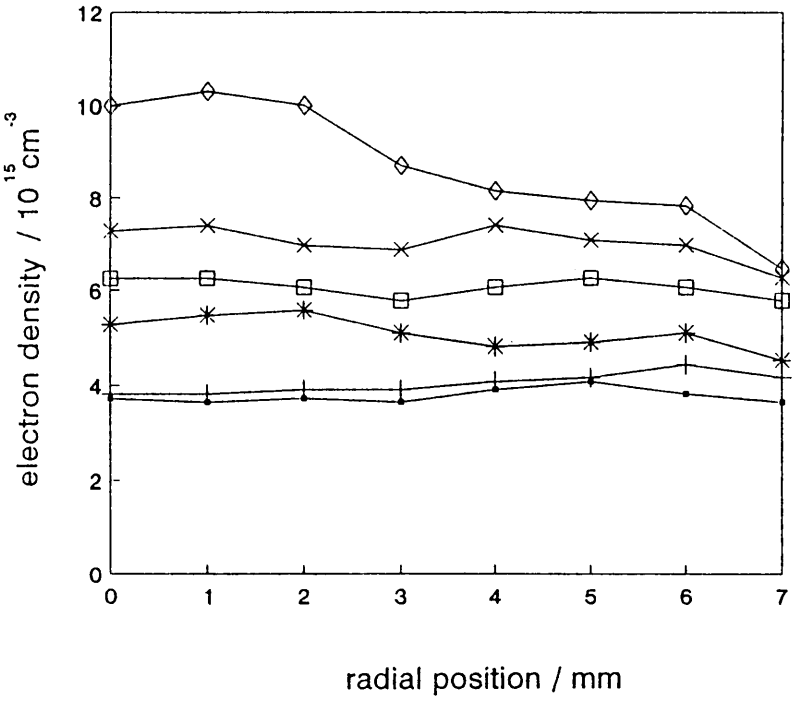

Figure 3.3a Radial electron density of the plasma across the torch for increasing ethanol concentrations, where (a) z = 0 mm, for: (⊡) 0 %, (+) 5 %, (✳) 10 %, (□) 15 %, (x) 20 % and (◇) 25 % ethanol.

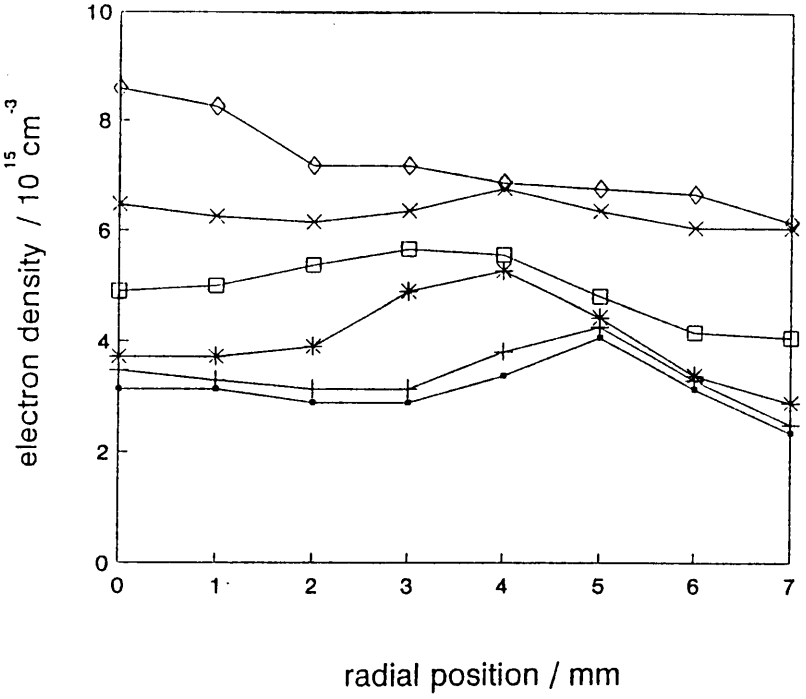

(b)

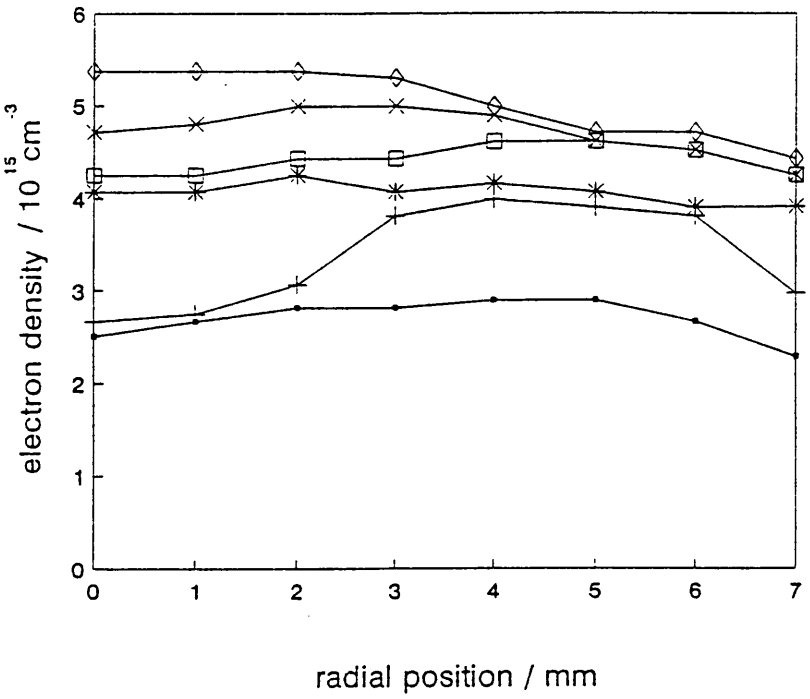

(c)

Figure 3.3b,c Radial electron density of the plasma across the torch for increasing ethanol concentrations, where (b) z = 5 mm and (c) z = 10 mm, for: (⊡) 0 %, (+) 5 %, (✳) 10 %, (□) 15 %, (x) 20 % and (◇) 25 % ethanol.

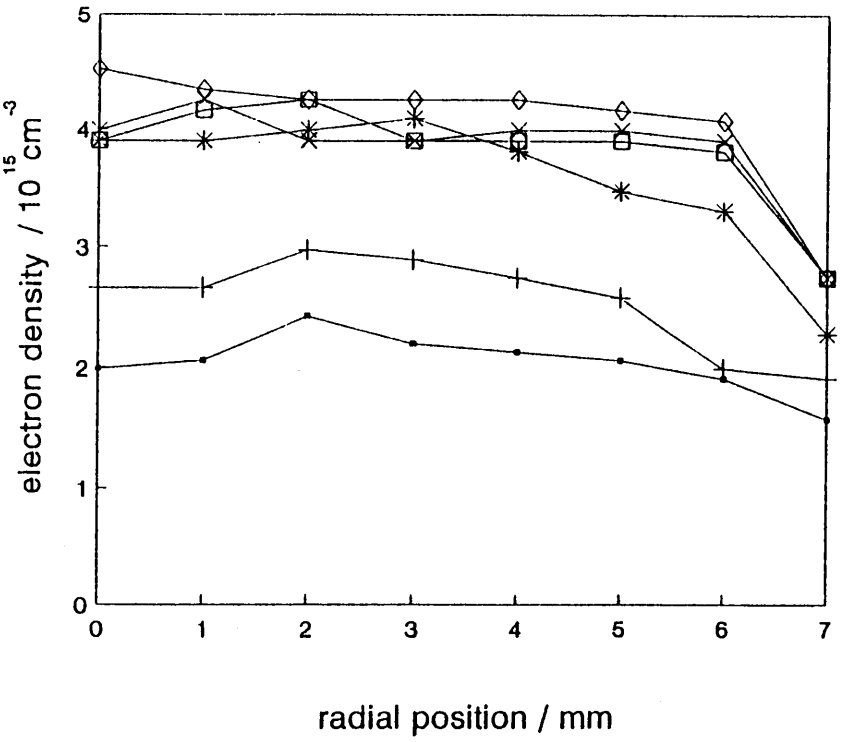

Figure 3.3d Radial electron density of the plasma across the torch for increasing ethanol concentrations, where (d) z = 15 mm, for: (⊡) 0 %, (+) 5 %, (✳) 10 %, (□) 15 %, (x) 20 % and (◊) 25 % ethanol.

The values that were obtained from Abel inversion were checked by determining the electron density for z = 0 mm, without inversion. The results may be found in Fig. 3.4. From the results presented in Figs. 3.3a - d and 3.4, it can be seen that the electron density increased as the concentration of the ethanol in the sample solution was increased. A further observation can be made from studying Figs. 3.3a - d. The electron density as shown in Fig. 3.3a reached a maximum 5 mm from the centre of the torch when water was aspirated. The position of this maximum changed as the ethanol concentration was increased, and was situated in the centre of the torch when the highest concentration, i.e. 25 % ethanol was aspirated. Similar observations may be made from the results shown in Fig. 3.3b, c and d, when z = 5, 10 and 15 mm.

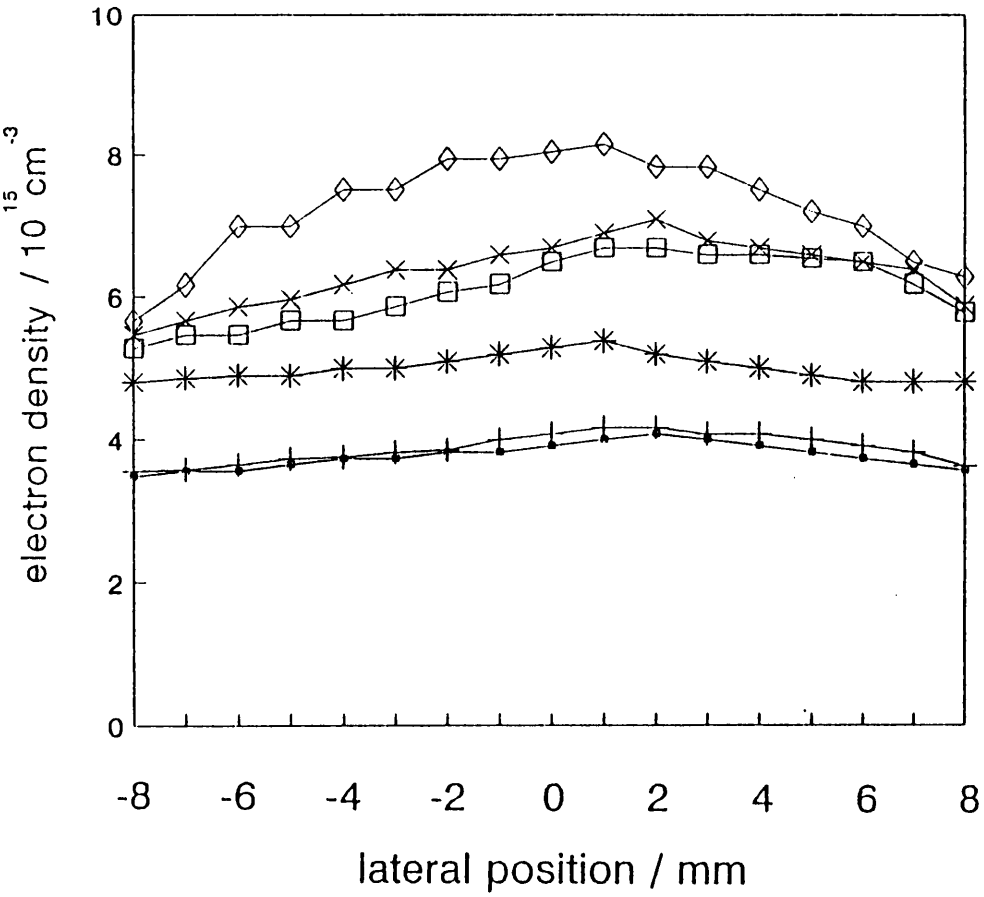

Figure 3.4 Electron density just above the load coil, without Abel inversion for: (⊡) 0 %, (+) 5 %, (✳) 10 %, (□) 15 %, (x) 20 % and (◊) 25 % ethanol.

These changes in electron density may also be noted in Fig. 3.4, but since the results have not been inverted they are not as easily evaluated. The increase in electron density with increase in ethanol concentration is obvious, however the change in the position of the electron densities' maximum was not so readily observed. If the changes in n_e are considered for the case when only water was aspirated, then the electron density increase by a factor of 1.17. This factor increased as the concentration of the ethanol increased, and reached a maximum of 1.44 when 25 % ethanol was aspirated.

3.3.2 Excitation Temperature

The changes in temperature of the plasma 15 mm above the load coil are given in Fig. 3.6 for various ethanol solutions. The difference in temperature between 0 and 5 %

ethanol was 600 K, and the temperature within the plasma continued to increase to a maximum when the solution contained 15 % ethanol. Thereafter the temperature decreased and at 25 % was almost equal to that obtained with pure water. The temperature was measured at 15 mm above the load coil since the signal intensities above that height became too small for accurate measurement (less than 5 % of the value at z = 0 mm). Below 15 mm the difference in temperature for the various ethanol concentrations was not as marked as a more uniform temperature was maintained.

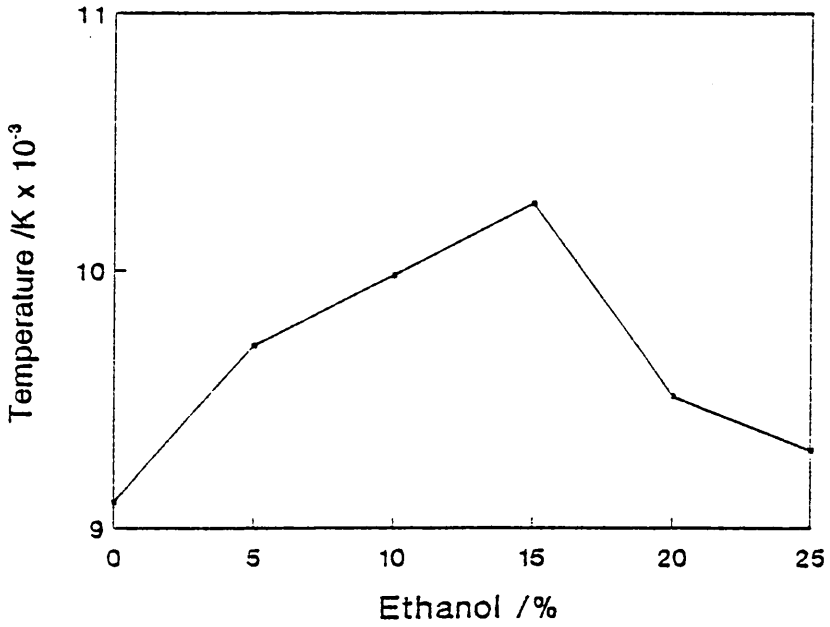

Figure 3.5 Excitation temperature of the plasma with increasing ethanol concentration. Viewed from the centre of the plasma at a height of 15 mm above the load coil.

The lateral change of excitation temperature, at the centre of the plasma, with observation height for an ethanol solution may be seen in Fig. 3.6. The temperature first increases to a maximum at 5 mm above the load coil, then proceeds to fall as the observation height was increased. This increase was found for all the solutions.

Electron density did not reach a maximum, for the ethanol concentrations used, in the same way as the excitation temperature. The increase in electron density was found

both at a distance of 5 and 0 mm from the centre of the plasma, but was most pronounced for r = 0 mm. This was found for all heights above the load coil, but demonstrated by the results given for just above the load coil (z = 0 mm), where the effect was greatest.

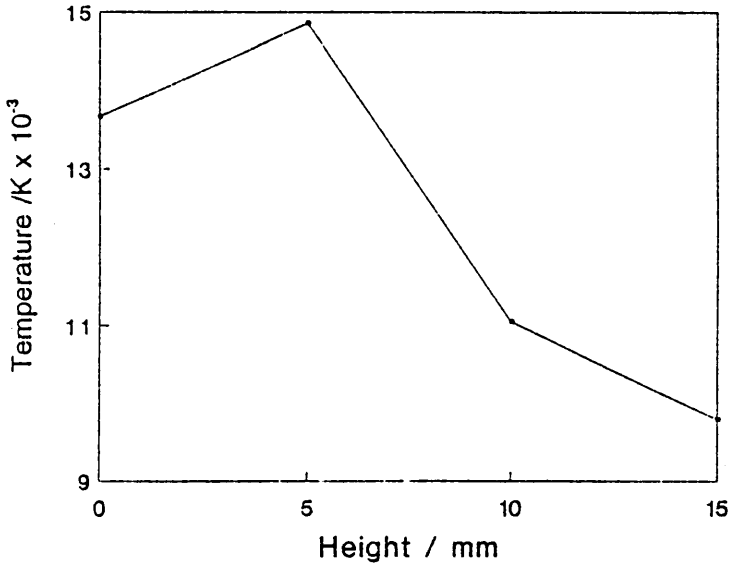

Figure 3.6 Excitation temperature of the plasma at various observation heights when 10 % ethanol solution was aspirated.

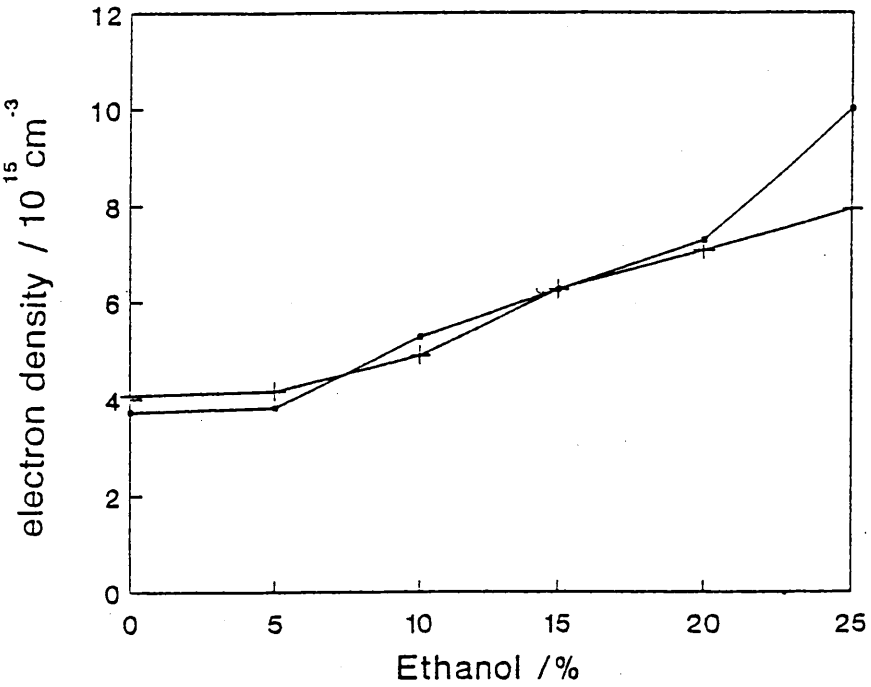

Figure 3.7 Electron density for increasing ethanol concentration, after Abel inversion, at z = 0 and at a radius of 0 (⊡) and 5 (+) mm.

The increase in excitation temperature with increasing ethanol concentration is in agreement with the findings of Benli (1983), but contrary to many other authors (Boorn and Browner: 1982, Goldfarb and Goldfarb: 1985, and Blades and Caughlin: 1985). In the case of Benli (1983), as with this investigation, he was concerned primarily with the influence of ethanol on aqueous solutions. In the case of the other authors, their primary goal was the investigation of other organic solvents and only in passing was ethanol included in the list of solutions investigated.

CHAPTER 4

AEROSOL DROP SIZE DISTRIBUTION AND MASS FLOW RATE

4.1 Introduction

The introduction of the sample and solvent into the flame or plasma is of fundamental importance to both atomic absorption spectroscopy (AAS) and ICP-OES. Both techniques require fine aerosol production, ICP-OES more than AAS (less than 1 μm in diameter for both techniques), and both usually use a pneumatic nebulizer and a spray chamber. For this reason it is of great importance to optimize the nebulizer-spray chamber system.

The drop size distribution of ethanol and ethanol/aqueous mixtures could be expected to differ from that of pure water because of the different physical characteristics of the two solvents. The physical parameters that would be of importance are those of density, viscosity and surface tension. The different characteristics would lead to changes in both the primary and tertiary drop size distribution. It was, therefore, necessary to investigate possible changes occurring in the physical properties of the material entering the plasma.

4.2 Review of the literature

Transport phenomena are processes that can modify the aerosol produced by the nebulizer on its way to the atomization cell. The first of these processes is the generation of primary aerosol. For concentric pneumatic nebulizers this processes has been governed by the Nukiyama-Tanasawa equation (Nukiyama and Tanasawa: 1940):

$$d_s = 585/V(\sigma/\rho)^{0.5} + 597(\eta/[\sigma\rho]^{0.5})^{0.45}(10^3 Q_l/Q_g)^{1.5} \qquad 4.1$$

where V (m s^{-1}) is the difference in velocities of the gas and liquids entering the nebulizer, σ (dyn cm^{-1}), ρ (g cm^{-3}) and η (dyn s cm^{-2}) are the surface tension, density and viscosity of the liquid respectively, and Q_l and Q_g (cm^3 s^{-1}) the volume flow rates of the liquid and gas respectively. The equation is used to determine d_s (μm) the Sauter median diameter of the droplets and is the measure of the ratio of total volume to total surface of the aerosol.

Equation 4.1 was derived for a particular type of concentric nebulizer operating at subsonic gas velocities. The liquids used had surface tension values between 30 and 73 dyn cm^{-1} and viscosities between 0.01 and 0.3 dyn s cm^{-2}. It is possible that because these specific applications are not necessary those required with pneumatic nebulizers and solutions associated with ICP-OES's that this equation has been thought to suffer from certain limitations (Gustavsson: 1983 and 1984). Furthermore, the two parts of the equation are not dimensionally alike, due to the fact that the equation was derived empirically. Consequently it does not provide a microscopic description of the processes which take place at the nebulization stage (Gustavsson: 1984).

W_{tot} and S_{tot}, the total mass of analyte and solvent transport rate respectively, are two parameters determined by the processes that occur during aerosol transport. These parameters, together with the characteristics of tertiary aerosol, are amongst the most important for determining aerosol processes which influence analytical signals. A second set of processes that will also influence the analytical signal is one which results from interactions of aerosol drops with the plasma (Browner, Canals and Hernandis: 1992).
Gustavsson (1987) listed eight different processes by which the separation of large droplets could take place in a spray chamber:

(i) Gravitational settling.
(ii) Inertial deposition.
(iii) Turbulence.
(iv) Flow-line interception.
(v) Diffusional deposition.

(vi) Electrostatic deposition.

(vii) Thermal precipitation.

(viii) Sonic agglomeration.

Only the first three processes are applicable to the standard spray chambers used in ICP-OES. This is not to say that other processes cannot play a role in the separation system as shown by Tracy *et al* (1982) who experimented with the influence of electrostatic forces on the aerosol. They found that both the signal and noise varied as they change the electrostatic field around the aerosol chamber.

The pre-atomization drop size, or tertiary drop size, is determined primarily by the evaporation of the solvent from the surface, according to Boorn *et al* (1980). In his work he found that the diameter at time t(s), d_t, could be calculated from:

$$d_t = (d_o^3 - E)^{1/3} \qquad 4.2$$

where d_o is the initial drop diameter (μm) and E the evaporation factor are given by:

$$E = 48\ D_v \sigma P_s M^2 (\rho TR)^{-2} \qquad 4.3$$

where D_v is the diffusion constant for the solvent vapour, P_s the saturated pressure, M the molecular mass, ρ the density, σ the surface tension, R the gas constant and T the absolute temperature. From the evaporation curves, Boorn and co-workers showed that evaporation, even in a short period of time (tenths of a second), caused a decrease at the micrometer level, in the diameter.

The spray chamber was regarded by Gustavsson (1987) as a filter with cutoff diameter d_c. Droplets with diameter greater than this will be retained and drained to waste, while smaller droplets pass through unaffected. This is an oversimplification as within the chamber these smaller droplets themselves will be exposed to a variety of different forces and processes as may seen from the above. According to Gustavsson, the final (tertiary) aerosol have mean diameter greater than d_c.

Various authors have supported the different processes for separation of droplets. In the review of the fundamental and theoretical aspects of spray chamber operations published by Gustavsson (1984), he concluded that the most important process determining the separation of larger droplets in the spray chamber was inertial impaction. Browner *et al* (1982) described the separation to turbulent losses in an ICP-OES aerosol chamber of the dual concentric type, having investigated gravitational settling, inertial deposition, turbulence, and centrifugal loss. Novak and Browner (1980) thought the separation to be due to gravitational settling. Skogerboe and Olson (1978) investigated inertial deposition and gravitational settling and found that the latter was responsible for primary limitations on aerosol transport, for the chambers they studied.

A mathematical model for the nebulization process in a spray chamber without an impact bead was proposed by Gustavsson (1983). From this the cutoff diameter could be calculated by considering the normal distribution, the efficiency and the aerosol concentration. The selection process for the primary generated aerosol in a spray chamber with a cutoff diameter d_c is given in Fig. 4.1.

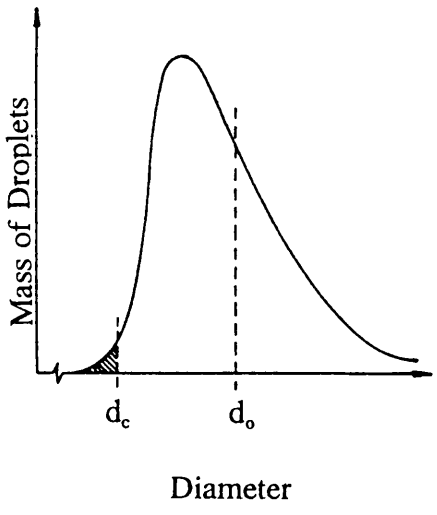

Figure 4.1 Selection of droplets from the primary aerosol in a spray chamber without impact bead (Gustavsson: 1987).

The shaded section represents the aerosol which will proceed into the torch. The proportion of aerosol represented by the shaded area, i.e. the percentage of the volume having droplets smaller than d_c, is given by the expression (Gustavsson: 1987):

$$\phi([\ln d_c - \ln d_s]/\sigma^*) \qquad 4.4$$

where σ^* is the standard deviation of the normal distribution given by the log-normal distribution, and ϕ is a function of the standardized normal distribution of the type:

$$\phi(x) = 1/(2\pi)^{1/2} \int_{-\infty}^{x} \exp(-t^2/2)\, dt \qquad 4.5$$

The University of Alicante in Spain, and particularly Antonio Canals and Vicente Hernandis have been involved in an in-depth investigation of the whole aerosol generation and transportation process. Together with Browner (Canals *et al*: 1990b), they looked at the evolution of drop size distribution for pneumatically generated aerosols in an ICP-OES. They used a laser Fraunhofer diffraction system at various positions along the trajectory of the aerosol within the spray chamber to measure the drop size distribution. With this system they investigated three factors which influenced the drop size:

(i) Nebulizing gas and liquid flow.

(ii) Design and dimensions of the nebulizers.

(iii) The effect that the physical properties of the solvent.

One cross-flow and three concentric glass nebulizers were used and the aerosol measured at four positions, the third being just at the outlet of the inner tube. The gas pressure within the spray chamber was only a few torr higher than in the atmosphere, once the glass tube had been removed so as to be able to measure at position 3. The bottom wall, which had been removed, would not influence the aerosol to any great extent, and the authors therefore felt that measurements at that position would correspond to the distribution that the aerosol would exhibit as it exited the inner tube. From this they deduced that they would be measuring the tertiary drop size distribution at that position (position 3).

When investigating the effect of solvent type on the drop size distribution, the above authors looked at water, methanol and n-butanol. They found that for the Sauter mean diameter for the different solvents was as follows; methanol < n-butanol < water. The progression followed the trend of the surface tension and they concluded that the surface tension was more important than the relative volatility. The order found for the Sauter mean drop size was followed at the first two positions, but by the fourth position the methanol was coarser than the other two solvents as may been in Fig. 4.2.

They used the following formula for the calculation of Sauter mean diameter:

$$d_s = \left[\int_{D_o}^{D_m} D^3 \, n(D) \, dD \right] / \left[\int_{D_o}^{D_m} D^2 \, n(D) \, dD \right] \qquad 4.6$$

where D was the drop diameter and n(D) the number of drops of diameter D. D_o and D_m were the lower and upper limits of the distribution, respectively.

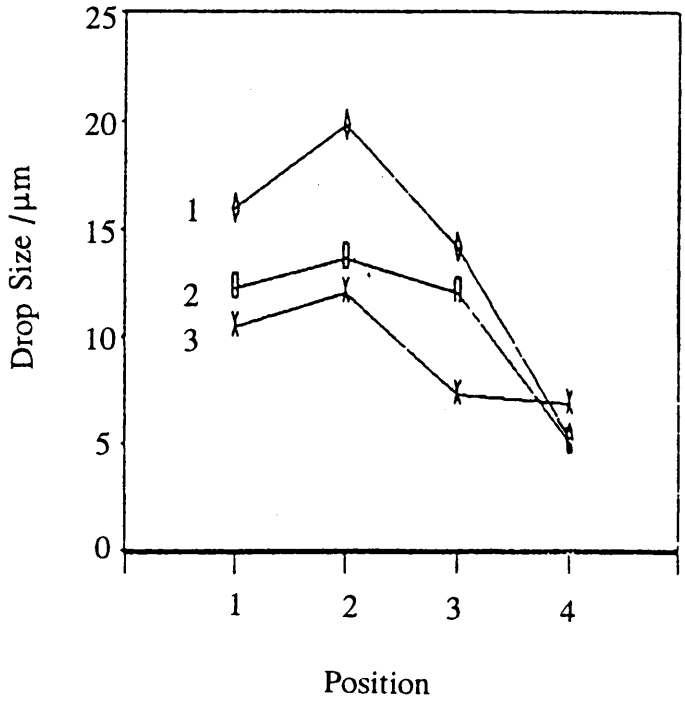

Figure 4.2 Changes in Sauter mean diameter along the trajectory for different solvent; (1) water, (2) n-butanol, and (3) methanol using a concentric nebulizer and gas flow rate of 0.65 l min^{-1} and liquid rate of 0.63 ml min^{-1} (Canals *et al*: 1990b).

The conclusions that they reached were as follows:

(i) the nebulizer gas flow had the greatest effect on the drop size distribution for both primary and tertiary aerosols,

(ii) the main processes that altered the primary aerosol were coalescence, evaporation, gravitational losses, impaction losses and inertial losses,

(iii) in the first section of the nebulizer, coalescence and evaporation were the main factors affecting drop size distribution,

(iv) in the second section of the spray chamber and just before the exit (position 3), a significant loss of liquid was found which was the result of impaction loss processes,

(v) between the final two positions the modification in aerosol distribution was due to inertial losses. The coarser the aerosol the greater these losses were and could even result in the drop size being reduced, and

(vi) low gas flow, high liquid flow, high surface tension, low relative volatility, large cross-sectional area for the gas outlet and cross-flow nebulizer all tended to increase the mean droplet size.

Canals, Hernandis and Browner (1990a) had in an earlier article compared the measurements they made of the Sauter mean drop size using the instrumentation and solvents discussed above and compared them to the results calculated from the Nukiyama and Tanasawa equation (equation 4.1). In the investigation they again altered the design of the nebulizer nozzle, used the same three solvent and varied the gas and liquid flow rates. They found that there was poor agreement between experimental and predicted results. In all the conditions evaluated, the mean Sauter drop size calculated from equation 4.1 far exceeded those found using the experimental setup. According to the conclusion reached by the authors, the d_s values found for methanol and n-butanol were always lower than those for water, which was not the case with the results from the Nukiyama-Tanasawa equation. Here, the results for water were lower than those for n-butanol, but similar to those calculated for methanol.

From the results of their investigation they concluded that the concentric nebulizers were more effective than the cross-flow type in the production of fine aerosol. They also found that the most effective concentric nebulizer was one with low gas cross-section, since it yielded the aerosol with smallest drop size distribution.

In their next article Browner, Canals and Hernandis (1992) looked at the effect that the transport of analyte and solvent had on the signal intensities of an ICP-OES. Again the three solvents were used as well as one cross-flow and three concentric nebulizers. On this occasion the aerosol was measured 8 mm above the central injection tube of the ICP torch by their system. To complete data analysis additional parameters were introduced. Distinction was made between tertiary Sauter mean drop diameters, td_s ($tD_{3,2}$ in the article) and primary drop diameters, pd_s. Analyte and solvent transport efficiencies, ϵ_n and ϵ_s, were used to evaluate systems.

Major changes in primary drop size after passing through the spray chamber Browner *et al* (1992) found resulted in changes to the analyte transport efficiency, ϵ_n. An average decrease of 270 % was found for the analyte transport efficiency as Q_l was increased from 0.63 to 1.90 ml min^{-1}. The same percentage decrease was found for the ϵ_s. They deduced that the decrease in the analyte transport efficiency resulted from the increase in pd_s, which in turn meant that fewer droplets passed through the "filter" and into the torch.

The signal intensities determined in the investigation are reproduced in Table 4.1 below. The very high result they obtained for methanol when compared to water and n-butanol presented considerable difficulty. The authors decided that this was as a result of the laser Fraunhofer system they employed to determine the drop size. The instrumentation they used was unable to measure droplets of diameter smaller than 1.2 µm. An aerosol with distribution initially containing drops in the range 1.2 - 5 µm would, they decided, appear to the light scattering system to actually contain a higher volume fraction of larger drops than did the original, unevaporated aerosol.

Table 4.1 Effect of solvent type on tertiary aerosol drop size, transport parameters and emission intensities (Browner *et al*: 1992).

Solvent	td_s /µm	S_{tot} /µg s^{-1}	W_{tot} /µg s^{-1}	I_{net} /x 10^{-4}
water	5.2	320	0.09	1.4
n-butanol	5.0	542	0.41	4.9
methanol	6.6	2167	0.55	-

The fraction of small drops below 5 µm in diameter in the primary aerosol was quite low (< 2 %) of the total aerosol mass. After the loss of larger droplets which occurs within the spray chamber the resulting tertiary aerosol would have a substantially higher fraction of smaller drops. Since their system could not measure below 1.2 µm the authors argued that the contribution of these smaller drops was not included in the measurements made by the instrument. A false percentage of drops was given, accounting for the anomalously high value for methanol in Table 4.1.

They also concluded that the large increase found for W_{tot} and S_{tot} (methanol having a mass transport of analyte 6.8 times higher than water) was as a result of the solvent which had evaporated from the larger drops not being lost to the system, but travelling instead to the plasma as solvent vapour.

The methanol introduced into their measuring system resulted in the plasma being extinguished and hence the signal intensity for that amount of methanol could not be determined. They concluded that though the factors which resulted in the plasma being extinguished were complex, it probably was related to dissociation energy and gas dynamics. From Table 4.1 it can be calculated that for complete atomization of the 320 µg of water 3.9 cal would be required, while for the 2167 µg of methanol 32.6 cal would be required, a factor of 8.4. The combination of greater volume

expansion and energy absorption was considered by these authors to be the major contributing factor to the intolerance of the plasma to the methanol.

There are many similarities between the aerosol production in flame atomic absorption spectroscopy, FAAS, and ICP-OES, even though the solution is not pumped into the nebulizer as is the case in ICP-OES. Both make use of pneumatic nebulizers and both send larger drops to waste after a separation process. Robles, Mora and Canals (1992) evaluated the Nukiyama-Tanasawa equation for the pneumatically generation of aerosols in FAAS, while Mora, Hernandis and Canals (1991) looked at influences of solvent physical properties on drop size distribution, transport and sensitivity in FAAS. Both groups used a laser Fraunhofer diffraction system to measure the Sauter mean diameter, and investigated the effects of gas and liquid flows and physical properties of the solvent had on the drop size distribution. The results obtained by Robles *et al* showed that equation 4.1 correctly described the trends of Sauter mean diameter variations with aerosol changes, but that they far exceeded the experimental values obtained for the drop size.

The difference between predicted and experimental Sauter mean diameter was greatest at high liquid flow to nebulizing gas flow ratios. They found a 3.6 - 13.3 fold overestimation of drop size for methanol-water mixtures. The chief cause of this discrepancy, they suggested, was the second term of the Nukiyama-Tanasawa equation carrying too great a weight in the calculations of the Sauter mean diameter. Although the values of the physical properties appeared in both terms of the equation, they were more pronounced in the second term and would consequently have had a greater effect. Mora *et al* found that the analyte transport rate was improved by a high solvent volatility and by small drop size distribution. Absorbance values followed the same trend.

Two tables in the publication of Mora *et al* (1991), are of particular interest since they relate to the drop size distribution and transport efficiency of methanol and methanol mixtures in the FAAS. They are combined and the important information reproduced below in Table 4.2.

Table 4.2 Distribution parameters and transport details for water/methanol (v/v) mixtures according to Mora *et al* (1991).

Solvent Methanol /%	Water /%	D_{50} /μm	SSA /m^2 ml^{-1}	S_{tot} /ml min^{-1}	W_{tot} /μg min^{-1}	ϵ_s /%	OB
0	100	17.0	0.7092	0.41	0.41	9.1	0.1434
10	90	16.5	0.7503	0.52	0.48	11.2	0.1687
25	75	15.5	0.8020	0.64	0.57	14.2	0.1854
50	50	13.8	0.9111	1.06	0.89	23.0	0.1971
60	40	13.2	0.9538	1.42	1.56	28.7	0.2000
80	20	11.9	1.0519	1.77	2.24	36.3	0.2056
90	10	10.9	1.1013	2.00	2.56	40.9	0.2190
100	0	9.7	1.1966	2.26	2.82	50.2	0.2094

where D_{50} is the droplet distribution diameter below which 50 % of the cumulative aerosol volume was found, SSA the specific surface area of the aerosol and OB the obscuration, a value which indicated the proportion of incident light that was scattered out of the beam by the aerosol. The other symbol retain their meaning.

Clearly, from Table 4.2 it may be seen that the drop size decreased as the methanol concentration increased. The dramatic increase in transport efficiency of the solvent (ϵ_s) should also be noted. The laser Fraunhofer diffraction instrument used had a cutoff at 1.9 μm.

Greenfield *et al* (1976) studied the effect of high acid concentrations in the sample solution, on the signal intensity of a high-power plasma. In the case of mineral acids they found that the intensity was reduced by a factor which they could correlate to the increased viscosity, but with organic acids they concluded that the expected reduction

because of changed viscosity was outweighed by differences in surface tension and density. They attributed the dependence of all the effects to the solution properties rather than the plasma source. Using their results they had obtained, Greenfield *et al* proposed the following equation, determined empirically, which relates signal intensity to physical properties:

$$I_s = I_w\ [\eta/(\rho\,\sigma)^{0.5}][7.055/\eta\ +\ 1.245] \qquad 4.7$$

where I_s and I_w are the signal intensities of the solvent and water respectively, η, the organic solvents viscosity, σ, the surface tension and ρ, the density. The ratio, I_s/I_w, is the enhancement factor, since it gives the improvement in the intensity signal that the addition of the solvent would bring about.

Todorovic, Vidovic and Ilic (1993) investigated the effect of aqueous organic solvents for the determination of trace elements in both FAAS and ICP-OES. Unlike the previous group of Canals and Hernandis, the organic solutions were added to water in increasing percentages, they did not use the pure solvents. Additions of acetone, ethanol, ethylene glycol, glycerol and 1,4-dioxane to aqueous solutions were used to investigate the signal intensities of Ca, Cd, Cu and Fe. Their study found no relationship, linear or logarithmic, between the measured signal intensity and any physical parameter.

Using equation 4.4, Todorovic *et al,* found that additions of any of the solvents investigated to the analyte solution brought about an increase in signal intensity, but the order that the solvents followed was: ethanol > acetone > dioxane > ethylene glycol > glycerol. They also used the Nukiyama-Tanasawa equation to calculate the ratio of mean droplet diameter of the aqueous organic (d_s) to the aqueous (d_w) solvent when applying an ICP-OES. These results are reproduced in Table 4.3.

They finally concluded that the effect of the organic solvent addition depended not only on the physical properties of the solution, but also the atomization efficiency which is dependent on the element being investigated.

Table 4.3 Sauter mean diameter ratio for aqueous organic solvent to water in an ICP-OES, according to Todorovic *et al* (1993).

Organic solvent content /% (v/v)	Acetone	Ethanol	d_s/d_w Dioxane	Ethylene glycol	Glycerol
1.0	0.97	0.98	0.99	1.00	1.01
5.0	0.95	0.96	0.96	1.01	1.01
10.0	0.94	1.00	0.95	1.02	1.01
20.0	0.94	1.01	0.96	1.04	1.04
40.0	0.96	1.07	1.00	1.11	1.15

Yanping and Zhanxia (1994) recently developed a Monte Carlo simulation of the nebulization process within the ICP-OES. The study was based on the drop size distribution being Gaussian and that aerosol droplet loss due to gravitational settling, impaction, turbulence and centrifugation was random. They proposed a jet model for calculating the variations of the aerosol flow velocity in a spray chamber. The Monte Carlo program written by them for three nebulizer nozzles supplied by Canals *et al* (1990), yielded results for ϵ_n and W_{tot} which compared favourably with those obtained by Browner *et al* (1992).

Yanping and Zhanxia found that the aerosol flow velocity distribution was a function of the radial and axial distances of the chamber. The results of their work (Yanping *et al*: 1994) indicated that the predominant loss mechanism depended strongly on the gas flow. They hope to publish results on the relationship between signal intensity and aerosol particle behaviour, the vaporization, atomization and ionization processes within an ICP in a future paper.

4.3 Experimental

4.3.1 Reagents

The same ethanol and water mixtures were used as in Chapter 3, section 3.2.2.

4.3.2 Apparatus

4.3.2.1 Micro Laser Particle Spectrometer

A micro laser particle spectrometer by Particle Measuring Systems, Inc., PMS, model μLPS-16 was used to perform pulse height analysis (PHA). A gas viewing module sensor (GVMS), PMS model GVMS was used for the aerosol sampling. The GVMS used a He-Ne polarized laser operating in a TeM mode of operation (Operating and Servicing Manual: 1986). The laser (1), in Fig. 4.3 had an output mirror (2) at one end from which the polarized beam was sent to the polarizing beamsplitter cube (3).

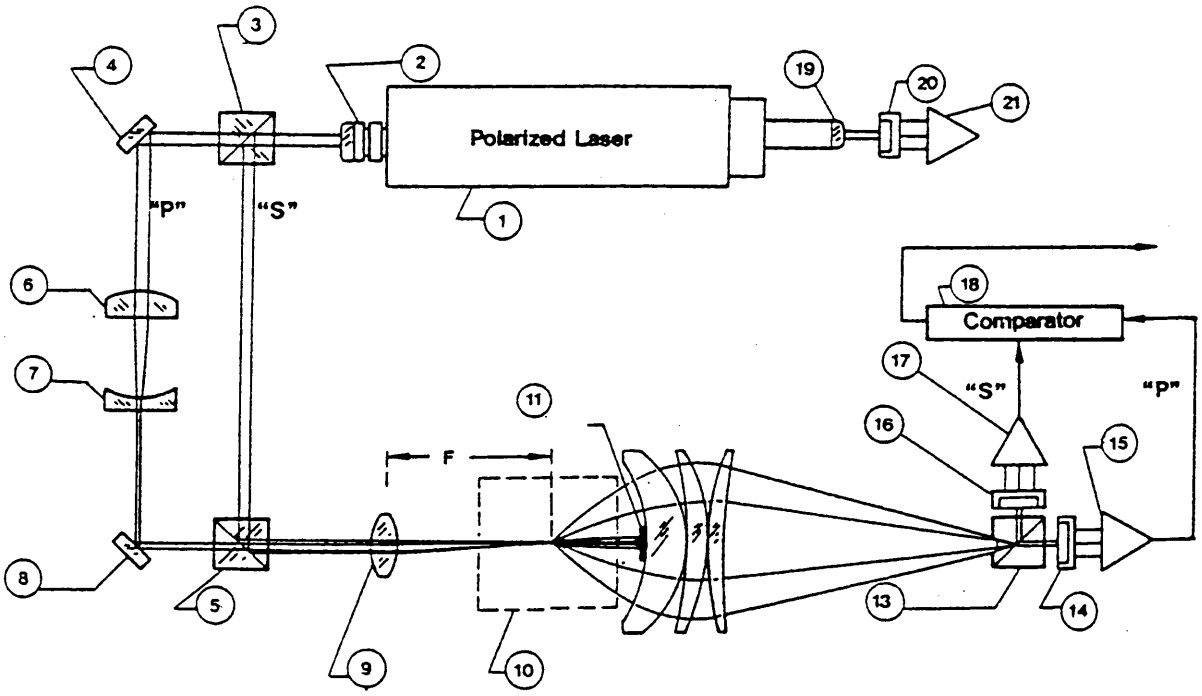

Figure 4.3 GVMS sensor optics used for particle size determination (Operating and Servicing Manual: 1986)

The light was split into two orthogonally polarized components "S" and "P" (the reflected beam was "S", the transmitted beam "P"). The two beams were treated independently. The "P" component was coupled to a mirror (4), while the "S" component remained collimated and was coupled to a recollimating beamsplitter cube (5). The "P" component was shaped in one dimension by the positive and negative cylindrical lenses (6 and 7). The now modified beam was reflected off the plane mirror (8) to the recollimating beamsplitter cube (5). At the cube (5), the "P" and "S" components were recombined to form a beam combination as may be seen in Fig 4.4. The beams had equal widths in one direction, but "P" was contracted in the other direction.

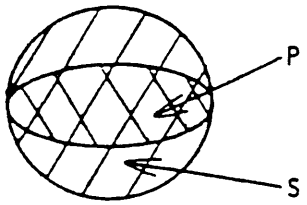

Figure 4.4 The recombined beams "P" and "S".

A condensing lens (9) focused the beam combination onto the sample chamber (10). At the focal point of lens (9), the elipticity of beam "P" was inverted as shown in Fig. 4.5. "P" was now elongated in the direction in which it was previously foreshortened. Particle flow in the sample chamber was at right angles to the elongated dimension. In the region near the focus of the condensing lens, the "S" polarized component converged more rapidly than did the "P" component. If the beams were of nearly equal power, then a central uniform intensity region would exist where the "S" component was equal or greater than the "P" component.

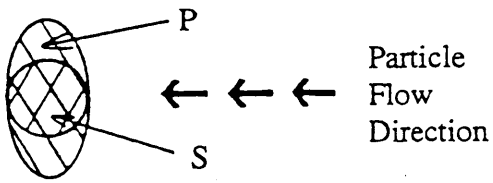

Figure 4.5 Beam construction as it passed through sample cell.

Light would be scattered from both the "P" and "S" component should a particle pass through the beam combination. The transmitted light (not scattered) was collected and absorbed by a dumping spot (11). The scattered light falling outside this spot was collected and refocused by a set of collecting optics coaxially positioned. This light was focused onto a collecting polarized beamsplitter cube (13), where the combined beam was again separated, "P" being coupled to the sizing photodiode (14) and associated preamplifier (15), the "S" component being coupled to the Acceptance photodiode (16) and its preamplifier (17).

The data acquisition system amplified the components "P" and "S", the "P" component being used to for particle measurement of the central uniform intensity region, while "S" simply established a region of localized interest. The "P" component acted as the measuring or sizing beam, while "S" was the acceptance beam. If "S" was greater than or equal to "P", the measurement of particle size given by "P" was accepted, if not, then it was rejected.

The laser supplied a reference output through a sealed mirror (19) to a reference photodiode (20) connected to a reference photodetector (21).

The GVMS was placed in the particle spectrometer and the electrical pulses sent out by the sensor were processed by the μLPS-16 and through a technique called PHA were correlated with particles of various sizes. Each pulse was interpreted as having come from a particle having a given size within a given range. The μLPS-16 counted all the particles detected in each of 15 fixed size classed. An example of one collection is given in Fig 4.6 for 25 % ethanol solution. Fig. 4.6 is a copy of the printout produced by the printer attached to the μLPS-16. The left-hand column of the first section gives the drop size measured, the second column the number of drops found of that size, and the final column gives the accumulated tally.

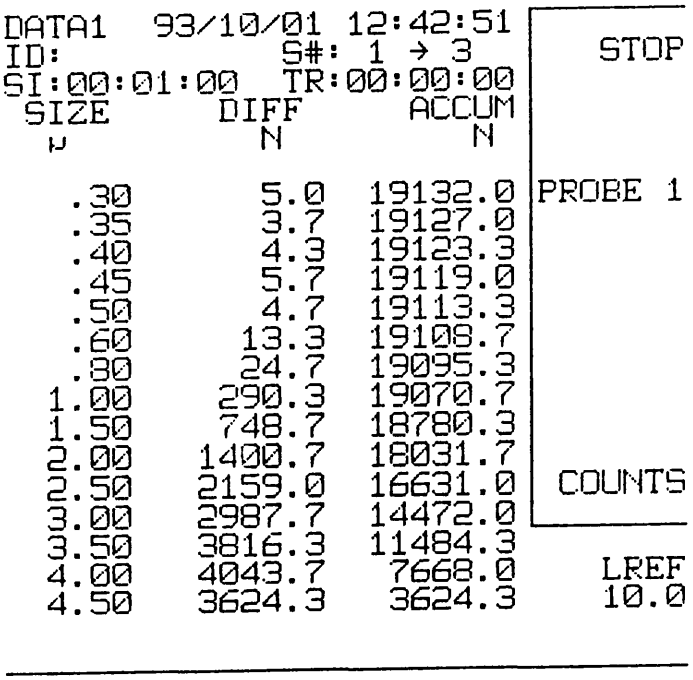

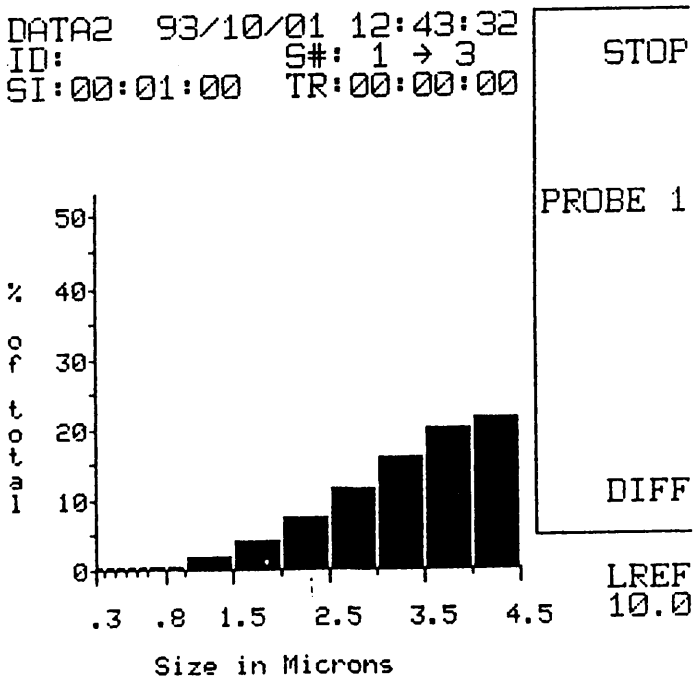

Figure 4.6 Example of particle size measurement using the µLPS-16. Sample solution contained 25 % ethanol.

4.3.3 Procedure

4.3.3.1 Drop-size distribution

The aerosol emitted from the sample injection tube of the ICP torch was transferred to the measuring cell of the laser particle counter by means of a plastic tube of internal diameter 5 mm. It was found that the aerosol flow was so dense that the laser beam was totally absorbed by the vapour cloud. In order to obtain comparative measurements the aerosol cloud had to be diluted. This dilution was achieved by inserting a T-piece into the tube from the sample injector immediately above the tip of the injector and passing argon at a fixed flow rate through one end of the T. This diluted the aerosol which now could be measured. The drop size was measured for water and the samples containing increasing amounts of ethanol.

4.3.3.2 Mass flow rate

The mass flow rate was determined by passing the aerosol from the sample injector tube into a U-tube containing anhydrous calcium chloride. The aerosol was collected in the U-tube for exactly 2 minutes and the mass determined gravimetrically. This gravimetric determination was carried out for the water and ethanol samples.

4.4 Results and Discussion

4.4.1 Mass transfer rate

The values obtained for the mass of aerosol aspirated for exactly 2 min for each of the water and ethanol solutions are given in Table 4.4. An increase of 5 % in the concentration of ethanol when starting from pure water caused very little increase in the mass flow rate (43.6 - 43.8 mg min^{-1}). The mass flow rate then increased more rapidly with increasing ethanol concentration (Table 4.4). Results are given as the average of triplicate determinations. The mass flow rate increased to 61.7 mg min^{-1} when 25 % ethanol was aspirated, an increase of 41.5 % over the amount of material coming out of the nozzle when pure water was nebulized. This must be compared to the increase of 6.3 % when the 10 % solution was aspirated.

Table 4.4 Mass of material released from sample injector tube in 2.000 min for increasing concentrations of ethanol.

Ethanol concentration /% (v/v)	Mass /g
0	0.0872
5	0.0876
10	0.0927
15	0.0995
20	0.1146
25	0.1234

4.4.2 Drop-size distribution

The drop size distributions for the various concentrations of ethanol investigated are given in Fig. 4.7a - f and summarized in Fig. 4.8.

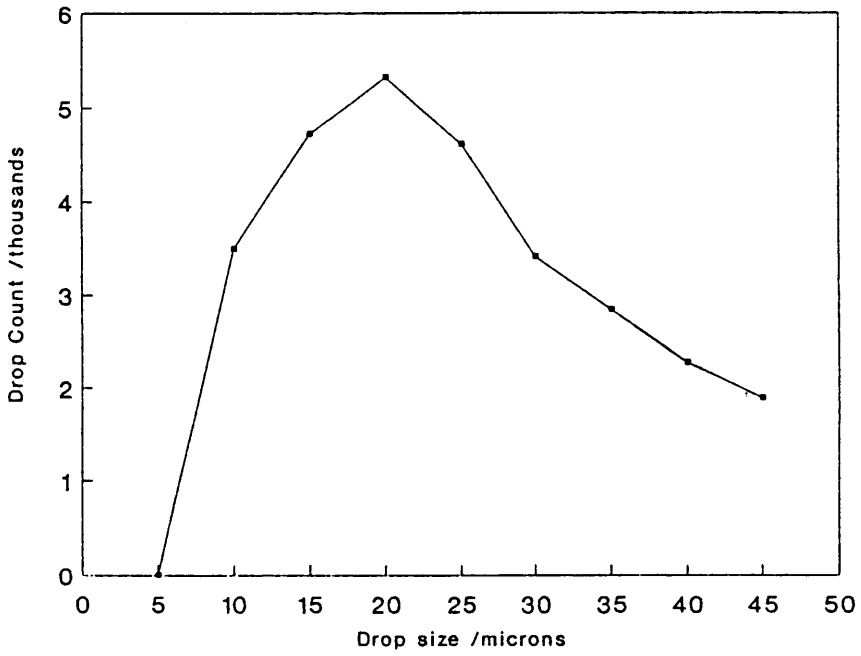

Figure 4.7a Drop size distribution for ethanol/water mixtures containing 0 % ethanol (v/v).

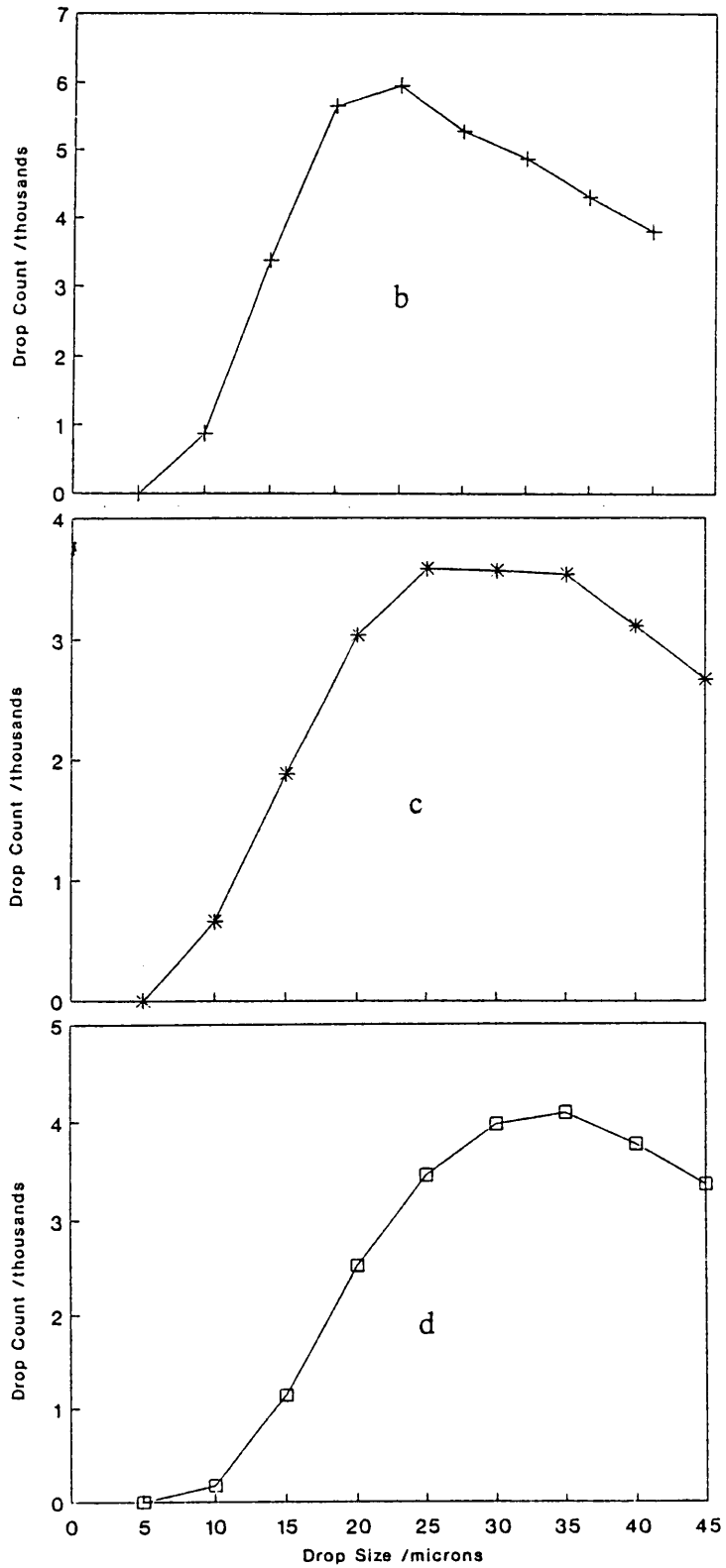

Figure 4.7b-d Drop size distribution for ethanol/water mixtures containing the following percentage of ethanol (v/v): (b) 5 %; (c) 10 %; (d) 15 %.

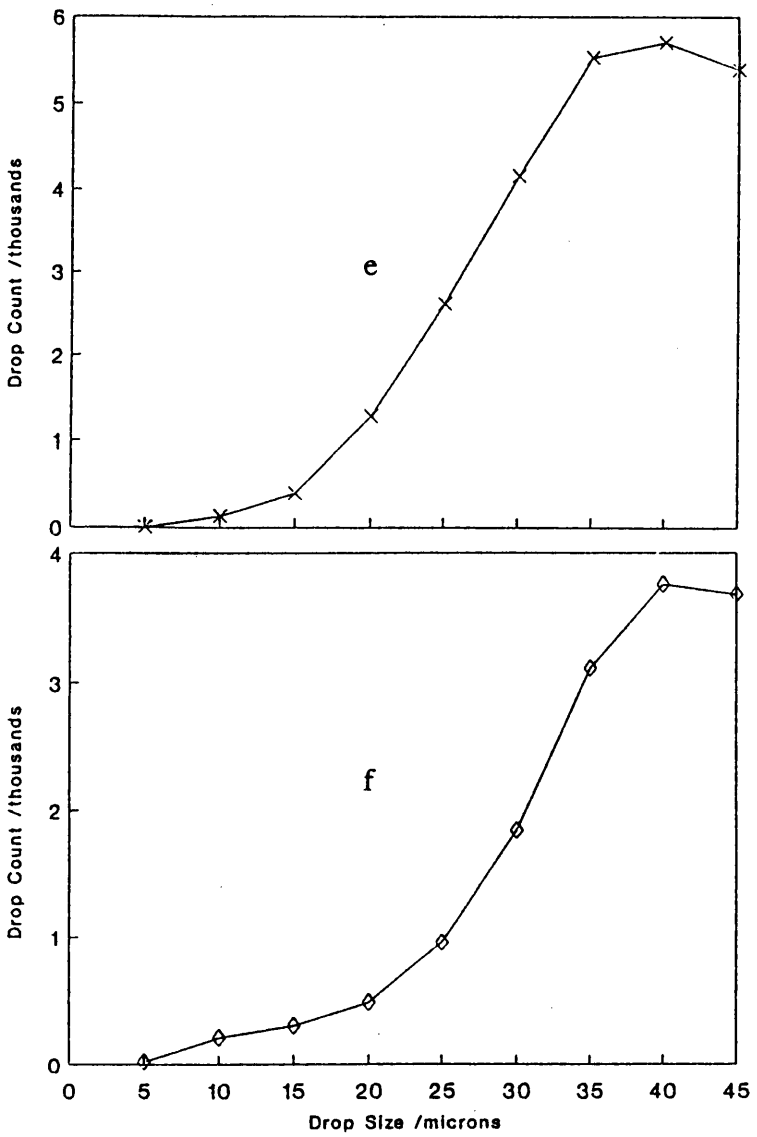

Figure 4.7e,f Drop size distribution for ethanol/water mixtures containing the following percentage of ethanol (v/v): (e) 20 % and (f) 25 %.

The instrument used to determine particle size distribution (a μLPS-16) is limited to the region 0.3 - 4.5 μm. The laser Fraunhofer diffraction system (Malvern Instruments Model 2600c) used by Browner *et al* (1992) had a lower limit of 1.2 μm. One other major difference between most of the work of Browner and co-workers (the exception being Mora *et al* (1991)) and that of Todorovic *et al* and is reflected in this work, is that Browner, Canals and co-workers always used pure solution, while Todorovic *et al* and the authors used various dilutions of organic solvents in water.

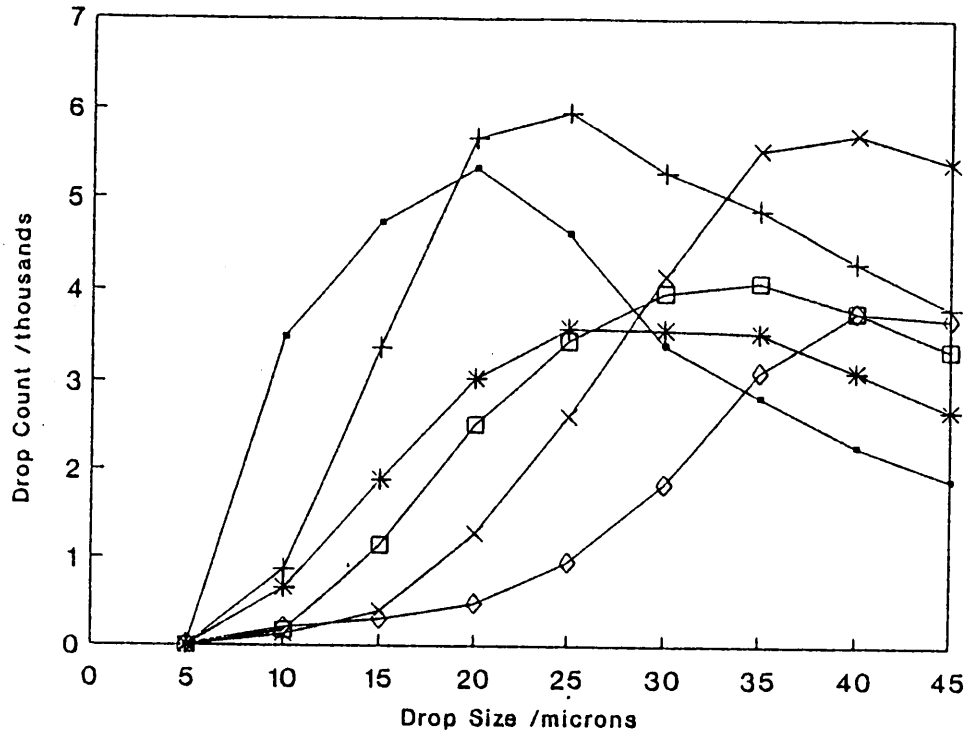

Figure 4.8 Drop-size distribution of the ICP-OES aerosol for increasing ethanol concentration: (⊡) 0, (+) 5, (✳) 10, (□) 15, (x) 20 and (◊) 25 % ethanol (McCrindle and Rademeyer: 1994).

Some uncertainty does exist with regard to the reproducibility of the determination of drop size distributions as given in Fig. 4.8. The aerosol was diluted by argon with a constant flow rate. Hence the measurement being made was not of the aerosol as it emerged from the nozzle, but rather of a diluted aerosol some distance away from the exit of the nozzle. The dilution was not identical in each case, resulting in the peak value for each dilution being arbitrary. Furthermore, the aerosol had to travel along a plastic tube before being diluted and entering the sample chamber of the laser particle analyser. All the changes that the aerosol would undergo as it passed through the system before entering the sample cell could result in the values obtained for particle distribution to be incorrect. Also, the argon used for dilution did not pass through a flow-meter which meant that the results were not reproducible. What was important, however, was that the **trend** reported and given in Fig 4.8 was reproducible.

The "anomalous" large droplet size found by Browner *et al* (1992) and given in Table 4.1 was explained by them as being the result of the lower limit that their instrument could read. The methanol had produced a large number of droplets with diameter smaller that this cutoff level and were not therefore counted. This led to the large average that they measured and presented in Table 4.1. In personal correspondence with Canals (Canals: 1995), the suggestion was made that the same error may have been repeated in the present work.

This suggestion is disputed by the authors (McCrindle and Rademeyer: 1994). Browner *et al* was using pure solvent. In the experiment, the results which are given in Fig 4.8, the concentration of the ethanol was increased and the results show clearly a **tendency for the mean drop size to increase**. **No** trace can be found that a collection of smaller drops had formed having a mean diameter smaller than 0.3 µm. Also, no real evidence was supplied by Browner *et al* that there was in fact an error in their calculations. It might be possible that the results as given by them do not suffer from corrections due to the cutoff value of 1.2 µm.

The evidence produced by Mora *et al* (1991) is much more convincing in that they did use increasing methanol concentrations and determined drop size. Certain comments are still valid. The measurements of drop size were made for a FAAS, and measured 28 mm from the nebulizer tip. The results that they found differed from those obtained with the same instrumentation a few months previously. One major advantage Mora and co-workers had was that the determination of the drop size was non-intrusive to the aerosol.

To substantiate previous proposals, namely that the cutoff value of 1.2 µl resulted in the average for the drop size being too large, Mora *et al* introduced the obscuration value (Table 4.2). This value indicated the portion of drops which could not be measured because of the cutoff value of the particle sizer. In going from pure water to 100 % methanol, the OB increased from 0.1434 to 0.2094 (in a prior Table in the publication the latter figure was given as 0.1607). At 25 % methanol the OB was 0.1854, i.e. it had increased by 29 % in going from pure water to 25 % methanol.

Assuming the same tendency for ethanol and considering that in the particle sizer used by McCrindle and Rademeyer the cutoff figure was 0.3 µl the amount of small particles excluded from the averaging process would not alter the final value to any great extent.

Another controversy is that of the Sauter mean diameter as calculated from the Nukiyama-Tanasawa equation. There is sufficient evidence (Browner *et al*: 1992, Robles *et al*: 1992, Canals *et al*: 1990) that the equation is only valid for certain nebulizer systems. In their calculations, Todorovic *et al* (1993), used the Nukiyama-Tanasawa equation to calculate the ratio of mean drop diameter of aqueous organic to that of water (Table 4.3). It must further be remembered that equation 4.1 determines the Sauter mean diameter of the primary aerosol. With the above in mind it is difficult to reach any conclusion regarding the tertiary drop size diameter. However, the tendency given in Table 4.3, which was calculated from increasing concentrations of organic solvent, is clear that, for ethanol, the drop size did increase as the concentration increased. That this increase applied to the primary drop size cannot be disputed, but if the primary drop size had increased then is it seems possible that the tertiary drop size would increase with increasing ethanol concentration as depicted in Fig 4.8.

CHAPTER 5

PRESENCE OF HYDROGEN IN AN ICP-OES

5.1 Introduction

Experience has shown that hydrogen can be detected in the ICP during the aspiration of water. During this investigation, the intensity of the emission signal on the PMT was determined by a removable aperture placed immediately after the exit slit (number 6 in Fig. 3.1) and before the PMT. The aperture consisted of a matt-black disk with a circle of diameter 8 mm cut out of the centre and fitted snugly into the PMT holder. This allowed only a limited amount of light to fall on the PMT. The dimensions of this aperture were to remain constant throughout the investigation as trends of temperature and electron density were to be determined. This constancy could only be achieved if the setup remained unchanged throughout the investigation. The size of the aperture was originally determined by optimizing the system for the emission signal from the ICP-OES when water was being aspirated. The size of the aperture was chosen so that the intensity of the light falling on the PMT was optimal (at the centre of the plasma, at position z = 0 mm, i.e. directly above the load coil). This ensured that with the appropriate voltage setting across the PMT, the H_β and H_α lines gave convenient readings (i.e. the signal to noise ratio was optimized as was the size and resolution of the emission lines).

As the ethanol concentration in the solvent was increased, the PMT became "flooded" and both the H_β and H_α peaks flattened. To reduce the intensity of the signal reaching the PMT, the size of the aperture was changed by using a disk with a smaller hole cut out (5 mm) and the measurements retaken. The increase in the emission intensity of the hydrogen lines could also have resulted from an increase of hydrogen in the plasma. The degree to which the hydrogen had increased and the implications with regard to analytical parameters were therefore further investigated.

5.2 Review of the Literature

Many researchers have reported on molecular gas additions to the argon plasma. The main aim of most of these studies was to try and find cheaper alternatives to argon for use in routine analysis or to obtain lower detection limits. The helium-argon mixture has also been investigated, but unless the determination of temperature and electron density was of interest, this, together with the wider one of general molecular addition (O_2, N_2 and air) is a topic removed from the current study and will not be reviewed.

Visser *et al* (1976) added a small amount of hydrogen (0.2 l min^{-1}) to the argon plasma to improve the measurement of intensity of the H_β, H_γ and H_δ lines. The measurements were made in order to determine the excitation temperature of the plasma using the two-line radiance ratio technique. They were using 9 MHz and 12 kW and the results at each position varied considerably. The temperature determined using the ratio of the H_β and H_γ lines was in the region of 6 000 K, while when using the H_β and H_δ lines the determined temperature was in excess of 10 000 K. The use of the H_γ and H_δ lines led to negative values for the excitation temperature. From their results they concluded that the negative pseudo-temperatures resulted because the Boltzmann distribution was not followed at 9 MHz.

The addition of hydrogen to the aerosol carrier gas was studied by Schramel (1983) while investigating the use of ICP-OES in bio-medical and environmental fields. He found that when a argon-hydrogen mixture (93.5 % Ar and 6.5 % H_2) was used as the carrier gas, all the elements he examined in the 200 - 400 nm range, yielded an increased signal intensity and a five-fold increase in detection limits.

Schramel returned to this topic and together with Li-qiang (Schramel and Li-qiang: 1984) continued the investigation of the argon-hydrogen plasma. By adding small amount of hydrogen to three different gas flows they studied the effects (signal, background intensity and signal to background ratios) on the analysis of fourteen elements (Fig.'s 5.1, 5.2 and 5.3). They then compared the results to those obtained with pure argon in the gas flows. The hydrogen was added to the aerosol carrier,

intermediate and outer gas flow and the observations made 9 mm above the load coil, at 55 % of generator output power.

They found that the signal for all the elements was enhanced by the addition of hydrogen, the increase for Al and Cu being small (as may be seen in Fig. 5.1). The background intensities also increased, except in the case of Ca and Mg. The signal to background ratio for most of the elements reached a maximum for low flow rates (between 0.05 and 0.15 l min^{-1}), while at higher flow rates the signal to background ratio decreased. They found the same effect to be valid for hydrogen added to the other gas flows.

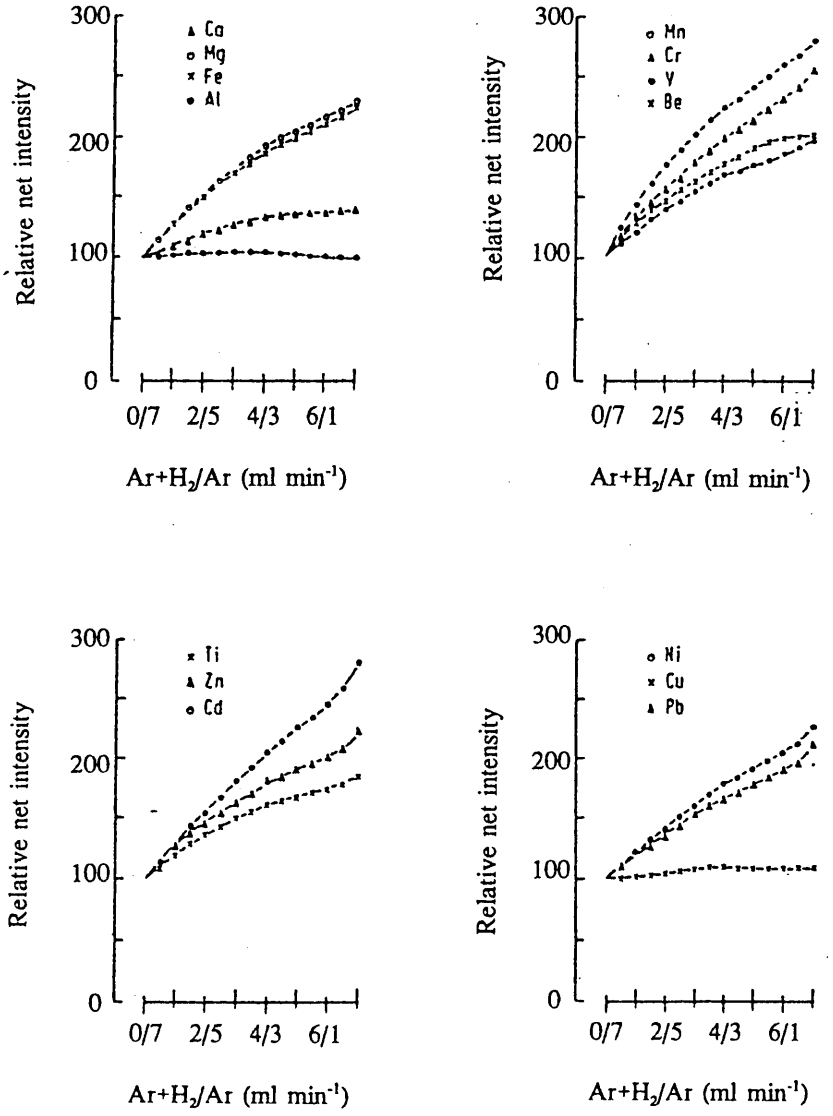

Figure 5.1 The influence of flow rate of argon-hydrogen aerosol carrier gas on the emission intensity of 14 elements (Schramel and Li-qiang: 1994).

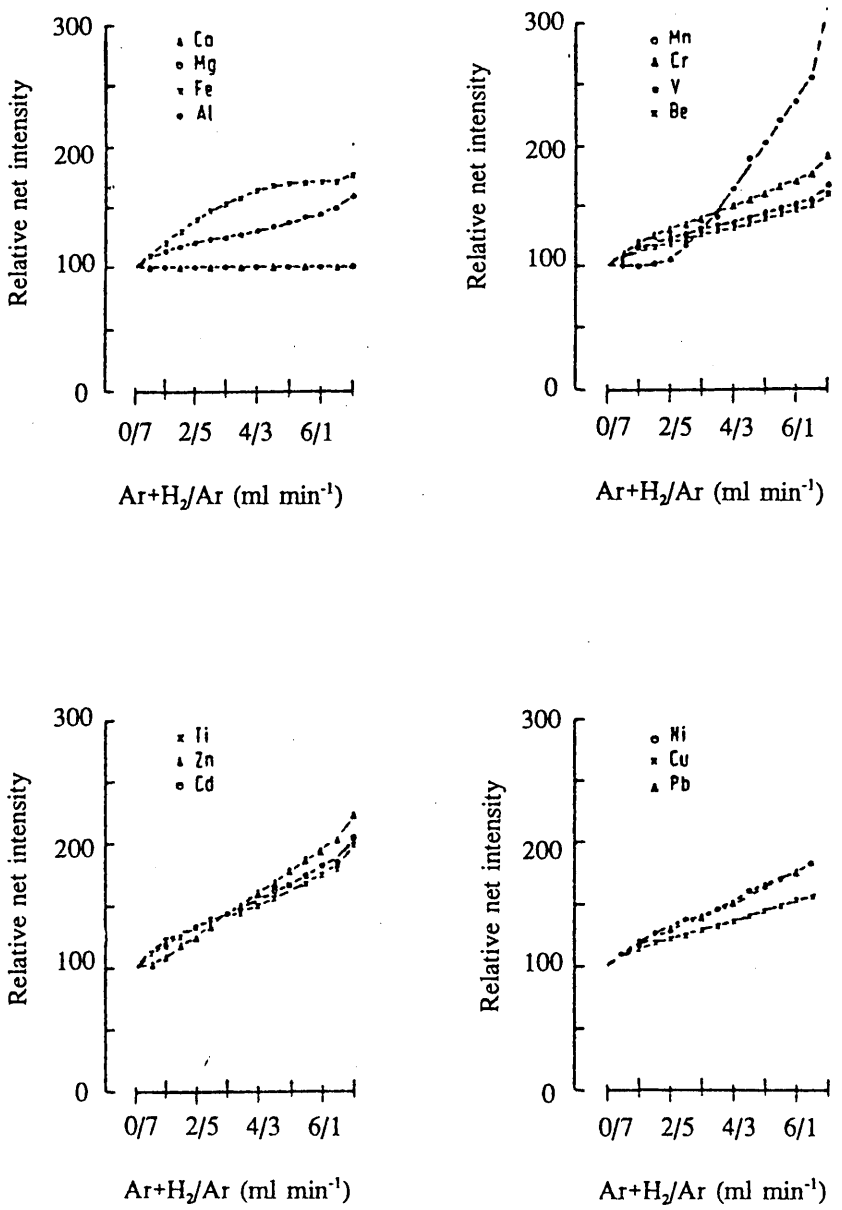

Figure 5.2 The influence of flow rate of argon-hydrogen aerosol carrier gas on the background emission intensity of 14 elements (Schramel and Li-qiang: 1994).

It was deduced that the increase in signal intensity was due to an increase in excitation temperature. They claimed that it was possible that this increase was because of the higher energy transfer from hydrogen species to the ions determined. This increase in temperature would thus result in a greater population of excited ions in the argon-hydrogen plasma.

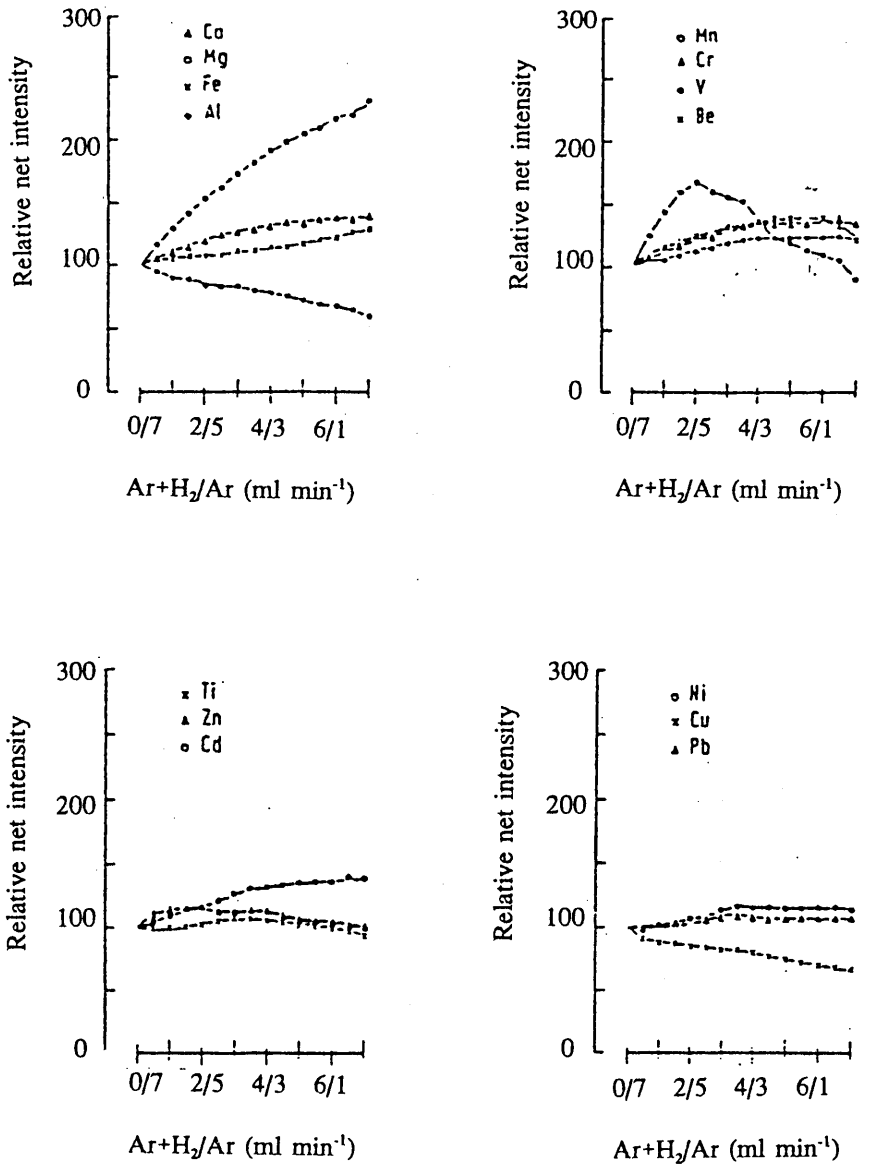

Figure 5.3 The influence of flow rate of argon-hydrogen aerosol carrier gas on the signal to background ratios of 14 elements (Schramel and Li-qiang: 1994).

Batal, Jarosz and Mermet (1982) investigated the continuum of a mixture of hydrogen and argon plasma at 430 nm when operating the plasma at 40 MHz. They found that the radial values obtained after Abel inversion for the hydrogen-argon mixture showed an increase of the continuum in the plasma, and a decrease at the outer edge of the torch, when compared to a pure argon plasma. A graphical representation of the results obtained may be seen in Fig. 5.4.

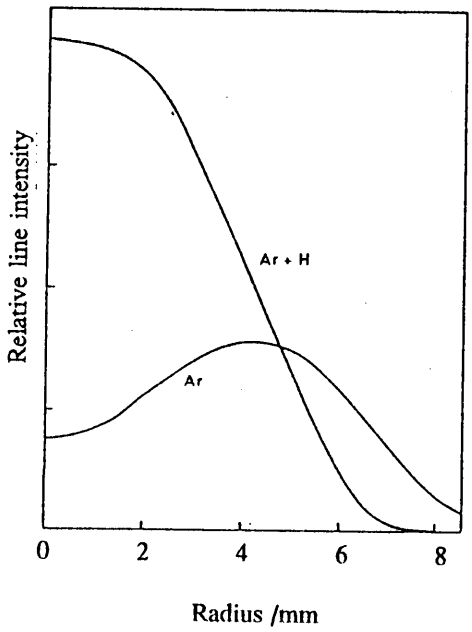

Figure 5.4 Comparison of the radial values of the continuum at 430 nm with and without 0.3 % hydrogen (Batal *et al*: 1982).

They found further that at 2 mm above the load coil, a 0.3 % addition of hydrogen to the intermediate gas changed the electron density (as calculated from the Stark effect on the H_β line). The changes to the electron density brought about by the addition of the hydrogen may be seen in Fig. 5.5.

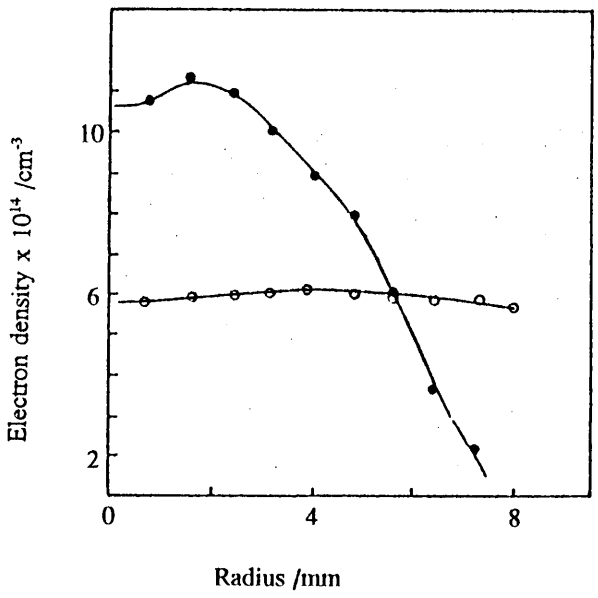

Figure 5.5 Electron number density of an argon (O) and argon-hydrogen plasma (Batal *et al*: 1982).

The excitation temperature was determined using the Boltzmann plots of the hydrogen lines, after the wide range of wavelengths covered had been taken into account. After Abel inversion, Batal *et al* (1982), calculated the axial excitation temperature for the pure argon plasma to be 5200 K, whereas the axial temperature after the addition of hydrogen to the argon was 7000 K. They concluded that the electron density and excitation temperature had increased. This increase, which corresponded to an increase in continuum, could be linked to a pinch effect resulting from the modified resistivity. Water, in the absence of any interferences, would yield the same increases because of the release of hydrogen. They found that the continuum, similar to that found in a pure argon plasma, was mainly due to radiative recombination below 500 nm. Above that wavelength, Bremsstrahlung had to be considered.

Alder *et al* (1980) found that water vapour could increase the electron density and excitation temperature. They thought that it was the hydrogen from the water that had increased the electron density. Tang and Trassy (1986) investigated this concept in detail. By using an ultrasonic nebulizer and a sheathing gas system they were able to investigate the effects that additions of water, with and without desolvation, as well as the additions of hydrogen, had on the plasma. The axial excitation temperature was determined, using the Boltzmann plot of ten ion lines, and was given without Abel transformation. The temperatures, as determined by Tang and Trassy, are given in Fig 5.6.

The Reynolds number for an ICP is between 100 and 300, which meant that the flows are laminar. Hence Tang and Trassy could estimate the heat transfer by conduction between the toroidal plasma and the central channel as being:

$$\delta Q = \theta(\delta T/\delta n)\, dS\, dt \qquad 5.1$$

where θ is the thermal conductivity, $\delta T/\delta n$ the thermal gradient, dS the exchange area and t the time.

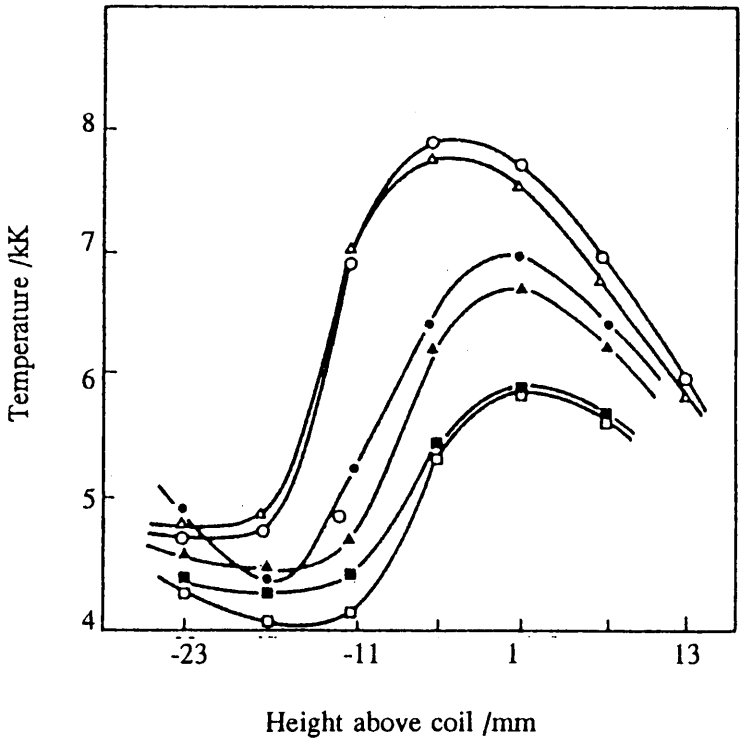

Figure 5.6 Axial excitation temperatures under various conditions (Tang and Trassy: 1986). Without desolvation (■)and with desolvation(□). With 0.05 l min^{-1} H_2 in aerosol carrier gas: without desolvation (▲), with desolvation (•). With 0.13 l min^{-1} H_2 in carrier gas flow: without desolvation (o), with desolvation (△).

After several assumptions, the exchange area they determined could be taken as:

$$S = \Pi d_d h_t \qquad 5.2$$

where d_d is the channel diameter and h_t the height above the injector nozzle. The equation for heat transfer by conduction may be written as:

$$d\theta/dt = \theta - (\delta T/\delta n)\ \Pi d_d h_t \qquad 5.3$$

Using equation 5.3 Tang and Trassy were able to calculate the thermal flow between channel and plasma. Fig. 5.7 indicates the thermal conductivities of the species investigated.

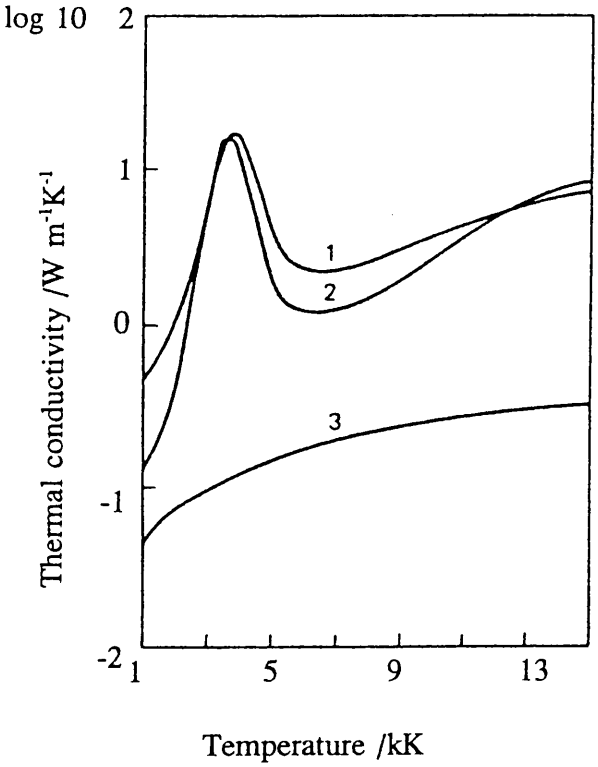

Figure 5.7 Logarithmic thermal conductance of hydrogen (1), water (2) and argon (3) as a function of temperature (Tang and Trassy: 1986).

They concluded that the most important role water played in the analytical plasma was the release of hydrogen. The hydrogen greatly enhanced the thermal conductivity and dominated the energy transfer processes from plasma to sample.

Hieftje *et al* (1987) also studied the energy transfer in an ICP. This transfer occurred mainly at the layer between the ring plasma and the channel in which the injected analyte was contained. They stated that the desolvation and volatilization processes depended on the thermal conductivity of the vapour and also on the thermal conductivity of the plasma gas. The volatilization of the solute particles was mass transfer controlled and lasted less than a millisecond. According to Tang and Trassy (1986), the desolvation of the droplets, however, was heat-transfer controlled and may be in the order of a millisecond. The dissociation of water required a large amount of energy and this may take as long as 3 ms for 0.3 mg s^{-1} of water (Tang *et al*: 1986). The total residence time in the plasma was between 5 and 10 ms depending on the discharge length and the carrier gas velocity, and so most of the time must be

spent in the atomization process. Excitation and ionization are probably much more rapid, in the order of nanoseconds. Thermal conductivity must be of great importance to the desolution, volatilization and dissociation processes.

From Fig. 5.7 it may be seen that the thermal conductivity of argon remained relatively constant at 0.1 W m^{-1} K^{-1}, while that of hydrogen and water reached values of 15 W m^{-1} K^{-1} at 3800 K (Tang *et al*: 1986). Hydrogen improved the heat transfer towards the central channel. This addition of hydrogen, via water, indicated that a delay would occur before the hydrogen became available via dissociation, while the addition of hydrogen directly to the aerosol carrier gas would eliminate that wait.

The improvement of energy transfer with hydrogen added in an ICP was also researched by Murillo and Mermet (1989). They reasoned that an addition of hydrogen on its own to the argon should not change the electron density, even if the amount of hydrogen was quite large, since there is little difference between the ionization energy of hydrogen and argon. Hence, the difference in electron density which is found, must have come from the change in shape of the plasma. The constriction effect, or thermal pinch, due to hydrogen, resulted in a different electron density gradient.

In their investigation, Murillo and Mermet (1989) studied the effects on the axial line intensity distributions, the temperature, the signals and background, and the detection limits for a variety of elements. In a previous paper (Murillo and Mermet: 1987), they divided temperature into "soft" and "hard". The "soft" temperature being one obtained below 5.5 eV, "hard" temperature above 5.5 eV. Addition of hydrogen to the carrier gas flow resulted in an increase, they found, of 1000 K on the "soft" temperatures, while the increase in the "hard" temperature was mainly at the level of the coil.

They found (Murillo *et al*: 1989) that hydrogen influenced the vertical spatial profile. For energies below 4 eV, hydrogen shifted the maximum signal to lower observation heights. Above 4 eV, the shift occurred to lower observation heights and signal enhancement took place. The shift confirmed that the addition of hydrogen led to a

more efficient energy transfer. When they investigated the effect of hydrogen on the continuum, they found that its addition resulted in an increase by a factor less than 2.

In studying the influence that addition of hydrogen had on line intensity, Murillo and Mermet (1989) found that, when comparing the ratios of atomic lines with and without hydrogen, they only realised an improvement in the signal of less than 3. When investigating the ionic lines they found that this ratio increased to a factor of 8. They concluded that only argon in the central channel resulted in a direct single step process being in operation to produce the excited ions, while the addition of hydrogen results in a two step process occurring. Because of the large increase when ion lines were used, they proposed that these, if used for analytical determinations, would result in improved detection limits, provided that hydrogen was added to the sheath gas. If less energy was applied, i. e. the atomic lines were being used, the increase in signal intensity would not compensate for the increase in continuum and the detection limits would not be improved.

Murillo and Mermet (1989) conclude that hydrogen, even at a flow of 0.05 l min^{-1}, in the central channel would improve energy transfer between the ring plasma and the injected species. The addition of hydrogen can overcome the low thermal conductivity of the argon and so assist with the atomization process.

The successful increase of signal intensity by small additions of hydrogen to the aerosol carrier gas led the group at Université Claude Bernard-Lyon I to investigate other applications for use in ICP-OES. Matousek and Mermet (1993) studied the effect of small amounts of hydrogen added to the carrier gas in electrothermal vaporization ICP-OES (ETV ICP-OES). They investigated the atomic and ion lines of Pb, Mn, Mg and Cr in order to elucidate the mechanisms involved and improve analytical performance. They found that the changes induced on the atomic lines by the addition of hydrogen was determined by a combination of three hydrogen-induced processes:

(i) a variation in the atomic/molecular population distribution in the ETV which

affected the analyte elemental mass entering the ICP;

(ii) enhanced excitation due to the increased excitation temperature and electron density;

(iii) enhanced atomization of the aerosol because of the increased energy transport between the plasma and the central channel due to the improved thermal conductivity of the hydrogen.

To this they added another factor for ionic lines, namely that with (i) and (iii) above the production of excited ions had increased. This improved production, they decided, was due to the single-step mechanism operating with argon alone, reverting to a two-step mechanism in the presence of hydrogen, as mentioned previously.

The work of Olesik and Fister (1991) and Hobbs and Olesik (1993) indicated that not all the droplets in the central channel were fully desolvated. The number of incomplete desolvated particles was found to be dependent on flow rate and applied power (Olesik and Fister: 1991). Improved heat transfer caused by the hydrogen would have the potential to enhance emission if a portion of the aerosol was not completely vaporized or atomized (Matousek and Mermet: 1993). The shift of the optimum viewing height to lower down in the plasma when hydrogen was added, could be explained by the better heat transfer, resulting in improved desolvation and atomization. This was especially true if the process had to take place in milliseconds (Matousek and Mermet: 1993).

When studying the Pb I line, Matousek and Mermet (1993) decided that the above was unlikely to be the reason for the improved signal of the analyte after hydrogen addition to the carrier gas. This improvement may be seen in Fig. 5.8. They reasoned that since they had used dry aerosol volatilization and dissociation of the Pb would not have been affected by the addition of hydrogen. The process they deduced must have been solely governed by enhanced excitation. The plot of peak area in Fig. 5.8 showed more clearly the changes in the excited atom population, as peak area is independent of the heating rate and the length of tubing used to transport the analyte to the plasma. The use of a dry aerosol to measure the changes due to the addition

of hydrogen was recommended by the authors. They further suggested that Pb could under these circumstances (dry aerosol) be used as a "reference" as to how the changes in the excitation conditions affect excitation of atomic lines.

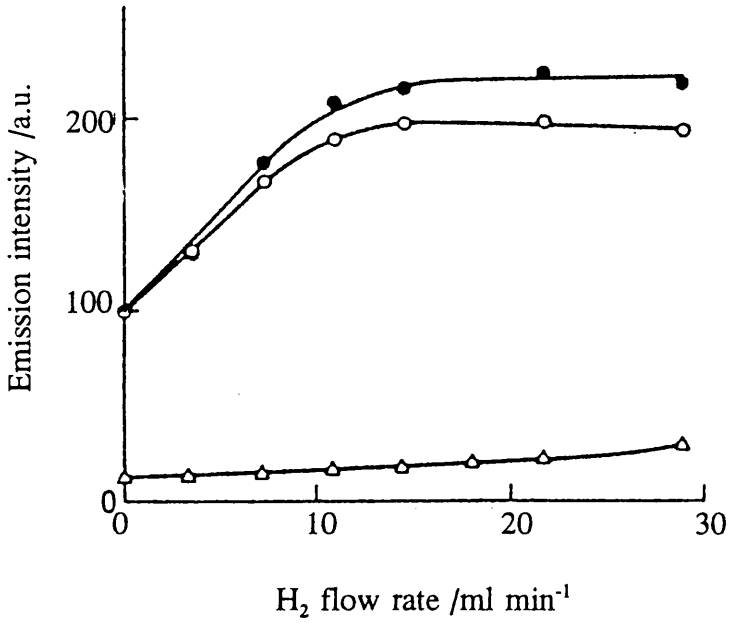

Figure 5.8 Effect of addition of hydrogen on peak height (●) and peak area (o) of Pb measured at 405.78 nm, with background (△) (Matousek and Mermet: 1993).

Matousek and Mermet (1993) found that when they investigated Mn it followed the same pattern as Pb, and concluded that again the enhanced emission signal was due to increased excitation. With two of the elements, Cr and Mg, the addition of hydrogen resulted in transport losses due to increased lifetime of free atoms in the hydrogen-containing atmosphere. The losses encountered were offset by the excitation processes being enhanced.

The Mg II/Mg I ratio is a useful and rapid tool to gain insight into the electron density of a plasma, and hence the effect of hydrogen on this intensity ratio was also investigated and their findings may be seen in Fig. 5.9. The ratio was improved by a factor of 5.3 when a dry aerosol was used, as opposed to a wet aerosol. This ratio was further enhanced to a factor in excess of 15 by the addition of hydrogen. The

increased electron density was due, they decided, to the hydrogen and this explained why the observed ratio was higher than the range of 10 to 13 that should be obtained for an ICP operating under LTE conditions. They deduced from Fig. 5.9 that the plasma has poor robustness without the hydrogen. The Mg II/Mg I intensity ratio also governed the way in which water affected excitation conditions within the plasma, and the wet aerosol, they claimed, improved atomization.

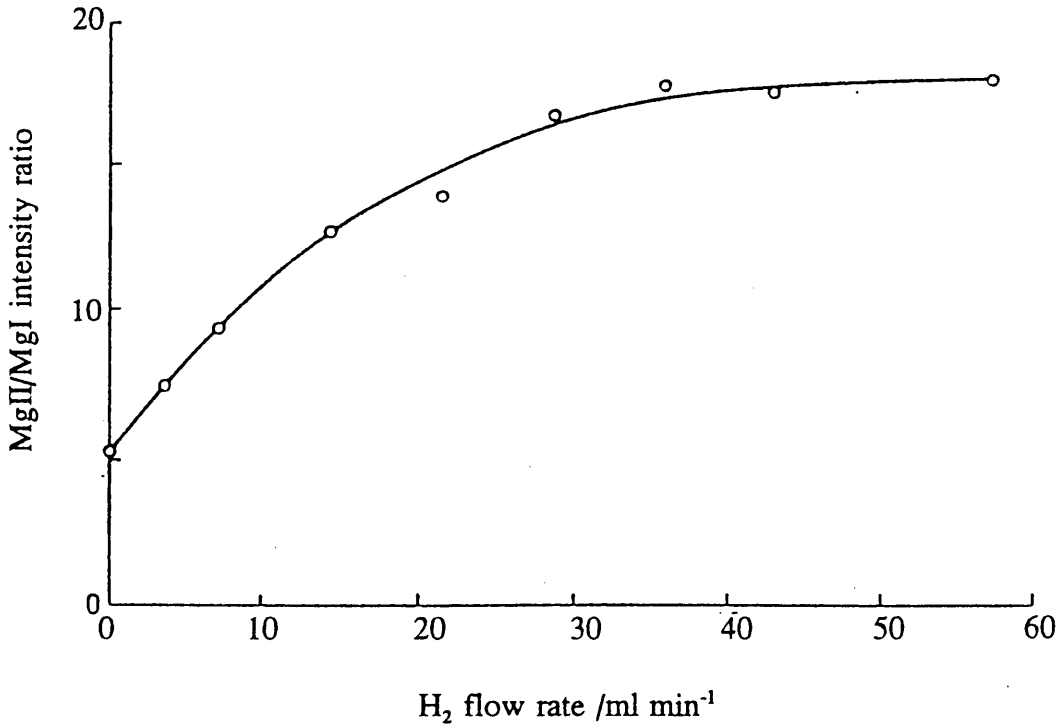

Figure 5.9 Effect of hydrogen on the Mg II/Mg I intensity ratio with the addition of hydrogen (Matousek and Mermet: 1993).

One further finding by the authors was that the intensity of the ion lines of the elements investigated all increased with addition of hydrogen. This they could describe to the drop in atomic population reaching the plasma and also the enhanced production of excited ions.

Matousek and Mermet found that the analytical performance was improved, especially when using the ionic lines. This resulted from the enhanced signal emission and improved relative standard deviations (RSD's) in the presence of hydrogen. The improvement of RSD compensated for the increased background continuum. The

amount by which the plasma was improved depended on the robustness of the plasma. The further the plasma was from LTE the greater the benefit from the addition of hydrogen.

Poussel *et al* (1994) investigated the dissociation of analyte oxide ions by using an ICP-Mass Spectrometer (ICP-MS). To understand more fully the analyte oxide formation and dissociation in the plasma, they investigated the role that energy transfer played. This they did by either degrading the efficiency of the plasma by using a sheathing gas or improved the efficiency by the addition of hydrogen. Additions of 0.02 l min^{-1} of hydrogen to the aerosol carrier gas resulted in significant modification of the spatial distribution of La^+ and LaO^+. Addition of hydrogen, they found, increased the rate of oxide dissociation.

After studying both the excitation temperature calculated from the Boltzmann plots of Ti ionic lines and the kinetic temperature using the Doppler line broadening of the Be I 234.86 nm line they found a decrease in the LaO^+:La^+ for an increase in temperature obtained by the addition of hydrogen to the carrier gas. There was a direct correlation between temperature, irrespective how it was measured, and production of LaO^+. They concluded that the formation of analyte oxides was related to the physical properties of the plasma.

Louie and Soo (1992) investigated the effect that the addition of either nitrogen or hydrogen had on the signal intensities of a wide range of elements when using an ICP-OES. The signals were increased for all the elements investigated, but that while the increase was the greatest for nitrogen additions, the addition of hydrogen did not result in any interferences. This was not the case with the nitrogen additions where polyatomic species of nitrogen did interfere.

Another use of added hydrogen was investigated by Ebdon and Goodall (1992). They studied the effect that additions of hydrogen would have on the atomization of slurries. Rotational temperature was determined by using vibrational rotation emission spectra of various molecular species. The addition of hydrogen to the inner gas resulted in

an increase of temperature from 2200 to 3900 K. The variations they found for rotational temperature with additions of hydrogen is given in Fig. 5.10.

Via a simple calculation, Ebdon and Goodall estimated that 5 % (v/v) hydrogen in argon mixture introduced into the injection gas, would result in an increase of 4.04 mmol of atomic hydrogen or an increase of 347 % in the hydrogen content of that gas. They then proceeded to estimate thermal conductivities of various injection gases. At 5000 K, "wet" argon aerosol carrier gas would have a thermal conductivity of approximately 52.66 J $(K\ s\ m)^{-1}$, while that of a hydrogen modified gas would be 99.5 J $(K\ s\ m)^{-1}$. This is almost twice that of "wet" argon and 2.6 times that of "dry" argon.

The increase in thermal conductivity is offset by the energy required to dissociate the molecular hydrogen. Following a similar type of calculation as used for the thermal conductivity above, Ebdon and Goodall estimated that it would require 1.3 kJ to bring 2.02 mmol molecular hydrogen from 298 K to atomic hydrogen at 5000 K. Remembering the 5 kJ calculated by Tang and Trassy (1986) to raise the temperature of "wet" argon through the same temperature range, Ebdon and Goodall reached the conclusion that the additional energy requirement was 26 %. This additional energy would result in the thermal conductivity being doubled.

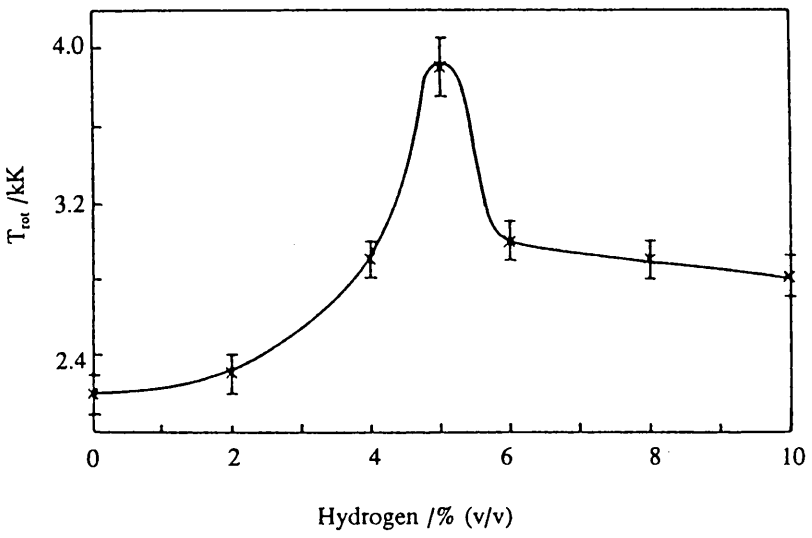

Figure 5.10 Variation of rotational temperature with hydrogen content (Ebdon *et al*: 1992).

Using the above calculations for the additional energy requirements and also for the thermal conductivity enabled Ebdon and Goodall (1992) to propose a mechanism for the increased energy transfer. Assuming a heat-transfer mechanism, and visualizing the ICP as a hot cylindrical tube through which the gas flowed, they suggested that the final temperature of the gas exiting the tube would depend on the total energy transferred and the specific heat capacity of the gas. The experimental values made them decide that there were two factors which countered the concept that it was the increased energy transfer due to thermal conductivity that caused signal enhancement. Their reasoning was as follows:

(i) The heat transfer via conduction depended on the residence time in the tube and the contact area. The residence time depended on initial gas flow, temperature and physical dimensions of the tube. Assuming a length of 30 mm and a diameter of 6 mm for the "tube", then at 5000 K the gas velocity would have been 990 m s^{-1} and the residence time 0.003 s. Hence, any increase in the gas temperature would act to decrease the residence time and therefore limit the effect of increased thermal conductivity.

(ii) The second factor concerned the thermal pinch effect. The plasma torus is contracted due to the increased transfer from the skin of the plasma in order to maintain charge carrier density and conductivity of the skin. This contraction results in the geometric contact area decreasing and the residence time would again be decreased because gas velocities would be increased. This final increase in gas velocities was probably the result of the narrowing of the central channel. Since the residence time is proportional to the square of the radius of this central channel, its decrease in size would be the major factor in determining heat transfer.

The authors concluded by stating that the increased energy transfer, due to hydrogen with high thermal conductivity being introduced into the plasma, was self limiting and that the contraction because of the thermal pinch effect was the determining process.

The role of desolvation and hydrogen addition on the excitation features of an ICP was investigated by Walters and Barnardt (1988). They optimized the desolvation temperature of an ultrasonic nebulizer and found that when operating it at that temperature an increase in the ionization temperature and electron density was obtained. The addition of about 4 % hydrogen to the aerosol carrier gas increased the electron density and ionization temperature even more, when operating the ultrasonic nebulizer at optimum temperature.

During the determination of excitation temperature and electron density as reported in Chapter 3 an increase in the signal intensity of the hydrogen lines (both H_α and H_β) had been noted. It was necessary to measure the magnitude of the increase and predict the possible effect that the increase in hydrogen concentration in the plasma would have on the fundamental and analytical characteristics of the plasma.

5.3 Experimental

5.3.1 Apparatus

The same apparatus as used for the determination of electron density and excitation temperature was used for the determining the emission intensity.

5.3.2 Procedure

To determine the relative hydrogen intensities when each ethanol solution was aspirated into the plasma the H_α line was used, because of its sensitivity.

5.4 Results and Discussion

The magnitude of relative intensities of the various concentrations of ethanol at the positions measured is given in Fig. 5.11. It should be noted that these are relative intensities and they are given in units as produced by the system employed. As each measurement was made under identical conditions, they may be compared to each other. The largest emission signal for the hydrogen emanated from just above the load coil (z = 0 mm). The intensity of the signal dropped by more than 20 % in moving 5 mm up the plasma (z = 5 mm). The intensity of the signal continued to decrease

to 15 mm above the coil where the signal was only 20 % of that obtained at z = 0 mm.

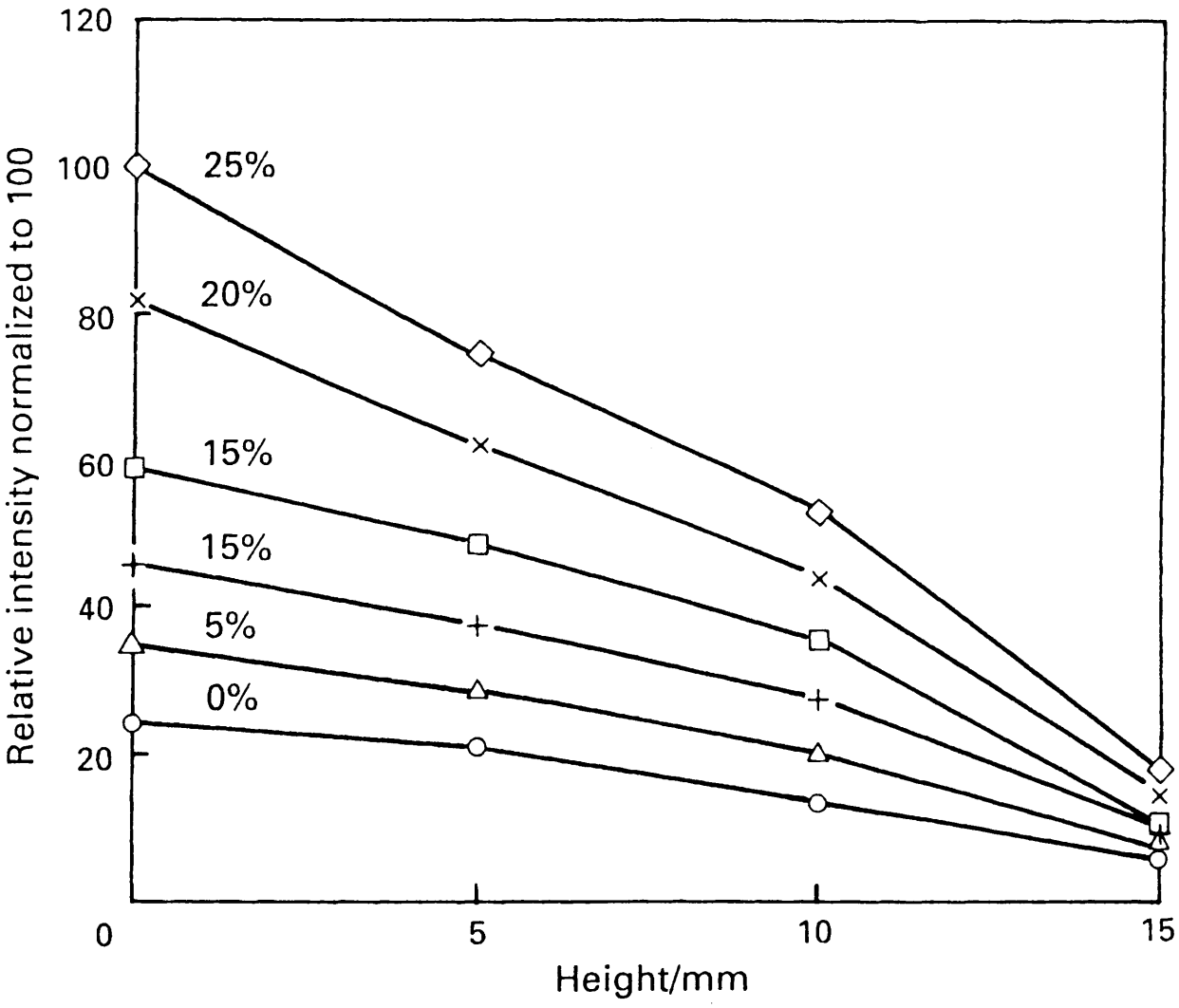

Figure 5.11 Relative intensity of the H_α line, at the centre of the torch, of various concentrations of ethanol for various positions above the load coil (McCrindle and Rademeyer: 1994).

The intensity, normalised to 100, increased as the ethanol concentration was increased, since by moving from water to 25% ethanol (the maximum ethanol concentration) a fourfold increase was obtained. As could be expected the intensity decreased away from the load coil, up to approximately fourfold (Fig. 5.11). The above graphs show that the hydrogen intensity was increased when ethanol was added to the sample solution. Some hydrogen was present when pure water was aspirated, but this amount

increased by a factor of 4, when 25 % ethanol was aspirated. The effects that this "addition" of hydrogen had on the system will be discussed in great depth later. The direct effect that the addition of ethanol to the analyte solution, by the "addition" of the hydrogen to the system, had on the analytical parameters, will be investigated in the next chapter.

CHAPTER 6

ANALYTICAL EVALUATION

6.1 Introduction

The use of organic solvents in Chemistry is diverse. As discussed earlier in Chapter 1, ethanol, while remaining one of the least expensive of organic solvents, and, because of its polarity one of the easiest to apply, is not extensively used in analyses with an ICP-OES. This lack of favour among analysts is due to the intolerance of 27 MHz plasmas, driven by crystal controlled rf generators, to high concentrations (above about 20 %) of ethanol in the solution. The majority of ICP-OES instruments in this country (South Africa) use crystal controlled rf-generators. The unwillingness to use ethanol occurs although ethanol enrichment of solutions is known to result in enhancement of signal intensity and hence an increase in sensitivity (Benli *et al*: 1991).

Enhancement of the signal intensity, which is found with organic solvents, both in atomic absorption spectrometry (AAS) and ICP-OES, has been the subject of many investigations. The physical properties of various alcohols, ketones, esters and other organic solvents were studied by Lemonds and McClellan (1973) and correlated to the signal enhancement found in AAS. Kreuning and Maessen (1987) reported that the solvent's saturation vapour pressure governed the plasma load, while the evaporation factor dominated the distribution of the solvent over the liquid and the vapour phase at the exit of the spray chamber. When investigating the excitation conditions in an ICP loaded with different organic solvents, Kreuning and Maessen (1989) found that the nature of the solvent and the solvent plasma load were decisive for the excitation conditions in an ICP.

An investigation into the analytical properties of the ethanol-loaded plasma was appropriate after finding the changes in fundamental characteristics that have been reported in earlier chapters. The effect that additions of ethanol to the sample matrix would have on the sensitivity, detection limits and background equivalent concentrations required investigation. Suitable elements to be investigated were selected.

6.2 **Experimental**

6.2.1 Apparatus

6.2.1.1 ICP Spectrometer

A Spectro Analytical Instruments Spectroflame ICP-OES was used operating under the conditions given in Table 3.1. It was fitted with the instruments standard cross-flow nebulizer and glass Scott spray chamber. The quartz torch was dismountable, with an internal diameter of 16 mm. A peristaltic pump provided a constant uptake rate. The signal intensity was transferred to the polychromator and scanning monochromator by means of optical fibres. Operating conditions for the pure aqueous solutions were according to the manufacturer's specification.

The power setting of 1.36 kW was used throughout since this had been used extensively for temperature and electron density determinations. The intermediate plasma gas flow rate was optimized as was the sample uptake rate. The latter measurement was limited by a fixed peristaltic pump rate, and so the sample uptake rate could only be altered in terms of tube size.

6.2.2 **Reagents**

Solutions containing 1, 5, 20, 60 and 100 $\mu g\ ml^{-1}$ of lead in pure water, and in 5, 10, 15, 20 and 25 % (v/v) ethanol were prepared from a 1000 $\mu g\ ml^{-1}$ Pb Titrosol standard in distilled and deionized water. The ethanol used was analytical-reagent grade. A second series of solutions were prepared in a similar fashion containing the

same concentrations as above but of Cd, Al, Cr, Mn, Fe and Na. Each solution contained all the elements at the required concentration. That is, there was a series of standards in pure water, another in 5 % ethanol, in 10 %, 15 %, 20 % and 25 %. A third series containing V and Mo was prepared in a similar way.

6.3 Sensitivity, Detection Limits and Background Equivalent Concentration

The sensitivity of the determinations is given as relative intensity/concentration, while the IUPAC definition of detection limit was used, i.e.

$$C_{DL} = 3\sigma_1/S \qquad 6.1$$

where, C_{DL} is the detection limit in concentration units, σ_1 the standard deviation of the limiting noise, and S the sensitivity.

The background equivalent concentration, BEC, is defined by

$$BEC = I_b/S \qquad 6.2$$

where I_b is the intensity of the background.

6.4 Results and Discussion

The effect on the analytical parameters of detection limits and signal enhancement, with increasing quantities of ethanol in the sample solutions, was investigated. The changes that accompanied the introduction of organic solvents in a sample were ascribed by literature to the physical properties of the solvent (Lemonds and McClellan: 1973, Greenfield *et al*: 1976, and Kojima and Iida: 1987). Density, viscosity and surface tension were the properties investigated by Todorovic *et al*: 1993). Several authors reported a decrease in excitation temperature (Kreuning and Maessen: 1987, Pan *et al*: 1990, Blades and Caughlin: 1985, and Boumans and Lux-Steiner: 1982) with the addition of organic solvent to the sample solution, while one (Benli: 1983) reported an initial increase, followed by a decrease as the concentration of ethanol increased.

Since the instrument used had a $\pi/4$ sr solid angle at which the intensity was measured, the height above the load coil could not be optimized. Further, the power applied was that of the manufacturer's recommendation, although a lower power was investigated. The lower power was limited to ethanol concentrations less than 15 %, when the plasma was extinguished. The nebulizer gas flow rate was initially kept constant for all the ethanol concentrations, but was later varied as indicated.

The percentage increase of the sensitivity for the different elements is shown in Fig. 6.1a, 6.1b, 6.2a and 6.2b as well as Table 6.1a and 6.1b. The elements chosen, Pb, Cd, Al, Cr, Mn, Fe, Na, V and M, were those fairly often determined and also to include both "soft" (Na) and "hard" (Cd) elements. They also included elements relatively easy to determine using ICP-OES like Mn and elements which may give spectral or chemical problems like Al. In Fig. 6.1a, the two different values for lead are given for 1.02 kW and 1.36 kW. A second lead line was used for comparison and the results obtained when using this line appear in Fig. 6.1b.

Slight deviation from linearity can be seen in the calibration curve for Pb when 20 % ethanol was present, but it is so small as to be insignificant. This was not the case for the calibration curve using the Pb line at 283.31 nm. The amount of curvature present would have made the selection of those parameters (20 % ethanol and 283.31 nm line) unsuitable for analysis. Calibration curves for ethanol concentrations up to and including 10 %, for both lines, are given for the lower power setting, since above 10 % and at 1.02 kW the plasma was extinguished. The calibration curve for the aqueous solution of Pb obtained with the 220.35 nm line at 1.36 kW corresponded to the curve obtained with 10 % ethanol at 1.02 kW. In the case of the line at 283.31 nm, the aqueous solution with 1.36 kW power, yielded slightly improved sensitivity when compared to the 10 % solution at 1.02 kW.

Additions of ethanol clearly enhanced the emission signal of both an atomic and ionic line as demonstrated in Fig. 6.1a and 6.1b.

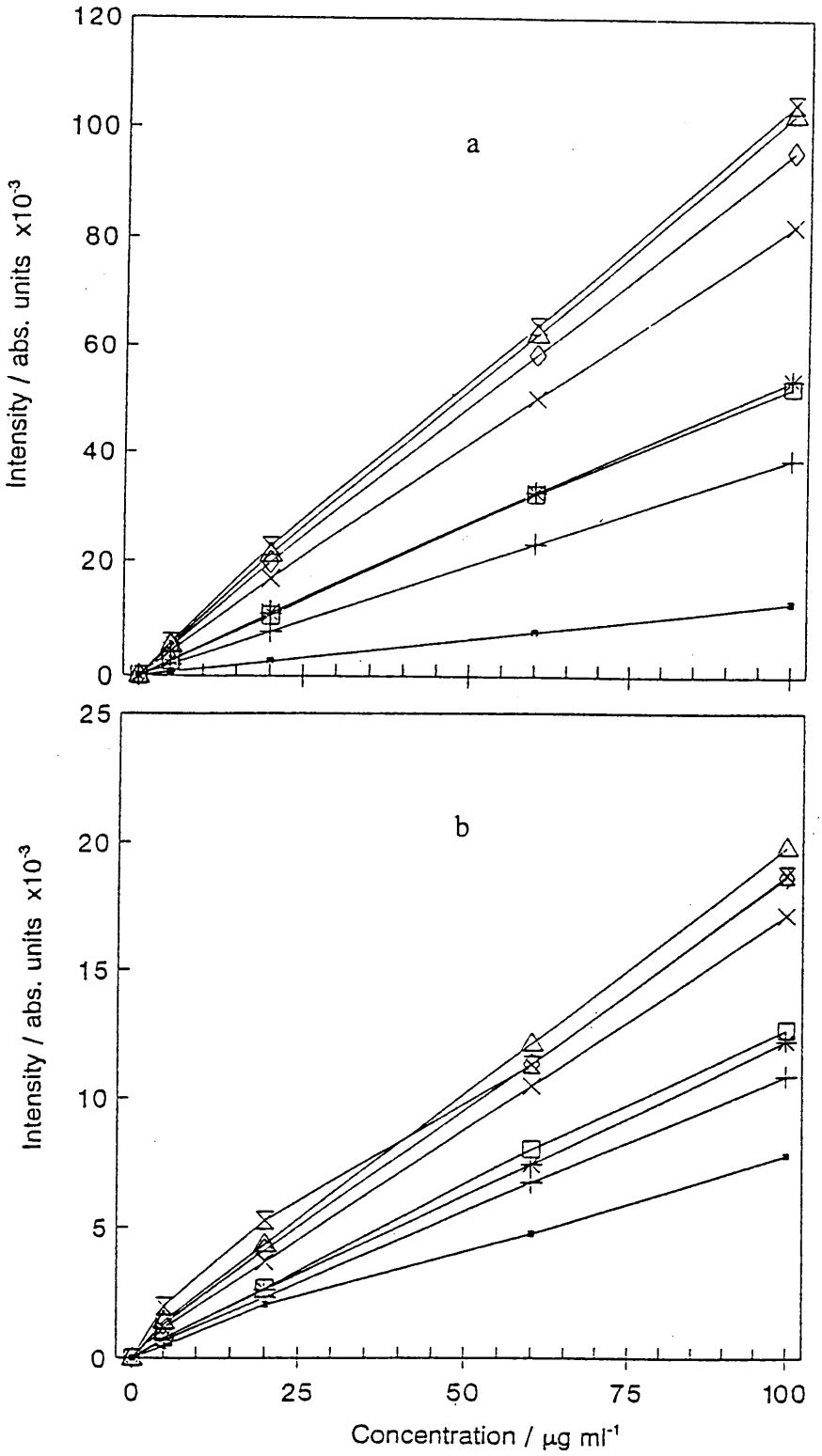

Figure 6.1a,b Calibration curves for (a) Pb at (220.35 nm) and (b) Pb at 283.31, with increasing ethanol concentration, at 1.02 (▣) 0; (+) 5; and (✳) 10 % and at 1.36 kW, (□) 0; (x) 5; (◇) 10; (△) 15 and (X) 20 % ethanol.

The difference between the increases in the sensitivities should be seen together with the changes in hydrogen emission signal given in Fig. 6.1c. At the lower power setting (1.02 kW), the hydrogen emission signal doubled when going from pure water to the 5 % ethanol solutions, and increased by a similar amount to the 10 % solution. Although the increases in hydrogen emission at the higher power setting were of the same order, the percentage increase was less (200 versus 150 %) due to the initial value being smaller. The changes found for the detection limits are given in Table 6.1a and 6.1b.

It should again be noted that at 1.02 kW the highest ethanol concentration that could be nebulized was 10 %. Consequently, the emission intensity of the hydrogen line at 1.02 kW is apparently incomplete.

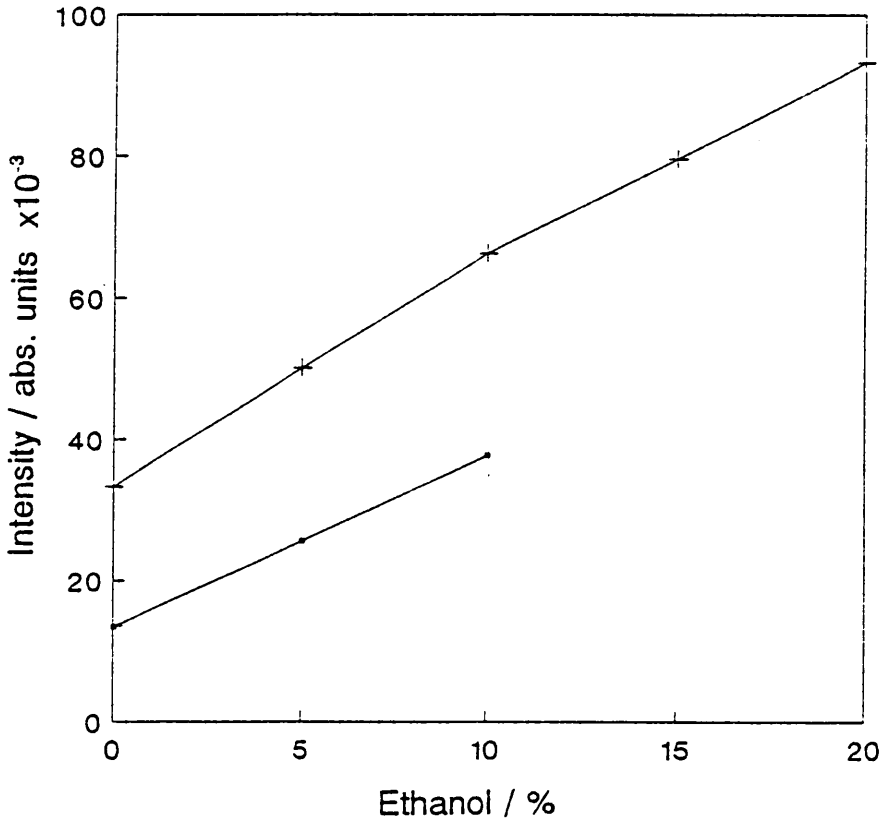

Figure 6.1c Emission intensity of hydrogen at 483.05 nm with increasing ethanol concentration (□) at 1.02 and (+) 1.36 kW power.

Table 6.1a Analytical parameters for Pb at different concentrations of ethanol at 1.02 kW and an aerosol carrier gas flow rate of 0.6 l min^{-1}.

	Ethanol /% (v/v)		
	0	5	10
Pb (283.31 nm)			
Sensitivity /a.u.($\mu g\ ml^{-1}$)$^{-1}$ x 10^{-3}	7.75	10.9	12.2
Detection Limit /$\mu g\ ml^{-1}$	0.45	0.91	1.30
BEC /$\mu g\ ml^{-1}$	14.6	30.1	42.5
Pb (220.35 nm)			
Sensitivity	128	388	537
Detection Limit	0.045	0.056	0.070
BEC	1.57	1.86	2.37

Table 6.1b Analytical parameters for certain elements at different concentrations of ethanol, 1.36 kW and a nebulizer flow rate of 0.6 l min^{-1}.

	Ethanol /% (v/v)				
	0	5	10	15	20
Pb (283.31 nm)					
Sensitivity /a.u.($\mu g\ ml^{-1}$)$^{-1}$ x 10^{-3}	12.7	17.5	18.7	19.8	18.8
Detection Limit /$\mu g\ ml^{-1}$	1.3	1.5	1.9	2.1	2.7
BEC /$\mu g\ ml^{-1}$	44.4	50.6	62.5	71.1	87.8

Pb (283.31 nm)					
Sensitivity /a.u.$(\mu g\ ml^{-1})^{-1} \times 10^{-3}$	52.3	82.2	95.7	102	104
Detection Limit /$\mu g\ ml^{-1}$	0.062	0.068	0.084	0.096	0.11
BEC /$\mu g\ ml^{-1}$	2.05	2.28	2.82	3.24	3.80
Cd (226.50 nm)					
Sensitivity	702	1040	1200	1260	1510
Detection Limit	0.0045	0.0051	0.0064	0.0075	0.012
BEC	0.221	0.258	0.313	0.363	0.549
Al (308.21 nm)					
Sensitivity	55.2	74.1	80.7	83.1	63.6
Detection Limit	0.15	0.18	0.22	0.26	0.46
BEC	4.99	5.93	7.47	8.69	14.8
Fe (259.94 nm)					
Sensitivity	188	268	304	327	254
Detection Limit	00.94	0.011	0.013	0.015	0.025
BEC	0.351	0.402	0.484	0.574	0.919
Cr (267.72 nm)					
Sensitivity	244	361	407	434	338
Detection Limit	0.010	0.011	0.014	0.017	0.028
BEC	0.381	0.433	0.540	0.622	1.04

Na (589.59 nm)					
Sensitivity /a.u.(μg ml^{-1})$^{-1}$ x 10^{-3}	4.13	5.14	5.57	5.85	4.44
Detection Limit /μg ml^{-1}	0.34	0.44	0.55	0.64	1.1
BEC /μg ml^{-1}	12.3	14.7	18.2	21.2	38.4
Mn (257.61 nm)					
Sensitivity	134	190	210	217	156
Detection Limit	0.019	0.022	0.027	0.032	0.058
BEC	0.672	0.776	0.979	1.16	2.00
Mo (281.61 nm)					
Sensitivity	850	1130	1130	1160	1170
Detection Limit	0.066	0.075	0.093	0.10	0.12
BEC	2.10	2.11	2.52	3.17	3.87
V (311.07 nm)					
Sensitivity	316	393	395	402	409
Detection Limit	0.018	0.022	0.028	0.032	0.034
BEC	0.650	0.776	0.976	1.08	1.16

The role of auxiliary gas in organic sample introduction was studied extensively by Pan *et al* (1990), who concluded that for optimum performance, the lowest possible auxiliary gas flow rate should be used. They deduced that the decrease in excitation temperature was due to the energy being consumed by the dissociation of the C_2 species. The decrease in excitation temperature was accompanied by a decrease in analyte emission intensity.

Sensitivities of the calibration curves for the different elements were investigated when the power was decreased (Pb in Fig. 6.1a), and when the nebulizer gas flow rate was changed. The changes that could be made to the aerosol carrier flow and the rf power

were limited because, above a certain flow rate (0.38 l min^{-1} for 25 % ethanol), and below an rf power setting of 1.02 kW for 15 % ethanol, the plasma was extinguished.

For a flow rate of 0.6 l min^{-1} and a forward power of 1.36 kW, the sensitivity of all the elements increased as the concentration of ethanol in the sample matrix was increased, the amount of increase being dependent on the element concerned, as may be seen in Table 6.1b. Lead underwent a maximum percentage increase (for increasing concentrations of ethanol) when the power was reduced to 1.02 kW (Fig. 6.1a). The greatest percentage increase in the concentration of hydrogen in the plasma (when ethanol concentration was increased), was also found when the forward power was 1.02 kW. In most cases the calibration curve with the greatest gradient was that obtained when the solution contained 15 % ethanol. The calibration curves for Pb was an example when this was not the case, and the most sensitive results were obtained with the 20 % ethanol solution.

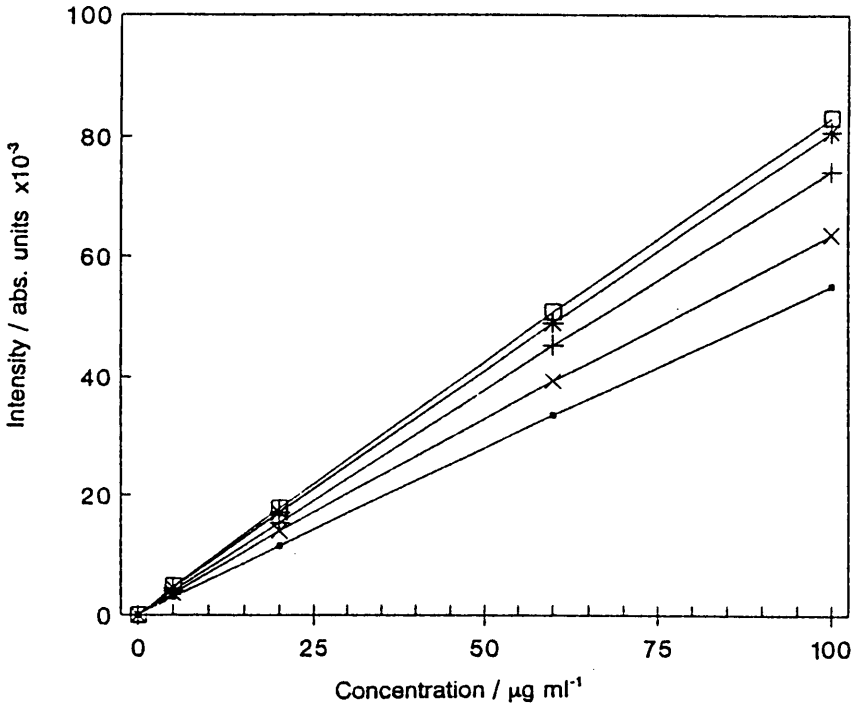

Figure 6.2a Calibration curves for Al (308.21 nm) with increasing ethanol concentration: (⊡) 0 ; (+) 5 ; (✳) 10 %; (□) 15 %; and (x) 20 %, at a flow rate of 0.6 l min^{-1} and 1.36 kW power.

The percentage increase in sensitivity with increasing ethanol concentration was in the same order for Pb, Cd , Fe, Cr and Mn, less for Al and Na and still smaller for Mo and V (Table 6.1b and Fig. 6.1a, 6.2a and 6.2b). Two of the calibration curves obtained are given in Fig. 6.2a and 6.2b and these are for Al and Mo as examples of the changes that occurred to signal intensity as the ethanol concentration was increased. The other calibration curves are included in the Appendix D.

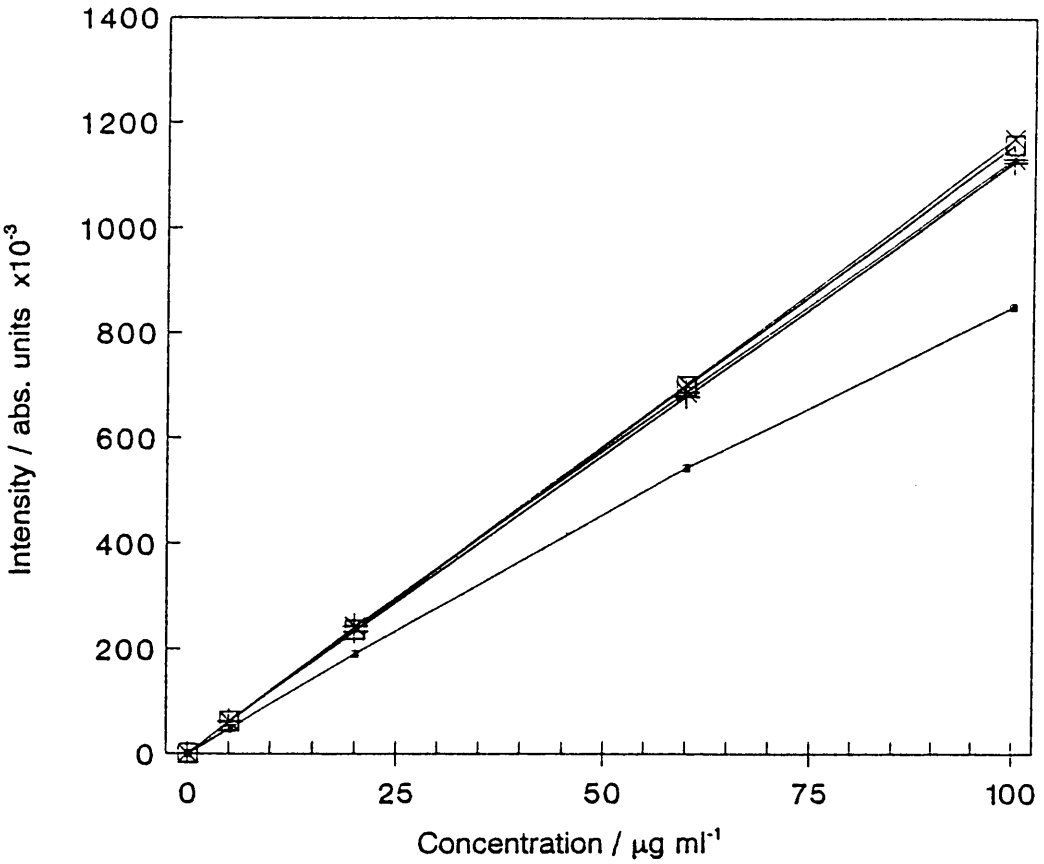

Figure 6.2b Calibration curves for Mo (281.61 nm) with increasing ethanol concentration: (⊡) 0 ; (+) 5 ; (✳) 10 %; (□) 15 %; and (x) 20 %, at a flow rate of 0.6 l min^{-1} and 1.36 kW power.

When the aerosol carrier gas flow rate was reduced to 0.40 l min^{-1}, the results changed, the sensitivity of all the determinations being reduced. Using the aqueous and 15 % solutions for Mo and V, the flow rate was increase from 0.40 l min^{-1} to 0.75 l min^{-1} (the maximum for the instrument) at 0.5 ml min^{-1} intervals the results being found in Table 6.2. The experiment was repeated for Cd, Al, Cr, Fe, Na and Mn, using the aqueous solution and comparing it with solutions containing 20 %

ethanol, examples of these being given in Fig. 6.3a - 6.3c (those for Al, Fe and Na). Results for the other elements may be found in Appendix D.

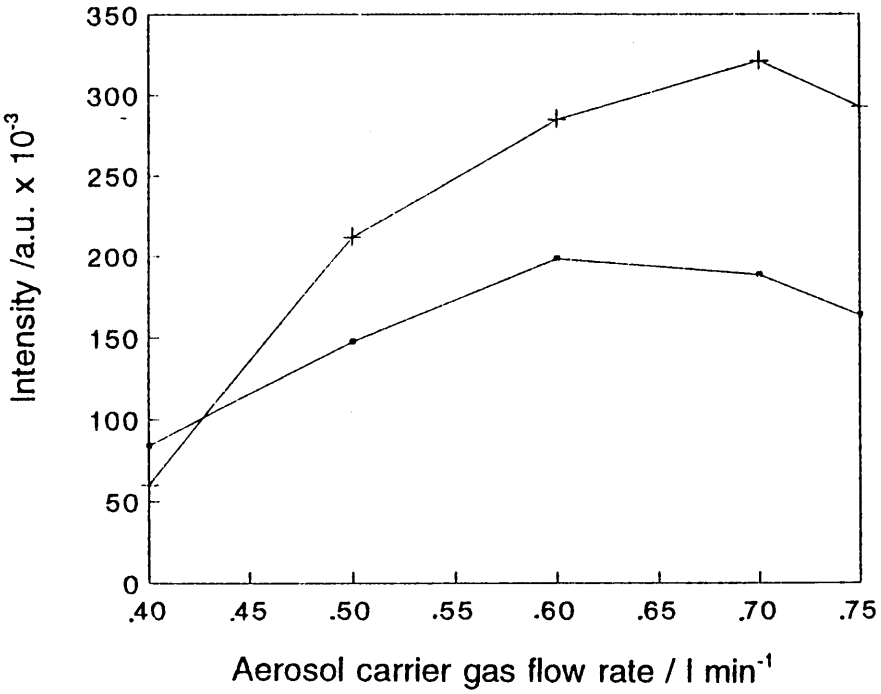

Figure 6.3a Emission intensity versus aerosol carrier gas flow rate for (⊡) aqueous and (+) 20 % ethanol solutions of Al.

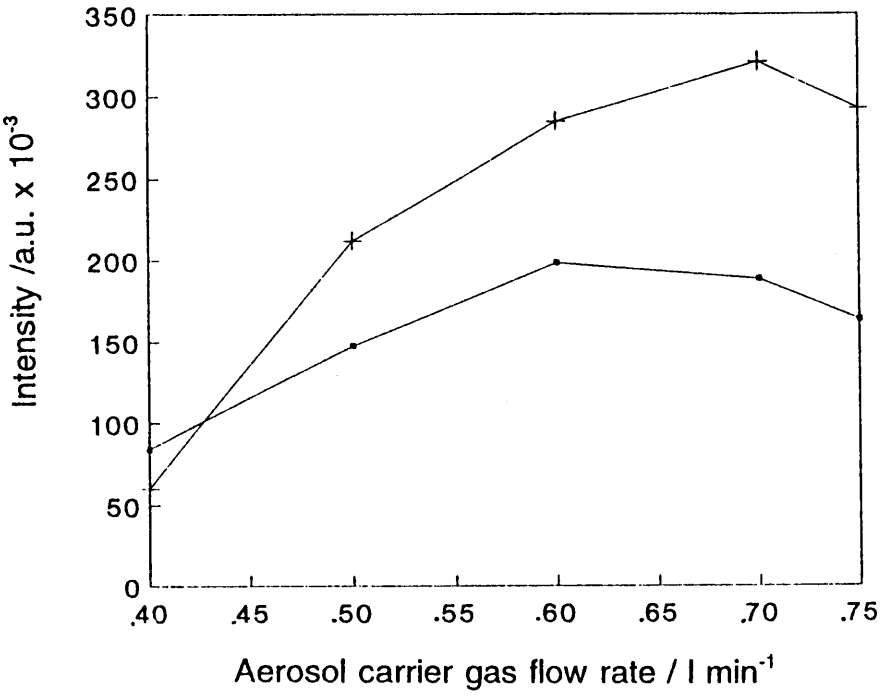

Figure 6.3b Emission intensity versus aerosol carrier gas flow rate for (⊡) aqueous and (+) 20 % ethanol solutions of Fe.

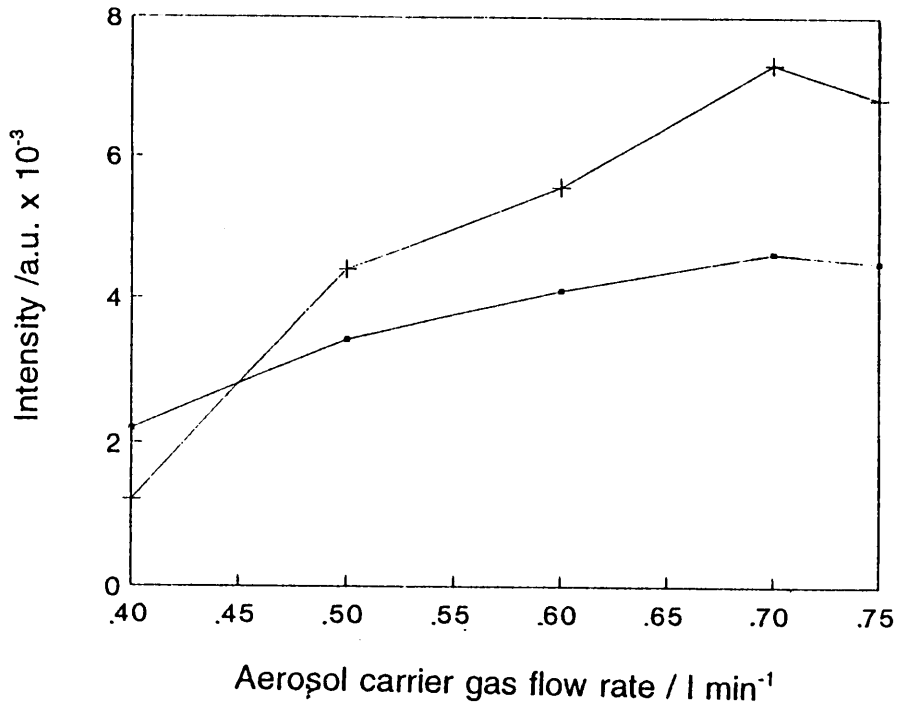

Figure 6.3c Emission intensity versus aerosol carrier gas flow rate for (⊡) aqueous and (+) 20 % ethanol solutions of Na.

An ethanol concentration of 15 % was chosen initially as that had produced the most sensitive calibration curve, but with the second experiment it was decided to use the highest ethanol concentration so as to produce the greatest changes in the background emission. Using the 20 % ethanol solution the intensity of the H_δ line at 434.05 nm was measured at different flow rates as may be seen in Fig. 6.4.

The sensitivity of the calibration curves of all the elements investigated increased from a flow rate of 0.4 l min^{-1} to a maximum when the flow rate was 0.6 l min^{-1} in aqueous solutions. In the presence of ethanol the maximum sensitivity was obtained when the flow rate was 0.70 l min^{-1}. Also the sensitivity increased by a factor of 2 for the aqueous solutions while for the ethanol solutions the factor was in excess of 5. The detection limits improved with increasing flow rates in both aqueous and ethanol solutions.

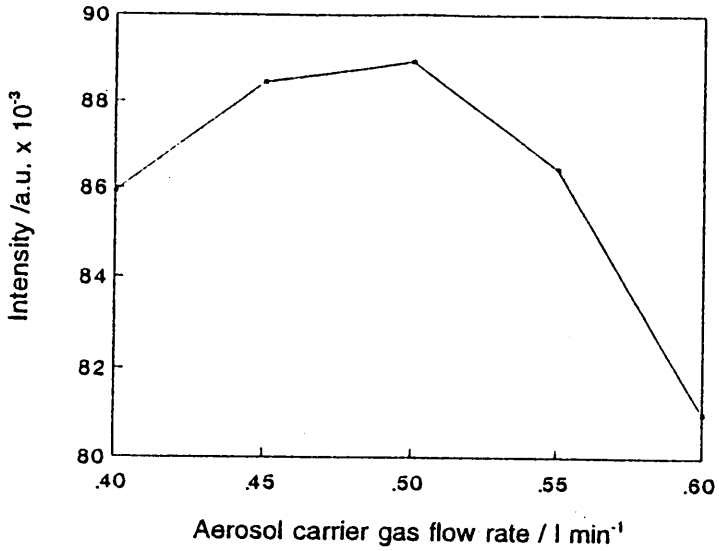

Figure 6.4 Emission intensity of the H_δ line at 483.05 nm when a 20 % ethanol solution was measured with increasing aerosol carrier gas flow rate.

The discovery that ethanol in the solution caused an increase in the hydrogen concentration within the plasma changed the direction of the investigation. The increase in hydrogen may have been expected since the ethanol molecule contains six hydrogen atoms as opposed to the two contained by a water molecule, but simple calculations show that there is in fact a 0.3 % increase in the actual number of hydrogen atoms in a 5 % ethanol solution as opposed to pure water. This increase in actual number of hydrogen atoms continues as the ethanol concentration increases, but is negligible (less than 0.3 %). It was found that hydrogen increased by more than 200 % (Chapter 5, Fig. 5.11). This discrepancy implied that the ethanol solutions could not have undergone the same dissociation mechanism as the water and that the hydrogen must be produced by some different mechanism and not merely by dissociation.

The background intensity found in the plasma is associated with a continuum emission due to Bremsstrahlung or recombination processes which are related to the electron density and temperature of the plasma (Long and Browner: 1988). Anything which changes the electron density and temperature may obviously affect the background. The addition of hydrogen to either sheathing or premix gas results in an increase in the continuum (Batal *et al*: 1982).

Table 6.2. Analytical parameters for different nebulizer flow rates when the solvent contained 0 and 15 % ethanol.

Element	Wavelength /nm	Flow rate /l min^{-1}	Sensitivity /a.u.($\mu g\ ml^{-1}$)$^{-1}$ x 10^{-3}	Det. Lim. /$\mu g\ ml^{-1}$	BEC /$\mu g\ ml^{-1}$	Ethanol /%
Mo	281.61	0.40	458	0.14	4.71	0
		0.50	687	0.094	3.09	0
		0.60	851	0.066	2.30	0
		0.70	849	0.064	2.12	0
		0.75	791	0.061	1.95	0
		0.40	367	0.41	13.6	15
		0.50	1070	0.13	4.42	15
		0.60	1300	0.083	2.83	15
		0.70	1330	0.043	1.82	15
		0.75	1230	0.040	1.69	15
V	311.07	0.40	137	0.053	1.81	0
		0.50	254	0.035	0.987	0
		0.60	316	0.018	0.650	0
		0.70	305	0.017	0.630	0
		0.75	289	0.015	0.573	0
		0.40	90.8	0.19	6.31	15
		0.50	328	0.047	1.61	15
		0.60	430	0.027	0.926	15
		0.70	476	0.012	0.441	15
		0.75	464	0.010	0.364	15

The addition of ethanol to the plasma clearly increased the background, the results being given in Table 6.1b. These results were obtained when the flow rate was 0.6 l min^{-1}, close to the instrument's recommended value rather than the optimum flow rate determined from Fig. 6.3a - 6.3c. Using the optimum flow rate the background was increased by the addition of ethanol. The increase in background was dependent on the flow rate and wavelength, in all cases Na at 589.59 nm yielding the largest BEC. At optimum flow rate, the increase in BEC due to the ethanol/hydrogen was equivalent to the increase in sensitivity which resulted from the addition and similar detection limits were obtained. In the case of 15 % ethanol the detection limits were improved (0.043 vs 0.066 µg ml^{-1} for Mo and 0.018 vs 0.012 µg ml^{-1} for V).

The indirect addition of hydrogen to the system, resulting in an increased electron density and excitation temperature led to an increase in sensitivity. Under optimum conditions (15 % ethanol), the increase in BEC was not as great as the increase in sensitivity and the addition led to an improvement in detection limits. For other concentrations of ethanol this was not the case even though the sensitivity increased the increase was not sufficient to offset the increase in BEC. The increase in sensitivity continued as the percentage of ethanol was increased to a maximum of 15 %. A further increase in ethanol resulted in the sensitivity decreasing, and the detection limits degenerated. This was particularly true when the flow rate was not optimized.

The residence time of the solvent within the plasma played a far greater role with the ethanol solutions than with pure water, as may be seen from Fig. 6.3a - 6.3c. Changes to the flow rate, when aqueous solutions were being nebulized, caused the detection limits and sensitivity to change. When pure water was used as solvent, an increase in the aerosol carrier gas flow rate from 0.4 l min^{-1} to maximum sensitivity, which was reached at 0.6 l min^{-1}, the sensitivity had only increased by a factor of 2. A similar change in flow rate resulted in an improvement by a factor of 7 for Al when 20 % ethanol was used as solvent. The importance residence time, as indicated by the aerosol flow rate, cannot be underestimated, and it further underlined the complex mechanism which the ethanol must undergo in the plasma.

The aerosol carrier gas flow rate was adjusted by changing the nebulizer pressure. Nebulizer pressure adjustment on most commercial instruments is made by means of a dial which is rotated to increase or decrease the pressure. The magnitude of the pressure is portrayed as an analogue measurement on a dial, normally with few sub-divisions, making it impossible to obtain sensitive responses. Small changes in pressure result in comparatively small changes in flow rate, but in the case of ethanol loading even an increase of 0.05 ml min^{-1} resulted in significant differences in sensitivity (140 %). Minor fluctuations in gas pressure (like the opening of a new argon cylinder) easily cause changes in flow rate of similar magnitude (0.05 l min^{-1}). The accuracy required in the measuring of flow rate is a topic which needs further investigation.

CHAPTER 7

CHARACTERISTICS AND APPLICATION OF 40 MHz ICP-OES

7.1 Introduction

Commercially available ICP-OES instruments in South Africa have used a frequency of 27 MHz. These were unable to maintain the plasma when high concentrations of ethanol were aspirated (above about 25 % ethanol depending on applied power). The development and commercial introduction of a new crystal controlled ICP-OES instrument with a more stable plasma using 41 MHz has made it possible to reconsider the analysis of ethanol samples. The recently introduced ICP-OES is the Varian Liberty which has a 40.68 MHz crystal controlled rf generator with direct serial coupling (DISC). DISC directly couples the rf circuitry to the load coil and so ensures that high plasma stability is maintained. The stability of the plasma was such that it was possible to investigate ethanol solutions containing 100 % ethanol. Since the new instrument did not make use of fibre optics the opportunity arose to investigate the viewing height as an adjustable parameter.

The influence of ethanol on organic solvents has not been investigated. This is probably the result of the ICP-OES's inability to work with high ethanol concentrations. Also, one of the most important applications for organic solvents is in the analysis of oil samples and oil is insoluble in ethanol and methanol. There is no information in the literature about the influence of ethanol on analyses carried out with ethanol additions to an organic solvent. The changes to excitation conditions within the plasma caused by the additions of ethanol to an organic solvent should complement the knowledge of the mechanisms occurring as the analyte progresses into the observation zone.

The introduction of a more stable ICP-OES has made investigations regarding the influence of ethanol in other organic solvents on the plasma possible. The effect of

the nebulization of ethanol in an organic solvent, on parameters such as observation height and flow rates was investigated. The intensity of the hydrogen line in the plasma was determined for various additions of ethanol. The analytical results were obtained using mixtures of xylene and ethanol and were compared to those obtained with pure xylene using Simplex optimization. Details of the Simplex procedures will be given in Section 7.2.2.

7.2 Review of the literature

7.2.1 Oil Analysis

There is an abundance of literature pertaining to the analysis of trace metals and wear metals in oil samples (Greenfield and Smith: 1972, Brown: 1983, Uchida: 1982 and Ng and Caruso: 1983). These are primarily carried out as diagnostic controls. The metals in the oil come from three sources: wear, contamination, and additive elements. The wear metals are products of frictional deterioration or corrosion and can be linked directly to the metallurgical composition of the engine. Dirt, leaks, and occasionally residual metal pieces are the cause of contamination. Additives are placed in the oil to reduce engine wear. Possibly the best known of the additives is "liquid moly" used to reduce engine wear when added to gearbox oil. Determination of which elements are present and at what concentration levels can be used for diagnostic purposes. Table 7.1 shows how determination of the type of metal present is linked to possible problem areas in a motor.

Oil analysis is usually carried out with xylene (Greenfield and Smith: 1972 and Brown: 1983) or 4-methyl pentan-2-one (MIBK) as solvent (Uchida: 1982 and Ng and Caruso: 1983). The methods have, in many instances, become routine and some laboratories are dedicated solely to the analysis and interpretation of oil samples. The South African Air Force, Mines, Transnet and most major transport companies all have laboratories where oils are analysed routinely. Advanced warning of possible engine failure is of vital importance for aircraft. The volume of oil required by train engines is enormous (hundreds of litres) and it is in the interest of the company concerned only to change the oil if it really is necessary. Analysis is therefore of considerable economic importance.

Table 7.1 Typical wear indicated by a specific element (McKenzie: 1981)

Element	Indicated conditions
Silicon	Indicates intrusion of soil or sand, usually from faulty air filter apparatus. Causes rapid engine wear and deterioration.
Iron	Indicates wear resulting from engine block, cylinders, gears, rings, camshaft, oil pump or crankshaft.
Copper	Indicates wear of the casing, injectors, valve shields or vacuum screws.
Nickel	Wear of plating on gears, and certain types of bearings.
Tin	Wear of certain types of bearings and iron pistons.
Lead	In diesel engines it indicates wear of bearings, in petrol motors a possible leak in the fuel.
Chromium	Indicates wear of rings or a leak in the cooling system if chromates are used as inhibitors.
Aluminum	Indicates wear of pistons and some types of bearings.
Molybdenum	Indicates wear of certain types of bearings and in oil coolers.
Sodium	Indicates a leak of the anti-freeze agents.
Boron	Indicates a leak of a cooling agent in a system in which boron is used as an inhibitor.
Barium	Used in cleaning oils and rust inhibitors.
Zinc	Primarily as an additive in oils to counter wear.
Phosphorus	As cleaner and anti-rust agent.
Calcium	Used in cleaners and dispersing agents.

There are many methods employed for the analysis of oil samples, but the ones most favoured are spark emission methods or ICP-OES. Both yield (or can yield) simultaneous measurements of many elements and therefore are capable of high throughput of samples. The rotating electrode spark source spectroscopy has the advantage that the samples do not require dilution before analysis, and many elements can be determined directly, without any sample preparation (Gambrill *et al*: 1971).

The introduction of the ICP-OES in the mid-seventies provided a simple alternative to the d.c. arc and spark sources (Barnes: 1978 and Fassel and Kniseley: 1974). This new technique was found to be well suited to oil analysis, although dilution of the oil was required (Fassel *et al*: 1976 and Brown: 1983). A list of detection limits for the analysis of lubricating oils by ICP-OES is given in Table 7.2. The need for dilution is two fold; to facilitate the nebulization of viscous samples by using a low viscous solvent, and to equalize the nebulization efficiency for various viscosities. This dilution could lead to the possibility of handling error, but it would definitely result in loss of sensitivity and increase in detection limits.

Algeo *et al* (1985) reported a method in which the Babington nebulizer was preheated and hence the oil could be nebulized directly into the plasma without the need for dilution. This eliminated possible errors. Despite the disadvantages of dilution, ICP-OES was soon to replace the arc or d.c.-plasma jet methods in most laboratories.

Granchi *et al* (1987) reported a method where a robot was used together with flow injection for fully automated sample preparation and determination of the wear metals in oils by ICP-OES. The automated system produced results identical to those obtained with manual used-oil analysis, but reduced the man-power requirements by two-thirds. Flow injection analysis for sample introduction improved the precision.

Table 7.2 Typical detection limits for the analysis of lubricating oils by ICP-OES, using MIBK for dilution (Fassel *et al*: 1976).

Element	Wavelength /nm	Detection limit /μg g^{-1}
Fe	259.940	0.04
Cu	324.754	0.006
Mg	279.553	0.007
Cr	283.563	0.03
Ag	328.068	0.02
Al	308.216	0.09
Zn	213.856	0.04
Si	288.160	0.07
Ni	341.476	0.1
Pb	283.306	0.3

Botto (1987) investigated matrix interferences in the analysis of organic solutions using ICP-OES. He found that these interferences arose during analyses if the composition and/or physical properties of the standards and samples were not identical. The analysis of widely different petroleum products was long and time-consuming if errors due to mismatching of sample and standard were to be avoided. This problem could partly be overcome, he found, if a suitable internal standard was used. He endeavoured to find a method which would reduce the problems of mismatching and addition of internal standards.

In the investigation, Botto looked at solutions of o-xylene and tetralin containing 2 - 20 % mass of solute and 1 μg g^{-1} of each of 21 elements in the solvents xylene, toluene, tetralin, 75 neutral lube base oils and bright stock. He measured the physical properties of each solution, which was then analysed by ICP-OES using calibration

standards consisting of pure xylene and tetralin. The intensity of the H_β line was also measured and normalized. H_β emission intensities were determined. The formula he used to calculate the normalized H_β intensities is given below:

$$\Delta\%H_\beta = \frac{\text{measured } H_\beta - \text{calculated } H_\beta}{\text{calculated } H_\beta} \text{ X } 100 \qquad 8.1$$

Since H_β is a "hard" line, the intensity will be suppressed or enhanced according to changes in the plasma that would affect "hard" lines. The addition of toluene, a more volatile solution than xylene, to the matrix, resulted in the intensity of the lines of two elements (Ag and Cu) being increased. Two "hard" lines (Cd and Zn), decreased in intensity. Botto deduced that these changes in intensity were due to the cooling effect caused by an increased plasma load. He found, further, that the signal observed for elements containing a 20 % solution of lube base stock in xylene was suppressed by between 5 and 25 %.

In work carried out by Rademeyer and Fischer (1993) metals in waxes were determined using ICP-OES. A Babington V-groove nebulizer was used with a heated spray chamber to enable the authors to nebulize the wax directly into the plasma. The same system was used to determine metals in both edible and lubricating oil (Fischer and Rademeyer: 1994). After optimizing the temperature of the spray chamber, oil flow rate and plasma power, detection limits obtained for the lubricating oils compared favourably with those reported elsewhere.

7.2.2 Simplex Optimization

It is self explanatory that the best possible results that can be obtained from the instrument should be reported. These results can be realized by optimizing the instrumental system before measuring emission intensities. The procedures which can be applied to obtain an optimized ICP-OES vary from "trial-and-error" methods to more systematic methods of which the Simplex procedure is one. Of the systematic techniques, the Simplex method is possibly the most rapid (Moore: 1985).

The sequential Simplex method was first proposed by Spendley *et al* (1962), and this was followed by the modified Simplex method of Nelder and Mead (1965) described by Morgan and Deming (1974) in a review article. A Simplex is a geometric figure which can move over a response surface in order to find the optimum position. A Simplex has one more top vertex (legs) than the number of variables, n, which need to be optimized. It moves across the response surface by lifting one leg (the poorest response obtained) and placing it on the surface in the direction in which the optimum response could be expected.

The modified Simplex method is an improvement on the original in that the simplex can expand when moving in a favourable direction and contract when the direction of movement is less favourable. This results in the optimum conditions being found more rapidly. More details may be found in other articles (Moore: 1985, Morgan and Deming: 1974 and Ebdon *et al*: 1980), while the rules and procedures for the Simplex method used is given in Appendix C.

The concentration of the same elements was determined in aqueous/ethanol mixtures using a 40 MHz ICP-OES, but additional standards prepared in 95 % ethanol were added to the series used in Chapter 6. The effect that high ethanol concentrations (up to 100 %) on parameters such as hydrogen intensity and electron density was also investigated. Changes in analytical parameters resulting from a high ethanol matrix were determined. The influence of aerosol carrier gas flow rate, observation height, and plasma power on signal intensity of several elements in various ethanol solutions was investigated.

The influence of ethanol in xylene had on mass flow rate, electron density and hydrogen intensity was investigated. Calibration curves were drawn for Fe, Al, Pb, Cu and Cr in the different xylene mixtures. Using secondary standards prepared from oil-based standards the concentration of elements in a standard reference oil were determined and compared to the certified values.

7.3 Experimental

7.3.1 Apparatus

7.3.1.1 ICP Spectrometer

A Liberty 220 ICP-OES made by Varian was used and operated under the conditions given in Table 7.3. The monochrometer was a 0.75 m Czerny Turner with a holographic grating of 1800 lines mm^{-1}. The grating was 100 x 90 mm in size. Stray light was reduced by using the holographic grating and a solar blind photomultiplier. Selected filters were used automatically, but it was not found to be necessary to apply any manually.

Table 7.3 ICP-OES operating conditions.

Rf power	1.00 to 1.50 kW
Argon plasma gas flow rate	15.0 l min^{-1}
Auxiliary gas flow rate	1.50 l min^{-1}
Pump speed	25.0 rpm
Nebulizer gas pressure	100 to 200 kPa
Torch	Quartz, low flow, low power
Spray chamber	Inert Sturman-Masters
Nebulizer	Glass concentric

Detection was by means of two photomultipliers, a R928 with a wide wavelength range (300 - 940 nm) and a R166 solar blind for the 160 - 300 nm range. Viewing height was computer controlled and allowed for a 6 mm horizontal and 40 mm vertical range. The rf generator was crystal controlled, solid state driven and water cooled, with an operating frequency of 40.68 MHz. Coupling was by means of DISC and the rf power was auto-tuned. The spectrometer was controlled by an IBM compatible PC and the software made it possible to optimize viewing height for each element by

means of a scan of emission intensity versus height. A "chiller" was used to control the temperature of the water used by the instrument.

7.3.2 **Reagents**

7.3.2.1 Aqueous/ethanol solutions

Solutions containing 1, 5, 20, 60 and 100 μg ml^{-1} of lead in pure water (distilled and passed through a Milli-Q water purification system of Millipore Corporation) were prepared from a 1000 μg ml^{-1} Merck Titrisol standard. The same concentrations of Pb were made up in 5, 10, 15, 20, 25 and 95 % (v/v) ethanol (seven series of solutions in total). A further series of standards were prepared in a similar fashion, containing the same concentrations as above but of Cd, Al, Cr, Mn, Fe and Na in the same ethanol solutions.

Since an aqueous 1000 μg ml^{-1} Titrisol was used, standards containing 20, 60 and 100 μg ml^{-1} dilutions of the combined elements could not be made in the same 95 % ethanol solution. Hence, separate standards for all the elements were made for the 20, 60 and 100 μg ml^{-1} standards in 95 % ethanol. Finally, another series was prepared in a similar way containing V and Mo. The higher standards (20 μg ml^{-1} and greater) in 95 % ethanol were again prepared separately. The ethanol used was analytical-reagent grade.

For the investigations into the effects of ethanol concentrations on the intensity of the hydrogen lines the series of solutions described above was used, since those had been experimented with previously (except the 95 % solution). A separate series of aqueous/ethanol solutions was prepared, in which the ethanol concentration was, respectively, 20, 40, 60, 80, and 100 % (v/v) ethanol in water. In this series, the ethanol concentrations were more evenly dispersed over the entire range.

A series of solutions of water, 25, 50, 75 and 95 % (v/v) ethanol solutions, each containing 50 μg l^{-1} of Mg was also prepared.

7.3.2.2 Oil Solutions

The oil samples were prepared from the following solutions:

(i) Conostan D oil-based organometallic standard solution for the determination of metals in lubricating oil, by Conostan Division of the Continental Oil Company, Ponca City, Oklahoma, USA. The standard oil solution contained 900 $\mu g\ g^{-1}$ of 12 elements, Al, Cu, Cr, Fe, Pb, Ag, Mg, Na, Ni, Si, Sn and Ti.

(ii) National Bureau of Standards, NBS, Standard Reference Material, SRM, 1084 containing approximately 100 $\mu g\ g^{-1}$ of the following elements; Al, Cr, Cu, Fe, Pb, Mg, Mo, Ni, Ag and Ti.

(iii) "Metal-free" oil (Conostan "Base oil") was used to prepare blank solutions and to maintain a constant oil content.

(iv) Xylene; Chemically pure grade was used as solvent for all standards and samples.

(v) Ethanol diluted as described above.

7.3.2.3 Preparation of Intermediate Standards

Intermediate standards were prepared, by mass, in polypropylene containers, using a three decimal-place balance. Oil and standard solutions were transferred to the containers by means of disposable syringes to avoid contamination.

* 10.0 and 100 $\mu g\ g^{-1}$ standards of 12 elements: 1.111 and 11.111 g of the Conostan D were placed in two separate polypropylene containers. Metal-free oil was then added to make the mass of each, 15.000 g.
* In the first series, the 10.0 and 100 $\mu g\ g^{-1}$ reference samples were made up to 100.000 g with xylene. No ethanol was added.
* A second series was prepared in a similar fashion to the first, except that after the addition of the metal-free oil, the solutions mass was made up to 70.000 g by the addition of xylene. After the oil had dissolved, the mass was made up to 100.000 g by the addition of ethanol.
* A third series was made in identical fashion, except that it contained

45 % (m/m) of ethanol.

* Blank solutions were prepared for each series by replacing the Conostan D 12 standard with metal-free oil.

7.3.2.4 Preparation of Sample

To prepare the sample 11.111 g of the NBS SRM 1084 was measured into three separate containers. Metal-free oil was added to each to a mass of 15.000 g. To the first, xylene was added to give a final mass of 100.000 g, while ethanol was added to the other two solutions (using the method described above) so that the ethanol concentrations were 30 and 45 % (m/m).

7.4 Sensitivity, Detection Limits and Background Equivalent Concentration

The sensitivity, detection limits and BEC were determined according to equations 6.1 and 6.2.

7.5 Mass Flow Rate

The mass flow rate of the xylene and xylene/ethanol solutions was determined in an identical manner as those for aqueous/ethanol mixtures and described in Section 4.3.4.2.

7.6 Simplex Optimization Procedures

A computer programme for optimizing instrumentation called GENMOD. PROG (obtained from the Analytical Science Division of the Council for Mineral Technology, MINTEK, Randburg, South Africa) was used for the Simplex optimization. The programme allows for n variables, where $1<n<11$, and may be used for up to 20 analytical lines simultaneously. It has provision for up to 100 Simplex moves. The programme offers a choice of three functions:

(i) net signal-to-background ratio (SBR),

(ii) net signal, or

(iii) minimum ionization interference.

It has been successfully applied to ICP-OES and to the optimization of graphite furnace techniques in AAS (Moore: 1986). A graphical display is used for monitoring and may be used as a record of optimization procedure.

The most common response function used is the SBR, as this should yield the lowest detection limits (Moore *et al*: 1984).

7.7 Results and Discussion

7.7.1 Aqueous/Ethanol Solutions

The Liberty software and instrumental procedure enabled the vertical height to be set for each element analysed even although it is a sequential instrument. Also, one of the operations carried out by the software was the optimization of the viewing height for each element after which the instrument automatically selected the optimized height. This commercial instrument had no flow rate readout for nebulizer gas, it was regulated by a nebulizer gas pressure adjustment. The setting of the peristaltic pump, tubing and the plasma gas flow rate followed the manufacturer's recommendations. Hence, there were three adjustments which had to be optimized for each element: viewing height, nebulizer gas flow rate and the power. For comparison, the power was maintained at a particular setting throughout an investigation, but considering that both "soft" and "hard" elements were present in the same mixture adjustments could have had different significance with each element.

The elements selected for determination by the Simplex method were those that had been investigated previously (Chapter 6), except for Mg, which was used for the investigation of electron density.

7.7.1.1 Effect of Viewing Height

It was impossible to meaningfully adjust the viewing height with the Spectroflame, since the instrument used fibre optics for the transfer of emission signal. As the optimal viewing height sheds some light on the type of reactions occurring in the plasma it was an important parameter to

determine. Consequently, the effect that the height above the load coil had on the hydrogen content of the ethanol enriched plasma, was determined using the Liberty. In Fig. 7.1 the emission intensity of the H_α line is given at a viewing height 2 and 10 mm above the load coil, when a 15 % ethanol solution was aspirated. It may be clearly seen that the viewing height had a considerable influence on the emission intensity. This could be expected, since recombination could take place rapidly and the hydrogen ion would be short-lived.

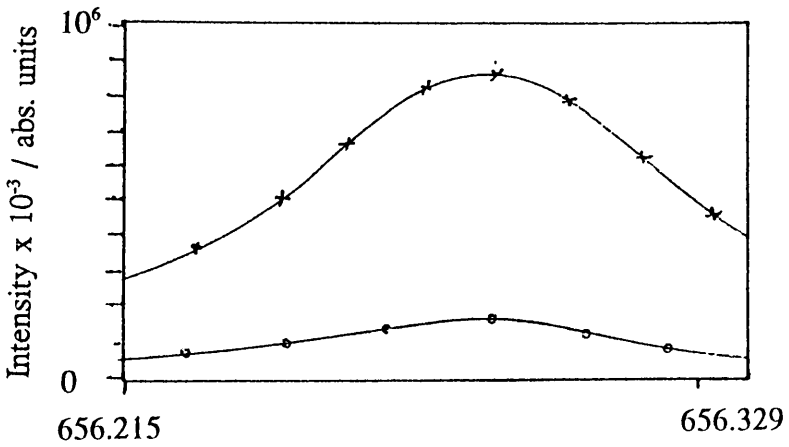

Figure 7.1 Emission intensity of the H_α line 2 (x) and 10 mm (o) above the load coil, 1.2 kW power.

The experiment was extended to find the changes that the optimal viewing height underwent with different ethanol concentrations. Results of this experiment may be seen in Fig. 7.2. Hydrogen intensity was lowest for 100 % ethanol, and reached a maximum when 20 % ethanol solution was aspirated. All the solutions gave a maximum reading for hydrogen intensity at 5 mm above the load coil. Values below 3 and above 8 mm were not recorded since the maximum measurement was clearly defined. Below 3 and above 8 mm the magnitude of the emission intensity continued falling.

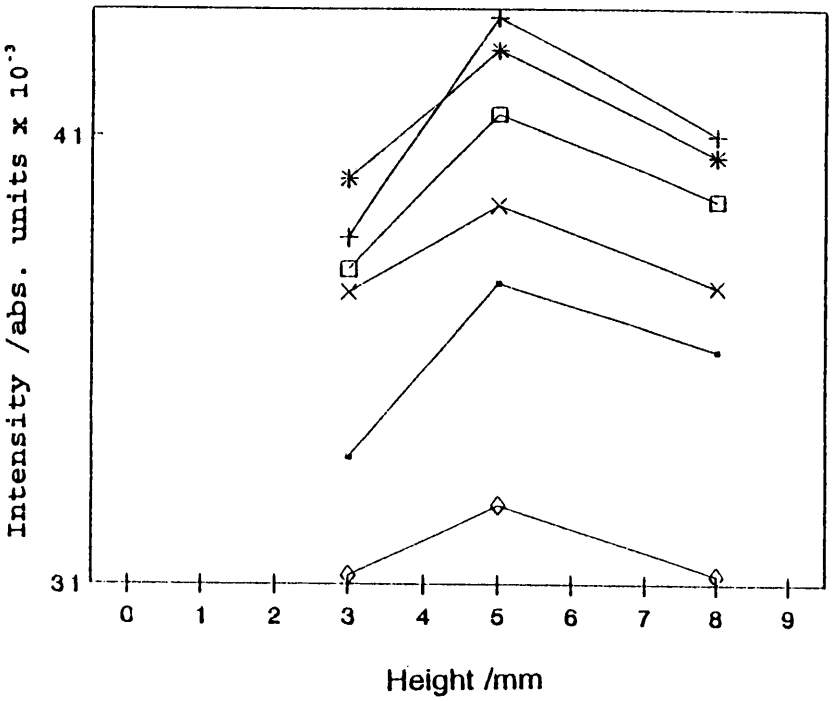

Figure 7.2 Changes in signal intensity of the H_α line at different viewing heights for increasing ethanol concentration: (▫) 0 %; (+) 20 %; (✳) 40 %; (□) 60 %; (x) 80 % and (◇) 100%.

7.7.1.2 Effect of Nebulizer Gas Pressure

The effect different nebulizer gas pressure settings (nebulizer gas flow rates) was also investigated. The results may be seen in Fig 7.3a and 7.3b, when various ethanol concentrations were nebulized at pressures of 100 and 200 kPa and at a viewing height of 14 mm. At a high flow rate, when the pressure was 200 kPa, the highest intensity of the hydrogen line was obtained when pure water when aspirated.

The intensity of the hydrogen line decreased as the ethanol concentration in the aspirates was increased (Fig. 7.3a). The reverse was found for a low flow rate (100 kPa pressure), where the intensity of the hydrogen line increased with increasing ethanol concentrations aspirated. Clearly, the emission resulting from the hydrogen in the plasma increased with ethanol concentration at low flow rates, whereas at high flow rates the ethanol resulted in the hydrogen signal decreasing.

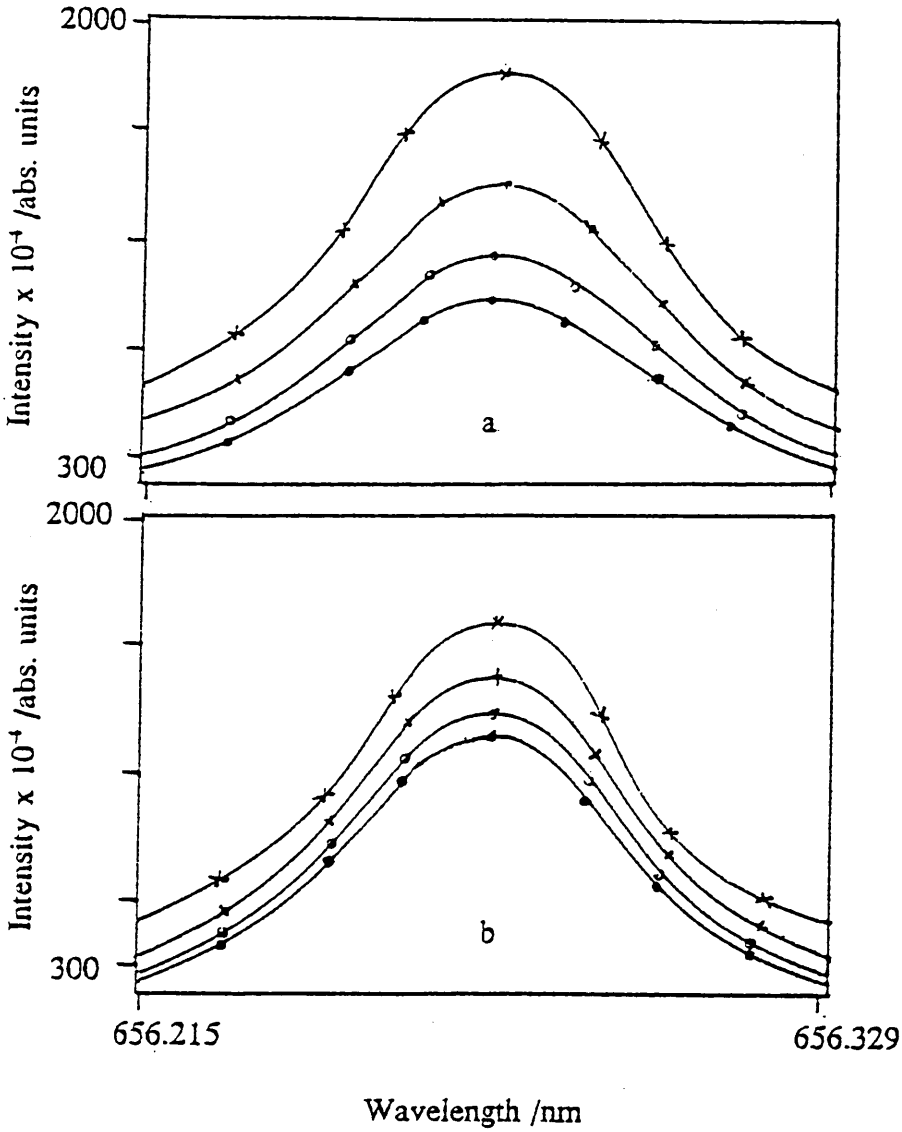

Figure 7.3 Emission intensity of hydrogen as measured by the H_α line for increasing ethanol concentrations at (a) 200 kPa: (x) 0 %; (+) 5 %; (o) 10 % and (●) 15% and (b) 100 kPa: (x) 15 %; (+) 10 %; (o) 5 % and (●) 0 %.

The effect of nebulizer gas pressure (aerosol carrier gas flow rate) on the emission intensity of the hydrogen line for various ethanol concentrations (up to 100 %) may be seen in Fig. 7.4. The signal obtained for hydrogen emission increased as the aerosol carrier flow rate increased, in the case of pure water, for all pressure values that were applied. This was not true for the ethanol solutions, for which the hydrogen intensity rapidly increased to reach a maximum at 80 kPa, before decreasing.

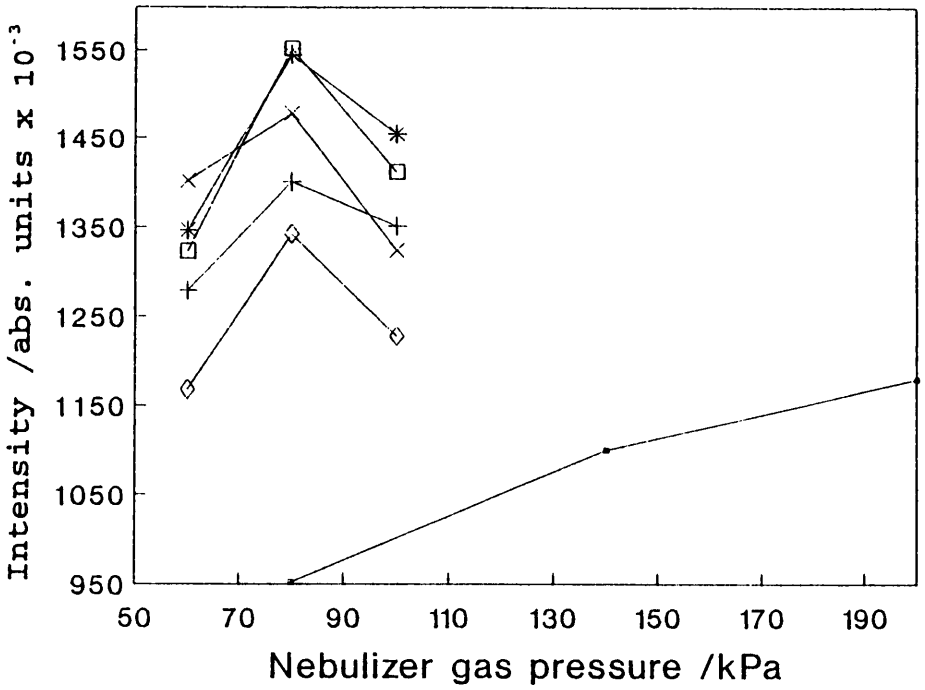

Figure 7.4 Influence of nebulizer gas pressure on the emission intensity of hydrogen as measured by the H_α line for increasing ethanol concentrations: (▫) 0 %; (+) 20 %; (✳) 40 %; (□) 60 %; (x) 80 % and (◊) 100 % ethanol.

The intensity of the hydrogen emission signal was only recorded for the ethanolic solutions in the region of 60 to 100 kPa. Above and below those values the signal decreased rapidly. The signal for water, on the other hand, was comparatively small initially and consequently the emission signal was only recorded above a nebulizer gas pressure of 80 kPa.

7.7.1.3 Effect of Ethanol Concentration when Nebulizer Gas Pressure was Held Constant

In Fig. 7.5 the effect that different concentrations of ethanol (0, 5, 10, 15, 25 and 95 %) had on the H_α emission intensity at 1.5 kW and 150 kPa nebulizer pressure may be seen. The pure water solution had the lowest intensity, and the 20 % ethanol the highest. The difference in intensities between the 15 and 20 % solutions was about 12 %. The order, in decreasing intensity was 20, 25, 100, 15, 10, 5, and 0 % ethanol. The magnitude of the signal increased from pure water, reached a maximum at 20 %, then decreased.

It should be noted that the conditions used in this investigation and those used for the other ethanol/aqueous series were different. This resulted in the ethanol concentration which gave the maximum intensity being 20 %. In the second experiment, when the 0, 20, 40, 60, 80 and 100 % solutions were used and with optimum conditions applied, the 60 % ethanol solution produced the greatest intensity as discussed in Section 7.7.1.5.

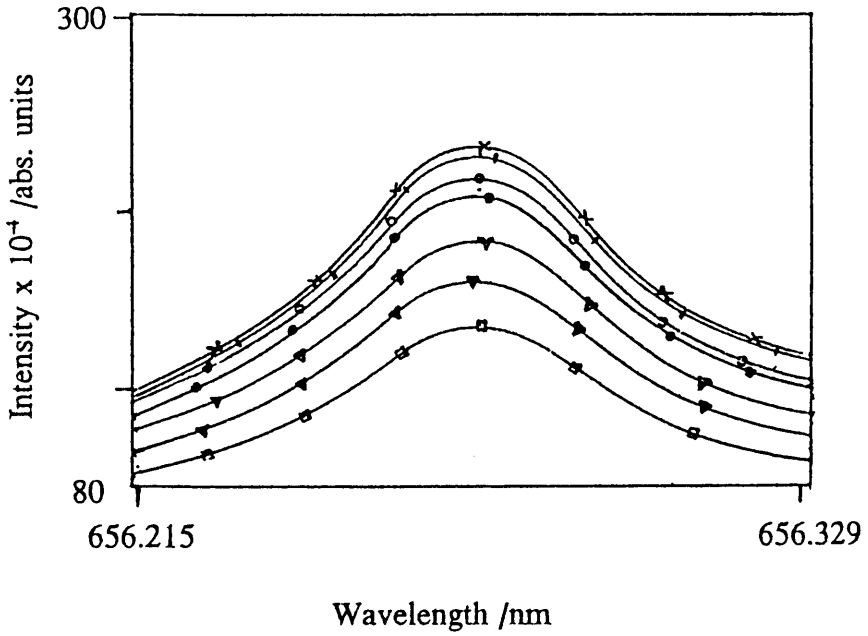

Figure 7.5 The emission intensity of hydrogen as measured by the H_α line for different concentrations of ethanol at 150 kPa and 1.5 kW: (▫) 0 %; (▾) 5 %; (▽) 10 %; (●) 15 %; (x) 20 %; (+) 25 %; (o) 100 %.

7.7.1.4 Effect of Power

The influence of power on the intensity of the hydrogen line was investigated. Aerosol carrier gas flow rate was kept constant, as was viewing height and then the power applied to the rf was varied. Results may be seen in Fig. 7.6. As the power increased so did the intensity of the hydrogen line. This increase was more significant for the solutions containing ethanol than for the pure water sample. The 80 and 100 % ethanol solutions were only measured from 1.40 kW, as below that value the plasma was extinguished.

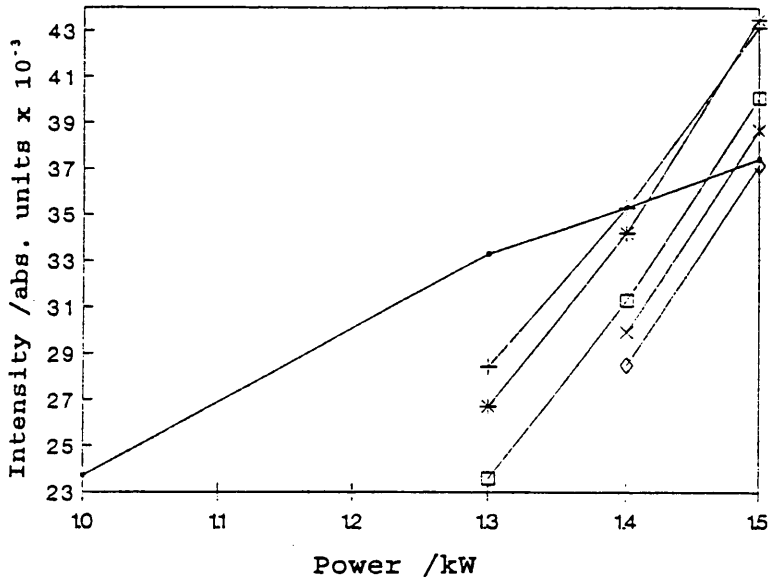

Figure 7.6 Influence of power on the intensity of the H_α line for increasing ethanol concentrations: (▫) 0 %; (+) 20 %; (✳) 40 %; (□) 60 %; (x) 80 % and (◇) 100 % ethanol.

The intensity of the hydrogen signal obtained from ethanolic solutions was only recorded for power values above 1.3 kW, and in the case of 80 and 100 % ethanol only above 1.4 kW. Below those values the signal decreased rapidly.

7.7.1.5 Using Optimized Values

Finally, using the optimum values for nebulizer gas pressure, power and viewing height, found when using different ethanol solutions , the intensity of the hydrogen line was determined (Fig. 7.7).

From the figure it may be seen that the intensity of the hydrogen line increased to a maximum when the solution contained 60 % ethanol, thereafter the intensity decreased, but the 100 % ethanol solution still yielding a value greater than that for pure water. The difference between water and the 60 % ethanol solution was a factor of 1.6. The difference in intensities of the 40 and 60 % ethanol solutions was negligible.

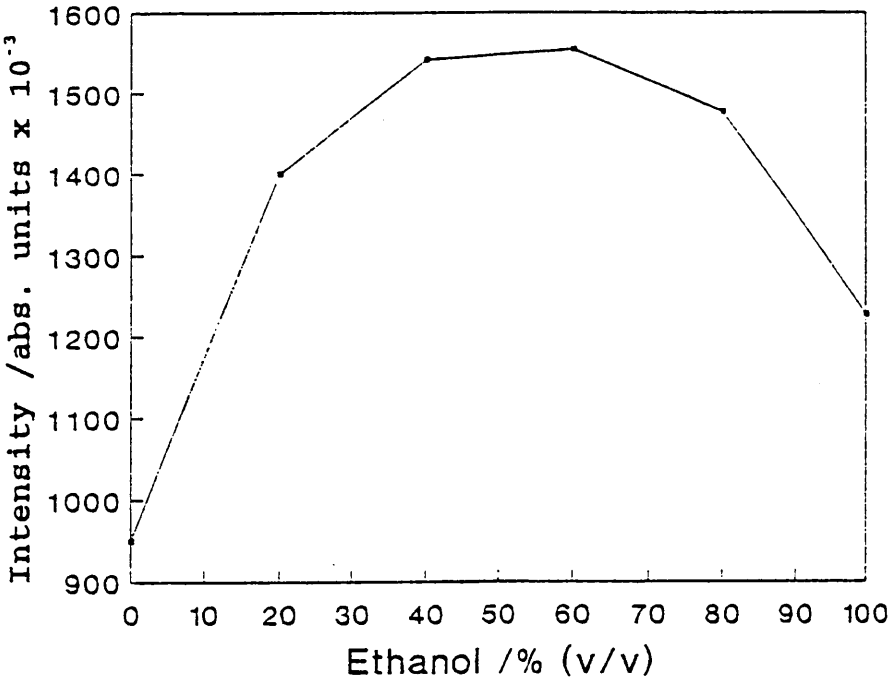

Figure 7.7 Influence of increasing ethanol concentrations on the intensity of hydrogen as measured by the H_α line.

7.7.1.6 Effect of Nebulizer Gas Pressure on Lead Lines

The influence that the nebulizer gas pressure had on the emission intensities of lead was investigated and is given in Fig. 7.8a and 7.8b. A series of ethanol solutions of 100 μg ml^{-1} Pb were investigated at nebulizer pressures of 100 and 200 kPa. In both cases the power setting was 1.2 kW. When the nebulizer pressure was 100 kPa (Fig. 7.8b) the emission intensity of Pb in the 15 % solution was considerably higher (34 %) than that of the 5 % solution. At 200 kPa, the difference was considerably smaller (6 %) and the 5 % solution then yielded the higher value (Fig. 7.8a).

The different scales in Fig. 7.8a and 7.8b should also be noted. The difference in intensities indicate the different sensitivities that may be achieved at the two gas settings. In Fig. 7.8c the emission intensity of the Pb line is given for 100 μg ml^{-1} Pb in 15 % ethanol at various nebulizer gas pressures.

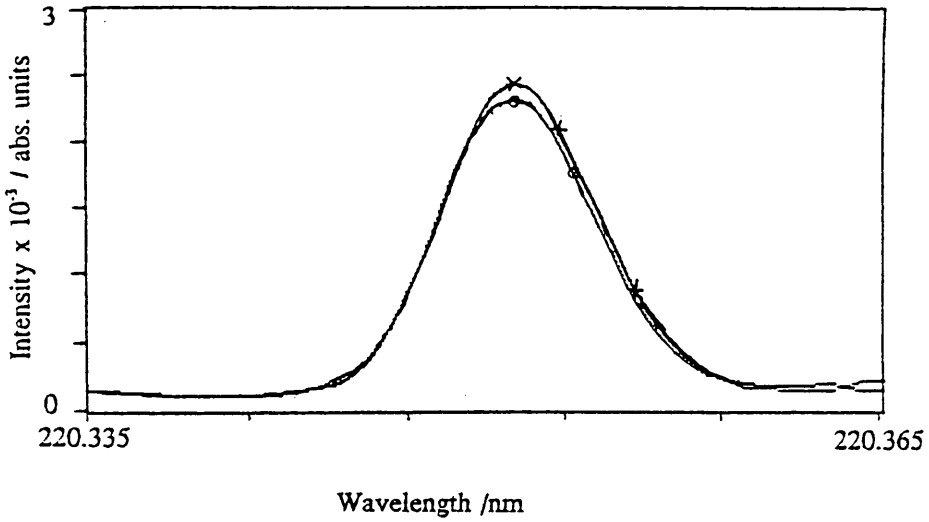

Figure 7.8a The emission intensities of 5 (x) and 15 (o) % ethanol solutions containing 100 μg ml^{-1} Pb. Nebulizer gas pressure was 200 kPa.

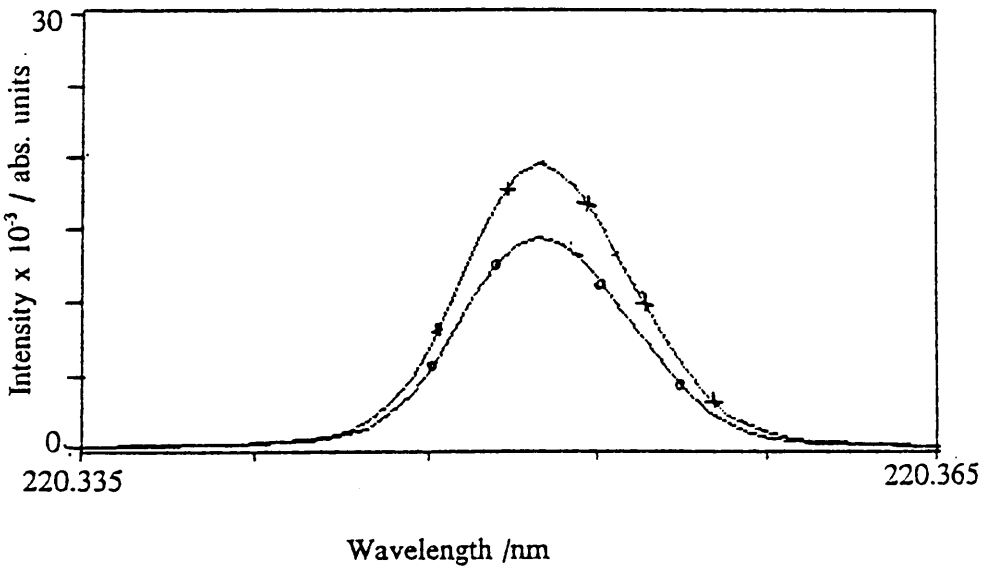

Figure 7.8b The emission intensities of 5 (o) and 15 (x) % ethanol solutions containing 100 μg ml^{-1} Pb. Nebulizer gas pressure was 100 kPa.

Again the importance of nebulizer gas flow rate is indicated as the intensity almost doubled when pressure was changed from 100 to 110 kPa, when the signal from the Pb line was at its greatest. The low pressure for the carrier gas indicated that the residence time of the aspirated solution should be relatively long, less than that for hydrogen, whose intensity reached a maximum at 80 kPa.

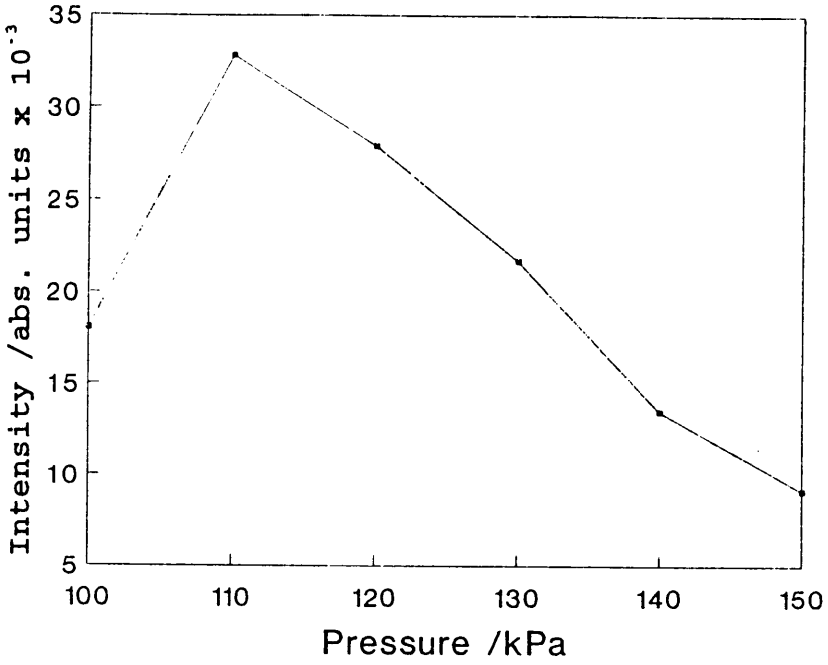

Figure 7.8c The emission intensity of 15 % ethanol solution containing 100 µg ml^{-1} Pb when the nebulizer gas pressure was increased.

7.7.1.6 Effect on Sensitivity of Analysis

Results obtained when different lead standards were nebulized were the same as found in Chapter 6, namely that the sensitivities increased to reach a maximum when the solution contained 15 % ethanol, then decreased as the ethanol concentration increased. There was one major difference in that the 95 % ethanol solution could now be determined at 1.2 kW, and the 25 % solution at 1.0 kW.

The effect on sensitivity was also obtained for the solutions containing V (Fig 7.9a) and Mo (Fig.7.9b). At the higher ethanol concentrations and at the lower power setting of 1.0 kW, the calibration curves for V showed clear deviations from linearity (Fig. 7.9a) and the calibration curve for the 95 % ethanol solution was not determined. In Fig. 7.9b it may be seen that Mo in 95 % ethanol and at 1.5 kW had a calibration curve only a little less sensitive that for the 25 % ethanol solution when the power was 1.2 kW.

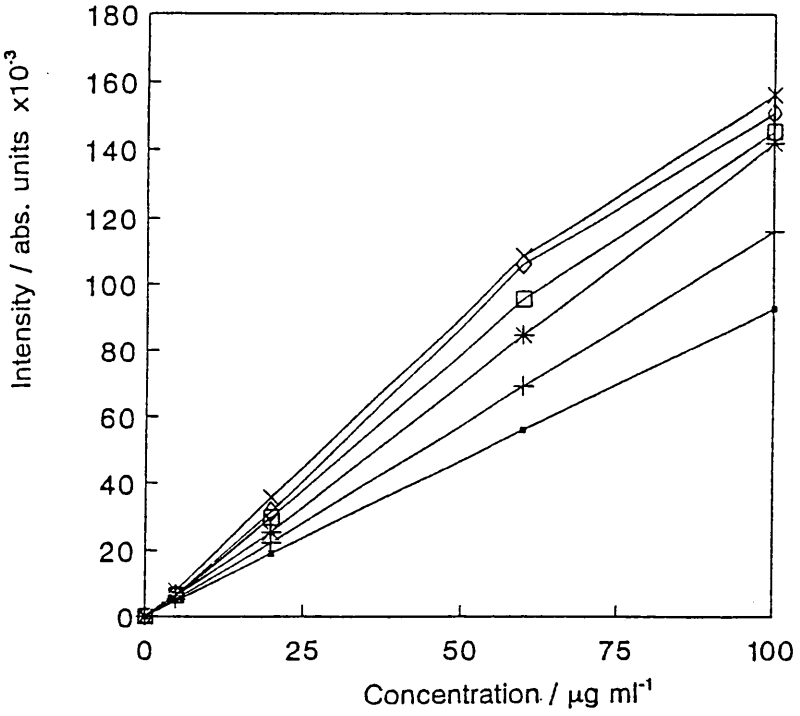

Figure 7.9a Calibration curves containing different ethanol solutions for V at 1.0 kW: (⊡) 0; (+) 5; (✳) 10; (□) 15; (x) 20 and (◊) 25 % ethanol.

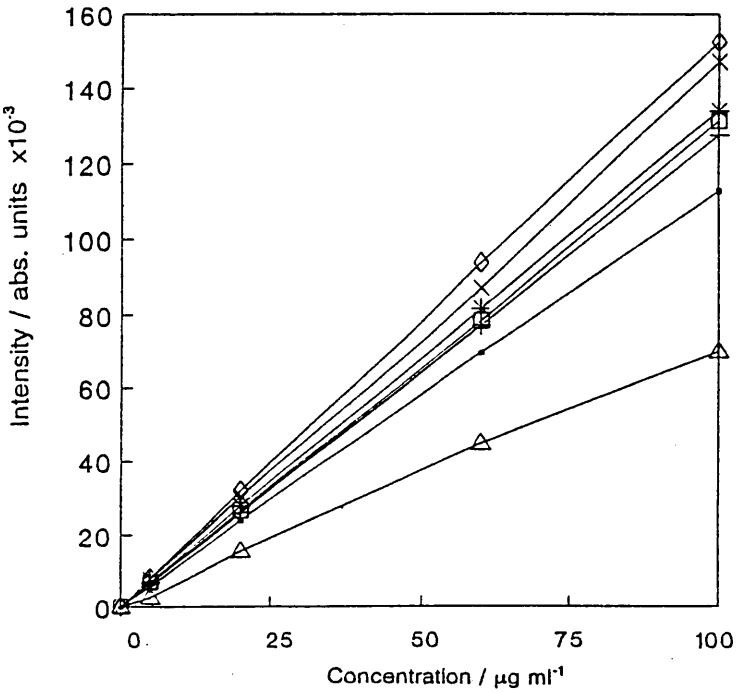

Figure 7.9b Calibration curves containing different ethanol solutions for Mo at 1.2 kW: (⊡) 0; (+) 5; (✳) 10; (□) 15; (x) 20; (◊) 25 and (Δ) 95 % ethanol.

At 1.5 kW the sensitivity for the series with the highest ethanol concentration was increased for all elements studied. Calibration curves for Cr and Na at different concentrations of ethanol are given as examples in Fig. 7.10a and 7.10b. The maximum power recommended by the instrument's manufacturer was 1.5 kW and this was, therefore, the highest value investigated. Sensitivity for both Cr and Na had more than doubled due to the presence of the high ethanol concentration (95 %). Sensitivity, detection limits and BEC for four elements (Cr, Cd, Mn and Na) are given in Table 7.4. The other elements investigated all followed the same trends as those four.

Two trends should be noted:

(i) The BEC increased drastically as the power was changed to 1.5 kW (Table 7.4). This drastic increase affected the detection limits then calculated. Changes in BEC also occurred when these elements were determined in aqueous solutions. The detection limits may suffer if higher sensitivity is required for "hard" lines, where it would be advantageous to use a high power setting. It depends on the determination involved, whether the instrument should be optimized for detection limits or sensitivity. In the case of high ethanol concentrations, the choice is not as simple. High power setting led to greater sensitivity, but in some cases, worse detection limits.

(ii) Regular increments in sensitivity as the ethanol concentration increased were not achieved in this investigation when several elements were determined using one set of conditions. This was because of the use of compromise conditions calculated for the nebulizer pressure. As has been described earlier, the flow rate was critical to the determination of sensitivity. It may seen from the results (Table 7.4), that as certain elements increased in sensitivity when the ethanol concentration was increased from 15 to 20 % (Al and Na), the sensitivity of other elements decreased slightly (Cd and Fe). As mentioned above, the viewing height was optimized for each element. In the case of Na in the 95 % ethanol solution, calibration curves were determined for a height of 2 and 6 mm. The results given in Table 7.4 show that the sensitivity almost

doubled when changing the height from 2 to 6 mm. Also, the calibration curve for Na at 2 mm did not pass through the origin due to the high background measurement.

Table 7.4 Examples of sensitivity, detection limit and BEC for aqueous organic solutions.

Element	Wavelength /nm	Sensitivity x 10^{-3} /a.u.(µg ml^{-1})$^{-1}$	Detection limit /µg ml^{-1}	BEC /µg ml^{-1}	Ethanol /%	Power /kW
Al	396.152	7.25	0.035	1.17	0	1.2
		5.62	0.034	0.991	10	1.2
		7.21	0.13	4.31	10	1.5
		8.42	0.085	2.82	15	1.5
		8.79	0.072	2.40	20	1.5
		17.3	0.054	1.80	95	1.5
Cr	267.716	3.28	0.0034	0.113	0	1.2
		4.03	0.0022	0.0732	10	1.2
		7.61	0.0069	0.231	10	1.5
		9.21	0.0042	0.142	15	1.5
		9.61	0.0037	0.124	20	1.5
		13.8	0.0019	0.0642	95	1.5
Cd	228.802	4.11	0.00082	0.0273	0	1.2
		2.91	0.0011	0.0362	10	1.2
		6.66	0.0030	0.100	10	1.5
		7.39	0.0020	0.0673	15	1.5
		7.14	0.0019	0.0636	20	1.5
		11.6	0.0016	0.0517	95	1.5

Element	Wavelength /nm	Sensitivity x 10^{-3} /a.u.(μg ml^{-1})$^{-1}$	Detection limit /μg ml^{-1}	BEC /μg ml^{-1}	Ethanol /%	Power /kW
Mn	257.610	25.8	0.00050	0.0167	0	1.2
		28.9	0.00035	0.0116	10	1.2
		51.2	0.0011	0.0377	10	1.5
		66.9	0.00062	0.0208	15	1.5
		66.8	0.00057	0.0190	20	1.5
		84.8	0.00046	0.0152	95	1.5
Fe	259.940	4.96	0.0032	0.107	0	1.2
		5.94	0.0024	0.0790	10	1.2
		9.89	0.0065	0.216	10	1.5
		13.0	0.0045	0.153	15	1.5
		13.1	0.0042	0.138	20	1.5
		19.7	0.0026	0.0817	95	1.5
Na	589.592	6.02	0.021	0.704	0	1.2
		5.07	0.035	1.17	10	1.2
		5.01	0.14	4.58	10	1.5
		8.42	0.085	2.82	15	1.5
		8.79	0.072	2.40	20	1.5
(view.	ht. 2 mm)	19.5	0.15	5.07	95	1.5
(view.	ht. 6 mm)	10.9	0.039	1.30	95	1.5

Optimum viewing height changed little for each element as the ethanol concentration increased. There was, however, a decrease in optimum height for the 95 % solutions (by about 2-3 mm). There was also a change in the optimum nebulizer gas flow rate

as adjusted by the pressure. As the power increased so did the optimum pressure, from 110 kPa for 1.0 kW to 180 kPa for the 1.5 kW and 95 % ethanol. The optimum viewing height varied considerably from element to element, for Na it was 2 mm, for Mo 10 mm. In the final analysis of Mn with 95 % ethanol, the viewing height was adjusted to 2 mm. The optimum height was 5 mm, but at that height the photomultiplier tube became saturated.

The changes to the sensitivities of the elements can be seen in the calibration curves given as example (Fig. 7.10a and b). The remaining calibration curves may be found in Appendix D.

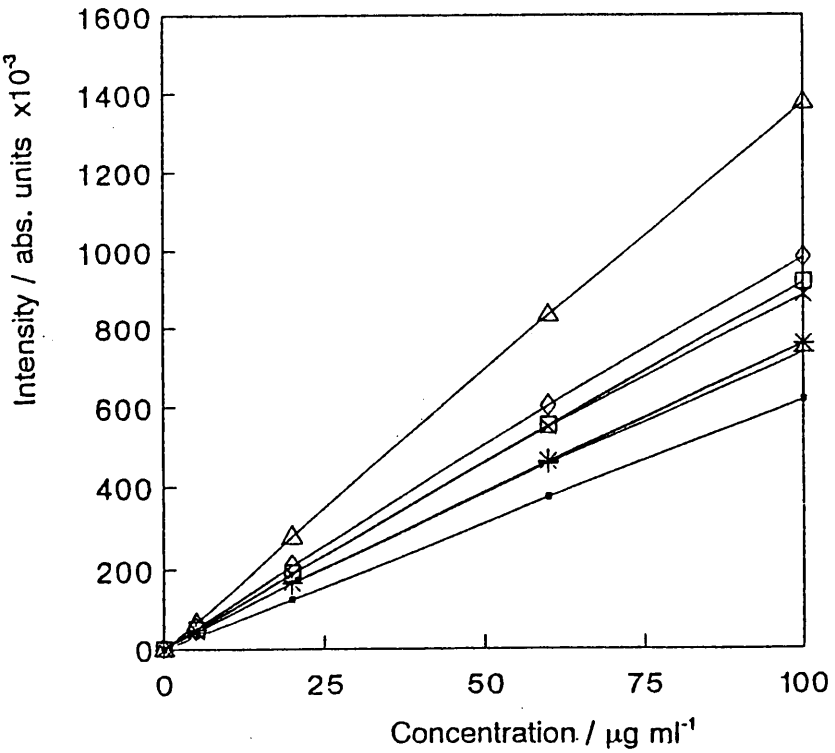

Figure 7.10a Calibrations curves containing different ethanol concentrations at 1.5 kW for Cr: (▫) 0; (+) 5; (✳) 10; (□) 15; (x) 20; (◊) 25 and (Δ) 95 % ethanol.

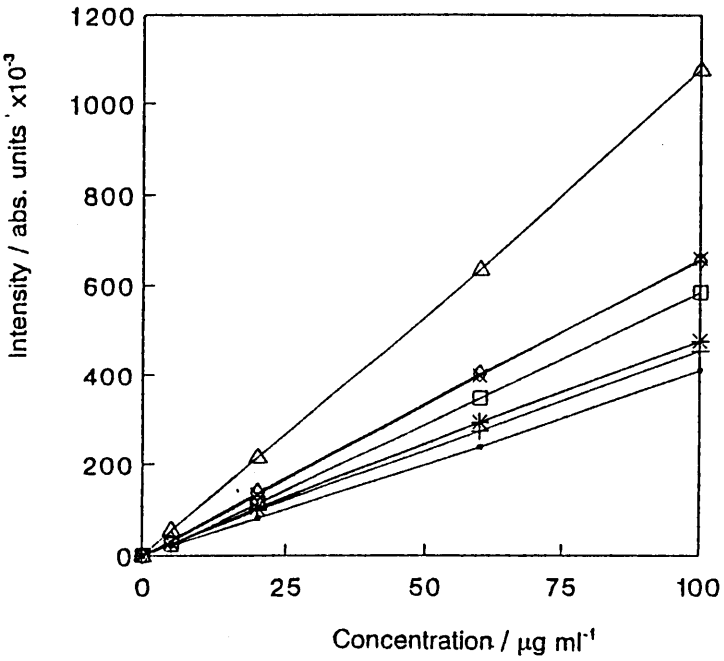

Figure 7.10b Calibrations curves containing different ethanol concentrations at 1.5 kW for Na: (▫) 0; (+) 5; (✳) 10; (□) 15; (x) 20; (◇) 25 and (Δ) 95 % ethanol.

Again the residence time was found to be of importance, the higher the ethanol concentration, the shorter the optimum residence time, but the lower the optimum viewing height.

If the ethanol concentration that the plasma can accommodate is limited, and ethanol be used for extraction purposes, then before elemental analysis can be performed the ethanol must somehow be removed, or its concentration reduced. Hence, the results obtained when using 1.5 kW power were most encouraging as they implied that it was no longer necessary when using ethanol for extractions, or other chemical manipulations, to remove the ethanol, or look for alternative solvents.

7.7.1.8 Electron Density

An approximate determination of the electron density of the plasma during the aspiration of different ethanol concentration was carried out using the ratio of the two Mg lines (Fig. 7.11) as discussed in Section 2.13.

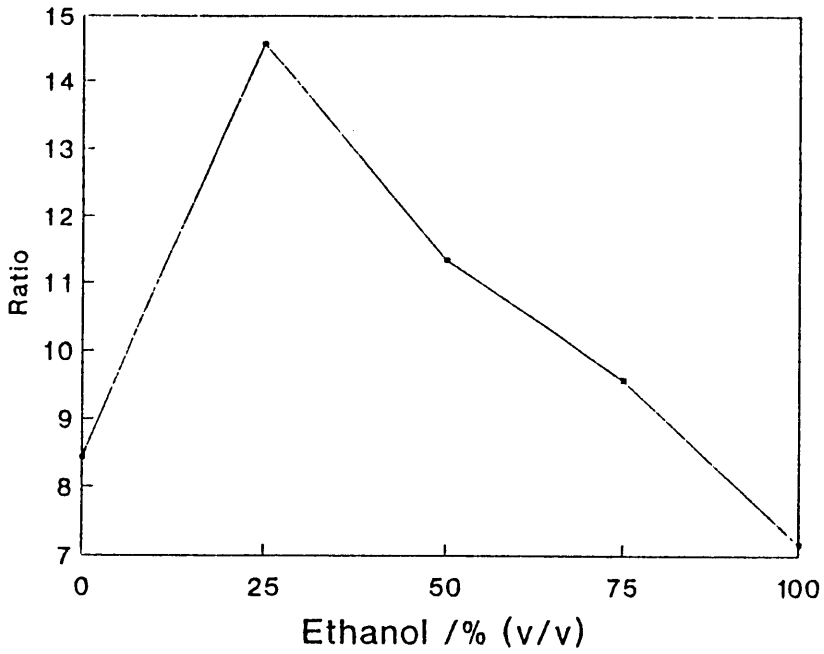

Figure 7.11 The ratio of the intensity of the Mg(II) line at 285.213 nm to the intensity of the Mg(I) line at 280.270 nm at 1.5 kW, corrected for background.

A ratio of between 10 and 13 implied, according to Mermet (1991), that the plasma was close to LTE.

When determining the intensity of the Mg lines at different ethanol concentrations it was found that the optimum viewing height was identical for water and the 25 % solution, but for the remainder the optimum height for the Mg(II) line was 1 mm less than for the Mg(I) line.

The ratio of the intensities of the Mg lines (Fig. 7.11), increased as the ethanol concentration increased, reaching a maximum for the 25 % ethanol solution, after which the ratio decreased. The maximum of 14.6 indicated that the plasma was in LTE when 25 % ethanol was being aspirated (Fig. 7.11).

7.7.2 Oil Solutions

Intensity of the hydrogen lines for various plasma conditions and ethanol concentrations has been fully investigated above. The question then arose as to the

intensity of the hydrogen line (and hence the concentration of hydrogen) in the absence of water. The next step, therefore, was to determine the effect ethanol would have on organic solvents.

Xylene was chosen as organic solvent since that would appear to be the most useful solvent for oil analyses (Boumans and Lux-Steiner: 1982). Oil is insoluble in pure ethanol so it could not be used on its own as solvent. Provided that the oil was first dissolved in xylene, the ethanol could make up half the final solution. To avoid solvent separation, the maximum ethanol concentration used was 45 %. A 30 % ethanol solution in xylene was also used for comparison.

The viewing height for the maximum intensity of the hydrogen line was investigated. Using pure xylene, the intensity of the hydrogen line (656.272 nm) reached a maximum 1 mm above the load coil. The magnitude of the signals at 1, 2, 3 and 5 mm above the load coil is given in Fig. 7.12.

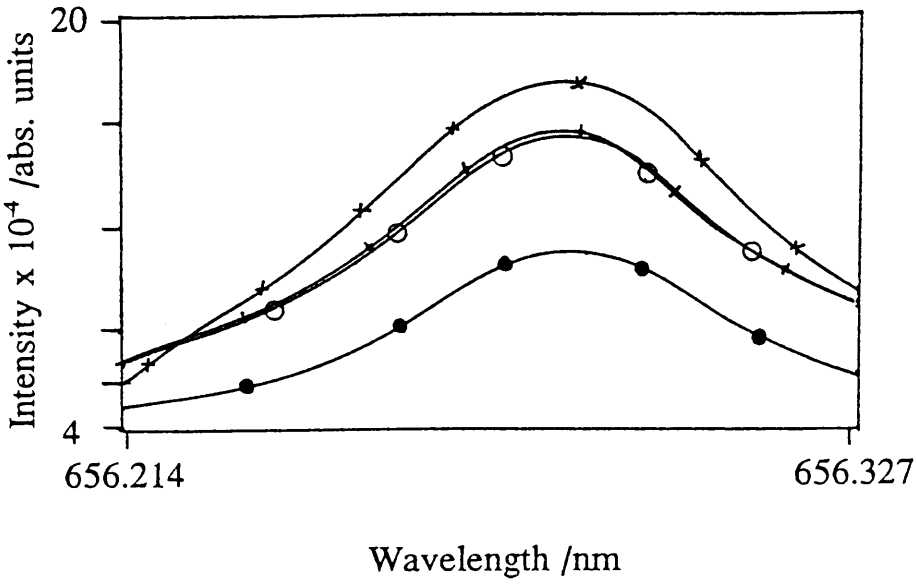

Figure 7.12 Emission intensity of hydrogen as measured by the H_α line at 1 (x), 2 (+), 3 (o) and 5 (●) mm above the load coil.

Making use of a viewing height of 1 mm and at 1.5 kW, the hydrogen intensity was measured when water, xylene, 30 % ethanol/70 % xylene and 45 % ethanol/55 % xylene were each aspirated in turn (Fig. 7.13a). The intensity of the hydrogen line, when water was aspirated, was almost 2.5 times that obtained when xylene was nebulized. Ethanol additions resulted in the intensity of the hydrogen line decreasing.

The difference between the magnitude of the hydrogen emission for water and the xylene solutions was so great that the difference between the two ethanol solutions was not easy to determine when all results appeared in one figure. The experiment was repeated, but on this occasion water was not used for comparison (Fig 7.13b).

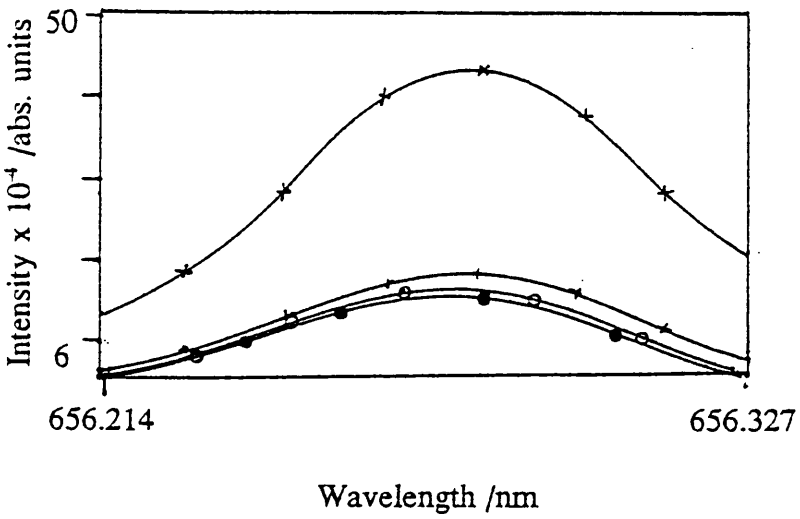

Figure 7.13a Intensity of hydrogen as measured by the H_α line when water (x), xylene (+), 30 % ethanol in xylene (o) and 45 % ethanol in xylene (o) was aspirated.

The intensity obtained from the xylene solution was almost twice the magnitude of the signal from the ethanol solutions. The solution containing 30 % ethanol had the smallest magnitude, though not very different from the 45 % solution (less than 10 % difference). The presence of ethanol led to a reduction of the amount of hydrogen in the plasma. Addition of ethanol to the xylene must have resulted in a decrease in the temperature of the plasma. This decrease would, in turn, lead to the reduction in

intensity of the hydrogen line. To determine possible causes for the decrease in temperature, it was necessary to measure the mass flow rate (Section 7.7.3.1).

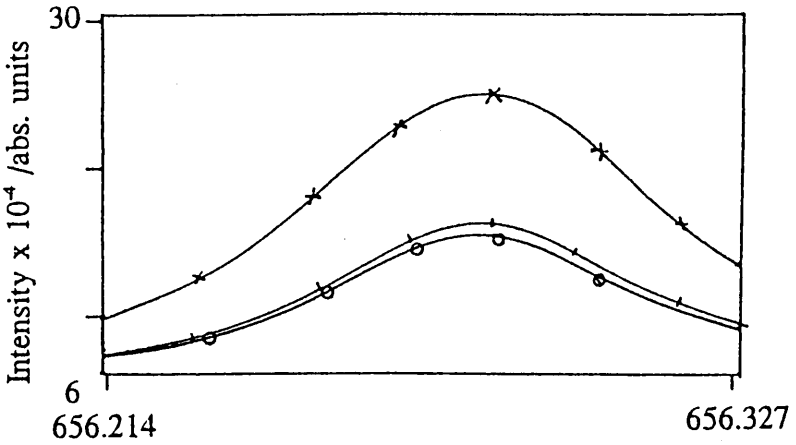

Figure 7.13b Intensity of hydrogen as measured by the H_α line when xylene (x), 30 % ethanol in xylene (+) and 45 % ethanol in xylene (o) was aspirated.

The Simplex method for optimizing instrumental parameters was applied to three variables i.e. viewing height, rf power and nebulizer gas pressure. Other parameters such as inner and outer gas flow rates were not included as it was easy for the programme to suggest a value which could damage the torch. The manufacturer's values were therefore used.

Adjusting those three parameters mentioned above, and using the optimization of Al as an example, without the use of the Simplex method the best SBR's for 10 $\mu g\ g^{-1}$ Al in xylene, 30 % ethanol and 45 % ethanol were 9.76, 4.73 and 5.86 respectively. Application of the Simplex programme improved the SBR's to 10.10, 6.06 and 6.11 for the same solutions. The values for the optimized parameters for Al are given in Table 7.5.

Results of the procedures followed by the Simplex method could be plotted and given as one of three values as discussed earlier. The SBR's were used in this investigation for determining optimum parameters. The effects of various adjustments are given as changes to the SBR in Fig. 7.14 where the Simplex method was applied to the

determination of Al in different solutions (xylene, 30 % and 45 % ethanol in xylene). In each case initial adjustments resulted in major changes to the SBR, but as the method proceeded variations in SBR decreased and finally reached a plateau. This value represented the SBR obtained from the optimized conditions.

Table 7.5 Optimized values for 10 μg g^{-1} Al using the Simplex method.

	xylene	30 % ethanol	45 % ethanol
Viewing height /mm	10.75	10.00	9.75
Rf power /kW	1.48	1.50	1.50
Nebulizer gas pressure /kPa	182.5	167	166
Signal /arb. units	50450	37880	38140
Background /arb. units	4545	6251	6242
SBR	10.10	6.06	6.11

Clearly, from both Table 7.5 and the optimization procedure given in Fig. 7.14, the pure xylene solution yielded the most sensitive results for Al, followed by the 45 % ethanol solution. The difference between the two ethanol solutions was again not very large (6.06 vs 6.11).

Using compromise conditions in order to measure the concentration of Al in all three solutions without further adjustments, led to a change in sensitivity of the 30 and 45 % ethanol solutions as may be seen in the calibration curves in Fig. 7.15. The solution which produced the most sensitive result (greatest slope) was clearly xylene, but it should be noted that the 30 and 45 % ethanol solutions had interchanged in sensitivity and also SBR, when compared to the results in Fig 7.14, in that the 30 % solution, as demonstrated in Fig. 7.15 was more sensitive than the 45 % ethanol solution.

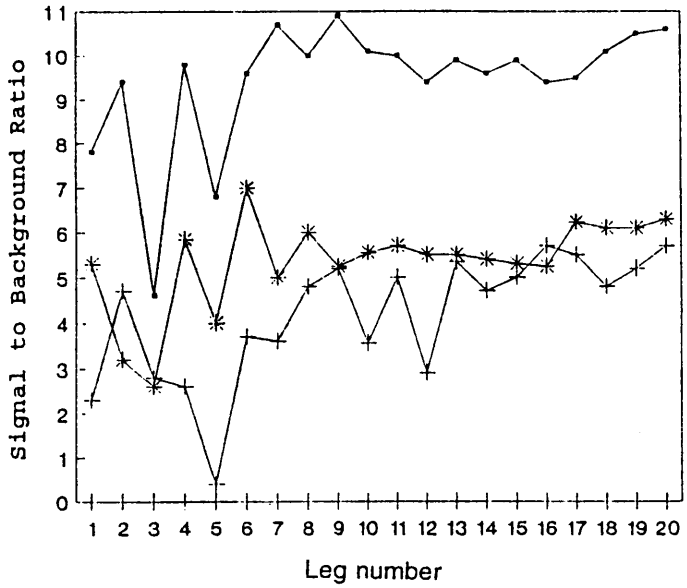

Figure 7.14 Response of SBR to changes in the optimization parameters for Al using the Simplex method in various solutions; (▫) xylene, (✳) 30 % ethanol and (+) 45 % ethanol.

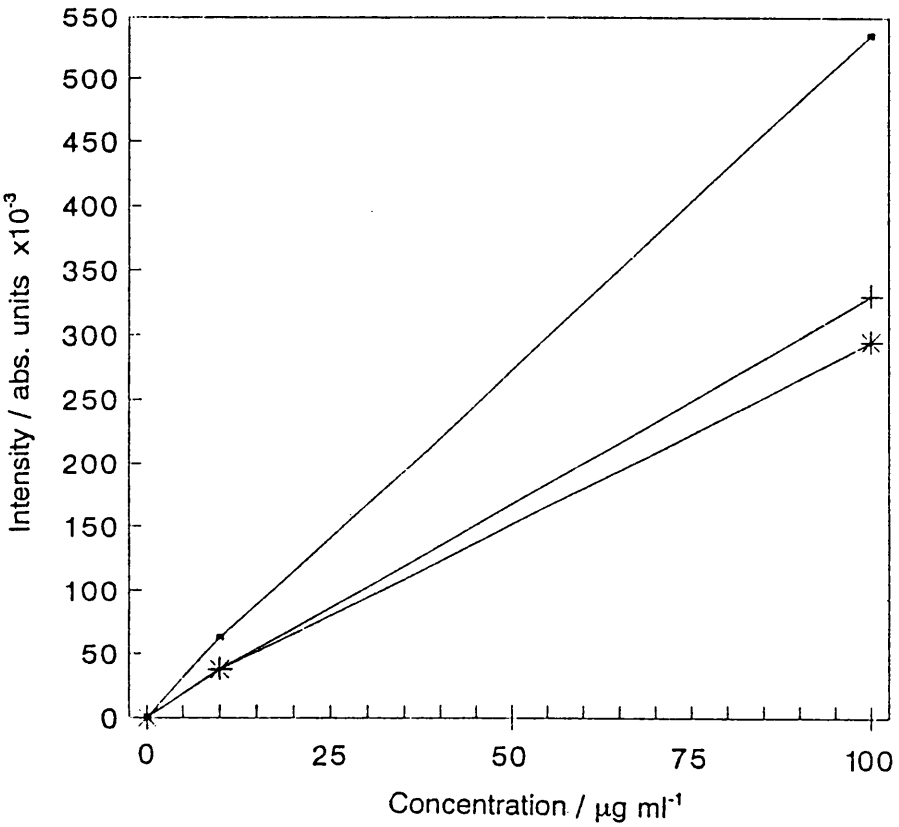

Figure 7.15 Calibration curve for Al in (▫) xylene; (✳) 30 % and (+) 45 % ethanol, in xylene.

The reason for this apparent change can be deduced from Fig. 7.14 where the value for the SBR's for the 30 and 45 % solutions are very similar, and for the 16th response the readings **had** interchanged. The compromise conditions used in the analysis could have resulted in a change in the sensitivities of the 30 and 45 % ethanol solutions. Slight deviation from linearity can be seen in the calibration curve for Al in 30 % and 45 % ethanol in xylene solutions.

Optimum compromise conditions (using the three different solutions) for the elements investigated are given in Table 7.6. Changes in the viewing height were computer controlled, while the power remained constant. Problems experienced previously regarding alterations to the nebulizer gas pressure were again encountered. Adjustments were made by means of a dial which was insensitive to movement. The revised pressure, as indicated by Simplex, or when measuring a different element, would be dialled, but drift in gas pressure would occur until the flow had stabilized. This could be several minutes and the exact pressure was not easily obtained with certainty.

Table 7.6 Optimum conditions for the elements investigated.

Element	Wavelength /nm	Viewing ht. /mm	Rf power /kW	Nebulizer pressure /kPa
Al	396.152	10.0	1.50	160
Pb	261.418	5.0	1.50	130
Fe	259.940	3.0	1.50	100
Cr	267.716	13.0	1.50	120
Cu	324.754	3.0	1.50	140

The calibration curve for Pb is also given (Fig. 7.16) since Pb was extensively investigated and reported in Chapter 6 and the initial part of this Chapter (Section 7.7.1.6).

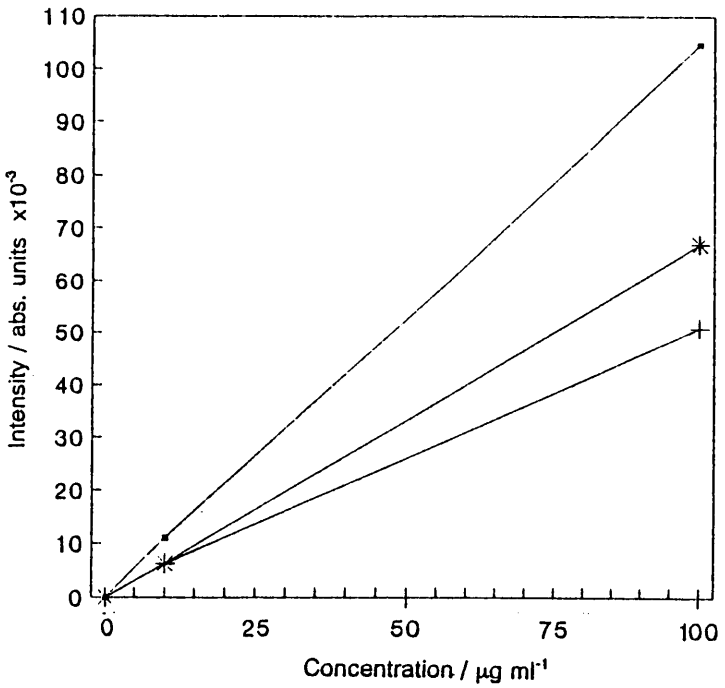

Figure 7.16 Calibration curves for Pb in (▫) xylene; (✳) 30 % and (+) 45 % ethanol, in xylene.

Again the xylene yielded the most sensitive results (as was the case for all the elements investigated), but the results obtained with the 45 % ethanol solution were considerably more sensitive than those for the 30 % solution, where some deviation from linearity can again be detected. A decrease in the temperature of the plasma would again account for the decrease in sensitivities when ethanol was added to the xylene.

The Varian Liberty ICP-OES has the facility that the viewing height can be changed for each element. The nebulizer gas pressure had to be manually changed, with the limitations discussed above, while the power was kept to the maximum recommended by the manufacturer (1.5 kW). Optimized conditions were applied to the analysis of the NBS reference material. The sample was made up as given in Section 7.8.3. The concentration of the elements were then measured using the conditions in Table 7.6 and the results are reported in Table 7.7.

Table 7.7 Results obtained for NBS standard reference oil 1084.

Element	Certified value /µg g^{-1}	Uncertainty /µg g^{-1}	Xylene /µg g^{-1}	30% ethanol /µg g^{-1}	45 % ethanol /µg g^{-1}
Al	98	± 2	102	105	108
Pb	101	± 4	105	102	100
Fe	100	± 3	105	95	93
Cr	100	± 3	103	103	106
Cu	98	± 4	102	100	104

Results obtained were close to the certified values, with two interesting exceptions. The value found for Al using the ethanol solutions increased as the ethanol concentration increased. Secondly, the result for Fe in xylene was higher than the certified value, but the results obtained for the ethanol solutions decreased with increasing ethanol concentration.

The BEC's were not reported for the different elements as they did not vary either with the element or with the different xylene/ethanol solvents.

7.7.3.1 Mass Flow Rate

If the temperature of the plasma was decreased as ethanol was added to the xylene solutions then one possible reason was that the mass flow rate had increased. This would result in the plasma temperature falling as the mass became too great for the plasma to sustain. In order to determine if this was the case, the mass flow rates of the xylene and xylene/ethanol mixtures were measured and the results are given in Table 7.8. These results represent the mass of material passing through into the plasma in precisely two minutes.

Table 7.8 Mass flow rates of various xylene mixtures nebulized into the plasma in precisely 2 minutes.

Solution	Mass /g
30 % ethanol in xylene	0.1572
45 % ethanol in xylene	0.1615
100 % xylene	0.0961

The mass flow rates of the ethanol xylene mixtures did not vary much (less than 3 %), but there was a drastic difference between the flow rate of xylene and the next ethanol mixture (an increase of 64 %). The effect of this increase in mass flow rate can be seen in the changes in electron density that occurred as the ethanol was introduced and increased. The energy of the plasma was dissipated in an attempting to vaporize the mass of material entering the plasma.

7.7.3.2 Electron Density

Changes in electron density were determined by calculating the ratio of the intensities of two Mg lines as discussed in Section 7.8.2 and given for aqueous/ethanol solutions in Fig. 7.11. The values obtained for the different xylene mixtures is given in Table 7.9.

While the ratio of the intensity of the two Mg lines when pure xylene was aspirated was below the minimum value of 10 for LTE as proposed by Mermet (1991), it was still considerably higher than that found for the ethanol mixtures. The drastic increase in mass of material in the plasma when ethanol was present in the mixture resulted in the electron density being suppressed.

Table 7.9 Ratio of the intensity of two Mg lines.

Solution	Ratio
30 % ethanol in xylene	5.63
45 % ethanol in xylene	2.47
100 % xylene	8.59

CHAPTER 8

DISCUSSION AND CONCLUSION

8.1 Introduction

Before embarking on a discussion, a summary of the findings of the previous chapters should be considered. Firstly with reference to aqueous solutions the following was found.

(i) Excitation temperature initially increased with increasing ethanol concentration, but above 15 % ethanol (v/v) the temperature decreased (Fig. 3.5). The excitation temperature was also found to be at its highest 5 mm above the load coil (Fig. 3.6).

(ii) Electron density increased as the ethanol concentration increased. The greatest increase was found in the region of the central channel. The electron density of aqueous ethanol solutions containing between 10 and 60 % ethanol, was such that the plasma could be regarded to be in a state of LTE, i.e. the ratio of two Mg lines was above 10 (Mermet: 1991).

(iii) Mass flow rate increased with increase in ethanol, but not in a linear fashion, i. e. the increase in mass flow rate versus ethanol concentration tended towards an exponential function.

(iv) Increase in hydrogen emission signal within the plasma was almost linear as the ethanol concentration increased to 30 %. Above that ethanol concentration, hydrogen concentration continued increasing more slowly until it reached a maximum at 40 % ethanol. This maximum was maintained until about 60 % ethanol. Above this the hydrogen emission signal decreased (Fig.'s 6.1c and 7.7).

(v) The drop size resulting from aqueous ethanol solutions increased as the ethanol concentration increased.

(vi) The sensitivity of determination for all the elements studied increased initially with ethanol concentration, using the Spectroflame ICP-OES. Signal enhancement reached a maximum however, at 15 % ethanol. This was not the case when the Liberty ICP-OES was used, when the signal enhancement continued as the ethanol concentration increased, reaching a maximum for almost pure ethanol.

Secondly, a series of ethanol concentrations in xylene were used as solvents for oil samples. The following was found:

(vii) Ethanol addition to oil dissolved in xylene solutions decreased the sensitivity.

(viii) Hydrogen signal in the plasma decreased when ethanol was added to samples in xylene.

(ix) The mass flow rate of the ethanol xylene mixtures was double that of pure xylene.

(x) Additions of ethanol to xylene, when aspirated in an ICP, reduced the electron density of the plasma.

These will be discussed further under different headings below.

8.2 Aqueous Ethanolic Solutions

8.2.1 Excitation Temperature

The excitation temperature was found to increase with the initial increase of ethanol concentration in the sample solution. This is in agreement with the findings of Benli (1983). Also in agreement with the findings of Benli, was that the temperature reached a maximum for 15 % ethanol and then proceeded to decrease with further increase in ethanol concentration (Fig. 2.6). Benli also reported an enhancement of emission signal with ethanol in the matrix.

The increase in excitation temperature reported by Benli (1983) was contrary to the findings of several other authors. They found that aspiration of an organic solvent into the plasma resulted in a decrease in excitation temperature (Boorn and Browner: 1982, Goldfarb and Goldfarb: 1985 and Blades and Caughlin: 1985). It must be stated that the interest of most of those authors had not been in ethanol as a solvent, but rather other organic solutions and none of them investigated the effects of ethanol fully. Also, as will be discussed later, the aerosol gas flow rate is critical to ethanolic solutions and it is possible that if compromise conditions, or conditions suitable to other solvents, were used deductions regarding the role of ethanol could have been misleading.

8.2.2 Electron Density

Electron density is a most useful parameter to determine, as it indicates how close the plasma is to a state of LTE (Matousek and Mermet: 1993). Electron density was determined both by using the Stark broadening of the H_β line and by the approximate method of intensity of Mg lines. Using both methods it was found that additions of ethanol to the sample matrix resulted in the electron density increasing. The greatest increase in electron density was found (after Abel inversion) in the region of the central channel (Fig. 3.3).

Unlike the excitation temperature, the electron density did not reach a maximum when 15 % ethanol was aspirated, but for 25 %. The ratio of the intensities of the two Mg lines (Fig. 7.11) was used to determine this figure. From the values obtained for the ratio, the plasma could have been regarded as being in a state of LTE for ethanol concentrations between 5 and 60 % (when the value for the ratio was greater than 10). That the plasma should be close to a state of LTE would imply greater accuracy in the determination of excitation temperature. This is because the method of calculating excitation temperature employed, i.e. using the "two line" method, was derived from the Boltzmann distribution and the Boltzmann equation is only valid for systems in state of LTE or close to it.

8.2.3 Mass Flow Rate

The mass flow rate increased throughout (Table 4.4.). The addition of a small amount of ethanol (5 %) resulted in only a small increase in mass reaching the plasma. Further additions of ethanol continued this trend, until the mass flow rate increased to such an extent that the energy was insufficient to vaporize all the material entering the plasma. Cooling of the plasma would then occur and the excitation temperature would decrease (Fig. 3.3).

8.2.4 Hydrogen Concentration

As mentioned in Chapter 5 it was the discovery that the emission signal of hydrogen in the plasma increased dramatically with increasing ethanol concentration that changed the direction of the investigation. The presence of hydrogen has been noted to change certain characteristics of the plasma. In the mechanism proposed by Ebdon and Goodall (1992), they suggested that it was the constriction of the plasma due to the pinch effect that was responsible for most of the changes to the fundamental parameters when hydrogen is introduced into the plasma. These changes included increased thermal conductivity and an increase in electron density.

Addition of hydrogen to the plasma gases would result in an increase in excitation temperature (Matousek and Mermet: 1993). Again this increase was related to the increase in thermal conductivity and the constriction of the plasma. The increase found in the excitation temperature may be seen in Fig. 3.5. The increase in excitation is in agreement with the findings of Ebdon and Goodall (1992) who found that addition of hydrogen caused an increase in rotational temperature.

Addition of ethanol to the sample solution could be seen visibly (Plates 1.1 to 1.5) to bring about physical changes within the plasma. One of these was the obvious change caused by the increasing presence of the hydrogen, namely that the background emission became brighter.

8.2.4.1 Relationship between Electron Density and Hydrogen Concentration

The decrease in radius of the plasma was certainly partly responsible for the increase in electron density however, the role of hydrogen should also be considered. The density increases as the square of the radius (Ebdon and Goodall: 1992) and by rough measurements from the plasma in the laboratory and from the photographs of water and ethanol being aspirated it appeared that the radius decreased by 1 mm for the 25 % ethanol (at z = 5 mm). This would result in an increase in electron density by a factor of 1.3, which was supported by the findings given in Fig. 3.4. The constriction of the plasma due to the pinch effect being responsible for this increase in electron density.

Nowak *et al* (1988) found that the introduction of water to the plasma resulted in an increase in electron density. They described this increase in electron density also to the constriction of the plasma. This increase they observed was most noticeable in the central channel of the plasma. They considered that a recombination channel had been formed in the central channel. At no stage did they consider that the increase in electron density was due to the addition of hydrogen via the water. This study indicated that hydrogen was at least in part responsible, as discussed below.

It was found that constriction of the plasma was partly responsible for the increase in electron density (Chapter 3), but a second factor which must be considered from Fig. 3.3, is that the electron density increased towards the central channel. Here the results found by Mermet and co-workers are important (Mermet: 1991, Murillo and Mermet: 1989 and Matousek and Mermet: 1993). They studied the effect of thermal conductivity of hydrogen on the temperature distribution within a plasma. An increase in hydrogen, with its improved thermal conductivity, would result in energy transfer occurring more readily to the cooler central channel. This would result in the electron density in that region increasing.

In the article by Murillo and Mermet (1988), the authors found that the thermal conductivity of the of the plasma increased from 0.1 $Wm^{-1}K^{-1}$ to 15 $Wm^{-1}K^{-1}$

with the introduction of hydrogen into the plasma. This increase in thermal conductivity allowed the heat generated by the load coil to be transferred more effectively to the central channel. An increase in thermal conductivity would result then in an increase in electron density in the region of the central channel. This increase may be seen in Fig. 3.3, after Abel inversion has been applied.

8.2.4.2 Relationship between Mass Flow Rate and Hydrogen Concentration

The mass flow rate increased throughout as mentioned previously (Table 4.4). The small increase in material reaching the plasma when 5 % ethanol was in the aspirated solution, would, provided it was completely vaporized, dissociated and atomized, result in the release of a small amount of additional hydrogen. This increase in hydrogen concentration in the plasma could cause an increase in temperature and electron density. Further additions of ethanol would continue this trend, until the energy of the plasma was insufficient to vaporize all the material and cooling occurred. The decrease in temperature resulting from the increased mass flow rate did not affect the continued increase in hydrogen emission signal. A contraction of the plasma and thermal conductivity are both related to changes in hydrogen concentration. The continued increase in hydrogen concentration would imply that further increases in thermal conductivity, and consequently electron density, could be anticipated. This may be seen in Fig. 3.7 where the electron density continued to increase even though the temperature had reached a maximum and in fact was decreasing.

8.2.4.3 Relationship between Reactivity and Hydrogen Concentration

As the aerosol passes through the magnetic field surrounding the coils and into the plasma, the temperature increases from ambient to 10 000 K. This takes between 5 and 10 ms depending on the torch dimensions and carrier gas flow rate (Tang *et al*: 1986). In that time the sample must be vaporized, desolvated, dissociated, atomized and excited. Volatilization takes less than a millisecond, desolvation about 1 ms and dissociation at long as 3 ms for every 0.3 mg s^{-1}

of water. Excitation and ionization are in the order of nanoseconds.

It is during this time scale that the processes that are of importance to analytical determinations must occur. Most authors concentrate on desolvation, for it is in this process that drop size will be of major importance. This a factor which will be discussed later. In all the processes the transfer of energy from the outer heated zone to the central channel through which the sample aerosol is passed must be important. It is with this transfer of energy, that hydrogen must play a vital role. The thermal conductivity of hydrogen is such that it assists in the transport of the energy to the sample. The change in shape of the plasma occurring together with the increase in temperature and electron density all increases the sensitivity of analyses.

The only reactions considered to be of importance are those of dissociation and atomization. These can take place in about 4 ms (Tang and Trassy: 1986), while if the aerosol carrier gas flow rate is low, the sample may be in the plasma for 10 ms. During this time the material is at 10 000 K (Fig. 3.6) and must therefore be very reactive. Additions of hydrogen to the plasma gases have been made by Ebdon and Goodall (1992) and Poussel *et al* (1994) so as to chemically change the environment within the plasma. In the first case the hydrogen was added to assist with the atomization of slurries, while Poussel *et al* added hydrogen to increase the rate of oxide dissociation when analysing La using an ICP-MS. Both works found the hydrogen increased the temperature, but in the case of Poussel *et al* they found that the ratio LaO^+:La had decreased. Hydrogen was added initially as a reducing agent and it may have been because of this factor that the ratio was improved. An increase in temperature would assist dissociation, but atomic hydrogen would aid reduction of difficult oxides.

It is this increase in temperature which has been ignored by most workers involved with ICP-OES research. An increase in the concentration of hydrogen in the plasma as ethanol was added was deduced from the increase

in intensity of the hydrogen lines (Fig.'s 6.1c and 7.7). Increased hydrogen could be the breakdown product of the ethanol in the plasma. The increase in electron density associated with the increase in hydrogen concentration could have resulted from one of three sources:

(i) breakdown of the ethanol to produce hydrogen, resulting in an increase of free electrons,

(ii) hydrogen produced by the breakdown is more easily ionizable by the rf source and an increase in electron density results. From the ionization potentials of hydrogen and argon it would seem likely that if hydrogen was present in atomic form, it would undergo ionization more readily than argon, and

(iii) a thermal pinch effect resulting in constriction of the plasma.

Thermal dissociation of ethanol is not likely to be much greater than that of water. The amount of hydrogen per mole increases only by 0.3 % when a 5 % ethanol solution is aspirated instead of water. Further increases in ethanol result in even less of an increase in hydrogen per mole. The surface tension, however, would decrease as the ethanol concentration increases. Less energy would be required to vaporize the droplets. The average energy required to break the interatomic bonds, calculated from thermodynamic data (Lide and Kehiain: 1994), decreases slightly as ethanol is added to water (5.10 eV for water as opposed to 4.22 eV for ethanol).

Likelihood of a chemical reaction in a plasma would be high because the rate of reactions is increased by temperature. The only factor negotiating reactions is the time constraint. The mechanism suggested for the formation of hydrogen in the plasma could follow the following path (McCrindle and Rademeyer: 1994).

Initial thermal decomposition of the ethanol would result in the release of CO and OH:

$$2C_2H_5OH + 7O_2 \rightarrow 4CO + 12OH$$

The CO and OH react to form CO_2 and atomic hydrogen

$$CO + OH \rightarrow CO_2 + H$$

It is the atomic hydrogen produced in this way that causes both the increase in intensity of the hydrogen lines and electron density and consequently an increase in excitation temperature.

8.2.5 Drop Size Distribution

It was found that the drop size increased as the ethanol concentration of the aspirated solution increased. The influence of the physical properties such as density, viscosity and surface tension cannot be ignored. All of these values would indicate that the drop size of ethanol and methanol should decrease with increasing concentrations of alcohol. At this point it must be made clear that the conclusions reached by Weir and Blades (1994) who studied methanol and suggested that three solutions could possibly summarize all types of solvents in ICP-OES was perhaps a little optimistic. That methanol and ethanol would behave substantially the same in the plasma should not be disputed.

In this work the effects of ethanol have been studied, but the findings would relate to methanol as well, because of their similar physical and chemical properties. The more viscous alcohols with chain lengths greater than three may behave differently, but they are not used as commonly as solvents as are methanol and ethanol. Ethanol was studied as it is the cheapest of the solvents and is not as toxic as methanol.

The postulations by the Alicante group that increase in drop size was an erroneous finding, were dubious, when considering the findings of Mora *et al* (1991). Mora *et al* found that when one experiment was repeated three months later, significantly different results for the obscuration value were obtained (Table 4.2). The cutoff in drop size diameter of 1.2 μm was large. It can be understood that if a considerable

number of droplets smaller than that were generated and they were not included in the calculation then an error would arise. This would lead to an incorrect value for drop size diameter. In the laser particle size counter used in the experiments associated with the findings described in Chapter 4, the cutoff drop size diameter was 0.3 μm. This is considerably smaller than the 1.2 μm of the Alicante group and should therefore not lead to the same type of error.

Although it was shown that drop size was increased by the addition of ethanol (Fig. 4.7) there were, unfortunately, problems associated with determination of drop size mean distribution. It should be stressed however, that the aim of this work was not to determine with great accuracy the actual drop size, but rather the effect that ethanol additions would have on that parameter. Conditions were such that there was a delay between the system being connected and before measuring commenced, so that an equilibrium situation could be recorded. However, once stabilized, the experiment was reproducible and in each case drop size increased as ethanol concentration increased.

8.2.6 Analytical Parameters

Several authors have reported an increase in emission intensity with the addition of hydrogen to the nebulizer gases (Schramel: 1983, Schramel and Li-qiang: 1984, Murillo and Mermet: 1989, Matousek and Mermet: 1993 and Louie and Soo: 1992). It would seem conclusive that if the addition of ethanol to the sample solution resulted in an increase in the hydrogen concentration of the plasma, then signal enhancement would result. This was found and is illustrated in Tables 6.1 and 7.4. Therefore hydrogen release is proposed as the mechanism by which ethanol addition caused improved sensitivity.

The results that changes of the fundamental characteristics of the plasma would have on sensitivity and analytical performance is most important. An increase in electron density and excitation temperature should result in enhanced emission signals. This enhancement may be seen in the calibration curves of all the elements investigated and could be directly related to increase in temperature (Fig.'s 6.2 and 7.10). Once the

temperature reached a maximum, then it could be expected that the signal would no longer continue to increase. This is illustrated in Fig. 6.2a and b and Table 6.1a and b, where sensitivity, as given by the slope of the calibration curve reached a maximum for different dilutions of ethanol.

It was difficult to determine the exact concentration of ethanol which resulted in the highest sensitivity. Although the temperature reached a maximum for 15 % ethanol, the electron density continued to increase to at least 25 % (Fig. 7.11). The lines which were more affected by the temperature reached a maximum at 15 % ethanol. Those lines for which the electron density were more important than the temperature reached maximum sensitivity for elemental analysis at 20 % ethanol. The effect that an increase in temperature had on signal enhancement resulted in Matousek and Mermet (1989) dividing temperature into "hard" and "soft". Additions of hydrogen resulted in the "soft" temperature (obtained below 5.5 eV) increasing by 1000 K. This increase should be in the order of the energy required to excite atoms, while ions would need greater energy.

According to Batal *et al* (1982), addition of hydrogen would result in an increase in background continuum. The increase being due to recombination below 500 nm and because of Bremsstrahlung above that wavelength. All the measurements were made below 500 nm and hence the optical effect probably resulted from recombination.

An increase in background emission was found throughout the investigation when ethanol was added to the aspirated solution, and its intensity, or rather, the effect of its intensity, depended on the element investigated. The importance for analytical determinations was that the BEC increased with additions of ethanol. The BEC is directly linked to detection limits calculated by equation 6.1, in that the BEC will be seen as part of the limiting noise in a determination. Hence, though sensitivity increased with increase in ethanol concentration, in most cases, this was not true for all elements. In most of the elements studied using the Spectroflame however, the detection limits increased in magnitude as the ethanol concentration increased (Table 6.1a and b).

The amount by which the BEC and sensitivity increased varied with each element analysed. If the increase in BEC was smaller than that of sensitivity, then an improvement in detection limits was obtained with increase in ethanol concentration (Cr, Mn and Fe in Table 7.4). This was not the case for other elements, such as Al and Cd. Sodium was an example of both scenarios, in that when the viewing height was 2 mm, the high BEC resulted in the detection limit increasing. When the Na was in a 95 % solution of ethanol, the decrease in BEC at 6 mm resulted in a detection limit comparable to that found with water. Selection of ethanol concentration in order to improve analysis would depend on the requirements, namely if the result desired is increased sensitivity or detection limits. It would appear from results obtained above, that the detection limits of "soft" elements would not be improved by the addition of ethanol, even though the sensitivity may be increased. In the case of "hard" elements, improvement in both sensitivity and detection limits would be obtained by the addition of ethanol.

Additions of ethanol to the sample matrix leads to greater sensitivity with regard to aerosol carrier gas flow rates. Aqueous solutions need to be optimized for flow rate. Optimization of aerosol carrier gas flow rates was found to be of even more importance with ethanolic solutions (Fig. 6.3a and b). Different aerosol carrier gas flow rates could result in the sensitivity doubling with aqueous solutions, while a fivefold increase was found with a 15 % solution of ethanol (Section 6.4, Fig. 6.3a). These findings were further substantiated by results obtained with xylene.

8.3 Xylene/ethanol Solutions

Once the electron density decreased, sensitivity and other analytical parameters would degenerate. The results obtained with the xylene/ethanol mixtures were further illustrations of the above phenomenon. When ethanol was added to the xylene a major change was caused in the amount of material reaching the plasma (almost a doubling). The plasma, while not being extinguished, was drastically affected by the increase in mass flow rate and the electron density fell dramatically. This was accompanied by a decrease in sensitivity.

Additions of ethanol to xylene resulted in the amount of material reaching the plasma increasing to an extent where the plasma could no longer vaporize all the droplets. Reduction in the temperature resulted in the amount of material that was excited or ionized being decreased. This decrease in the number of excited species was found in the reduction of the hydrogen and analyte lines intensity.

The mass flow rate found with the xylene/ethanol solutions could result in the plasma being unable to vaporize the material. Hobbs and Olesik (1993) showed a drastic decrease in atomic number density near incompletely desolvated droplets. The presence of these droplets resulted in a decrease of 2000 K in temperature and a decrease by more than one and a half decades in electron density. This was accompanied by a drop in the degree of ionization. All these factors were present when the xylene/ethanol mixtures were aspirated and it may be concluded that the increased mass flow rate resulted in incomplete desolution.

8.4 Plasma Stability

Boorn and Browner's (1987) comments on the inability of the ICP-OES to cope with increasing ethanol concentrations appear extremely relevant. According to them, the instability results from the gradual quenching of the luminous plasma core from beneath the load coil and when this quenching reaches the core region the plasma is extinguished. The extent of plasma instability is partly controlled by the matching network of the plasma coupling box and this must accurately follow changes within the plasma. In the case of ethanol, the reflected power increases and the automatic matching may not be able to maintain the plasma. It was suggested by Boorn and Browner that this difficulty could be overcome by improved matching networks. It would appear that the new developments in ICP-OES's used were able to cope with the increase in forward power and maintain a stable plasma.

8.5 Conclusions

The aim of the investigation was to determine the fundamental properties of an ICP when ethanolic solutions were aspirated. These parameters have been thoroughly investigated and their influence on analytical procedures notarized. Changes that

occurred with the addition of ethanol have been determined and reasons for the changes found. The discovery that increasing amounts of hydrogen were released as the concentration of ethanol nebulized and atomized was increased, explained fully the increases in electron density and signal enhancement. Changes within the plasma as hydrogen is released leads to the possibility that rapid chemical reactions other than those usually associated with ICP-OES's should be considered.

A method has been developed for elemental analysis using pure ethanol solutions, with the aid of new technology. The sensitivity obtained from such solutions is greater than that for aqueous solutions. The detection limits improved for some elements, but this depended on the element determined. In general, detection limits of elements with "hard" lines improved when analysed from pure ethanol. The ability to carry out sample analysis using organic solvents is of great assistance to the chemist.

REFERENCES

Abdullah, H. M., and Mermet, J. M., Spectrochim. Acta, **37B**, 391 (1982).

Alder, J. F., and Mermet, J. M., Spectrochim. Acta, **28B**, 421 (1973).

Alder, J. F., Bombelka, R. M., and Kirkbright, G. F., Spectrochim. Acta, **35B**, 163 (1980).

Alkemade, C. Th. J., Hollander, T. J., Snellerman, W., and Zeegers, P. J. Th., *Metal Vapours in Flames*, Pergomon Press, Oxford (1982) p41-63.

Barnes, R. M., and Schleicher, R. G., Spectrochim. Acta, **36B**, 615 (1981).

Bastiaans, G. J., and Mangold, R. A., Spectrochim. Acta, **40B**, 885 (1985).

Batal, A., Jarosz, J., and Mermet, J. M., Spectrochim. Acta, **36B**, 983 (1981).

Batal, A., Jarosz, J., and Mermet, J. M., Spectrochim. Acta, **37B**, 511 (1982).

Benli, H., Spectrochim. Acta, **38**, 81 (1983).

Benli, H., Yang, J., Pei, A., Zeng, X., and Boumans, P. W. J. M., Spectrochim. Acta, **46B**, 3 (1991).

Blades, M. W., Spectrochim. Acta, **37B**, 869 (1982).

Blades, M. W., Appl. Spectrosc., **37**, 371 (1983).

Blades, M. W., and Caughlin, B. L., Spectrochim. Acta, **40B**, 579 (1985).

Blades, M. W., Caughlin, B. L., Walker, Z. H., Burton, L. L., PROG. Anal. At. Spectrosc., **10**, 57 (1987).

Boorn, A. W., Cresser, M. S., and Browner, R. F., Spectrochim. Acta, **35B**, 823 (1980).

Boorn, A. W., and Browner, R. F., Anal. Chem., **54**, 1402 (1982).

Boorn, A. W., and Browner, R. F., in *Inductively Coupled Plasma Emission Spectrometry*, ed. Boumans, P. W. J. M., John Willey and Sons, New York, (1987), p169.

Boss, C. B., and Fredeen, K. J., in *Concepts, Instrumentation and Techniques in Inductively Coupled Plasma Atomic Emission Spectrometry*, Perkin-Elmer Corporation, USA, (1989), p3-4 and 3-5.

Botto, R. I., Spectrochim. Acta, **42B**, 181 (1987).

Boumans, P. W. J. M., *Theory of Spectrochemical Excitation*, Hilger Watts, London/Plenum Press, New York, (1966), p79.

Boumans, P. W. J. M., and Lux-Steiner, M. CH., Spectrochim. Acta, **37B**, 97 (1982).

Brown, R. J., Spectrochim. Acta, **38B**, 283 (1983).

Browner, R. F., Boorn, A. W., and Smith, D. D., Anal. Chem., **54**, 1411, (1982).

Browner, R. F., Canals, A., and Hernandis, V., Spectrochim. Acta, **47B**, 659 (1992).

Burton, L. L., and Blades, M. W., Spectrochim. Acta, **45B**, 139 (1990).

Capelle, B., Mermet, J. M., and Robin, J. P., Appl. Spectrosc., **36**, 102 (1982).

Canals, A., Hernandis, V., and Browner, R. F., J. Anal. At. Spectrom., **5**, 61 (1990a).

Canals, A., Hernandis, V., and Browner, R. F., Spectrochim. Acta, **45B**, 591 (1990b).

Canals, A., Private Correspondence (1995).

Caughlin, B. L., and Blades, M. W., Spectrochim. Acta, **39B**, 1583 (1984).

Caughlin, B. L., and Blades, M. W., Spectrochim. Acta, **40B**, 1505 (1985).

Cremer, C. J., and Birkebak, R. C., Appl. Opt., **5**, 1057 (1966).

Crosley, D. R., and Smith, G. P., Combustion and Flame, **44**, 27 (1982).

De Galan, L., Spectrochim. Acta, **44B**, 829 (1989).

Dickerson, G. W., and Fassel, V. A., Anal. Chem., **41**, 1021 (1969).

Ebdon, L., Cave, M. R., and Mowthorpe, D. J., Anal. Chim. Acta, **115**, 179 (1980).

Ebdon, L., and Goodall, P., J. Anal. At. Spectrom., **7**, 1111 (1992).

Faires, L. M., Palmer, B. A., Engleman R., and Niemczyk, T. M., Spectrochim. Acta, **39B**, 819 (1984).

Faires, L. M., Palmer, B. A., and Brault, J. B., Spectrochim. Acta, **40B**, 135 (1985).

Fischer, J. L., and Rademeyer, C. J., J. Anal. At. Spectrom., **9**, 623 (1994).

Foley, H. M., Phys. Rev. **69**, 616 (1946).

Freeman, M. P., and Katz, S., J. Opt. Soc. Am., **53**, 1172 (1963).

Furuta, N., Nojiri, Y., and Fuwa, K., Spectrochim. Acta, **40B**, 423 (1985).

Goldfarb, V. M., and Dresvin, S. V., High Temp., **3**, 303 (1965).

Goode, S. R., and Deavor, J. P., Spectrochim. Acta **39B**, 813 (1984).

Granchi, M. P., Biggerstaff, J. A., Hilliard, L. J., and Grey, P., Spectrochim. Acta, **42B**, 169 (1997).

Greenfield, S., Jones, I. L., and Berry, C. T., Analyst, **84**, 713 (1964).

Greenfield, S., and Smith, P. B., Anal. Chim. Acta, **59**, 34 (1972).

Greenfield, S., McGeachin, H. McD., and Smith, P. B., Anal. Chim. Acta, **84**, 67 (1976).

Grieg, J. R., Lim, C. P., Moo-Yourig, G. A., Palumpo, G., and Greim, H. R., Phys. Rev., **172**, 148 (1968).

Griem, H. R., *Plasma Spectroscopy*, McGraw-Hill, New York (1964).

Griem, H. R., *Spectral Line Broadening by Plasmas*, Academic Press, New York (1974).

Gustavsson, A., Anal. Chem., **55**, 94 (1983).

Gustavsson, A., Anal. Chem., **56**, 815 (1984).

Gustavsson, A., in *Inductively Coupled Plasmas in Analytical Atomic Spectroscopy*, ed. Montaser, A., and Golighny, D. W., VHC Publishers, New York (1987).

Hanselman, D. S., Sesi, N. N., Huang, M., and Hieftje, G. M., Spectrochim. Acta, **49B**, 495 (1994).

Hasegawa, T., and Haraguchi, H., Spectrochim. Acta, **40B**, 123 (1985a).

Hasegawa, T., and Haraguchi, H., Spectrochim. Acta, **40B**, 1505 (1985b).

Hasegawa, T., and Winefordner, J. D., Spectrochim. Acta, **42B**, 637 (1987).

Hasegawa, T., and Haraguchi, H., in *Inductively Coupled Plasmas in Analytical Atomic Spectroscopy*, ed. Montaser, A., and Golighny, D. W., VHC Publishers, New York (1987).

Hausler, D. W., and Taylor, L. T., Anal. Chem., 1227 (1981).

Herzberg, G., *Atomic Spectra and Atomic Structure*, Dover Publications, New York (1944).

Helbig, V., and Nick, K.-P., J. Phys., **B14**, 3573 (1981).

Hieftje, G. M., Miller, R. M., Pka, Y., and Wittig, E. P., Anal. Chem., **59**, 2861 (1987).

Hill, R. A., J. Quant. Spectrosc. Radiat. Transfer, **7**, 401 (1967).

Hobbs, S. E., and Olesik, J. W., Spectrochim. Acta, **48B**, 817 (1993).

Houk, R. S., Svec, V. H., and Fassel, V. A., Appl. Spectrosc., **35**, 380 (1983).

Houk, R. S., Montaser, A., and Fassel, V. A., Appl. Spectrosc., **37**, 425 (1983).

Houk, R. S., Schoer, J. K., and Crain, J. S., Spectrochim. Acta, **42B**, 841 (1987).

Huang, M., and Hieftje, G. M., Spectrochim. Acta, **40B**, 1387 (1985).

Huang, M., and Hieftje, G. M., Spectrochim. Acta, **44B**, 291 (1989).

Huang, M., Marshall, K. A., and Hieftje, G. M., Anal. Chem., **58**, 207 (1986).

Hughes, D. W., and Wooding, E. B., Phys. Lett., **24A**, 70 (1967).

Human, H. G. C., and Scott, R. H., Spectrochim. Acta **31B**, 459 (1976).

Inglis, D. R., and Teller, E., Appl. Spectrosc., **33**, 206 (1979).

Jinno, K., Nakanishi, S., and Fujimoto, C., Anal. Chem., **57**, 2229 (1985).

Johnston, P. D., High Temp., **20**, 499 (1966).

Kalnicky, D. J., Kniseley R. N., and Fassel, V. A., Spectrochim. Acta, **30B**, 511 (1975).

Kalnicky, D. J., Fassel V. A., and Kniseley, R. N., Appl. Spectrosc., **31**, 137 (1977).

Kepple, P., and Greim, H. R., Phys. Rev., **173**, 317 (1968).

Kirkbright, G. R., and Sargent, M., *Atomic Absorption and Fluorescence Spectroscopy*, Academic Press, London (1974).

Kleinmann, I., and Cajko, J., Spectrochim. Acta, **25B**, 657 (1970).

Kojima, I., and Iida, C., J. Anal. At. Spectrom., **2**, 463 (1987).

Kornblum, G. R., and de Galan, L., Spectrochim. Acta, **37B**, 541 (1974).

Kornblum, G. R., and de Galan, L., Spectrochim. Acta, **32B**, 71 (1977).

Kornblum, G. R., and Smeyers-Verbeke, J., Spectrochim. Acta **37B**, 83 (1982).

Kosinski, M. A., Uchida, H., and Winefordner, J. D., Talanta, **30**, 339 (1983).

Kreuning, G., and Maessen, F. J. M. J., Spectrochim. Acta, **42B**, 677 (1987).

Kreuning, G., and Maessen, F. J. M. J., Spectrochim. Acta, **44B**, 367 (1989).

Krupa, R. J., Long, G. L., and Winefordner, J. D., Spectrochim. Acta, **40B**, 1485 (1985).

Lemonds, J. A., and McClellan, E. B., Anal. Chem., **45**, 1455 (1973).

Lide, D. R., and Kehiain, H. V., in *CRC Handbook of Thermophysical and Thermochemical Data*, CRC Press, Florida, U. S. A., (1994).

Lochte-Holtgreven, W., Plasma Diagnostics, North-Holland, Amsterdam (1968) p13.

Long, S. E., and Browner, R. F., Spectrochim. Acta, **43B**, 1461 (1988).

Long, S. E., and Browner, R. F., Spectrochim. Acta, **44B**, 831 (1989).

Louie, H., and Soo, S. Y.-P., J. Anal. At. Spectrom., **7**, 557 (1992).

Masamba, W. R. L., Ali, A. H., and Winefordner, J. D., Spectrochim. Acta, **47B**, 481 (1992).

Matousek, J. P., and Mermet, J. M., Spectrochim. Acta, **48B**, 835 (1993).

McCrindle, R. I., and Rademeyer, C. J., J. Anal. At. Spectrom., **9**, 1087 (1994).

McKenzie, T., in *Varian Instruments at Work*, Varian Techtron, Australia, **AA-10**, 1 (1981).

Meeks, F. R., Spectrochim. Acta, **48B**, 1537 (1993).

Mermet, J. M., Spectrochim. Acta, **30B**, 383 (1975).

Mermet, J. M., Spectrochim. Acta, **44B**, 1109 (1989).

Mermet, J. M., Anal. Chim. Acta, **250**, 85 (1991).

Montaser, A., and Fassel, V. A., Appl. Spectrosc., **36**, 613 (1982).

Montaser, A., Fassel, V. A., and Larson, G., Appl. Spectrosc., **35**, 385 (1981).

Moore, G. L., Humphries-Cuff, P. J., and Watson, A. E., Spectrochim. Acta, **39B**, 915 (1984).

Moore, G. L., in *Council for Mineral Technology, Report No. M179*, Randburg, South Africa, 1 (1985).

Moore, G. L., Private communications (1986).

Mora, J., Hernandis, V., and Canals, A., J. Anal. At. Spectrom., **6**, 573 (1991).

Murillo, M., and Mermet, J. M., Spectrochim. Acta, **42B**, 1151 (1987).

Murillo, M., and Mermet, J. M., Spectrochim. Acta, **44B**, 359 (1989).

Nelder, J. A., and Mead, R., Comput. J., **7**, 308 (1965).

Ng, K. C., and Caruso, J. A., Anal. Chem., **55**, 2032, (1983).

Niebergall, K., Brauer, H., and Dittrich, K., Spectrochim. Acta, **39B**, 1225 (1984).

Nojiri, Y., Tanabe, K., Uchida, H., Haraguchi, H., Fuwa, K., and Winefordner, J. D., Spectrochim. Acta, **38B**, 61 (1983).

Novak, J. W., and Browner, R. F., Anal. Chem., **52**, 287 (1980).

Nowak, S., van der Mullen, J. A. M., van Lammeren, A. C. A. P., and Schram, D. C., Spectrochim. Acta, **44B**, 411 (1989).

Nukiyama, S., and Tanasawa, Y., Trans. Soc. Mech. Eng., Tokyo, 1938-1940, 4, 5 and 6, (transl. Hope, E., *Experiments in the Atomization of Liquids in an Air Stream*, Defence Research Board, Dpt. of National Defence, Ottawa, Canada, 1950).

Olesik, J. W., and Fister III, J. C., Spectrochim. Acta, **46B**, 851 (1991).

Omenetto, N., Nikden, S., Reeves, R. D., Bradshaw, J. B., Bower, J. N., and Winefordner, J. D., Spectrochim. Acta, **35B**, 507 (1980).

Operating and Servicing Manual, Particle Measuring Systems, Inc., Boulder, U. S. A., 1986.

Pan, C., Zhu, G., and Browner, R. F., J. Anal. At. Spectrom., **5**, 537 (1990).

Pan, C., Zhu, G., and Browner, R. F., J. Anal. At. Spectrom., **7**, 1231 (1992).

Pei-qi, L., Pei-zhong, G., and Tie-zheng, L., Spectrochim. Acta, **43B**, 273 (1988).

Poussel, E., Mermet, J. M., and Deruaz, D., J. Anal. At. Spectrom., **9**, 61 (1994).

Prost, M. M., Spectrochim. Acta, **37B**, 541 (1982).

Raaijmakers, I. J. M. M., Boumans, P. W. J. M., van der Sidje, B., Schram, D. C., Spectrochim. Acta, **38B**, 697 (1983).

Rademeyer, C. J., and Fischer, J. L., J. Anal. At. Spectrom., **8**, 487 (1993).

Raeymaekers, R., Broekaert, J. A. C., and Leis, F., Spectrochim. Acta, **43B**, 941 (1988).

Reeves, R. D., Nikden, S., and Winefordner, J. D., Appl. Spectrosc., **34**, 477 (1980).

Reif, I, Fassel V. A., and Kniseley, R. N., Spectrochim. Acta, **28B**, 105 (1973).

Russo, R. E., and Hieftje, G. M., Appl. Spectrosc., **36**, 92 (1982).

Schramel, P., Spectrochim. Acta, **38B**, 199 (1983).

Schramel, P., and Li-qiang, X., Fresenius Z. Anal. Chem., **319**, 229 (1984).

Scott, R. H., Fassel, V. A., Kniseley, R. N., and Nixon, D. E., Anal. Chem., **46**, 75 (1974).

Seeverens, P. J. H., Klaassen, E. J. M., and Maessen, F. J. M. J., Spectrochim. Acta, **38B**, 727 (1983).

Skogerboe, R. K., and Olson, K. W., Appl. Spectrosc., **32**, 181 (1978).

Spendley, W., Hext, G. R., and Himsworth, F. R., Technometrics, **4**, 441 (1962).

Uchida, H., Kosinski, M. A., Omenetto, N., and Winefordner, J. D., Spectrochim. Acta, **38B**, 529 (1983).

Tang, Y. Q., and Trassy, C., Spectrochim. Acta, **41B**, 143 (1986).

Thomsen, C., and Helbig, V., Spectrochim. Acta, **46B**, 1215 (1991).

Todorovic, M., Vidovic, S., and Ilic, Z., J. Anal. At. Spectrom., **8**, 1113 (1993)

Tracy, D. H., Myers, S. A., and Balitsee, B. G., Spectrochim. Acta, **37B**, 739 (1982).
Uchida, H., ICP Newslett., **8**, 155 (1982).

Uchida, H., Kosinski, M. A., Omenetto, N., and Winefordner, J. D., Spectrochim. Acta, **39B**, 63 (1984).

Van der Mullen, J. A. M., Nowak, S., Van Lammeren, A. C. A. P., Schram, D. C., and Van der Sijde, B., Spectrochim. Acta, **43B**, 317 (1988).

Van der Mullen, J. A. M., Spectrochim. Acta, **44B**, 1067 (1989).

Van der Mullen, J. A. M., Spectrochim. Acta, **45B**, 1 (1990a).

Van der Mullen, J. A. M., Spectrochim. Acta, **45B**, 233 (1990b).

Vidal, C. R., Cooper, J., and Smith, E. W., Astrophys. J. Suppl., No. 214, **25**, 37 (1972).

Visser, K., Hamm, F. M., and Zeeman, P. B., Appl. Spectrosc., **30**, 34 (1976).

Walters, P. E., and Barnardt, C. A., Spectrochim. Acta, **43B**, 325 (1988).

Walters, P. E., Gunter, W. H., and Zeeman, P. B., Spectrochim. Acta, **41B**, 133 (1986).

Ward, A. F., Sobel, H. R., and Crawford, R. L., ICP Information Newslett., **3**, 90 (1977).

Weir, D. G. J., and Blades, M. W., Spectrochim. Acta, **49B**, 1231 (1994).

Weldt, R. H., and Fassel, V. A., Anal. Chem., **37**, 920 (1965).

Willard, H. H., Merritt, L. L. jr., Dean, J. A., and Seattle, F. A. jr., *Instrumental Methods of Analysis*, 7th ed., Wadsworth Publishing Co., Belmont, USA, (1988), p274.

Xiao, J., Li, Q.-Y., Li, W.-C., Qian, H.-W., Tan, J.-Y., and Zhang, Z.-X., J. Anal. At. Spectrom., **7**, 131 (1992).

Yanping, H., Zhanxia, Z., J. Anal. At. Spectrom., **9**, 701 (1994).

Zeeman, P. B., Terblanche, S. P., Visser, K., and Hamm, F. H., Appl. Spectrosc., **32**, 572 (1978).

APPENDIX A

A.1 Introduction

The programme atodconv.exe converts analogue signals to digital values. It is contained in the directory "atod" and may be initiated by typing "atodconv".

A.2 Programme

The screen will give the following:

SPACE	:	Begin acquisition
F	:	Set frequency of acquisition
N	:	Set number of data points to acquire
M	:	Measure maximum frequency again
C	:	Calibrate input
Q	:	Quit program

Maximum frequency /Hz	:	100.0000
Maximum number of data points	:	1000

Current frequency	:	1.0000
Current number of data points	:	100
Calibration correlation	:	1.0000000
Calibration (y = a + bx)	a :	0.0000
	b :	1.0000

A.3 Procedure

The desired number of data points must be determined. In the case of the acquisition from the PMT the number was 256 when the excitation temperature and electron density was determined and reported in Chapter 3. The time interval in which the

points must be acquired should also be determined. From those two values (number of points and time) the frequency can be calculated. By pressing "F" the frequency may be set as the programme requests "Enter new frequency" and by pressing "N" the required number of points may be set after "Enter new number of data points to record: ". "M" remeasures the maximum frequency.

The default value for the number of data points is "100", but the value will change as "N" is entered. Similarly the default value for frequency is "1.0000", but will alter as a value is entered via "F".

Measurement, or conversion, commences after "space" has been pressed. Conversion will continue at the set frequency until the predetermined number of points have been converted, afterwhich the message "Acquisition in progress Please wait!" leaves the screen.

The results may be calibrated if a device generating a known value is used to as a source for the analogue signal. The calibration correlation is altered according to the results obtained from the standard device. The calibration curve is then calculated and reported as a linear function, with "a" and "b" given from the determination.

The programme is ended by pressing "Q".

APPENDIX B

1. Introduction

The following manual is given with the permission of Prof K Visser of the University of Stellenbosch. The programme contains two directives, one to apply Abel inversion, the other to calculate the temperature and electron density.

2. Abel Inversion

The program *ABEL* calculates the Abel integral inversion, I(r) from a series of laterally measured parameters $I(x_i)$ determined at equidistant lateral x_i-coordinates of a cylindrical symmetric source on an IBM-PC. The program is menu driven and can be initiated after inserting the disk containing the program and other related files into the active diskdrive and typing *ABEL*.

3. Data Input

Data can be imported either from files or edited via the keyboard. Data imported from files must conform to the following criteria:

3.1 Input data must be in the form of a set of related files, one file for each particular x_i-coordinate and the values in each such file represent the spectral intensity Ix_j, x_i at successive equally spaced wavelengths λ_j.

3.2 Files are named in terms of the index, i of the lateral position represented:

E.g. XXXX-8XX.XXX is the data for the lateral position with index -8.

File-names may consist of up to 8 characters of which two is used for identification of the lateral index i and optionally an extension of up to three characters conforming to the standard MSDOS file-names. The specific position for the lateral index

identification label in the file-name is arbitrary, but must be identical for a set of related files as must be the rest of the characters in the name. The lateral index identification label must be symmetrical with respect to zero and positive indexes must be written in the form **00,01** etc. A maximum of 33 files may be placed for successive lateral positions.

3.3 In each file of a related set, the intensity values should correspond to identical wavelength step size and for all such files the data in successive order should correspond with similar increasing or decreasing wavelengths. The wavelength is determined from the peak of the spectral profile and the spectral dispersion and then synchronized for the different files in a related set. A maximum of 330 wavelength positions in each file can be accommodated.

3.4 The format of the input data files is the standard text file format with ASCII code representation of integer, fixed or exponential real values separated from one another by a space, a comma or a carriage return. The period is used as decimal symbol.

4. Main Menu

The main menu consists of the following explanatory options:

MAIN MENU FOR *ABEL* INTEGRAL INVERSION

0 : EXIT FROM PROGRAM

1 : SET DEFAULT VALUES

2 : IMPORT DATA

3 : CALCULATE *ABEL* INVERSION

4 : DISPLAY VARIABLES GRAPHICALLY

5 : EXPORT DATA FILES

Select from 0..5

5. **Default Menu**

The default values are obtained from the configure file *ABEL.CNF* which was saved upon exit from the previous run of the program *ABEL* or from initial default values if this file does not exist. The default menu consists of the following options:

DEFAULT MENU

0 : EXIT TO MAIN MENU

1 : PATH b:

2 : IMPORT FILE NAME A??.LAT

3 : EXPORT FILE NAME A??.RAD

4 : Maximum wavelength index in [1..330]] **256**

5 : Maximum lateral index in [1..16] **8**

Select from 0..5

Option **1 : PATH** is used to specify the drive and optional subdirectory where the data files containing the input reside.

Option **2 : IMPORT FILE NAME** contains the mask for the set of file names containing the input data with the wildcard characters ?? reserved for the lateral index labels.

Option **3 : EXPORT FILE NAME** contains the mask for the set of file names serving as destination for the radial output data with the wildcard characters ?? reserved for the radial index labels.

Option **4 : Maximum wavelength index in [1..330]** contains the number of wavelength positions in the set of files. If any of the input files contains more values, this counter is automatically increased till the end of file code is read.

Option **5 : Maximum lateral index in [1..16]** contains the maximum positive index

of the number of lateral indexes and thus controls the lateral index label in the names of the set of files being searched to import.

6. **Data Import Menu**

The data import menu consists of the following options:

DATA IMPORT MENU

0 : EXIT TO MAIN MENU

1 : PATH b:

2 : FILE NAME MASK A??.LAT

3 : DIR

4 : IMPORT DATA FILES

5 : NUMERIC DISPLAY

6 : EDIT THE DATA

Select from 0..6

Option **1 : PATH** is used to specify the drive and optional subdirectory whose directory can be read or where the data files containing the input can be searched.

Option **2 : FILE NAME MASK** contains the mask for the set of file names to be searched for either directory identification or for reading the input data files. Wildcard characters ?? can be used for substitution of a single character in a file name or for substituting the file name or file name extension. Before selecting the option **4 : IMPORT DATA FILES**, the mask must be set correctly with the wildcard characters **??** reserved for the lateral index labels.

Option **3 : DIR** can be used to test if the files conforming to the file name mask specified in the previous option **2 : FILE NAME MASK** do exist at the drive and subdirectory. It can also be used to search the directories.

Option **4 : IMPORT DATA FILES** is used for importing the data from the files specified by the path file name mask. During data import the user will be informed of the particular file being read as well as errors encountered, if any.

Option **5 : NUMERIC DISPLAY** displays data imported from the set of data files to memory in numerical format. The lay-out of the data in a two dimensional matrix is such that the vertical columns correspond with the successive lateral indexes which is indicated on top of each column on a highlighted background. The rows correspond to the intensities at successive wavelength indexes, which is indicated in the leftmost column on a highlighted background. The display window containing 6 columns and 23 rows can be moved from left to right over the data matrix of up to 33 columns by 330 rows by means of the *right arrow key* and from right to left by means of the *left arrow key*. Upward scrolling can be accomplished by means of the *up arrow key, the page up* and the *home key*, while downward scrolling is affected by means of the *down arrow key, the page down key* and the *end key*. To exit from this option the *escape key* is to be used.

Option **6 : EDIT THE DATA**. The data can be edited (if necessary). Movement of the cursor for selecting the specific data value to be changed, is similar to that of the previous option. The convention for representing integer or real values upon entering, is according to the Turbo Pascal standard. To exit from this option the *escape key* is to be used.

7. **Calculate Abel Inversion**

This option calculates the Abel integral inversion according to the technique of Freeman and Katz (1963).

8. **Display Graph Menu**

The display graph menu consists of the following options:

DISPLAY GRAPH MENU

0 : EXIT TO MAIN MENU

1 : LATERAL DATA VERSUS WAVELENGTH

2 : LATERAL DATA VERSUS LATERAL POSITION

3 : COMPOSITE GRAPH LATERAL DATA VERSUS WAVELENGTH

4 : RADIAL DATA VERSUS WAVELENGTH

5 : COMPOSITE GRAPH RADIAL DATA VERSUS WAVELENGTH

Select from 0..5

Once a graph is displayed the *print screen key* can be used to obtain a hard copy by means of a graphic screen dump to the printer.

Option **1 : LATERAL DATA VERSUS WAVELENGTH** provides graphically an intensity versus wavelength profile at any of the selected lateral positions. It corresponds with the data from one particular input file as a function of wavelength index. Autoscaling is used for each graph.

Option **2 : LATERAL DATA VERSUS LATERAL POSITION** provides graphically a lateral intensity distribution versus lateral position at any of the selected wavelength indexes. It is useful to decide whether the input data does indeed fulfill the requirement of being cylindrical symmetric for the *ABEL* integral inversion. Wavelength synchronization for the different files is taken in account in plotting these graphs. Autoscaling is used for each graph.

Option **3 : COMPOSITE GRAPH LATERAL DATA VERSUS WAVELENGTH** provides a composite graph of four intensity versus wavelength profiles at four successive lateral positions. Scaling is done according to the peak value of the whole set of lateral dat. After viewing one group the next may be viewed by hitting any key, till the end of the cycle. This option is just a condensed version of option 1 enabling the user to view more than one graph simultaneously with the same scaling factor.

Option **4 : RADIAL DATA VERSUS WAVELENGTH** provides graphically an intensity versus wavelength profile at any of the selected radial positions after performing the Abel integral inversion. It corresponds with the data that can be exported to one particular output file as a function of wavelength index. Autoscaling is used for each graph.

Option **5 : COMPOSITE GRAPH RADIAL DATA VERSUS WAVELENGTH** provides a composite graph of four calculated intensity versus wavelength profiles at four successive radial positions. Scaling is done according to the peak value of the whole set of radial data. After viewing one group the next may be viewed by hitting any key, till the end of the cycle. This option is just a condensed version of option 4 enabling the user to view more than one graph simultaneously with the same scaling factor.

9. **Data Export Menu**

The data export menu consists of the following options:

DATA EXPORT MENU

O : EXIT TO MAIN MENU

1 : PATH b:

2 : FILE NAME MASK A??.RAD

3. DIR

4. EXPORT DATA FILES

5. NUMERIC DISPLAY

Select from 0..5

Option **1 : PATH** is used to specify the drive and optional subdirectory whose directory can be read or where the data files containing the radial output data can be saved.

Option **2 : FILE NAME MASK** contains the mask for the set of file names to be

searched for either directory identification or for saving the radial output data files. Wildcard characters **??** can be used for substitution of a single character in a file name or for substituting the file name or file name extension. Before selecting the option **4 : EXPORT DATA FILES**, the mask must be set correctly with the wildcard characters **??** reserved for the radial index labels.

Option **3 : DIR** can be used to test if the files conforming to the file name mask specified in the previous option **2 : FILE NAME MASK** are existing file names at the drive and subdirectory. It can also be used as a general search in the directories.

Option **4 : EXPORT DATA FILES** is used for exporting the data from the files specified by the path file name mask. During data export the user will be informed of the particular file being written as well as errors encountered, if any. Should a file already exist the user will be asked whether the programme would rewrite it or not.

Option **5 : NUMERIC DISPLAY** can be used to display the calculated radial data in numerical format. The lay-out of the data in a two dimensional matrix is similar to the display of the lateral data and scrolling is also identical. To exit from this option the *escape key* is to be used.

10. Purpose of the Program *TEMP*

The program *TEMP* (Temperature and Electron Density Calculations) calculates the temperature and electron number density from spectral intensity measurements on the Hydrogen Balmer Lines H_α and H_β on an IBM-PC. The program is menu driven and can be initiated after inserting a disk containing the program and other related files into the active diskdrive and typing *TEMP*.

11. Data Input

Data must be imported from files, which must conform to the following criteria:

11.1 Input data for each of the two spectral lines (from the same stationary plasma volume) must be in a separate file, and the values in each such file represent the spectral intensity I_j.

11.2 Filenames may consist of up to 8 characters and optionally an extension of up to three characters conforming to the standard MSDOS filenames.

11.3 Provision is made for a maximum of 330 wavelength positions in each file.

11.4 The format of the input data files is the standard text file format with ASCII code representation of integer, fixed or exponential real values separated from one another by a space, a comma or *ENTER*. The period is used as decimal symbol.

12. Main Menu

The main menu consists of the following self explanatory options:

MAIN MENU FOR TEMPERATURE CALCULATION

0 : EXIT FROM PROGRAM

1 : SET DEFAULT VALUES

2 : IMPORT DATA

3 : DISPLAY VARIABLES GRAPHICALLY

4 : CALCULATE TEMPERATURE

Select from 0..4

13. Default Submenu

Default vales are obtained from the configure file *TEMP.CNF* which was saved upon exit from the previous run of the program *TEMP* or from initial default values if this file does not exist. The default menu consists of the following options:

DEFAULT SETTINGS MENU

0 : EXIT TO MAIN MENU

1 : Maximum wavelength index in [1..330] **256**

3 : Intensity Calibration

4 : Wavelength Calibration

5 : Spectral Line Constants

Select from 0..5

13.1 **Path and Filenames Submenu**

This sub-Submenu provides the setting of the access path and names of the files containing the spectral intensities of the two lines H_α and H_β.

DEFAULT PATH AND FILENAME SUB-SUBMENU

0 : EXIT TO PREVIOUS MENU

1 : Path **b:**

2 : ALPHA filename **A07.RAD**

3 : BETA filename **B07.RAD**

Select from 0..3

13.2 **Maximum wavelength index in [1..330]**

This variable contains the number of wavelength positions in the set of files. If any of the input files contains more values, this counter is automatically increased till the end of file code is read.

13.3 **Intensity Calibration Submenu**

In order to calculate the excitation temperature by means of the intensity ratio of the two spectral lines originating from the same homogeneous volume of plasma, the intensities of the two lines relative to each other must be calculated.

INTENSITY CALIBRATION SUB-SUBMENU

0 : EXIT TO PREVIOUS MENU

1 : Calibration signal at ALPHA

2 : Calibration signal at BETA

3 : Radiance at ALPHA

4 : Radiance at BETA

13.4 **Wavelength Calibration Submenu**

In order to calculate the electron number density from the spectral profiles of the two Hydrogen spectral lines, H_α and H_β, their halfwidth has to be calculated and accordingly the wavelength interval corresponding to the range of intensity points needs to be calibrated. This wavelength span must be given in units of *m*.

WAVELENGTH CALIBRATION SUB-SUBMENU

0 : EXIT TO PREVIOUS MENU

1 : Wavelength interval at ALPHA

2 : Wavelength interval at BETA

Select from 0..2

13.2 **Spectral Line Constants Submenu**

To perform the excitation temperature measurement from the line intensity ratio a number of constants pertaining to the specific spectral lines are needed. The default vales of these spectral line constants are applicable to the H_α and H_β lines.

SPECTRAL LINE CONSTANTS SUB-SUBMENU

0 : EXIT TO PREVIOUS MENU

1 : ALPHA degeneracy **g1 = 18**

2 : BETA degeneracy **g2 = 32**

3 : ALPHA transition probability **A1 = 4.410E+07**

4 : BETA transition probability **A2 = 8.419E+07**

5 : ALPHA wavelength **l1 = 6.56280E-07**

6 : BETA wavelength **l2 = 4.86132E-07**

7 : ALPHA energy (/cm) **E1 = 9.74920E+04**

8 : BETA energy (/cm) **E2 = 1.02824E+05**

Select from 0..8

The excitation energy of the two lines must be specified in units of cm^{-1} for the calculation, but the units of the other spectral constants are arbitrary, since their ratios are taken in the calculation causing the units to cancel out.

14. Data Import Submenu

The data import menu consists of the following options:

DATA IMPORT SUBMENU

0 : EXIT TO MAIN MENU

1 : PATH **b:**

2 : ALPHA FILE NAME MASK **A07.**

3 : BETA FILE NAME MASK **B07.**

4 : ALPHA MASK DIR

5 : BETA MASK DIR

6 : IMPORT DATA FILES

7 : NUMERIC DISPLAY /Select from 0..7

Option **1 : PATH** is used to specify the drive and optional subdirectory whose directory content can be read or where the data files containing the input can be searched.

Option **2 : ALPHA FILE NAME MASK** contains the mask for the file name(s) to be searched for either directory identification or for reading the input data file containing the H_α spectral intensities. Wildcard characters **??** can be used for substitution of a single character in a file name or for substitution of the file name or file name extension, during file searches. Before selecting the option **6 : IMPORT DATA FILES**, the mask must be set correctly.

Option **3 : BETA FILE NAME MASK** contains the mask for the file name(s) to be searched for either directory content identification or for reading the input data file containing the H_α spectral intensities. Wildcard characters **??** can be used for substitution of a single character in a file name or * for substitution of the file name or file name extension, during file searches. Before selecting the option **6 : IMPORT DATA FILES**, the mask must be set correctly.

Option **4 : ALPHA MASK DIR** can be used to test if the file conforming to the file name mask specified in the option **2 : ALPHA FILE NAME MASK** does exist at the specified drive and subdirectory. It can also be used in a general search of the directories.

Option **5 : BETA MASK DIR** can be used to test of the file conforming to the file name mask specified in the option **3 : BETA FILE NAME MASK** does exist at the specified drive and subdirectory. It can also be used in a general search in the directories.

Option **6 : IMPORT DATA FILES** is used for importing the data from the files specified by the path and file name mask. During data import the user will be informed of the particular file being read as well as errors encountered, if any.

Option **7 : NUMERIC DISPLAY** can be used to display data imported from the two data files to memory in numerical format. The lay-out of the dat in a two dimensional matrix is such that the two vertical columns correspond with the intensities of the H_α and H_β lines respectively. The rows correspond with the intensities at successive wavelength indexes, which is indicated in the leftmost column on a highlighted background. The display window containing 2 columns and 23 rows can be scrolled. Upward scrolling can be accomplished by means of the *up arrow key*, the *page up* and the *home key*, while downward scrolling is affected by means of the *down arrow key*, the *page down key* and the *end key*. To exit from this option the *escape key* is to be used.

15. **Display Graph Menu**

The display graph menu consists of the following options:

DISPLAY GRAPH SUBMENU

0 : EXIT TO MAIN MENU

1 : ALPHA INTENSITY VERSUS WAVELENGTH

2 : BETA INTENSITY VERSUS WAVELENGTH

3 : COMPOSITE GRAPH

Select from 0..3

Once a graph is displayed the *print screen key* can be used to obtain a hard copy by means of a graphic screen dump to the printer.

Option **1 : ALPHA INTENSITY VERSUS WAVELENGTH** provides graphically an intensity versus wavelength profile of the H_α line.

Option **2 : BETA INTENSITY VERSUS WAVELENGTH** provides graphically an intensity versus wavelength profile of the H_β line.

Option **3 : COMPOSITE GRAPH** provides graphically an intensity versus wavelength profile for both lies on the same graph.

16. **Calculate Temperature**

This option calculates the excitation temperature (in K) using the two line intensity ratio technique. The nett line intensities are obtained by summing over the wavelength profiles (negative intensity values are ignored) and normalizing according to the intensity calibration factors. The full-width-half-maximum values of the two spectral lines (in Å) are calculated from the spectral profiles and the wavelength calibration factors. The electron number densities (cm^{-3}) are calculated by means of interpolation from the tables of Vidal *et al* (1972) using the calculated temperature and halfwidth of the H_α and H_β lines as parameters. For values outside the listed range the program responds with a remark "No solution found".

APPENDIX C

RULES FOR THE SIMPLEX METHOD (From Moore: 1985)

Once the initial simplex has been established, the following rules and steps apply.

1. After each single response measurement, a move is made.

In the interests of speed, replicate measurements are not normally made. The method is designed so that any false high responses generated are eliminated.

2. The simplex moves by rejection of the point that shows the worst response and replacement of that point with its mirror image across the hyperface of the remaining four points.

If the vertices of the four-dimensional simplex are represented by the coordinate vectors S1, S2, S3, S4 and S5, where S5 has the worst response, then elimination of the most undesirable response leaves the hyperface S1, S2, S3 and S4 with centroid C, where

$$C = (S1 + S2 + S3 + S4)/4 \qquad C.1$$

The new simplex is defined by this hyperface, and a new vertex S6 is generated by the reflection of S5 across the hyperface through C:

$$S6 = C + (C - S5) \qquad C.2$$

If the new vertex yields the worst response in the new simplex, the application of Rule 2 would result in the reflection of the simplex back to the previous simplex, and it would become standard. Hence, Rule 3 is needed.

3. **If the new vertex shows the worst response in the new simplex, the vertex associated with the second-worst response is rejected, and the moves continue.**

4. **If a vertex has not been replaced in 5 simplexes before Rule 2 was applied, the response at the persistent vertex must be retested.**

This rule is necessary so that the simplex will be prevented from circling a possible false high response.

The simplex may start to move beyond the permitted hyperspace by exceeding one or more of the four plasma variables (i.e. a boundary violation). A new vertex may call for an observation height lower than the top of the quartz torch or a power higher than can be supplied by the generator. In such an event, Rule 5 is applied.

5. **If the new vertex lies beyond the boundaries of the interdependent variables, the response must not be observed but a very undesirable response must be assigned to that vertex.**

The application of Rules 2 and 3 will then result in the simplex returning to a position inside the boundary limits.

The identification of a situation in which a limitation on a variable prevents the attainment of a better response is one of the beneficial practical results of the simplex method of optimization.

Once an optimum has been found, the rules force the simplex to circle around the optimum region. The smaller the simplex at this stage, the more accurately the optimum can be defined. Once the simplex shrinks to such a size that the indeterminate errors involved in the response measurement mask the true differences between the vertex responses, the simplex will wander erratically near the optimum.

The **modified simplex procedure** employs the Rules for the basic simplex, but also allows for the contraction or expansion of the simplex to enable it to travel faster over the response surface and to define the final optimum more precisely. The operations of expansion and contraction are added to the operation of reflection.

If an initial simplex has the responses R1, R2, R3, R4, R5 in descending order, the following procedure must be followed.

For any particular parameter,

V_W represents the value of the parameter associated with the worst response, R5.

The new parameter V_R will then be defined by the equation:

$$V_R = C + Z(C - V_W), \qquad C.3$$

where the centroid C is given by:

$$C = (V_1 + V_2 + V_3 + V_4)/4, \qquad C.4$$

and the expansion coefficient Z is taken as 1. V is the value of a parameter associated with a particular response.

If the response at the new vertex is greater than R1, expansion of the simplex may be justified, and new parameters are calculated by the use of equation C.3 when Z = 2. If the response at this expanded vertex is better than at the reflected vertex, the expanded vertex is used to define the new simplex. If the response is worse, the original reflected vertex is used.

If the response at the new vertex is less than R1 but greater than R3, the reflected vertex (Z = 1) is used to define the new simplex, i.e. no expansion or contraction is attempted.

If the response at the new vertex is less than R3 but greater than R5, a positive contraction is attempted, and new parameters are calculated by the use of equation C.3 when Z = +0.5. If the response at the contracted vertex is better than at the reflected vertex, the contracted vertex is retained in the new simplex. If the response is worse, the original reflected vertex is retained.

If the response at the new vertex is less than R5, a negative contraction is applied, and the new parameters are calculated by the use of equation C.3 when Z = -0.5. Irrespective of the success or failure of this negative contraction, the contracted vertex is retained in the new simplex but, in the latter event (failed negative contraction), the second-worst response is rejected on the next simplex cycle. As in the case of a boundary violation, this causes the simplex to change to a direction that may be more favourable.

When the differences in response or step sizes of the plasma parameters become smaller than a certain value, the simplex can be stopped.

APPENDIX D

The following consists of a series of calibration curves for the elements investigated. They were determined under various circumstances, which will be detailed below. The first six were determined using an aerosol carrier gas flow rate stipulated by the manufacturer (Spectroflame) and at 1.36 kW.

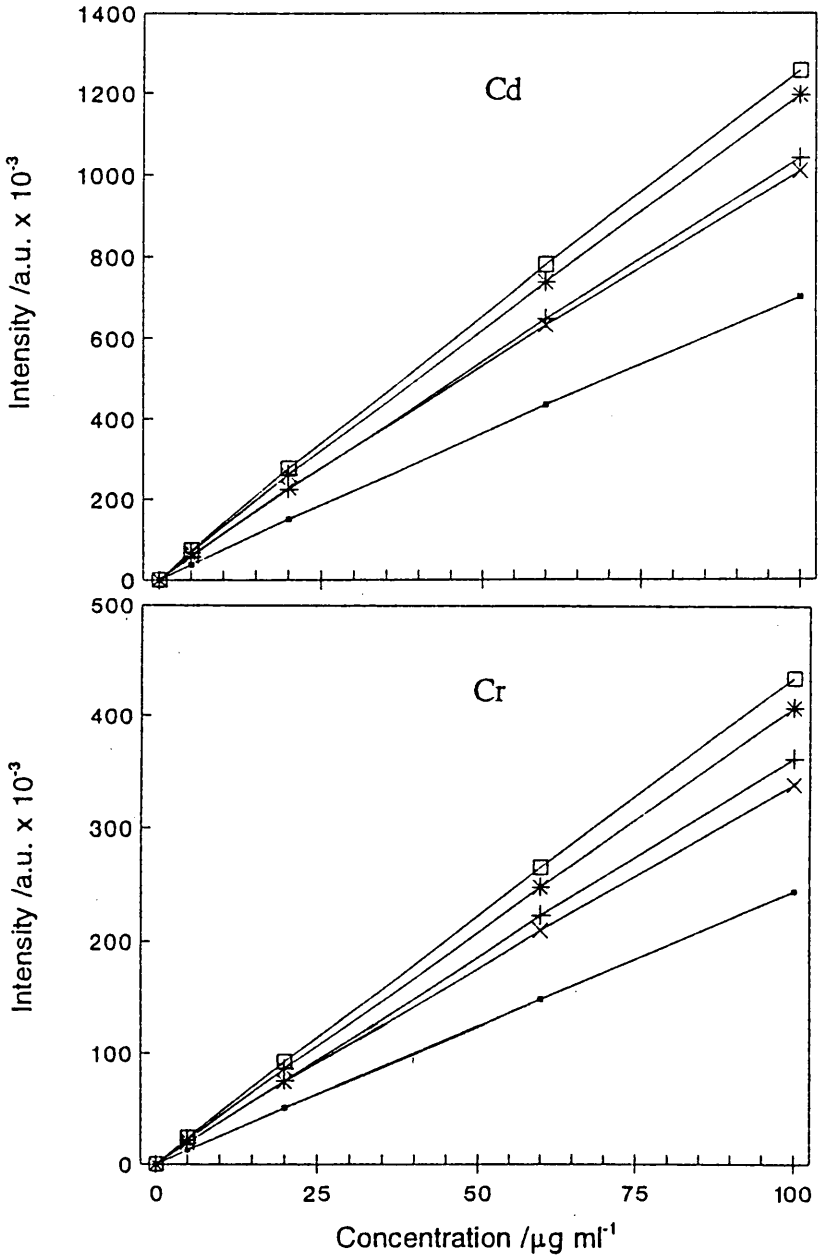

Figure D.1 Calibration curves for elements in (⊙) 0, (+) 5, (✳) 10, (□) 15 and (x) 20 % ethanol.

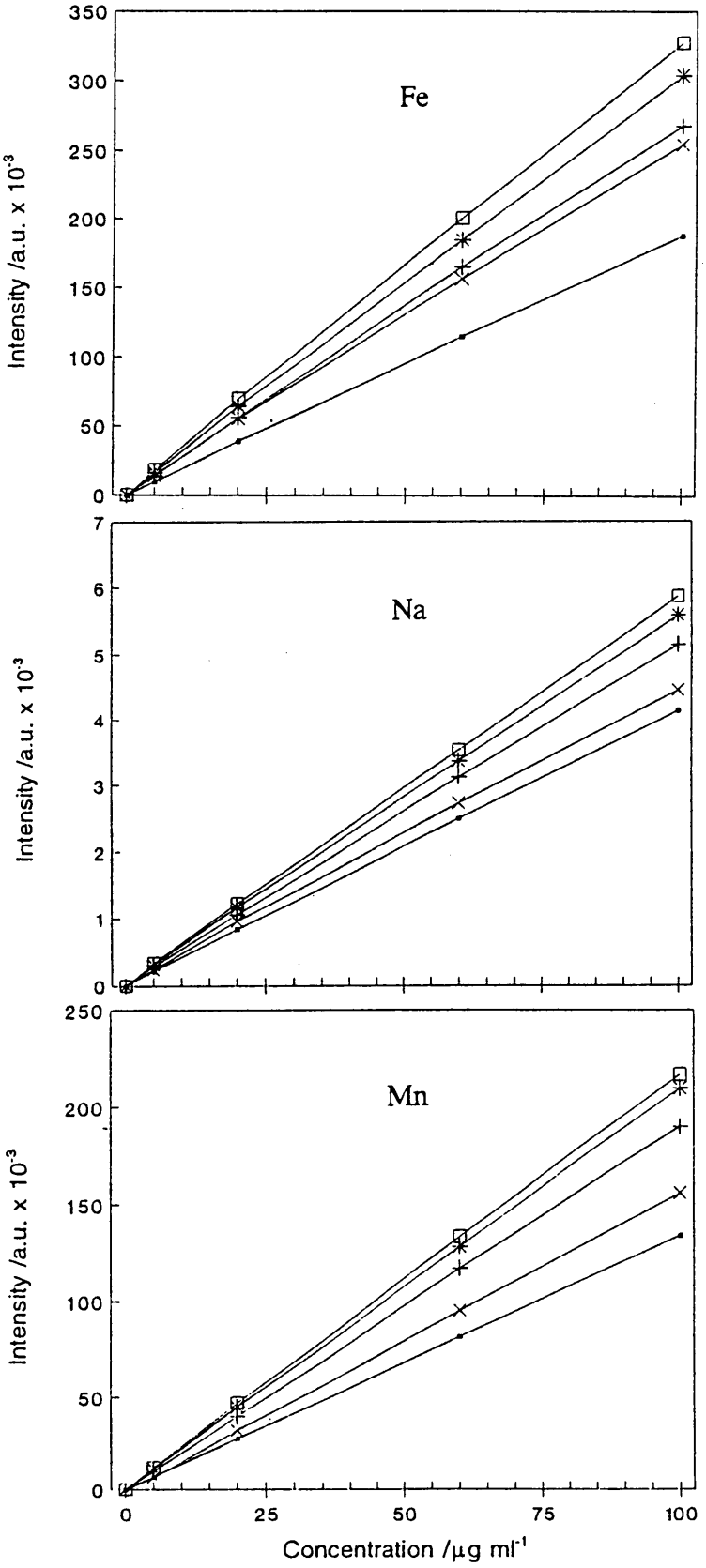

Figure D.2 Calibration curves for elements in (⊙) 0, (+) 5, (✳) 10, (□) 15 and (x) 20 % ethanol.

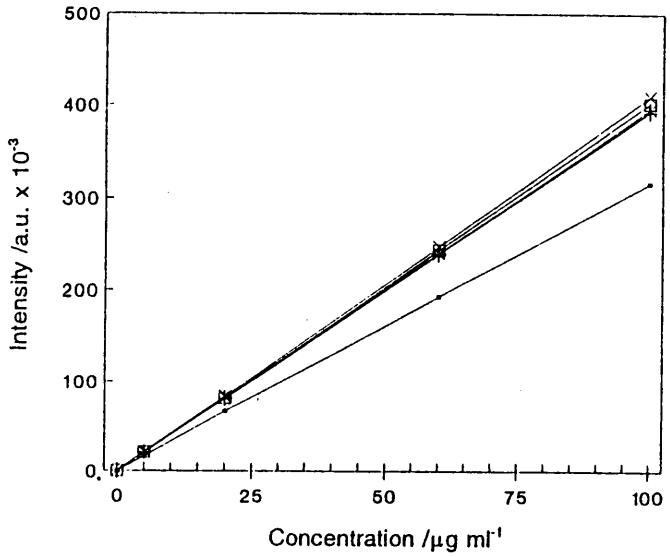

Figure D.3 Calibration curves for V in (⊙) 0, (+) 5, (✳) 10, (□) 15 and (x) 20 % ethanol.

The following is a series of calibration curves for the elements investigated, but at low aerosol carrier gas flow rates. The rates were such that the intensity of the highest standard for 20 % ethanol could not be measured. The concentration of ethanol which resulted in the greatest sensitivity has also changed from that reported in the text and obtained using a suitable flow rate. The differences in sensitivity between these calibration curves and those presented earlier can be seen in an examination of the intensity scale.

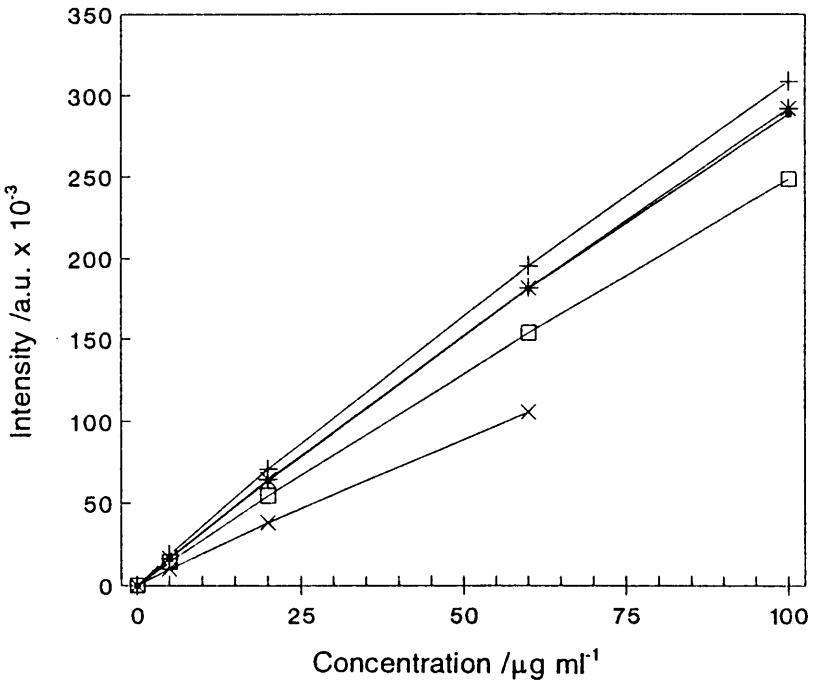

Figure D.4 Calibration curves for Cd in (⊙) 0, (+) 5, (✳) 10, (□) 15 and (x) 20 % ethanol.

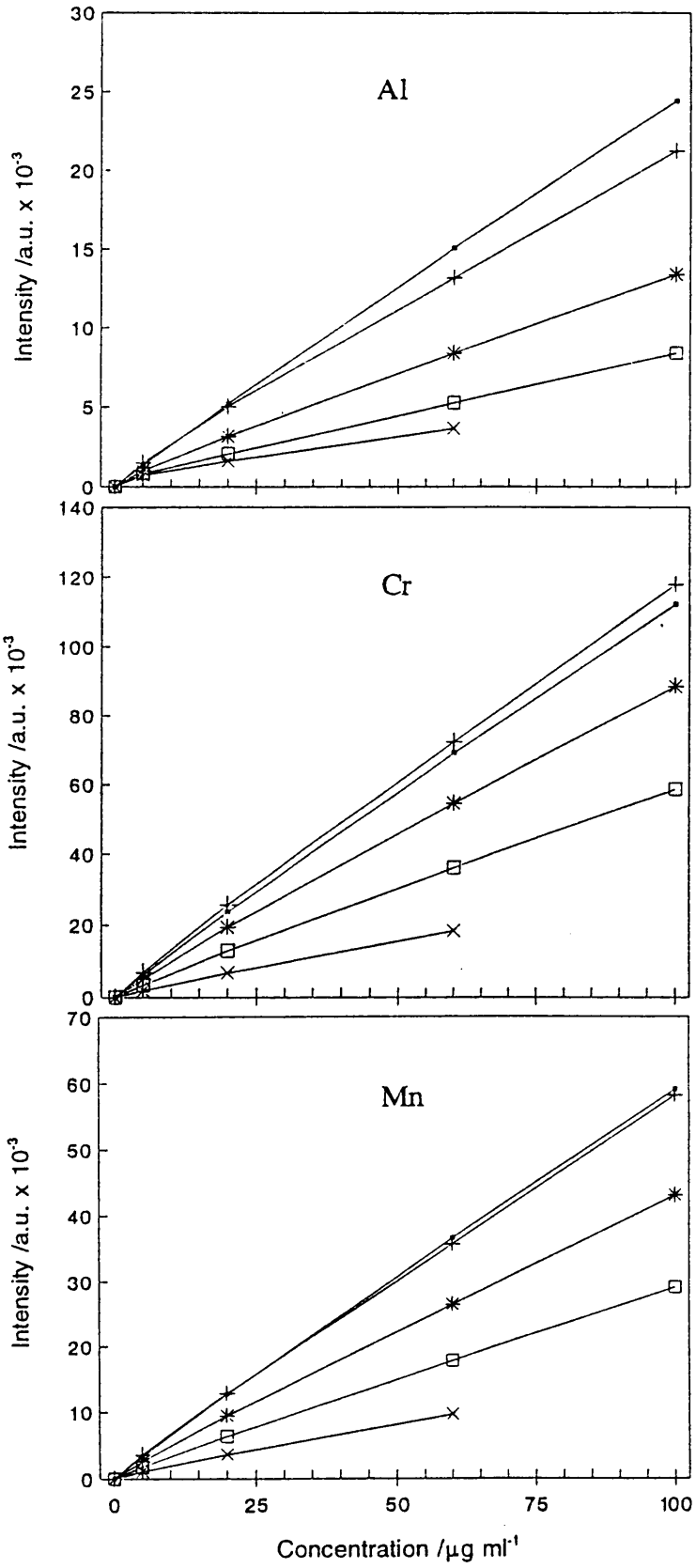

Figure D.5 Calibration curves for elements in (⊙) 0, (+) 5, (✳) 10, (□) 15 and (x) 20 % ethanol.

In the following two calibration curves, at the slower aerosol carrier gas flow rate, it was possible to obtain the measurement for the highest standard in 20 % ethanol.

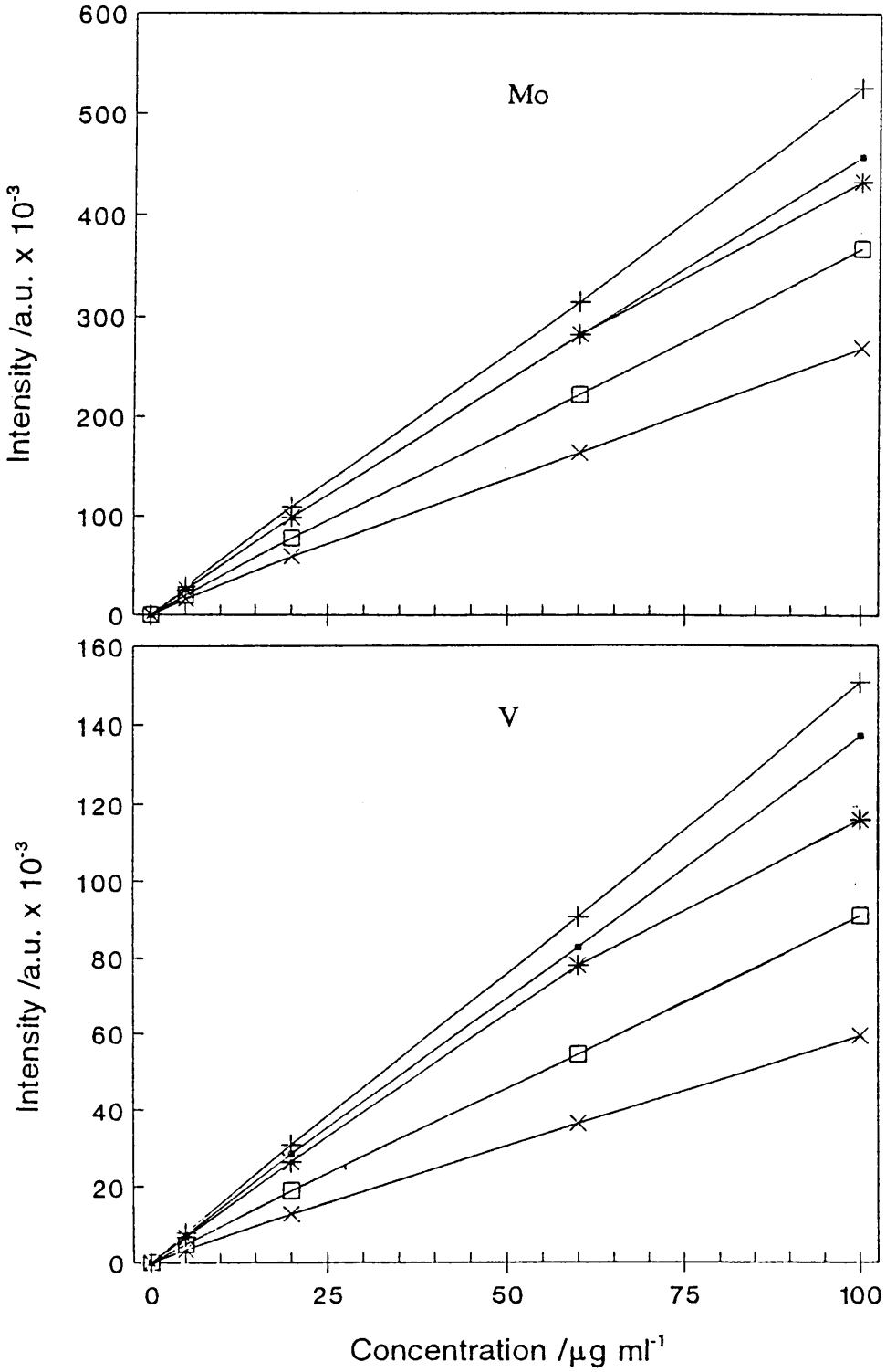

Figure D.6 Calibration curves for Mo and V in (⊙) 0, (+) 5, (✳) 10, (□) 15 and (x) 20 % ethanol.

The following calibration curves for Mo and V were obtained at different aerosol carrier gas flow rates. Standards were in 15 % ethanol.

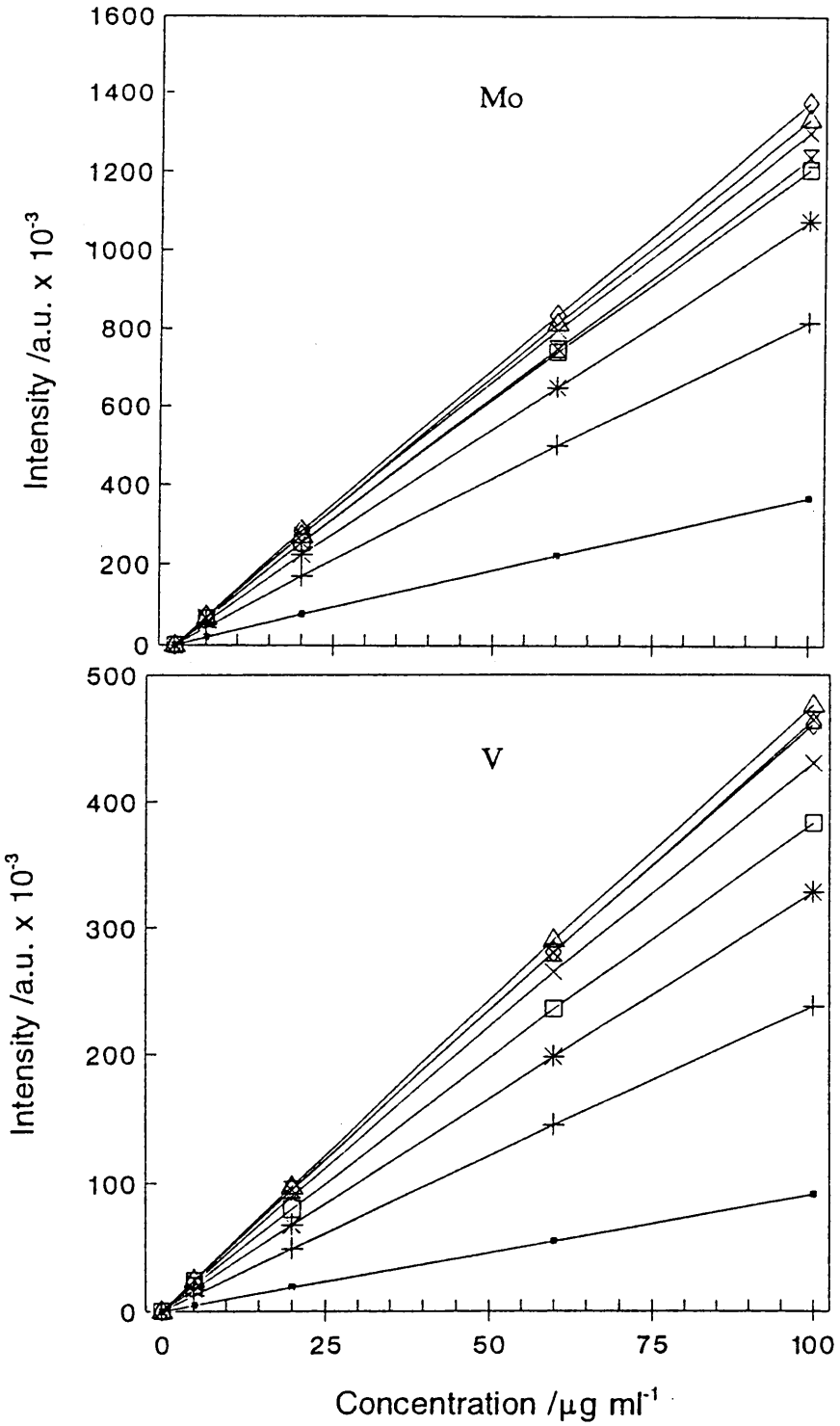

Figure D.7 Calibration curves for Mo and V in 15 % ethanol at aerosol carrier gas flow rates of (⊙) 0.40, (+) 0.45, (✳) 0.50, (□) 0.55, (x) 0.60, (◊) 0.65, (Δ) and (X) 0.75 l min^{-1}.

Effects of aerosol carrier gas flow rates can be seen in the following figures were signal intensity of 100 µg ml^{-1} of the elements was determined in water and 20 % ethanol.

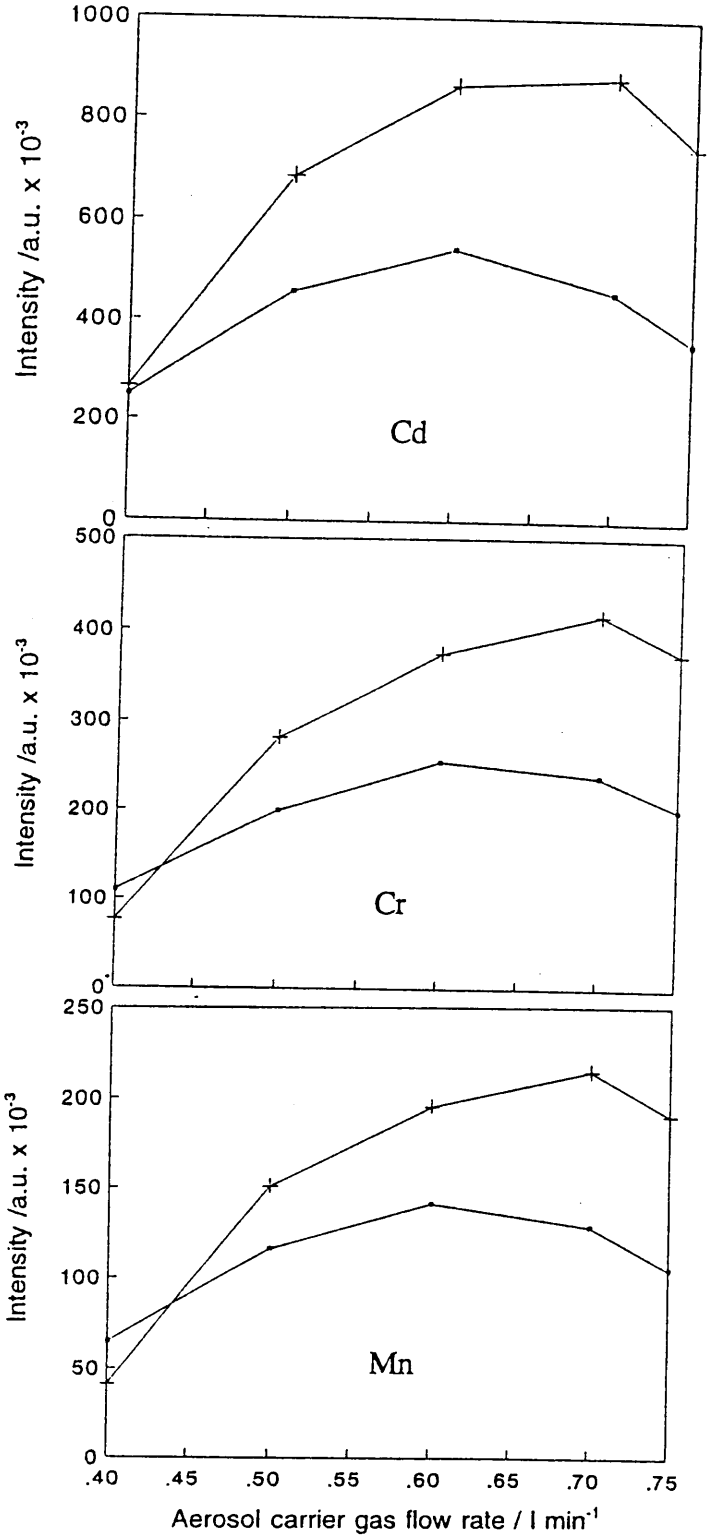

Figure D.8 Signal intensity of 100 µg ml^{-1} of Cd, Cr and Mn in water (⊙) and 20 % (+) ethanol with increasing aerosol carrier gas flow rate.

The Varian Liberty ICP-OES was used to obtain the following calibration curves.

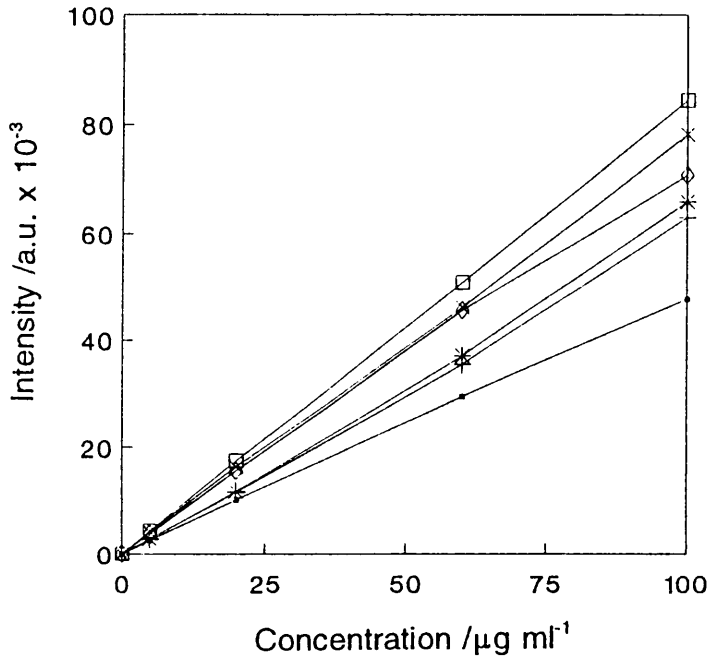

Figure D.9 Calibration curves at 1.0 kW of Mo in 0 (⊙), 5 (+), 10 (✳), 15 (□), 22 (x) and 25 (◊) % ethanol.

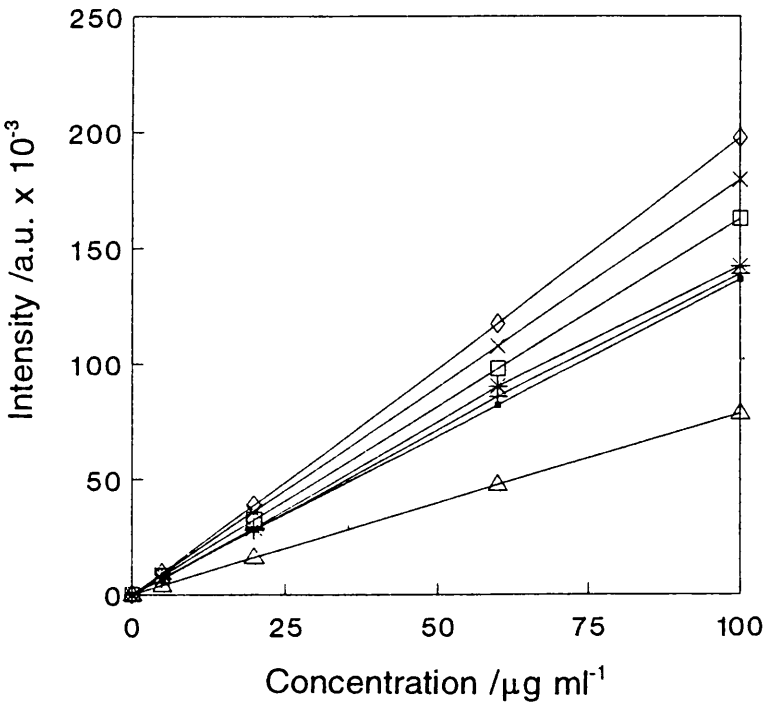

Figure D.10 Calibration curves at 1.2 kW of V in 0 (⊙), 5 (+), 10 (✳), 15 (□), 20 (x), 25 (◊) and 95 (Δ) % ethanol.

The following series were obtained using 1.5 kW.

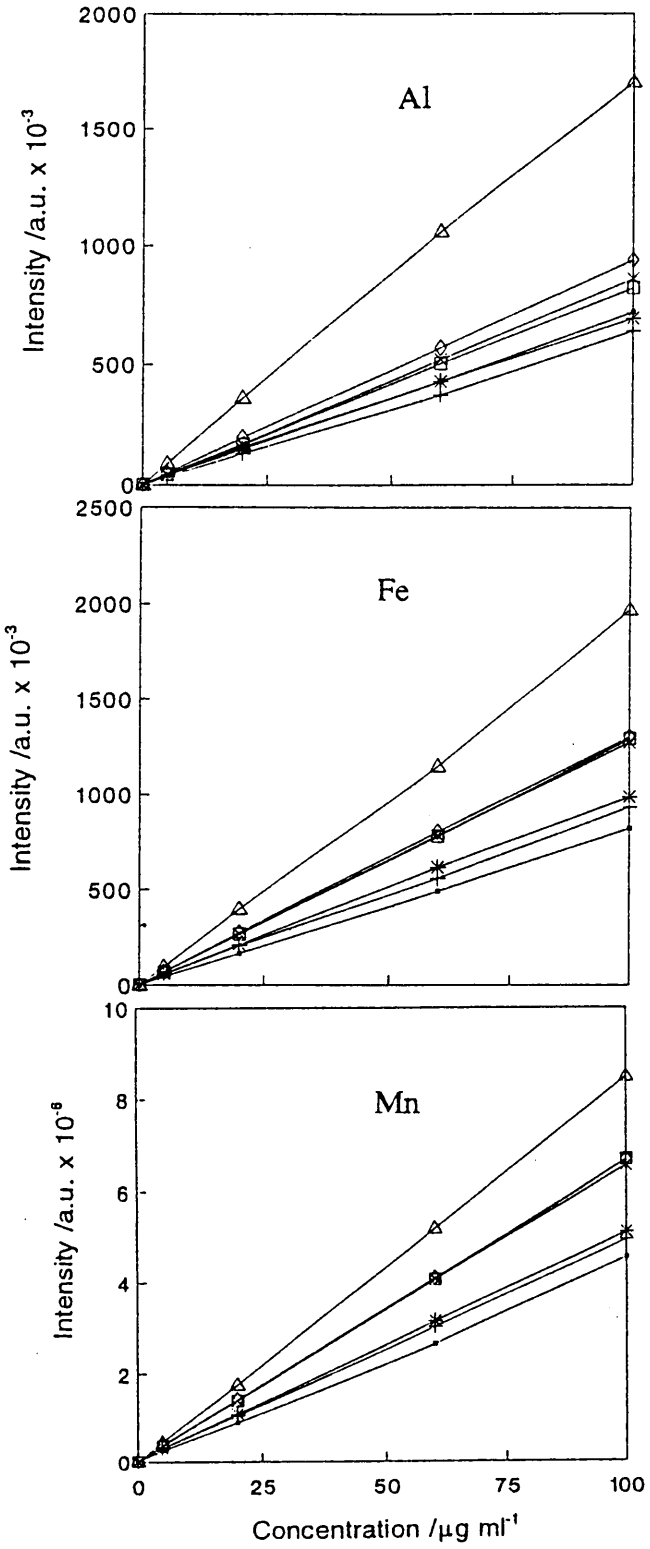

Figure D.11 Calibration curves of elements in 0 (⊡), 5 (+), 10 (✳), 15 (□), 20 (x), 25 (◊) and 95 (Δ) % ethanol.

Using xylene and xylene/ethanol mixtures the following calibration curves were obtained using conditions obtained from Simplex optimization.

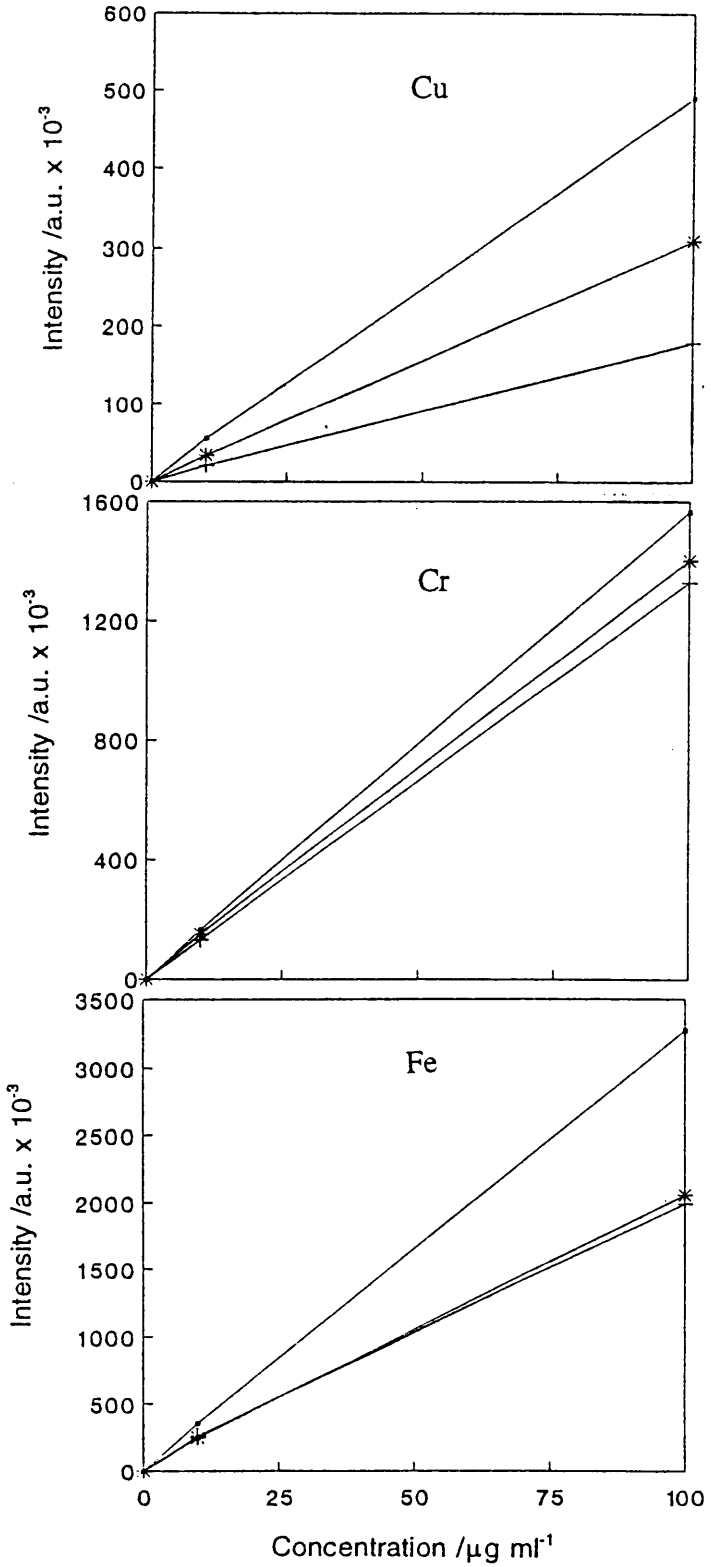

Figure D.12 Calibration curves for elements in (⊡) xylene, (+) 30 % and (✳) 45 % ethanol in xylene.